Development of an Optical Fiber Biosensor with Nanoscale Self-Assembled Affinity Layer

Ziwei Zuo

Dissertation submitted to the Faculty of the
Virginia Polytechnic Institute and State University
In partial fulfillment of the requirements for the degree of

Doctor of Philosophy

In

Physics

James R. Heflin, Chairman
Jean J. Heremans
Hans D. Robinson
Thomas J. Inzana

Nov 20, 2013
Blacksburg, Virginia

Keywords: long-period-gratings (LPG), ionic self-assembled multilayer (ISAM) films, fiber optical sensor, methicillin-resistant *S. aureus* (MRSA), *Brucellosis*, *Francisella tularensis*, monoclonal antibody (Mab)

Abstract

Development of an Optical Fiber Biosensor with
Nanoscale Self-Assembled Affinity Layer

Ziwei Zuo

Optical sensor systems that integrate Long-Period-Gratings (LPG) as the detection arm have been proven to be highly sensitive and reliable in many applications. With increasing public recognition of threats from bacteria-induced diseases and their potential outbreak among densely populated communities, an intrinsic, low-cost biosensor device that can perform quick and precise identification of the infection type is in high demand to respond to such challenging situations and control the damage those diseases could possibly cause.

This dissertation describes the development of a biosensor platform that utilizes polymer thin films, known as ionic self-assembled multilayer (ISAM) films, to be the sensitivity-enhancing medium between an LPG fiber and specific, recognition layer. With the aid of cross-linking reactions, monoclonal antibodies (IgG) or DNA probes are immobilized onto the surface of the ISAM-coated fiber, which form the core component of the biosensor.

By immersing such biosensor fiber into a sample suspension, the immobilized antibody molecules will bind the specific antigen and capture the target cells or cell fragments onto the surface of the fiber sensor, resulting in increasing the average thickness of the fiber cladding and changing the refractive index of the cladding. This change occurring at the surface of the fiber results in a decrease of optical power emerging from the LPG section of the fiber. By comparing the transmitted optical power before and after applying the sample suspension, we are able to determine whether or not certain bacterial species have attached to the surface of the fiber, and as

a consequence, we are able to determine whether or not the solution contains the targeted bacteria.

This platform has the potential for detection of a wide range of bacteria types. In our study, we have primarily investigated the sensitivity and specificity of the biosensor to methicillin-resistant *Staphlococcus aureus* (MRSA). The data we obtained have shown a sensitive threshold at as low as 10^2 cfu/ml with pure culture samples. A typical MRSA antibody-based biosensor assay with MRSA sample at this concentration has shown optical power reduction of 21.78%. In a detailed study involving twenty-six bacterial strains possessing the PBP2a protein that enables antibiotic resistance and sixteen strains that do not, the biosensor system was able to correctly identify every sample in pure culture samples at concentration of 10^4 cfu/ml. Further studies have also been conducted on infected mouse tissues and clinical swab samples from human ears, noses, and skin, and in each case, the system was in full agreement with the results of standard culture tests. However, the system is not yet able to correctly distinguish MRSA and non-MRSA infections in clinical swab samples taken from infected patient wounds. It is proposed that nonspecific binding due to insufficient blocking methods is the key issue.

Other bacterial strains, such as *Brucella* and *Francisella tularensis* have also been studied using a similar biosensor platform with DNA probes and antibodies, respectively, and the outcomes are also promising. The *Brucella* DNA biosensor is able to reflect the existence of 3 *Brucella* strains at 100 cfu/ml with an average of 12.2% signal reduction, while negative control samples at 10^6cfu/ml generate an average signal reduction of -2.1%. Similarly, the *F. tularensis* antibodies biosensor has shown a 25.6% signal reduction to LVS strain samples at 100 cfu/ml, while for negative control samples at the same concentration, it only produces a signal reduction

of 0.05%. In general, this biosensor platform has demonstrated the potential of detecting a wide range of bacteria in a rapid and relatively inexpensive manner.

Acknowledgement

First of all, I would like to thank my advisor, Dr. James R. Heflin, for giving me the opportunity to work on this project, and for his precious research advice, enormous support and encouragement through years of laboratory work. Without his insight and expertise on the obstacles I have encountered in this project, I could never be able to finish my research on this project. I can't express enough appreciation for all the time Dr. Heflin has devoted in my research, and I would like to dedicate this dissertation to him.

I also thank Dr. Thomas J. Inzana for his valuable advice and suggestions on the biochemistry issues we met during the research, and without his support and Dr. Aloka B. Bandara's hard work on providing the strain samples, this project won't be possible. I value highly of our collaboration, and I would like to give my deep thanks to them.

Thanks to my committee members: Dr. Hans Robinson and Dr. Jean J. Heremans, for offering all the help I asked for. Thanks to Dr. Jimmy Ritter, for his support and assistance in this research project and offering great ideas on issues we have constantly come across.

And I can't afford to forget to give thanks to Mr. Moataz Khalifa, for offering me the opportunity to conduct AFM studies, and accompany me over many unforgettable nights in the laboratory. Without his expertise on AFM, his impressive smell and humor, I would enjoy much less of my laboratory time. Also thanks to Ms. Kelly Mccutcheon for helping me oversee the experiments when I have to focus on the dissertation writings.

During my years in pursuing my degrees in Virginia Tech, I have met so many great faculty and staff who I want to thank. I want to give my special thanks to Ms. Christa Thomas, for her great help during all these years, on so many trivial or important matters. Thanks to Dr. Uwe

Täuber for his wonderful advice during my first year in the graduate program of Physics department.

I would like to thank my parents, Mr. Ming Zuo and Ms. Hui Cheng. Their unending support and love have given me great encouragement to carry on my study in Virginia Tech. And I thank them for offering me good education and opportunities without having any regrets or asking for returns.

I am deeply thankful to have received many helps and spiritual nourishment from Dr. Johnny Yu and Dr. Jessie Yu-Chen, they have made my stay in Blacksburg as like home. Also thanks to Dr. Y.A Liu, Dr. Chao Shang, Dr. Liwu Li, Dr. Peter Lo, Dr. Caisy Ho, Dr. Paul Carlier, Dr. Don Mckeon, Dr. Randall Cliff. You have been great example to me and have taught me lessons I won't get anywhere else.

And thanks to my good old friends, Dr. Qiang Li, Mr. Lester Jay, Dr. Jay Sullivan, Dr. Tongli Zhang, Mr. Lifeng Li, Mr. Gang Wu, Ms. Luman Chen, Ms. Yanjun Ma, Ms. Ying Xu, Mr. Di Zeng, Mr. Yao Li, Mr. Renyuan Fu, Mr. Waifong Chan, Ms. Yiming Tang, Dr. Chih-ling Liou, Ms. Yueying Yu, Mr. Yitao Zhu, Ms. Yinglian Yang, Ms. Bing Yan, Mr. Christoph Paulus, Dr. Ni Shen, Dr. Cheng Ma, Mr. Zhipeng Tian, and many more that I can't list here. Friendship never will grow old with you fellows. And special thanks to Ms. Qing Li and Dr. Jing Zhang. Thanks to my best "bad" friend Mr. Zhao Liu and Mr. Xiao Lv, killing time with you can't be more fun. And thanks to Dr. Danielle Jao for giving my great advice on graduation.

And I can't forget my dear friend Mr. Chuck Schumann, I know you are happy for me in heaven.

Contents

List of Figures

List of Tables

Chapter 1 Introduction

1.1 Review of Biosensing Technology

A biosensor is a type of device that converts the presence of biological targets to an electronic, physical or chemical signal variation that can be macroscopically observed, measured and quantitatively processed.

The most common commercial-available biosensor is the blood glucose biosensor, which translates the glucose concentration of the blood sample to the current traversing between two detection electrodes, and in turn is able to monitor the glucose level of the diabetes user, and warn the user for dangerously high or low sugar level.[1,2,3]

In general, a biosensor consists of three major parts: the sample preparation compartment, which treats the raw source for test (*i.e.* air collected from environment, swabs taken from a patient's wound, cell cultures) into the reaction-ready form for the biosensor; the sensor compartment, where the transducer or the detector element is located and the main biochemical reactions occur, triggering a physicochemical, optical, piezoelectric or electrochemical signal variation of the sensor that can then be easily collected and quantified; and the signal processing compartment, which amplifies the transformed signal the sensor compartment generates, interprets and displays the results through a user-friendly interface.

[1] A Farmer, A Wade, E Goyder, et al., "Impact of self-monitoring of blood glucose in the management of patients with non-insulin treated diabetes: open parallel group randomized trial". *BMJ,* **335 (7611):** 132, (2007).
[2] H. C. Gerstein, M. E. Miller, et al. "Effects of intensive glucose lowering in type 2 diabetes". *The New England Journal of Medicine*, **358(24):** 2545–59, (2008).
[3] M. E. Khamseh, M. Ansari, M. Malek, , G. Shafiee, H. Baradaran, "Effects of a structured self-monitoring of blood glucose method on patient self-management behavior and metabolic outcomes in type 2 diabetes mellitus". *Journal of diabetes science and technology*, **5(2):** 388–393, (2011).

In the heart of the biosensor system lays the biological receptor, which must meet the following criteria to qualify for the detection element of the sensor system:

(a) The receptor must be able to effectively interact with the target analyte, such as binding or reacting with the analyte.

(b) The result of the receptor-analyte interaction must yield a measurable change to the biosensor system, for example, increasing the physical size of the receptor compound, changing the pH values or salt concentration of the buffer solution environment the receptor is located in, and so on.

(c) The receptor must be very specific, meaning the receptor must not interact with background components of the sample, and/or other biomolecules coexisting with the target analyte in the sample.

Based on the interaction principle or the targeting region of the analyte, biosensor designs can be classified as one of the following categories:[4] antibody-antigen sensor;[5] enzyme sensor; DNA probe sensor;[6] cellular structures/living cells sensor;[7,8,9,10] or biomimetic materials sensor.[11] Based on the type of signal the transducer generates from the biological signal, the biosensor can

[4] T. Vo-Dinh, B. Cullum, "Biosensors and biochips: Advances in biological and medical diagnostics". *Fresenius' Journal of Analytical Chemistry*, **366 (6–7):** 540, (2000).

[5] E. Marazuela, A. Moreno-Bondi, "Fiber-optic biosensors - an overview". *Analytical and Bioanalytical Chemistry* **372(5-6):** 664–682, (2002).

[6] Donzella V, Crea F. "Optical biosensors to analyze novel biomarkers in oncology." *J Biophotonics.* **4(6):**442-52, (2011).

[7] R. Rizzuto, P. Pinton, M. Brini, A. Chiesa, L. Filippin, T. Pozzan, "Mitochondria as biosensors of calcium microdomains". *Cell Calcium*, **26(5):** 193–199, (1999).

[8] M. Bragadin, S. Manente, R. Piazza, G. Scutari, "The Mitochondria as Biosensors for the Monitoring of Detergent Compounds in Solution". *Analytical Biochemistry,* **292 (2):** 305–307, (2001).

[9] C. Védrine, J.-C. Leclerc, C. Durrieu, C. Tran-Minh, "Optical whole-cell biosensor using Chlorella vulgaris designed for monitoring herbicides." *Biosensors & bioelectronics*, **18(4):** 457–63, (2003).

[10] R. S. Dubey, S.N. Upadhyay, "Microbial corrosion monitoring by an amperometric microbial biosensor developed using whole cell of Pseudomonas sp." *Biosensors & bioelectronics*, **16(9-12):** 995–1000, (2001)..

[11] M. Campàs, R. Carpentier, R. Rouillon, "Plant tissue-and photosynthesis-based biosensors". *Biotechnology Advances*, **26(4):** 370–378, (2008).

be classified as: electrochemical sensors;[12,13] optical sensors;[14] electronic sensors;[15] mass-sensitive and piezoelectric sensor;[16] surface accoustic biosensors; thermometric[17] and pyroelectric sensors.

Though the biosensor designs vary widely, all biosensor designs must involve sensor-preparation steps to attach the corresponding receptor to the sensor surface and ensure the receptor region that would interact with the analyte is accessible to the applied analyte sample. This procedure can be tricky and problematic, as the organic receptor cannot be easily directly attached onto commonly seen transducer materials, such as metals, silica or inorganic polymers. Usually the transducer surface needs to be treated with organic thin films or gold nanoparticle films that can bind activated receptor molecules through so called cross-linking reactions. The choice of the crosslinking chemistry and bridging organic film must not modify the structure or analyte-reactive region (denoted as paratope) of the receptor, or block the signal channel for the transducer. Otherwise, the receptor would lose activity and cease to react with the analyte, or the transducer may be deafened for sensing any biological variations taking place to the receptor layer. Identifying a proper biochemical reaction chain and respective materials to immobilize the receptor have thus been a central issue for biosensors designed to target particular analytes.[18,19,20]

---

[12] S.Q. Lud, M.G. Nikolaides, I. Haase, M. Fischer and A.R. Bausch, "Field Effect of Screened Charges: Electrical Detection of Peptides and Proteins by a Thin Film Resistor" *ChemPhysChem,* **7(2):** 379-384, (2006).

[13] G Liu, Y. Lin, "Nanomaterial labels in electrochemical immunosensors and immunoassays." *Talanta*. **74(3):**308-17, (2007).

[14] María Dolores Marazuela, María Cruz Moreno-Bondi, "Fiber-optic biosensors – an overview." *Anal Bioanal Chem* **372**:664–682,(2002).

[15] I. Vockenroth, P. Atanasova, W. Knoll, A. Jenkins, I. Köper, "Functional tethered bilayer membranes as a biosensor platform". *IEEE Sensors 2005 the 4-th IEEE Conference on Sensors*: 608–610, (2005).

[16] Kyung Wook Weea, *etc.,* "Novel electrical detection of label-free disease marker proteins using piezoresistive self-sensing micro-cantilevers." *Biosensors and Bioelectronics*, **20(10):** pp. 1932–1938, (2005)

[17] Bong Seop Kwaka, *etc*.,"Quantitative analysis of sialic acid on erythrocyte membranes using a photothermal biosensor." *Biosensors and Bioelectronics,* **35(1):** pp.484–488, (2012).

[18] Guan H, Cai M, Chen L, Wang Y, He Z., "Label-free DNA sensor based on fluorescent cationic polythiophene for the sensitive detection of hepatitis B virus oligonucleotides." *Luminescence*. **25(4):**311-6,(2010).

The transducer of the biosensor needs to be first of all a sensitive device to the signal variation it is devised to monitor, as the biological variation is almost always small and can be inconveniently buried in the background noise. Immunoassay based biosensors usually use automatic screening devices to monitor the signals (such as using a CCD to detect the color variation or the wavelength shifting of the sample solution, or examine the fluorescence trace of the labeled receptor) of the on-plate assays. Electronic or electrochemical sensors may use capacitors, potentiometric, electrophoresis effect or circular oscillator as the transducer. For instance, a parallel plate capacitor is highly sensitive to the distance between the parallel plates and the material medium between the plates. Therefore, the receptors that capture analytes to the substrate surface may modify the average distance between plates and the dielectric constant of the intermedium biofilm, and in turn can be detected via supplementary circuits.[21] Recent studies[22,23] have found interesting applications of field-effect transistors (FETs) as the transducer of the biosensor, which could exhibit exceptional sensitivity to the density of the captured biomolecules on the FET surface, and can therefore be extremely responsive to small amount of analyte binding.

Biosensors for commercial use usually require the sensor system to be highly sensitive and selective to the target analyte, and capable of being easily deployed and maintained in a variety of environments. Most current biosensor platforms are either too expensive for vast deployment

---

[19] M. Zhang, S. Ge, W. Li, M. Yan, X. Song, J. Yu, W. Xu, J. Huang, "Ultrasensitive electrochemiluminescence immunoassay for tumor marker detection using functionalized Ru-silica@nanoporous gold composite as labels." *Analyst.* **137(3):**680-5,(2012).

[20] Li P, Sherry AJ, Cortes JA, Anagnostopoulos C, Faghri M., "A blocking-free microfluidic fluorescence heterogeneous immunoassay for point-of-care diagnostics." *Biomed Microdevices.* **13(3):**475-83,(2011).

[21] Anjum Quershia, Yasar Gurbuza, Weng P. Kangb, Jimmy L. Davidson, "A novel interdigitated capacitor based biosensor for detection of cardiovascular risk marker." *Biosensors and Bioelectronics,* **25(4):** 877-882, (2009).

[22] Deblina Sarkar, Kaustav Banerjee, "Proposal for tunnel-field-effect-transistor as ultra-sensitive and label-free biosensors." *Appl. Phys. Lett.,* **100:** 143108 (2012).

[23] Ankit Jain, Pradeep R. Nair, Muhammad A. Alam, "Flexure-FET biosensor to break the fundamental sensitivity limits of nanobiosensors using nonlinear electromechanical coupling". *PNAS*, **109(24):** 9304-9308, (2012).

or daily maintenance, or require complex supporting systems that limit the application of the biosensor. However, recent research on optical sensors has proven that such sensor systems are more adaptable and compact compared to other sensor platforms, and their exceptional sensitivity could help expand the regime of applications in medical diagnostics, forensics, military, environmental protection and so on.[24,25,26] This dissertation will focus on a specific fiber optic biosensor, which is based on the ultra-sensitivity of the long-period-grating (LPG) fiber sensor. The next section will concentrate on the development of the optics-related biosensors.

1.2 Current Development of Optical Biosensors

The development of modern molecular biology has helped advance the research on optical sensors to design and build ultra-sensitive, compact and mobile, rapid diagnostic sensor systems.

A variety of immunoassays have been associated with the optical property of the target labeling molecules in the early days. The labeling dye molecules could color the assay solutions under suitable reaction conditions with the product, and mark the existence of the label-fixed target. Therefore the most intrinsic optical biosensor designs are devised to collect the color-changing signals or weak light signals generated by the labeling molecules (mostly enzymes). Various fluorescence microscopy biosensors,[27,28,29] which measure the fluorescence intensity

[24] E. Anderson, J. Graham Smith, *et al.,* "Investigation and verification of a bioluminescent biosensor for the quantitation of ara-CTP generation: A biomarker for cytosine arabinoside sensitivity in acute myeloid leukaemia", *Biosensors and Bioelectronics,* **52:** 345-353, (2014).
[25] S. Rodriguez-Mozaz, M. de Alda, D. Barceló, "Biosensors as useful tools for environmental analysis and monitoring." *Anal Bioanal Chem,* **386**: 1025–1041, (2006).
[26] CA Rowe-Taitt, JP Golden, MJ Feldstein, JJ Cras, KE Hoffman, FS. Ligler, "Array biosensor for detection of biohazards." *Biosens Bioelectron.* **14(10-11):**785-94, (2000).
[27] Daniel Berdat, Annick Marin, Fernando Herrera, Martin A.M. Gijs, "DNA biosensor using fluorescence microscopy and impedance spectroscopy." *Sensors and Actuators B,* **118**:53–59, (2006).
[28] Andreas P. Abel, Michael G. Weller, Gert L. Duveneck , Markus Ehrat , H. Michael Widmer,"Fiber-Optic Evanescent Wave Biosensor for the Detection of Oligonucleotides." *Anal. Chem.,* **68 (17):** pp 2905–2912,(1996).
[29] Tempelman LA, King KD, Anderson GP, Ligler FS , "Quantitating Staphylococcal Enterotoxin B in Diverse Media Using a Portable Fiber-Optic Biosensor."*Anal Biochem,* **233**:50–57, (1996).

have been explored through CCD or microcircuits to read the weak radiation of fluorescent labels and transform such signals to analog electric or digital signals for quantitative analysis.

As the detection of fluorescence light can always be difficult due to its generally weak signal strength and masking by background noise, some biosensors use external light or UV excitation[30] to amplify the fluorescence signal, or use resonant cavities[31] to image the binding of analyte to the sensor surface. Researchers have also explored the use of interferometers for biosensing tasks, which focus on identifying small phase shifts of the sensor-ray-channel compared to the reference-ray-channel.[32,33,34]

Other technologies such as measures of absorbance, refraction, or Raman shift of the incident light have been explored for sensing the variation of optical properties of the sensor surface film due to analyte bindings. This includes sensors known as surface plasmon resonance (SPR) biosensors, which measure the interaction between incident light and the surface electronic plasma's optical properties. It was first demonstrated by Liedberg et al. in 1983,[35] and has been studied in depth in several implementations of biosensing,[36] such as:[37] prism coupling,

[30] Bartolomeo Della Ventura, Luigi Schiavo, Carlo Altucci, Rosario Esposito, Raffaele Velotta, "Light assisted antibody immobilization for bio-sensing." *Biomedical Optics Express*, **2(11):** pp.3223-3231,(2011).
[31] D. A. Bergstein, E. Ozkumur, A. C. Wu, A. Yalcin, J. Needham, R. Irani, J. Gershoni, B. B. Goldberg, C. DeLisi, M. F. Ruane, M. S. Ünlü, "Resonant Cavity Imaging: A Means Toward High-Throughput Label-Free Protein Detection," *IEEE Journal of Selected Topics in Quantum Electronics*, **14(1)**:131-139, (2008).
[32] B.H Schneider, E.L Dickinson, M.D Vach, J.V Hoijer, L.V Howard, "Highly sensitive optical chip immunoassays in human serum." *Biosens. Bioelectron.* **15(1-2)**:13-22, (2000).
[33] M.M. Varma, H.D. Inerowicz, F.E. Regnier, D.D. Nolte, "High-speed label-free detection by spinning-disk micro-interferometry." *Biosens. Bioelectron*. **19**(11):1371-1376, (2004).
[34] M. Zhao, D. Nolte, W. Cho, F. Regnier, M. Varma, G. Lawrence, J. Pasqua, "High-Speed Interferometric Detection of Label-Free Immunoassays on the Biological Compact Disc." *Clin. Chem.* **52:**2135-2140, (2006).
[35] B. Liedberg, C. Nylander, I. Lunstrom, "Surface plasmon resonance for gas detection and biosensing" *Sens. Actuators,* **4:** 299-304, (1983).
[36] Xudong Fan, Ian M. White, Siyka I. Shopova, Hongying Zhu, Jonathan D. Suter, Yuze Sun, "Sensitive optical biosensors for unlabeled targets: A review", *Analytica Chimica Acta,* **620**: 8–26, (2008).
[37] Homola J., "Present and future of surface plasmon resonance biosensors." *Anal Bioanal Chem.,* **377(3):**528-39,(2003).

waveguide coupling, fiber and grating coupling, and long-range and short-range surface plasmon (LRSP and SRSP).

With the development of optical fiber fabrication and manufacturing techniques, researchers begin to use fibers as the substrate for the biosensor, as the observer can monitor the absorbance, refraction, phase shifting, energy leaking and other optical properties occurring to the fiber all at once with the help of versatile fiber fabrication options. The advantages of fiber optical sensors are that they can be easily and cheaply mass-produced; the sensor supporting devices (diode laser and photodetectors) are small in size and the whole system can be built into a "lab-in-box". The fiber as a waveguide can carry a continuous range of wavelengths and allow propagation of multiple modes, each of which can be chosen as a "detection channel" to yield the multiple-diagnosis capacities. Fiber manufactured from silica can host a vast range of organic materials, which have been proven very useful for biochemical reactions, and therefore is capable for assembly of complex biosensor structures. And fiber can be more resistant to the background environmental fluctuations and therefore easier to be deployed and maintained in the open environment.

Generally fiber optic biosensors are built on top of two fiber structures: FBG[38,39,40] (Fiber-Bragg-Grating) and LPG [41 , 42] (Long-Period-Gratings). The former evaluates the power attenuation and wavelength shifting of the reflected light, which can be useful if the biosensing components are built upon the tip at one end of the fiber and the spectrum is monitored from the

[38] K.H. Smith, B.L. Ipson, T.L. Lowder, A.R. Hawkins, R.H. Selfridge, S.M. Schultz, "Surface-relief fiber Bragg gratings for sensing applications." *Appl. Opt.,* **45**:1669, (2006).
[39] T.L. Lowder, J.D. Gordon, S.M. Schultz, R.H. Selfridge, "Volatile organic compound sensing using a surface-relief D-shaped fiber Bragg grating and a polydimethylsiloxane layer." *Opt. Lett.,* **32:**2523, (2007).
[40] W. Liang, Y. Huang, Y. Xu, R.K. Lee, A. Yariv, "Highly sensitive fiber Bragg grating refractive index sensors." *Appl. Phys. Lett.* **86**: 151122, (2005).
[41] M.P. DeLisa, Z. Zhang, M. Shiloach, S. Pilevar, C.C. Davis, J.S. Sirkis, W.E. Bentley, "Biofunctionalized tilted Fiber Bragg Gratings for label-free immunosensing." *Anal. Chem.,* **72:**2895, (2000).
[42] L. Rindorf, J.B. Jensen, M. Dufva, L.H. Pedersen, P.E. Hoiby, O.Bang, "Photonic crystal fiber long-period gratings for biochemical sensing." *Opt. Express*, **14:**8224, (2006).

other end. This type of biosensor is especially good at reaching a region of interest that cannot be easily accessed by other devices designs. The latter measures the power attenuation and wavelength shifting of the transmitted light spectrum, the sensitivity generally grows proportionally to the length of the fiber grating region. And since its grating period is much longer than for the FBG, the cost per sensor unit can be much lower. Since the designed purpose for our biosensor project is to develop an affordable, rapid diagnostic sensor system that can be easily operated, the LPG fiber sensor platform is a more suitable choice, and such sensor design and sensing capability will be explored in detail in this dissertation. In particular, we focus on how the combination of a turn-around-point LPG and self-assembled polyelectrolyte films with large refractive index can yield an exceptionally sensitive, highly specific and versatile biosensing platform with measurement times of less than an hour.

1.3 Turnaround Point Long-Period-Gratings with Ionic Self-Assembled Multilayers

In order to address the urgent need of a fast-diagnosing, low-cost, accurate and versatile biosensor system, this dissertation will describe a novel approach to building an optical fiber based biosensor platform that satisfies all these criteria.

Inspired by and based upon the long-period-grating (LPG) based fiber sensors, this biosensor system displays outstanding sensitivity to the nanometer scale variation of surface thickness on the cladding, where the adhesion of the target analyte indicates the existence of such elements in the tested sample solution. The data obtained from pure culture trials demonstrates that the biosensor platform has the capability of sensing the presence of target strains at a level of 100 cfu/ml. As the analyte adhesion progresses, which leads to the increment of fiber sensor's cladding film thickness, the fiber sensor is capable of instantly reflecting the changes, thereby

making the biosensor system a possible candidate for a real-time monitoring and diagnostic device.

This dissertation will study the LPG optical fiber sensor, which consists of three essential elements: turnaround point LPG fiber, nanoscale ionic self-assembly multilayers (ISAM) organic thin film, and the cross-linked bioreceptor films. The turnaround point LPG fiber serves as the core element of the biosensor system, which is the transducer and responsible for converting the signal from the attachment of the corresponding analyte to the variation of transmitted optical power through the LPG fiber segment. The ISAM organic thin film will be the intermedium between fiber substrate and the bioreceptor thin film, which will provide desired biochemical functional groups for crosslinking reactions and help tune the LPG fiber to the optimum performance region. The bioreceptor film is the sensing arm of the biosensor platform. Based on the type of bacteria to be detected, the bioreceptor film can be constituted by proteins, antibodies, enzymes or DNA probes. These biological macromolecules can recognize and match with the cognate antigen expressions, and end up with binding the antigen analyte to the fiber surface, which induces the variation of transmitted optical power at the LPG fiber core.

A series of experiments have been conceived and deployed to explore the specificity and sensitivity of the biosensor system. It has been found that the Methicillin-resistant *Staphylococcus aureus* (MRSA) biosensor using monoclonal antibodies to the PBP2a penicillin-binding protein is capable of sensing MRSA strain 1556 at concentrations as low as 100 cfu/ml, with signal reduction at 21.78% in the pure culture samples, and ignoring Methicillin-sensitive *Staphylococcus aureus* (MSSA) strains, which are essentially identical with MRSA strains in a patient's initial symptoms and not distinguishable by many low-accuracy immunoassay tests. Broad screening assays of pure culture samples of 26 MRSA strains and 16 non-MRSA strains

have been performed at concentration 10^4 cfu/ml to examine the biosensor's capacity of general MRSA strain detection and differentiation. All 26 MRSA strain samples have shown positive responses with optical power attenuations of 9.1% to 34.6% (higher than the threshold—7% of optical power attenuation). In contrast, all 16 non-MRSA strain samples were also tested negative, all with power reductions less than 2.7%. The system was all tested on swabs taken from human volunteer ears, noses, and skin. In all 19 samples, the biosensor's MRSA diagnostic results were in complete agreement with BBL CHROMagar standard culture test at identifying the 9 positive and 10 negative samples. Mouse tissue samples were also tested with the MRSA biosensor platform. Tissue samples collected from MRSA infected mice have yielded optical power attenuation of 19.2% ± 6.4% for spleen tissues, 50.1% ± 11.9% for liver tissues and 11.7% ± 3.0% for lung tissues respectively; while by contrast, the tissue samples collected from MSSA infected mice have yielded optical power attenuation of 1.6% ± 8.3% for spleen tissues, 0.7% ± 1.0% for liver tissues and -0.9% ± 1.1% for lung tissues respectively. The data have shown clear distinction between the two experimental groups, therefore the biosensor system is proven to be capable of handling complex tissue samples and generating reliable results.

Tests on swabs taken from infected wounds of human clinical patients have not been as successful, presumably due to the much more complex mixture of materials present in such samples. As a result, we developed a modified version of the MRSA sensor using a DNA probe as the receptor. While the results of this approach are more reproducible, they still suffer from a substantial number of false-positive results. This is hypothesized to be due to non-specific binding from the complex samples and suggests that improved approaches to blocking the non-specific binding sites need to be developed.

Assays with an *F. tularensis* antibody-based biosensor that is built with the same biosensor platform to the MRSA biosensor system have also been designed and conducted, and the results are promising. In a consecutive assays test, the WBTI (*F. tularensis* negative) pure culture samples at 100 cfu/ml, 10^4 cfu/ml and 10^6 cfu/ml have generated signal reduction of 0.05%, 3.28% and -11.67% respectively; while the LVS (*F. tularensis* positive) pure culture samples at the same concentration level have generated signal reduction of 25.6%, 44.9% and 39.6% respectively. The signal yields from LVS samples are much higher than those from WBTI samples at the same concentration, therefore it can be concluded the *F. tularensis* antibody biosensor has a good sensitivity and specificity in detection of *F. tularensis* positive pure culture samples.

Similar results were also obtained from *Brucella* DNA probe biosensor and *H. Somni* DNA probe biosensor assays. Assays with three main *Brucella* strain types: *B. Suis, B. Abortus,* and *B. Melitensis* have yielded an average 12.2% ± 2.4% signal reduction for 100 cfu/ml pure culture samples, and 19.15% ± 0.68% signal reduction for the 10^4 cfu/ml pure culture samples; while three negative control strains (*P. aeruginosa, E. Coli* and *Salmonella*) at concentration of 10^6 cfu/ml yielded an average -2.1% ± 1.6% signal reduction, which is even smaller than the responses from *Brucella* strain samples at 100 cfu/ml concentration. Therefore, the *Brucella* DNA biosensor is very specific and sensitive to the *Brucella* strain types tested. Assays with the *H. Somni* DNA probe biosensor have suggested a good differentiation between *H. Somni* strain samples and culture samples as well. *H. Somni* pure culture samples at concentration of 100 cfu/ml, 10^4 cfu/ml and 10^6 cfu/ml have generated a signal reduction of 0.92%, 7.14% and 14.5% respectively, while the control strain (*E. Coli*) samples tested at the same time yet at high concentration of 10^6 cfu/ml always returned a negative reading, with an average -0.39% ± 0.18%

signal reduction. The strain concentration threshold for an effective *H. Somni* DNA biosensor detection is at the concentration level of 10^4 cfu/ml, where the biosensor has clearly differentiated signals generated from *H. Somni* strains and control strains.

The production cost of this optical fiber biosensor is low compared to its competitors, such as real-time PCR or quantitative PCR systems, which could cost more than $25,000 for the system and $100 for each individual test. This biosensor design takes full advantage of mature fiber fabrication techniques and biochemistry interactions, where the ingredient materials are widely and commercially available, and compatible with mass production. The total cost for the biosensor system is estimated to be in the range of a few thousand dollars, while the biosensing kit containing the fresh biosensor would not exceed a few tens of dollars, therefore it would be suitable for performing vast sample screening tasks and providing rapid diagnostic information for medical professionals of small community clinics. More importantly, the optical fiber biosensor system is easy to operate and can be fully automated, meaning the staff training and maintenance costs can be minimized.

Furthermore, the biosensor platform is feasible for easy expansion to detection of various bacteria or viruses. The crosslinking chemistry used for the biosensor assembly is compatible with conjugating most proteins, biotinylated DNA probes, and enzymes to the surface film of the fiber, therefore providing flexible and versatile options for the receptor of the biosensor, which makes the biosensor platform expandable and capable of the detection and diagnosis of a vast range of bacteria and viruses, far beyond those examined in this study. This can help lower the R&D expenses for further development and expansion of this biosensor system, and offer a long product line in the commercial version, which could also be easily customized to meet the client's needs of the sensor system.

1.4 Outline

This dissertation will present detailed discussion of the theories and principles of the proposed biosensor platform in Chapter 2, describe the experimental details in Chapter 3, and discuss versatile applications in determination and differentiation of several bacteria strains in Chapters 4 and 5. Chapter 6 will summarize the results obtained through the development and studies of the proposed biosensor system, and discuss future research directions and possible improvement of the system.

More specifically, section 2.1 will focus on the sensing theories of the LPG fiber sensor, which utilize mode-coupling between the propagating core mode and the cladding mode to advance in both sensitivity and stability of the signal. Section 2.2 will focus on the ISAM organic thin film technique, which dramatically increases the sensitivity of the system, and connects the bio-receptors to the fiber sensor surface, making the biosensor compatible with expansion to other targets. Section 2.3 will explore the cross-linking chemistry, and explains how various receptors can be easily immobilized onto the ISAM film via amide bond, and still maintaining their functionality and activity.

Section 3.1 will discuss the biochemistry interactions between receptors and their specific analyte, and section 3.2 will introduce the full assembly procedures of the biosensor system and how the system operates.

Chapter 4 will focus on the initial exploration of the biosensor system's capability with the detection of MRSA, with monoclonal antibodies (section 4.2) or biotinylated DNA probes (section 4.3) as receptor. Results will be presented on pure culture samples with a variety of MRSA and non-MRSA strains, swabs taken from human ears, noses, and skin, and swabs from

the tissues of infected mice. Issues related to measurements using clinical swab samples from human patient wounds will also be discussed.

Chapter 5 will explore expansion of the biosensor platform to the detection and differentiation of other bacteria types, such as *F. tularensis, Brucella,* and *H. Somni*.

Chapter 6 will include conclusions and future work to the biosensor project. Section 6.1 summarizes all the results obtained from the previous studies, and section 6.2 will propose possible topics worth exploring in the future development of the biosensor system and interesting ideas that can be tested.

Chapter 2 Long-Period-Gratings (LPG) based Biosensor

2.1 Long Period Gratings

2.1.1 Single-mode Fiber

An optical fiber is a waveguide that confines the propagation direction of the light waves along the axis of the fiber, and only allows the light modes that fall within the cutoff frequency.

Due to versatile application purposes, there are a range of fiber designs, such as step-index fiber, gradient-index fiber, tapered fiber, photonics crystal fibers (PCFs) and so on. A most simple and commonly used fiber is the silica step-index fiber, which is fabricated with cylindrical symmetry and constitutes three main components: the fiber core, which guides the majority of the power of the light and has a higher refractive index (R.I.); and the fiber cladding, which surrounds the core and has a lower refractive index to confine the propagating mode to the core through total internal reflection; the jacket, which is the outmost layer of the fiber, and adsorb the leaked optical power from the core or cladding.

Figure 2-1 shows the typical structure of the step-index fiber.

(a) (b)

Figure 2-1: a) A typical structure of a step-index optical fiber: (A) core of the fiber, (B) cladding region, and (C) the buffer jacket protecting the fiber. b) Cross sectional view of a step-index single-mode fiber (SMF).

The diameter and R.I. aperture of the fiber will determine the boundary conditions for Maxwell's equations of the propagation light modes, where the electromagnetic wave modes can be obtained from possible solutions of Maxwell's equations. A single-mode fiber (SMF) is an optical fiber whose diameter is normally less than 10 μm [43], and the core-cladding refractive indices difference is in order of 0.01~0.1, and less than that of the multimode fiber. The frequency cutoff of the single-mode fiber imposes the existence of only one transverse mode ($LP_{0,1}$ mode) available in the fiber core.

Theoretically, for a step index SMF, the fiber parameters have to satisfy the normalized frequency (V-number) criterion. V-number is defined by:

$$V = \frac{2\pi a}{\lambda}\sqrt{{n_1}^2 - {n_2}^2} < 2.405 \qquad (2\text{-}1)$$

where a is the radius of the core, λ is the wavelength of the propagating wave in vacuum, and n_1 and n_2 represent the refractive index in the core and the cladding, respectively. And $V = 2.4048$ is the cutoff frequency for the next core mode, and therefore this number sets the upper boundary for the V-number of SMF.

As shown in Figure 2-2, the light wave propagates parallel to the length of the optical fiber. Multimode-fiber (MMF) has a larger core radius and can accommodate more light modes; by comparison, SMF can only host one single $LP_{0,1}$ mode (also known as fundamental mode) in its core.

[43] ARC Electronics (2007-10-01). "Fiber Optic Cable Tutorial"

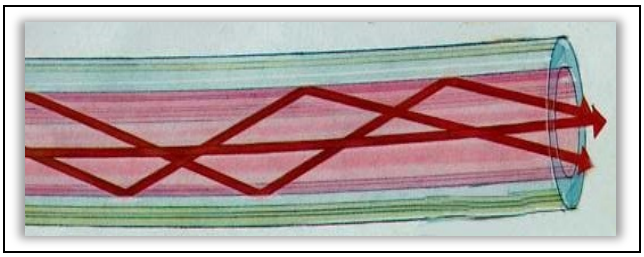

(a)

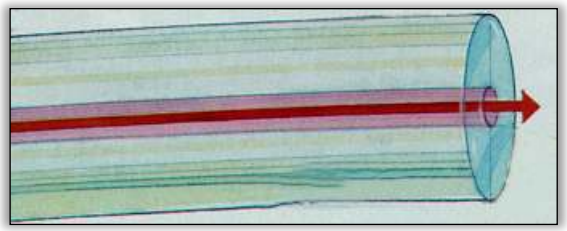

(b)

Figure 2-2 : a) Multimode fiber is able to support multiple modes within its core, and these modes will spread out and lose its shape, and will be received separately at the receiving point. b) Single-mode fiber. Source:[44].

2.1.2 Cladding Mode

For a single-mode fiber, only the fundamental guided mode is permitted for long distance propagation, which is the LP_{01} mode, where $l = 0$ and $m = 1$ represent the first solution to the Maxwell's equations under the step-index SMF symmetry. However, the RI aperture between the cladding and jacket/ambient-media of the optical fiber also forms a waveguide, which could accommodate propagation modes known as cladding modes. Normally, there could be up to 10^4 cladding modes guided in the cladding with protection coatings stripped off.[45] These modes are originated from the fraction of power when the injected laser beam entered the single-mode fiber, and from the dispersed modes from the core.

The cladding modes are generally short-lived, due to leakage into the coating buffer or adsorption by the fiber jacket, which will strongly attenuate the power of the cladding modes and eliminate its propagation after a few meters of entering the fiber.

For most applications, the cladding modes are not desired, since the photo-detector could not distinguish the core modes from cladding modes, therefore the interference between the fundamental mode which carries the useful information and the cladding modes, which generally

[44] http://www.arcelect.com/fibercable.htm
[45] "Long-period grating theory", http://gratings.fo.gpi.ru/index.php?page=11#ref

become background noise, can introduce additional signal dispersion or distortion. Nevertheless, the cladding modes rarely affect the propagation of the fundamental mode in the core, since they have different propagation constants, often denoted as symbol β. The propagation constant of a mode contains the phase and propagation direction information of the electromagnetic wave that travels with such mode. According to the fiber-mode theory,[46,47] only the modes which satisfy certain phase matching conditions will exhibit coupling capacities with each other.

Propagation constant is defined as:

$$\beta = \frac{2\pi}{\lambda} n_{eff} \tag{2-2}$$

where n_{eff} is the effective refractive index of the waveguide the light is propagating in and λ is the vacuum wavelength of the mode. The effective refractive index n_{eff} is determined by the R.I. aperture and geometry parameters of the waveguide the wavelength of the transmitting light ray, and the considered modes.

2.1.3 Mode Coupling and Phase-matching in a Single Mode Fiber

The radius of the cladding of a typical SMF is much larger than that of its core, usually 100 microns or more in diameter, which enables the cladding to host high-order modes (as the number of modes is proportional to the square of the cutoff V-number, and from equation (2-1), V is determined by radius a, therefore large a implies a square-more number of modes).

Though optical fibers are designed to avoid the interaction between core modes and cladding modes, certain perturbation (e.g., external binding of the fiber, the impurity in the fiber core, or geometry imperfection of the fiber) along the light path of the core mode can disperse a fraction of power into the cladding.

[46] T. Tamir, ed., "Integrated Optics", Vol.7 of Topics in Applied Physics, Springer-Verlag, 1975.
[47] T. Erdogan, "Fiber grating spectra", *J. Lightwave Technol.,* 15, pp. 1277-1294, 1997.

More specifically, the coupled-mode theory predicts that when this perturbation is met at a periodic form, the core mode and one cladding mode can phase-match and yield a resonant coupling. In addition, the mode-coupling theory restricts that the cladding mode is possible to phase-match the core mode only when the phase-matching condition is satisfied:

$$\beta_{core} - \beta_{clad} = k\frac{2\pi}{\Lambda} \tag{2-3}$$

Where β_{core} and β_{clad} are propagation constants of the core mode and cladding mode, respectively, Λ is the grating period in the fiber core that perturbs the core mode, and k represents the diffraction order of the light wave in the grating. We can conveniently set k = 1, since the first-order diffraction takes the main role in the grating calculations. Figure 2-3 shows one scheme of such mode-coupling gratings.

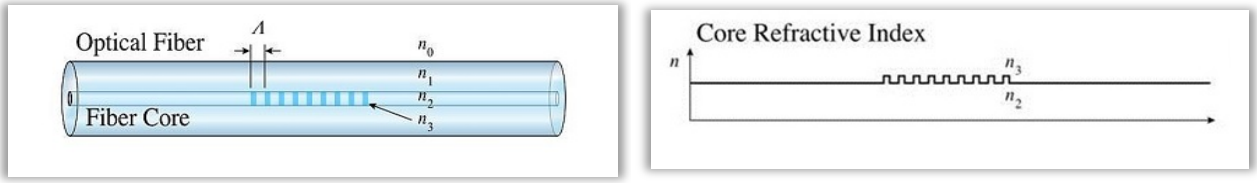

(a) (b)

Figure 2-3: a) a periodic perturbation grating in the core of the fiber, with the grating period Λ, with the original core refractive index as n_2 and the grating region refractive index n_3. The cladding refractive index is n_1 and the surrounding medium's refractive index is n_0. b) a rectangular profile of the refractive index change in the core, where along every Λ in length, the core refractive index n_2 will step-jump to n_3 and back to n_2, periodically. Source: [48].

Based on the definition of the propagation constant in equation (2-2), we can simplify equation (2-3) to the following form:

$$(n_{eff}^{\ core} - n_{eff}^{\ clad})\Lambda = \lambda \tag{2-4}$$

[48] http://en.wikipedia.org/wiki/Fiber_Bragg_grating

where n_{eff}^{core} and n_{eff}^{clad} are effective refractive indices of the core and the cladding modes, Λ represents the grating period, λ is the wavelength where the resonant coupling occurs. Due to the materials dispersion, the effective refractive indices of the core and the cladding modes are wavelength dependent.[49,50,51] As a consequence, equation (2-4) predicts that with a chosen grating period, it is possible to perform selective mode coupling at certain wavelengths.

According to the length of the grating period, there are two general grating types. One is the fiber Bragg grating (*FBG*),[52,53] whose typical grating period is around a few hundred nanometers and in the order of the length of the wavelength, and it couples wave modes reflected at each periodic perturbations to the corresponding cladding mode. Therefore, a reflected signal at the resonant wavelength can be observed from an FBG fiber at the source end.

The other type of fiber grating is the long-period-grating (*LPG*), whose grating period is on the order of hundreds of microns, which is larger than the wavelength of most SMF allowed modes. Compared to an FBG, an LPG has a much larger gratings period which significantly reduce the fabrication cost and difficulties. Resonant coupling between core and the cladding modes will transfer a fraction of the optical power at the resonant wavelength to the cladding, which will then be lost due to adsorption and dispersion. Therefore, the transmitted light at the resonant wavelength of an LPG will lose most of its power when hitting the fiber grating segment. As the LPG will couple the modes travelling in the same direction, an LPG fiber

---

[49] Patrick H J, Kersey A D and Bucholtz F, "Analysis of the response of long period fibre gratings to external index of refraction", *J. Lightwave Technol*. 16 1606–42, (1998).

[50] S. A. Vasiliev, E. M. Dianov, A. S. Kurkov, O. I. Medvedkov, V. N. Protopopov, "Photoinduced in-fibre refractive-index gratings for core-cladding mode coupling", *Quantum Electron*., 27, pp. 146-149, (1997).

[51] T. Erdogan, "Cladding-mode resonances in short- and long-period fiber grating filters", *J. Opt. Soc. Am. A*, 14, pp. 1760–1773, (1997).

[52] S.W. James, R.P. Tatam, "Optical fibre long-period grating sensors: characteristics and application", *Meas. Sci. Technol.*, 14, R49–R61 (2003).

[53] O.V. Ivanov, S.A. Nikitov, Yu.V. Gulyaev, "Cladding modes of optical fibers: properties and applications", *Physics-Uspekhi*, 49, 175-202 (2006).

experiment measures the transmission spectrum, and one or more dips can be observed in the spectrum at the resonant wavelength where a phase-matching occurs.

Based on the materials of the optical fiber and the purpose of the LPG, different types of grating structures and grating approaches have been developed. Some of the applications exert external force or pressure on a portion of the originally uniform optical fiber to create periodic refractive index variations, and in this case the LPG structure is reversible, and the grating period can be modified or adjusted on the same fiber. Other applications will introduce tilted grating fringes, where the grating section will have an angle with the cross-section of the fiber core. In our biosensor applications, we simply adopt the uniformly distributed gratings design, in which the distance between each perturbation grating is a constant.

2.1.4 Phase Matching Curve

In this section, we examine more closely the principle of the LPG fiber as a sensor, and the phase matching curve (PMC) will be presented to illuminate why and how an LPG fiber react to the change of the corresponding parameters, and what are anticipated to emerge on the transmission spectrum.

Studies on the mode-coupling theory[54,55] introduce the detuning parameter δ to define the coupling efficiency between two modes,

$$\delta = \frac{1}{2}(\beta_{core} - \beta_{clad} - \frac{2\pi}{\Lambda_{LPG}}) = \pi(n_{eff}^{core} - n_{eff}^{clad})(\frac{1}{\lambda} - \frac{1}{\lambda_R}) \quad (2\text{-}5a)$$

with $$\lambda_R = (n_{eff\_core} - n_{eff\_clad}^{(i)})\Lambda_{LPG} \quad (2\text{-}5b)$$

[54] Turan Erdogan, "Fiber Grating Spectra", *Journal of Lightwave Technology,* 15, 1277-1294, (1997).
[55] Vengsarkar A M, Lemaire P J, Judkins J B, Bhatia V,Erdogan T and Sipe J E, "Long-period fibre gratings as band rejection filters", *J. Lightwave Technol.,* 14 58–64, (1996)

In equation (2-5), n_{eff_core} and $n_{eff\_clad}^{(i)}$ are effective refractive indices of the core and the *i*th cladding mode respectively, and these parameters are determined by the engaged modes, geometric symmetry and fabrication parameters of the LPG fiber. λ_R is the resonant coupling wavelength where the core mode phase matches a cladding mode and creates a resonance takes place under the period Λ_{LPG}.

In a weakly-guided LPG, in which the R.I. aperture of the core and cladding by a small amount, an approximate solution of the coupled mode equations can be made and yields the normalized power conversion rate $R(z)$ as:

$$R(z) = \frac{\eta^2 \sin^2(z\sqrt{\eta^2 + \delta^2})}{\eta^2 + \delta^2} \tag{2-6}$$

where the fiber axis is along z-axis and the beginning of LPG is set as $z = 0$. η is the coupling coefficient, which under the context of approximation is a constant and can be determined by the overlap integral between the electric field of the core mode and the cladding mode, the index difference in the grating and the resonant wavelength. $R(z)$ defines the fraction of power transferred between two modes, and the larger $R(z)$ becomes, the more power is leaked into the cladding mode. Figure 2-4 shows the relation between the detuning parameter δ and power conversion rate $R(z)$ based on equation (2-6) with chosen parameters.

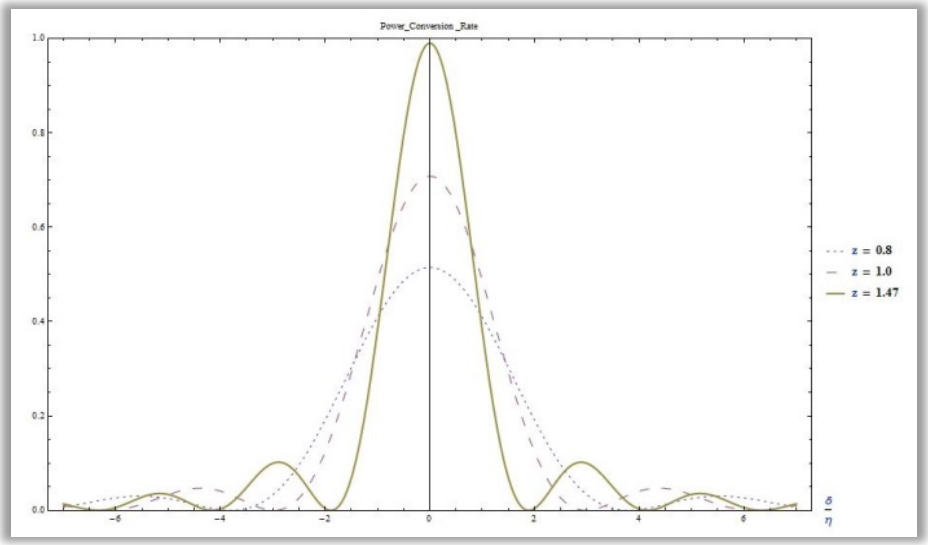

(a)

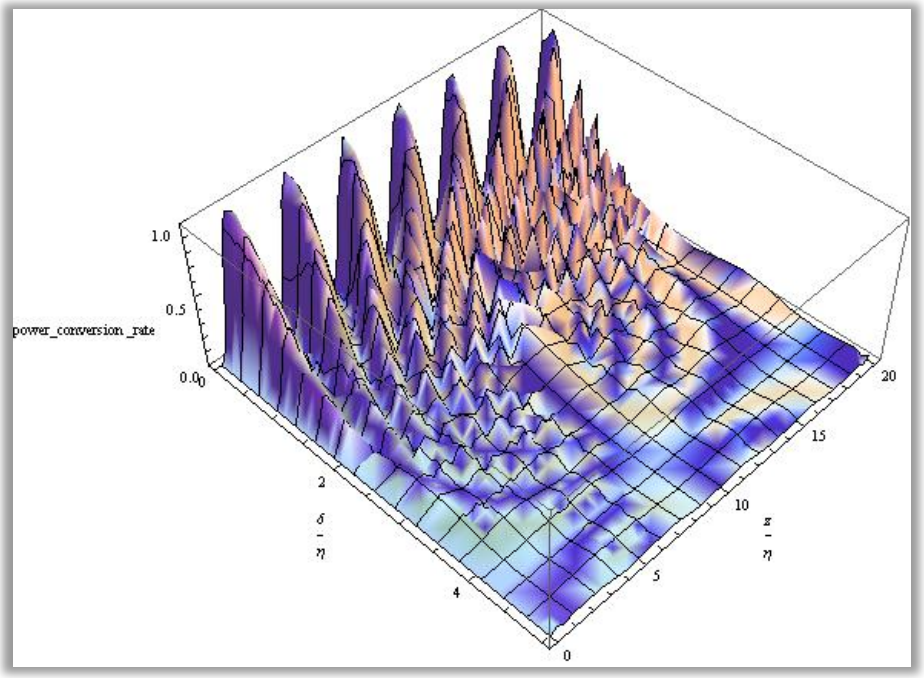

(b)

Figure 2-4: Power conversion rate $R(z)$. a) at z = 1.47, and δ/η = 0, 99% of the core mode power at the resonant wavelength has been transferred to the cladding mode. While at z = 0.8, at most only 50% of the core mode power is lost. b) the power conversion along the propagation direction (z-axis).

Figure 2-4(a) shows clearly that at $\delta = 0$, the resonance is at its maximum degree. The guided wave (the core mode) losses the most power at such wavelength that is corresponding to

the dip in the transmission spectra. When δ moves away from zero, detuning starts to dominate the mode-coupling and diminish the power conversion between the core mode and the cladding mode.

Equation (2-5b) reflects the phase matching condition between the core and the coupled cladding mode. Since both effective refractive indices presented in the equation are wavelength-dependent only, such equation can be transformed to a function:

$$\Lambda_{LPG}(\lambda) = \frac{\lambda}{n_{eff\_core}(\lambda) - n_{eff\_clad}^{(i)}(\lambda)} \tag{2-7}$$

This equation predicts a phase-matching-curve (PMC), which provides a more intuitive picture of the modes-coupling within the LPG fiber. Calculation methods[56,57] can be used to evaluate $n_{eff\_core}(\lambda)$ and $n_{eff\_clad}^{(i)}(\lambda)$ based on Sellmeier's equation and the weakly-guided field approximation. Figure 2-5 from Dr. Zhiyong Wang's dissertation[58] shows simulation of the PMC in an LPG fiber with core radius *a*=3.2 μm, fiber cladding radius *b*=59.2 μm, and refractive index of core and cladding of 1.455 and 1.45, respectively.

[56] A. Yariv, Optical Electronics, 3rd ed. New York: Holt, Reinhart and Winston, 1985, pp. 57–77.
[57] K.S. Kim and M.E. Lines, "Temperature dependence of chromatic dispersion in dispersion-shifted fibers: Experiment and analysis," *J.Appl. Phys.*, vol. 73, pp. 2069–2074, (1993).
[58] Zhiyong Wang, "Ionic Self-Assembled Multilayers Adsorbed on Long Period Fiber Gratings for Use as Biosensors", Ph.D Dissertation, ETD-12082005-094018, (Virginia Tech, 2005)

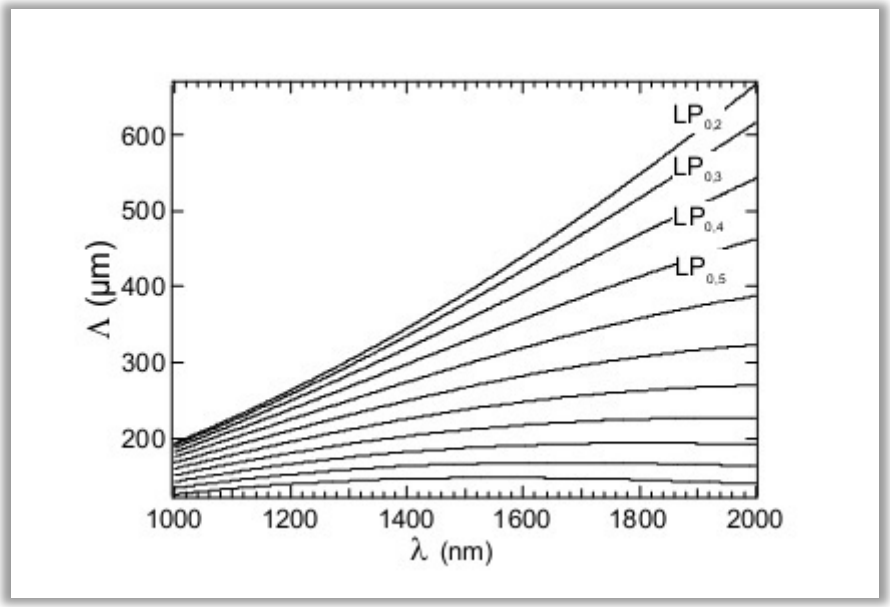

Figure 2-5: Phase matching curves of the simulated LPG fiber. Each curve, from top to bottom, refers to the phase matching conditions between the fundamental LP_{01} mode and the coupled cladding LP_{0m} mode (m from 2 to 12 in this figure). Source:[58].

Figure 2-5 reveals a very intriguing feature of the LPG fiber under selected parameters. The phase matching function $\Lambda_{LPG}(\lambda)$ is monotonically increasing for low-order cladding mode coupling (say, LP_{02} - LP_{04}), though for higher-order modes, the PMC becomes more concave and shows a parabola-like trajectory. Mathematically, $d\Lambda_{LPG}/d\lambda$ decreases by increasing the value of mode number m (corresponding to the LP_{0m} cladding mode). Moreover, some studies[59] have shown that with a high mode number (for example, m=25), the PMC can become monotonically decreasing.

The fiber cladding allows the existence of a large number of cladding modes, which in turn renders multiple resonances, as each intersection between a given grating period Λ_{LPG} and the PMCs denotes to a phase-matching coupling. In the transmission spectrum this phenomena will translate into multiple dips at each resonant wavelength, as shown in Figure 2-6. Nevertheless,

[59] S.W. James, R.P. Tatam, "Optical fiber long-period grating sensors: characteristics and application," *Meas. Sci. Technol.* 14 R49–R61, (2003).

the coupling coefficient may vary for each mode coupling under constant gratings period Λ_{LPG}, which is then reflected in discrepant power loss amount at each resonant wavelength.

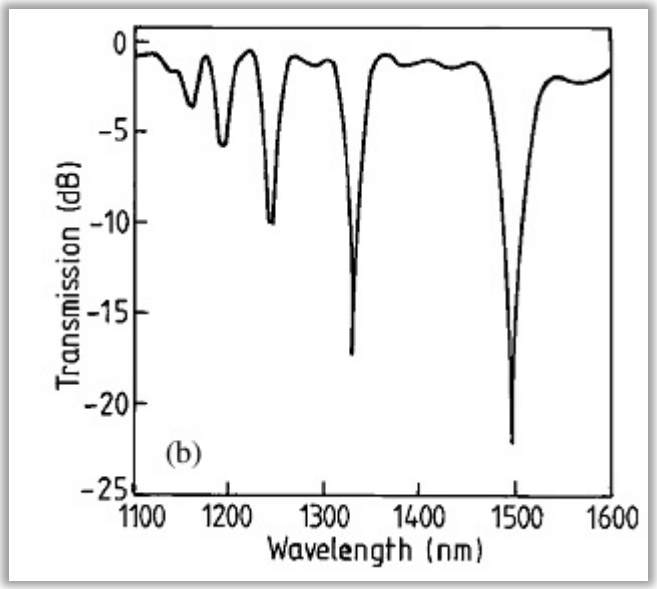

Figure 2-6: Transmission spectrum of a typical LPG. Multiple dips can be observed in this spectrum, indicating the resonant coupling between the core mode and four separate cladding modes within the range of 1100 nm to 1600 nm. Source: [59].

In this dissertation, the coupled modes that display parabola-like PMCs are the central focus. In such cases, resonant couplings at two separate wavelengths can appear to an LPG fiber with fixed grating period. Moreover, a parabola-like PMC will exhibit an extreme point on its trajectory, where $d\Lambda_{LPG}/d\lambda = 0$. Around such point, even a slight detuning will wipe away the majority power loss obtainable at the resonant wavelength, which offers an advanced sensitivity when operating experiments at such coupling modules.

2.1.5 Turnaround Point in an LPG Fiber

2.1.5.1 Principal of the Turnaround Point

Unlike the monotonic PMC of low-order coupling modes and higher-order coupling modes, the parabola-like PMC always has an extreme point on its trajectory. Such a point is referred to as a turnaround point (TAP). The shape of the PMC is critical in determining how the transmission spectrum shifts due to the shifting of the modification of the PMC. Based on simulations run by Dr. Zhiyong Wang[58], figure 2-7 can be drawn and it depicts the how the $LP_{0,4}$ coupling mode and $LP_{0,12}$ coupling mode will respond to the increment of the cladding radius, and what the observer would expect from the transmission spectrum.

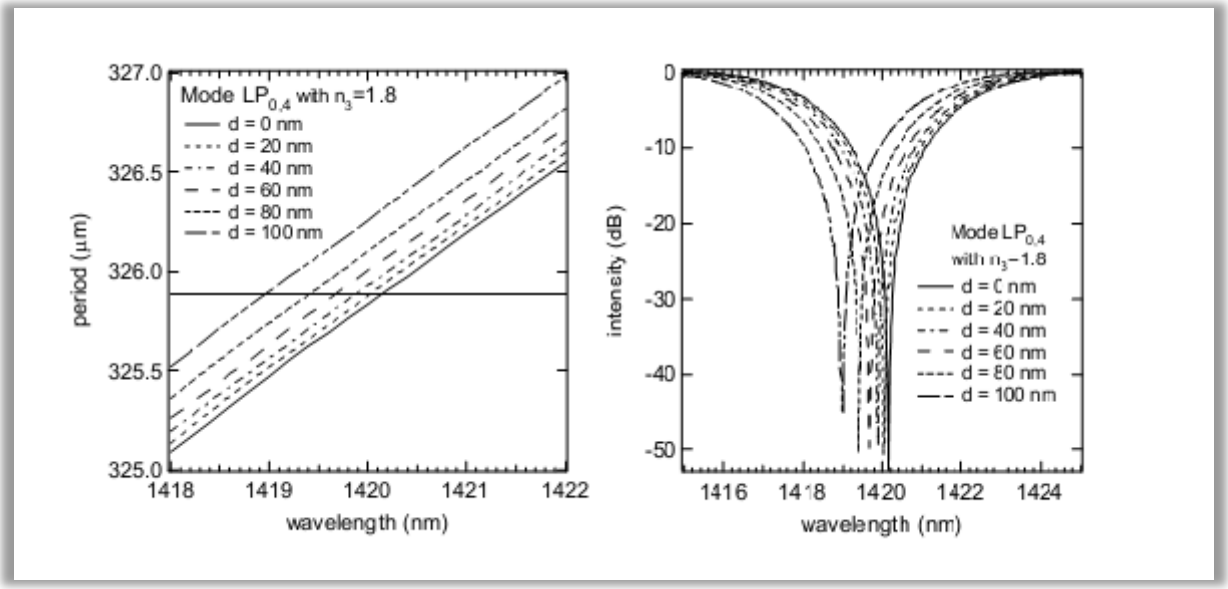

(a)

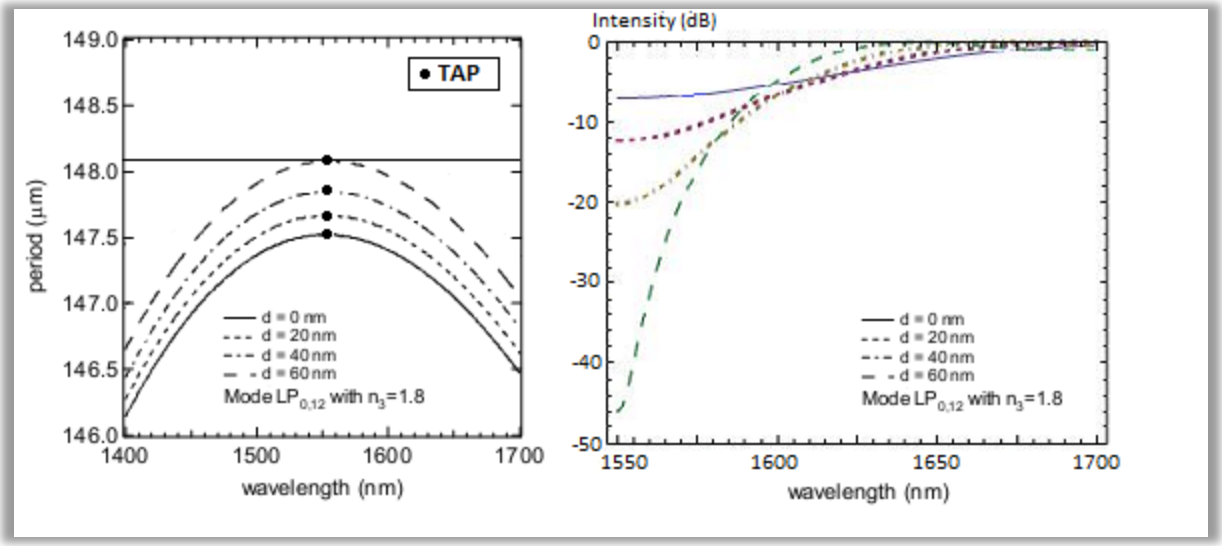

(b)

Figure 2-7: Coupling to different modes can deliver distinct behavior on the increment of the cladding radius. The horizon line indicates the grating period in the simulated LPG fiber, *d* refers to the additional thickness added to the cladding. n_3=1.8 is the refractive index of the material added to the cladding. The PMC shifts upwards with thicker materials over the cladding. a) Monotonic PMC of the $LP_{0,4}$ coupling mode results in a resonant wavelength shifting in the transmission spectrum. b) A TPA PMC of the $LP_{0,12}$ coupling mode delivers a power loss peak shifting along a single wavelength at 1550 nm. Source:[58].

Figure 2-7 illustrates a picture of the LPG resonant behavior, that by adding or material from the surface of the cladding, the PMC of the coupled modes will shift upwards or downwards correspondingly.

For a monotonic increasing PMC, the curve shifts upwards or downwards roughly proportionally to the thickness of the ambient material. However, the inscribed LPG grating period Λ_{LPG} is at a fixed value and will not be altered due to the deposition of materials, which results in the shifting of the resonant wavelength to the left with thicker material layer, and to the right with a thinner ambient material layer.

Whereas, for a parabola-like PMC, with deposition of more materials, the curve moves up and the TAP gets closer to the grating period. The detuning vanishes rapidly and the resonant

coupling is forming, transferring the power of the core mode at the coupling wavelength to the coupled cladding mode. The magnitude of the transmitted power is varied but the resonant wavelength remains fixed. In other words, a change of thickness only affects the transmitted power at a fixed wavelength rather than appearing as a shift in resonant wavelength.

Since the TAP PMC involves the resonant coupling of the core mode with high-order cladding mode, the grating period of the TAP LPG is generally smaller than the conventional LPG with the monotonic PMC. There are several advantages for adopting the TAP LPG: 1) unlike a conventional LPG in which the power loss peak shifts in wavelength, a TAP LPG's power loss peak only shifts up or down at the fixed wavelength, therefore, a broadband light source and an optical spectrum analyzer are no longer needed for TAP LPG experiments and this can help reduce the cost for setting up the experiment system as well as expanding such LPG's potential applications in the field. 2) In the PMC, the region around the TAP has a very small $d\Lambda_{LPG}/d\lambda$ value, therefore when the TAP of PMC is close to the grating period even a slight shift of the PMC towards the grating period can amplify the resonant coupling significantly, or *vice versa*. Such feature suggests an extremely high sensitivity when the LPG grating period is close to that of the TAP. Carefully choosing the fiber inscription parameters will render an ultra-sensitive TAP LPG sensor. 3) Resonant coupling occurs instantly when phase-matching condition is met, and once such coupling is formed, the power-loss will be reflected to the transmission spectrum almost simultaneously. The quick response of the TAP LPG fiber is hence able to perform real-time monitoring and sensing tasks with constantly polling the transmitted power at the resonant wavelength.

2.1.5.2 Sensitivity of the TAP

In order to study the sensitivity relevance of the TAP LPG, it is helpful to define the mode dispersion function[60] as:

$$\Phi(\lambda) = \frac{2\pi(n_{core} - n_{clad})}{\lambda} \tag{2-8}$$

Clearly, $\Phi(\lambda_{LPG}) = \frac{2\pi}{\Lambda_{LPG}}$ satisfies the phase matching condition and therefore mode dispersion reaches its maximum value. Consequently, the mode dispersion measures how strong the coupling is formed at the specific coupling module. With Taylor expansion at the vicinity of λ_{LPG}, the dispersion function can be rewritten as:

$$\Phi(\lambda) - \Phi(\lambda_{LPG}) = a_1(\lambda - \lambda_{LPG}) + a_2(\lambda - \lambda_{LPG})^2 + \mathrm{L} \tag{2-9}$$

In a conventional LPG fiber, the first term always dominates the equation, reflecting the monotonic property of the PMC under coupling module. However, as has been shown in preceding discussions, at a slightly higher mode coupling models, $a_1 = 0$ and hence the quadratic term a_2 emerges and dominates the equation (2-9), making the PMC to be parabolic-like. In depth study has proven that in such cases the relationship between $\delta\lambda$ and $\delta\Lambda_{LPG}$ is determined by:

$$\delta\lambda = \pm(-\frac{2\pi}{a_2\Lambda_{LPG}^2}\delta\Lambda_{LPG})^{1/2} \tag{2-10}$$

As stated in the preceding section, the LPG fiber has a fixed period of grating once the fabrication is completed, which means Λ_{LPG} remains a constant after that, therefore in the theoretical analysis, only $n_{eff\_clad}(\lambda)$ can be changed with the wavelength. However, the

[60] Victor Grubsky and Jack Feinberg, *"*Long-period fiber gratings with variable coupling for real-time sensing applications*", OPTICS LETTERS*, Vol.25 203-205, (2000).

expansion of the refractive index of the cladding over the vicinity of λ_{LPG} is complex and the physics picture is too vague to clearly reflect the resonant coupling in LPG. Accordingly, a series of similarly crafted TAP LPGs with diversified grating periods will be studied to show the sensitivity of such fibers.

The positive and negative signs in the equation (2-10) suggest the parabolic-like shape of the PMC at this mode-coupling level. The negative sign inside the square root indicates that a_2 has a negative value, which validates the concave property of the TAP PMCs. Replacing $\lambda - \lambda_{LPG} = \delta\lambda$ in equation (2-9) and using equation (2-10), it can be found that the dispersion function is proportional to the small change of the grating period $\delta\Lambda_{LPG}$:

$$\Phi(\lambda) - \Phi(\lambda_{LPG}) \propto \frac{2\pi}{\Lambda_{LPG}^2}\delta\Lambda_{LPG} \tag{2-11}$$

Therefore the resonant strength can be expressed with the dispersion function (2-11), and such strength at every wavelength depends primarily on the distance between the corresponding points on the PMC and the grating period. The closer such points are to the grating period, the stronger the resonant coupling takes place at respective wavelengths.

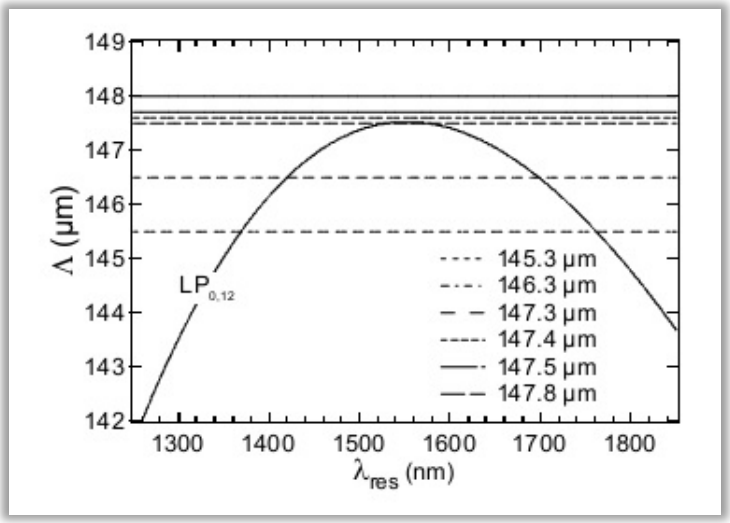

(a)

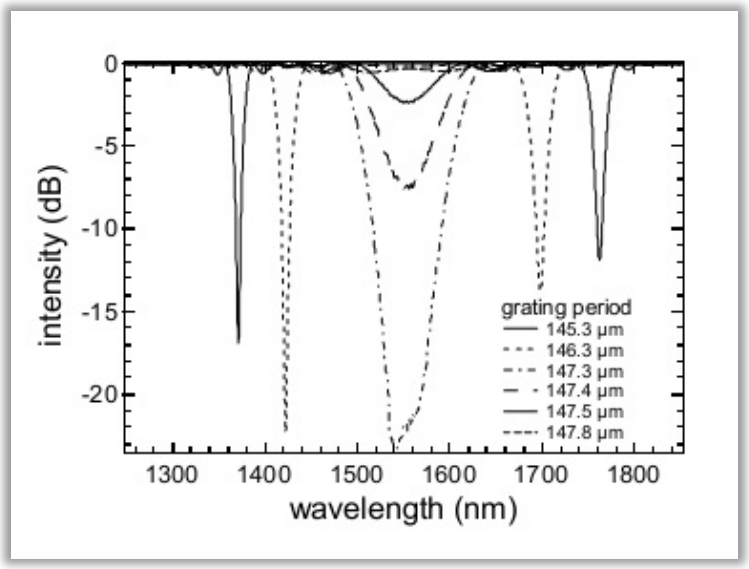

(b)

Figure 2-8: PMC location to the grating periods reveals the corresponding transmission spectrum. a) Grating periods with various distances to the TAP of the LPG. Horizontal line indicates the grating periods, from bottom to top are 145.3μm, 146.3μm, 147.3μm, 147.4μm, 147.5μm and 147.8μm, respectively. b) The corresponding transmission spectrum based on the PMC. Source:[58].

Figure 2-8 shows Dr. Zhiyong Wang's simulation work[58] over a series of TAP LPGs whose gratings period varies from 145.3 μm to 147.8 μm, with the coupling module as core mode coupled to the $LP_{0,12}$ cladding mode. Notably, with the increment of the grating period over 0.2 μm from 147.3 μm to 147.5 μm, the attenuation at the resonant wavelength 1550 nm decreases from -25 dB to -2 dB, referring to a 99.5% change of the transmitted power with a less than 0.14% period variation when close to TAP. The figure also reflects the fact that with shorter grating periods, 146.3 μm for instance, the power attenuation at 1550 nm disappears entirely under total detuning. Also, dual intersections can be seen for the grating period of 146.3 μm on the PMC, and the transmission spectrum indicates two resonant peaks at wavelengths of around 1420 nm and 1700 nm, respectively.

Similarly, if evaluating the dispersion function at the perspective of the PMC shifting due to the change of the cladding radius and/or its refractive index, we can expect same exceptional sensitivity.

We have conducted experiments to examine the mode-coupling theory discussed above, and the results confirm that the sensitivity increases as additional materials are deposited to the cladding and push the PMC close to the TAP.

Figure 2-9 displays the transmitted power loss of a TAP LPG evolving with the deposition of the adsorbed materials over the cladding. In this experiment, the TAP LPG is tuned to make sure the engaged mode-coupling PMC lies slightly before hitting the turn-around-point. An adsorbed material (ISAM films, as described below) with controllable thickness were added sequentially to the LPG fiber, which increased the radius of the cladding gradually. Measurement of the transmitted optical power was recorded at the resonant wavelength of the TAP LPG.

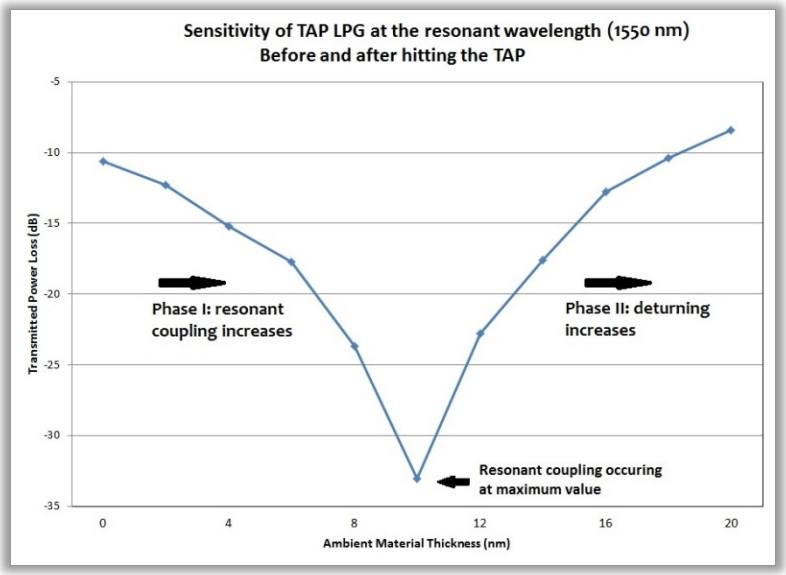

(A)

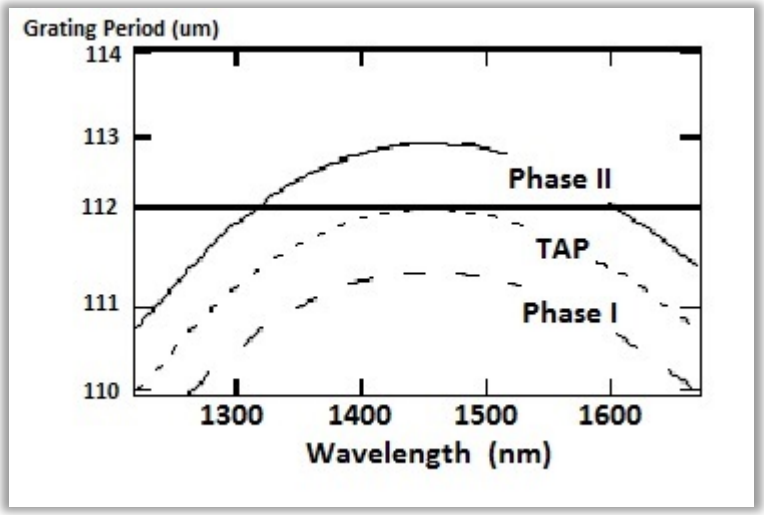

(B)

Figure 2-9: (A) a TAP LPG transmitted power loss evolution with more adsorbed materials deposited on the cladding of the fiber. (B) Phase I, TAP and phase II are displayed under the PMC view. The fiber is tuned slightly before hitting TAP. In phase I, with a few nanometers ambient materials added to the cladding, the transmitted power loss increases exponentially. Then at one point between 8 *nm* and 12 *nm*, the phase-matching-condition is met, and then in phase II, detuning takes place and transmitted power loss soon recovered.

Figure 2-9 exhibits two distinct phases with the increment of the thickness of the cladding. In the Phase-I, as the PMC shift upward with more material added to the fiber, the resonant coupling gains strength and the transmitted optical power at the resonant wavelength becomes more strongly attenuated. At the TAP, the phase-matching condition is met and the attenuation reaches its maximum. The amount of the power losses at this point is determined by the coupling coefficient. As additional material is deposited on the fiber, the TAP of the PMC crosses the grating period horizontal line and detuning increases in Phase-II. The resonant then occurs at two separate wavelengths that shift further apart as additional material is deposited on the cladding.

Considering Phase-I and Phase-II separately, the sensitivity of the TAP LPG at each phase can be analyzed in each category.

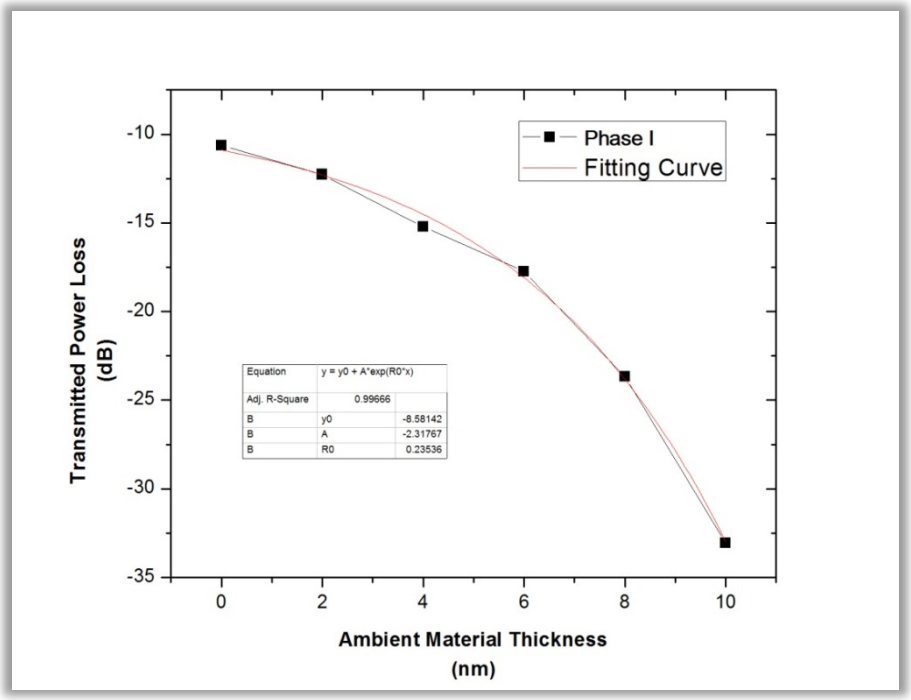

(a)

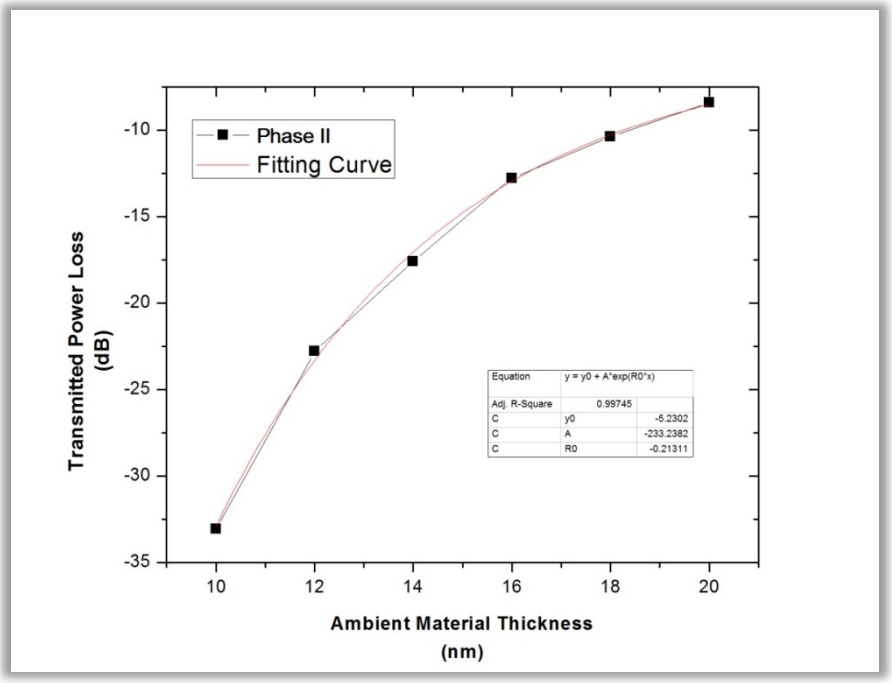

(b)

Figure 2-10: Curve trajectory fitting and comparison in Phase I and Phase II. a) in Phase-I before hitting the TAP, the transmitted light losses power exponentially when the thickness of cladding rises. b) in Phase-II, after hitting the TAP, the detuning occurs, and the mode-coupling vanishes as the power losses recovers from the dip.

Figure 2-10 shows the numerical fitting curve to the change of the transmitted power loss in phase I and phases II respectively. The base function used for fitting analysis is:

$$y = y_0 + A\exp(R_0 x) \tag{2-12}$$

Regardless of the constants y_0 and A that shift and relocate the fitting curve, the constant R_0 indicates the curvature of the fitting curve and reveal the sensitivity of the LPG fiber. The R^2 value shows the goodness of the fit. R^2 value of phase I fitting curve is 0.9967, and R^2 value of phase II fitting curve is 0.9975, both indicate a good fitting to the data. In phase I, the curvature constant $R_0 = 0.235$, while in phase II, the curvature constant $R_0 = 0.213$, these two values are close, and it reveals that the sensitivity of TAP LPG is similar before and after hitting the TAP.

Therefore, the transmitted power loss of a TAP LPG is exponentially increasing or decreasing at a constant increment rate of the thickness of the ambient material layer, depending on which sides of the TAP the LPG is operated.

2.1.5.3 Measurement Techniques

The previous section concludes that the sensitivity of a TAP LPG is similar in phase I (before TAP is reached by the grating period) and in phase II (after the TAP passes the grating period), therefore both regions can be used to conduct sensing tasks with measurement at the resonant wavelength.

The most notable feature of a TAP LPG in phase II is its dual resonant peaks, where a change is induced in the effective index of the cladding (ambient materials, change of refractive index, etc.), and causing the peaks to shift away from each other. This is trivial for the TAP PMC, where $\frac{d\Lambda}{d\lambda} > 0$ when $\lambda < \lambda_{TAP}$, and $\frac{d\Lambda}{d\lambda} < 0$ when $\lambda > \lambda_{TAP}$, where λ_{TAP} is the corresponding wavelength at the turn-around-point of the PMC. Therefore when PMC continues to shift up, the

dual intersections of the PMC and the grating period's horizontal line move further apart. Some studies focus on the peaks shifting of the TAP LPG operating in phase II, and use the amount of the wavelength shifting as the beacon and the sensor indicator. However, tune the TAP LPG to operate in Phase-I can be more convenient and help maintain the fiber sensitivity, such measures will be adapted to the experiment design.

In summary, sensing tasks can be conducted in either phase I or phase II of the TAP LPG, and transmitted optical power can be measured and compared prior to the biosensor study, to check if the TAP LPG fiber operates under the experiment designs, and what shall be anticipated. A positive response for fiber sensor operating in phase I denote to the attenuation of transmitted power at and around resonant wavelength; and for fiber sensor operating in phase II, it refers to a reverse shifting of transmitted power at or around the resonant wavelength, respectively.

Nevertheless, if the fiber is tuned too close to the TAP, there may be additional concerns.

First, if sensing tasks are performed in phase I and close to the TAP, the change of the effective refractive index of the cladding may push the PMC into phase II and cause a peak splitting. Data points collected from phase I and phase II should not be compared, since the transmitted light wave gains power in phase II, rather than losses power in phase I as the PMC moves up. The may cause confusion and false negative results when monitoring the transmitted power at a single wavelength. Possible solutions include using a full-span optical spectrum analyzer and to examine if the dual peaks emerge in the larger scale of the spectrum, or check if the single peak has flattened, which is a good indicator of the fiber reaching the TAP region. Generally, it will be helpful to tune the fiber into the sensitive region of phase I yet avoid getting too close to the TAP.

Secondly, a more careful study towards the sensitivity issue of the TAP LPG led by Dr. Jimmy Ritter of Virginia NanoTech Inc. has found that at the exact location of the TAP, the fiber is rather insensitive to the change of the thickness of the ambient layer, as shown in figure 2-11.

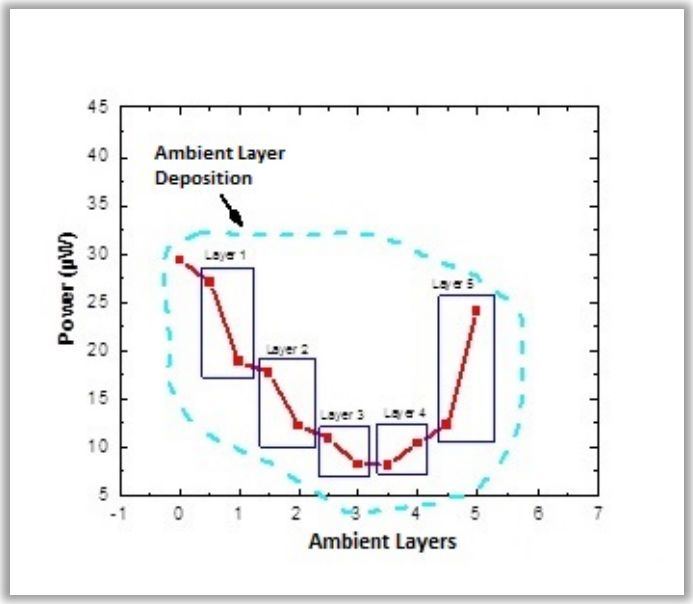

Figure 2-11: The insensitive region at the TAP. Thickness of each ambient layers are considered constant. Through layer 1 to layer 3, the fiber stays in phase I region and the transmitted light loses power. Similarly, through layer 4 to layer 5, the fiber stays in phase II region, and the light regains. However, between layer 3 and layer 4, the fiber is right at the TAP, and the change of the power is slow given same amount of material is added. (From Eric Carlson and Dr. Ritter's study)

Such phenomena are more common in TAP LPG fibers whose PMC of the coupling model has a sharp tip, or mathematically speaking, $d^2\Lambda/d\lambda^2$ has a large value around the TAP. Therefore, when the TAP is passed, the dual peaks won't split very rapidly, an overlap of the dual peaks at TAP's resonant wavelength keep the transmitted power remaining at the same level and prevent the detuning effect to emerge at this wavelength.

Testing the LPG fiber to find out the location of the TAP will help avoid the insensitive region around the TAP. Also, when inscribing the TAP LPG, it's also helpful to use the

parabolic-like PMCs with a relatively small coupling number, since for those coupling mode the PMCs are more flat and the insensitive region can be minimized.

2.1.6 Applications of the TAP LPG as a Sensor

TAP LPG fibers have demonstrated exceptional sensitivity perturbations induced by the variation of the effective indices at the core, the cladding, or the grating period. Numerous studies have been conducted to use the LPG for sensing subtle variation of temperature, strain, the surrounding medium's refractive index and so on.

The temperature and strain LPG sensors transform the variation in the grating period in the core to the change of transmitted optical power. Higher temperature will cause the silica and quartz fiber to extend in length due to the adsorption of the heat. Meanwhile, the grating period increases, and consequently shifts the PMC of the LPG fiber. Such changes eventually reflect in the transmission spectrum and the shift of the wavelength is measured and quantitatively determined. Theoretically, the LPG sensor responds to the change of the temperature is based on:[11]

$$\frac{d\lambda}{dT} = \frac{d\lambda}{d(\delta n_{eff})}\left[\frac{dn_{eff}}{dT} - \frac{dn_{clad}}{dT}\right] + \Lambda\frac{d\lambda}{d\Lambda}\frac{1}{L}\frac{dL}{dT} \tag{2-13}$$

where δn_{eff} is the difference of the refractive indices of the core mode and the cladding mode. Bhatia[61] *et al.* and Shu[62] *et al.* have demonstrated two distinct designs of the temperature sensors and their corresponding measurement techniques.

[61] V. Bhatia "Applications of long-period gratings to single and multi-parameter sensing", *Opt. Express*, **4** 457–66, (1999).
[62] Xuewen Shu, et. al., "Sensitiv ity Characteristics of Long-Period Fib e r Gratings", *J. Lightwave Technol., 20*, pp. 255–266, (2002).

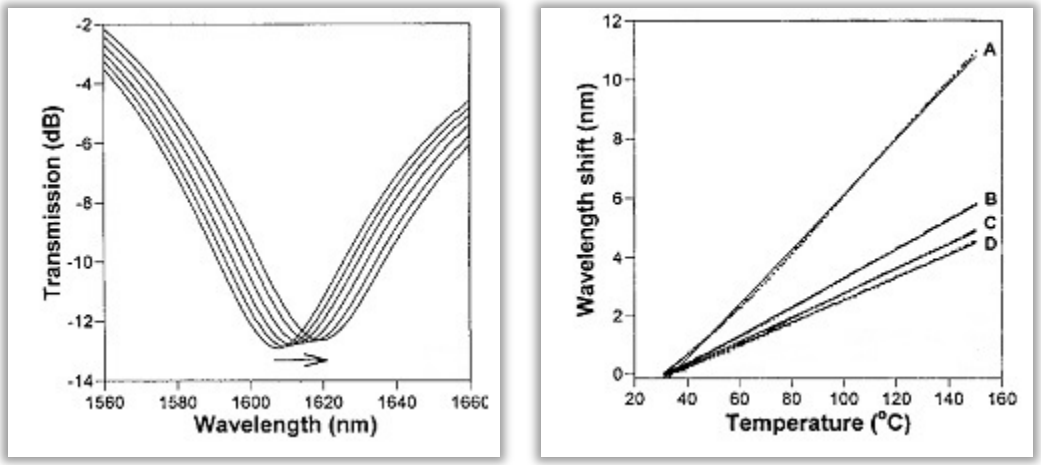

(a)

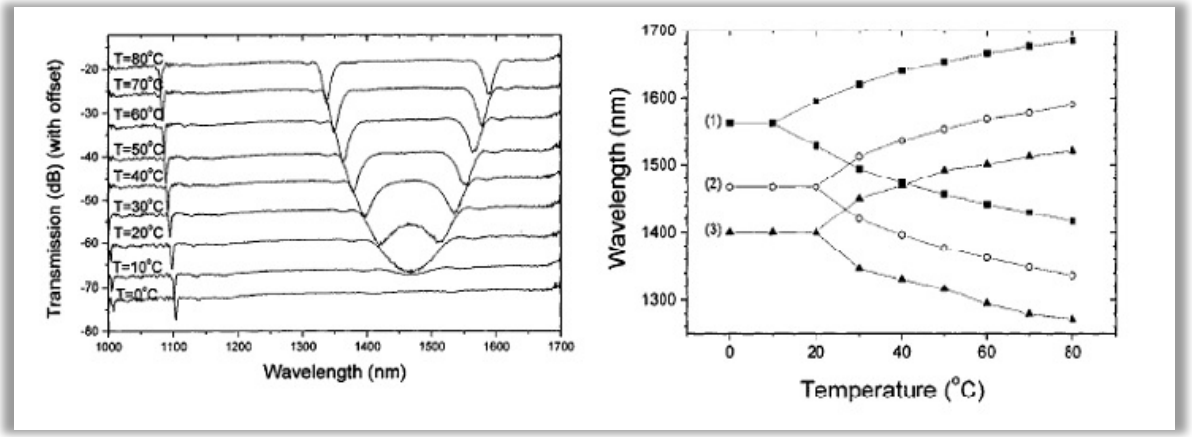

(b)

Figure 2-12: LPG temperature sensor developed by V. Bhatia (From [16]), and X. Shu (From [17]) a) Bhatia's sensor showed the transmission spectra readings of the single attenuation peak locations under 22.7, 49.1, 74.0, 100.9, 127.3 and 149.7 °C respectively. The linear shifting of the wavelength at different bands. Bands A-D are located at 1608.6 nm, 1332.9 nm, 1219.7 nm and 1159.6 nm respectively at 31.2 °C. b) Shu's sensor showed dual peaks shifting in his LPG sensor application. In this case, the separation of the dual peaks is observed. The higher the temperature rises, the further away the dual peaks move from each other. Curves 1, 2 and 3 refers to the coupling modes of the core mode with the 11^{th}, 12^{th} and 13^{th} cladding modes, respectively.

Similarly, the strain exerted on the optical LPG fiber will stretch the, and accordingly extends the grating period. Responses from the shifting of the attenuation peak can be expressed as:

$$\frac{d\lambda}{d\varepsilon} = \frac{d\lambda}{d(\delta n_{eff})}\left[\frac{dn_{eff}}{d\varepsilon} - \frac{dn_{clad}}{d\varepsilon}\right] + \Lambda\frac{d\lambda}{d\Lambda} \tag{2-14}$$

where ε is the measure of the strength of the external stress exerted. A conventional strain LPG sensor is built as a peak-shifter, such as work done by Shu[17] *et al.*. However, Grubsky[15] *et al.* have proven that the TAP LPG can also be used as the strain sensor. Their works are displayed and compared in figure 2-13 below.

(a)

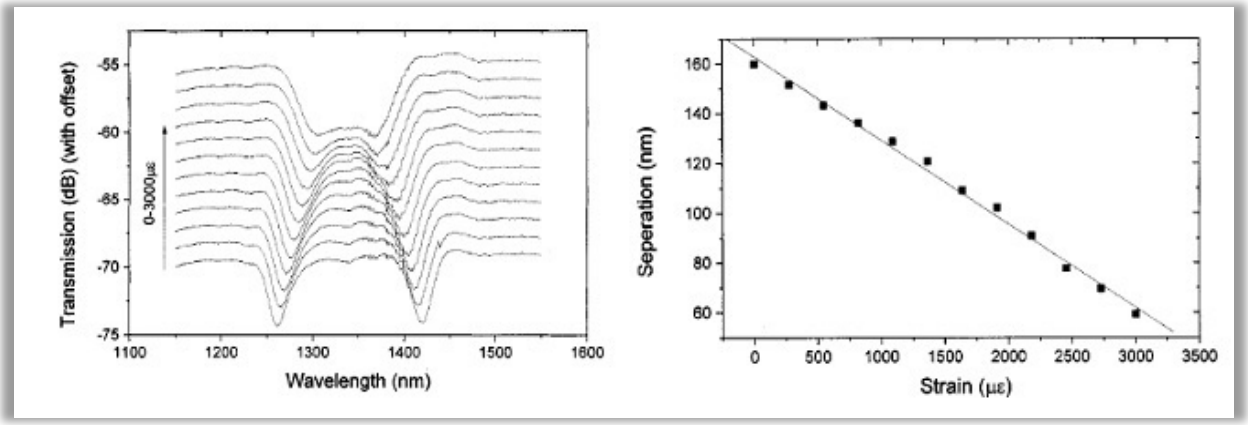

(b)

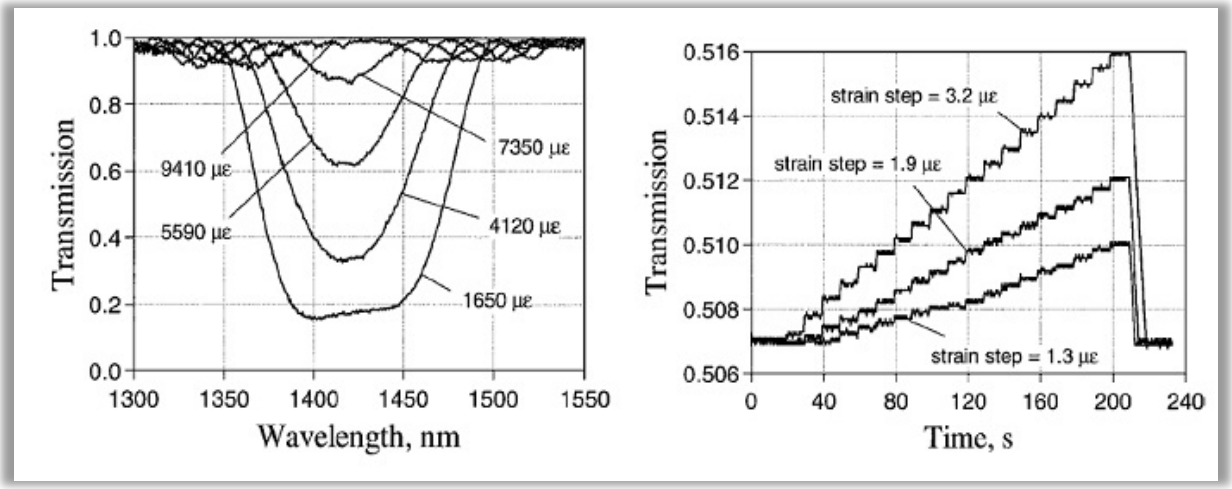

Figure 2-13: Two designs of the LPG strain sensors. a) Shu's design (From [17]) measure the wavelength separation between dual peaks, where with higher strain exerted to the LPG fiber, the further away dual peaks shift from each other. b) Grubsky's design (From [15]) utilized a TAP LPG, where the strain was added at a constant step-ratio. Larger strain change rate showed a steeper response from the change of the transmission.

The change of the refractive index of the surrounding medium also impacts the behavior of the cladding mode, and therefore changes the position and shape of the PMCs of the LPG fiber. Studies[63] have been performed on this issue and Figure 2-14 shows the peak shifting to different wavelength with changes in the refractive indices of the surrounding medium.

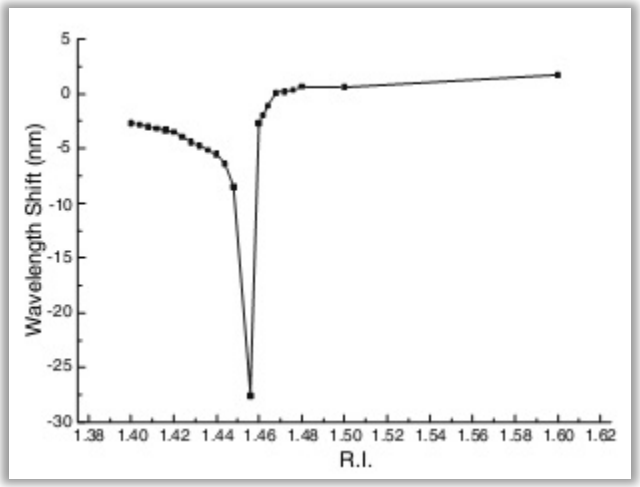

Figure 2-14: Refractive index sensor (From [18]) displays the peak shifting characteristic of the LPG, when the refractive index of the surrounding medium has been changed.

The refractive index sensor is sensitive to the refractive index variation of the ambient medium, and as a consequence, it can be used as a monitor for the liquid level of a container. The study[64] below exhibits that the transmission spectrum is almost linear to the amount of the LPG region immersed in the medium liquid, whose refractive index differs from that of air.

[63] S. Khaliq, S. W. James and R. P. Tatam, "Enhanced sensitivity fibre optic long period grating temperature sensor," *Meas. Sci. Technol.,* 13792–5, (2002).

[64] Khaliq S, James S W and Tatam R P, "Fibre-optic liquid level sensor using a long-period grating," *Opt. Lett.,* **26** 1224–6, (2001).

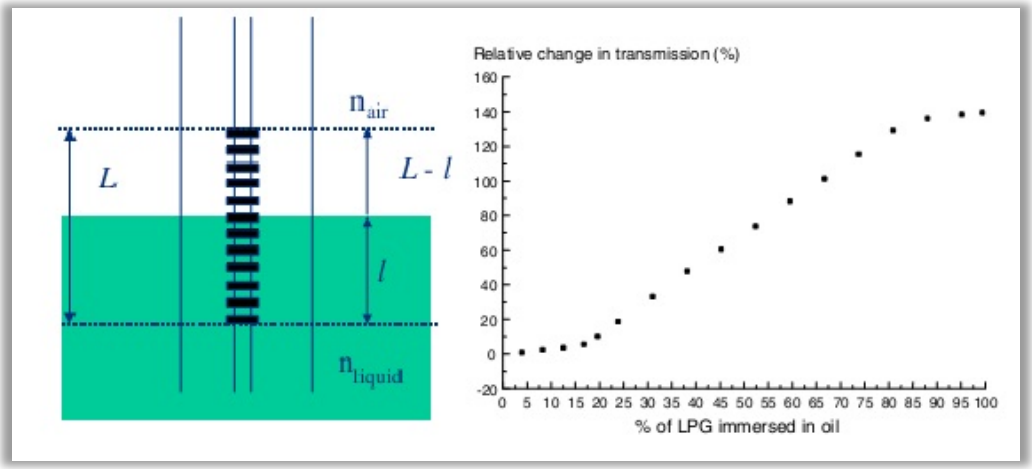

Figure 2-15: The amount of the LPG fiber immersed by the liquid medium will affect the transmission spectrum or the value of the attenuated transmitted optical power more specifically. Therefore a variation of the liquid level will be displayed in the transmission spectrum in real time (From [18]).

Studies have also been performed to apply the LPG fiber as biosensor, which has been extensively discussed in the introduction part. In conclusion, the LPG fiber sensor is capable of performing many environmental or event-controlled monitoring tasks, such as measuring the temperature of the power cable or oil line at distant locations and transmitted the signal through light signal transmitter, or monitoring the structure stress parameters of a bridge. LPG sensor designs have found many roles in the field of optical sensing applications.

2.2 Ionic Self-Assembled Multilayers (ISAM)

2.2.1 Introduction to Ionic Self-assembled Multilayer Thin Films

As shown in the previous section, the TAP LPG has demonstrated extensive sensitivity potential to detect thickness and the refractive index variation of the materials coated over the fiber. Building specific receptors on the TAP LPG will transform the fiber into a specific sensor for the respective analyte. Such receptors can recognize targets upon contact and capture them to the fiber surface, resulting in increasing the average thickness of the ambient layer and

translating the physical existence of the targeted molecule into the optical signal. However, typical quartz or silica optical fibers are made of inorganic materials and lack suitable functional groups to establish stable bonds with most biology receptors. Therefore, an intermedium organic thin film is useful to serve as a bridge to link the receptors with the fiber, as well as enhancing the sensitivity of the LPG fiber sensor.

Ionic self-assembled multilayers (ISAM) are a thin film fabrication technology that is well known for its thermal stability and mechanical durability, precise thickness control, rapid deposition and versatile biochemistry reactive capabilities. ISAM films are formed by a layer-by-layer (LBL) deposition technique and organize the polymer film structure in the vertical orientation. Such nanoscale film fabrication and manipulation technique was pioneered by Decher[65] *et al.*to replace the so-called Langmuir-Blodgett film deposition technique, which has limitations on the choices of polymer classes, as well as the strict requirement for the size and surface properties of the substrate and is far less stable. The LBL technique quickly attracted broad attentions, and it has been exploited in many applications such as sensors,[66,67,68] surface coating and substrate protection,[69,70] biological molecular labeling,[71] nonlinear optical,[72] *etc.*.

---

[65] G. Decher, "Fuzzy Nanoassemblies: Toward Layered Polymeric Multicomposites", *Science*, **277:** pp.1232-1237, (1997).

[66] F. Caruso, K. Niikura, D.N. Furlong, Y. Okahata, "Assembly of Alternating Polyelectrolyte and Protein Multilayer Films for Immunosensing," *Langmuir*, **13**: 3427–3433 (1997).

[67] G. Mijares, D. Reyes, M. Gaitan, B. Polk, D. DeVoe, "Polyelectrolyte multilayer-treated electrodes for real-time electronic sensing of cell proliferation". *Journal of Research of the NIST*., **115**: 61(13), (2010).

[68] Z. Wang, J.R. Heflin, K. Van Cott, R.H. Stolen, S. Ramachandran, S. Ghalmi, "Biosensors Employing Ionic Self-Assembled Multilayers Adsorbed on Long-Period Fiber Gratings," *Sensors and Actuators B*, **139**:618-623, (2009).

[69] H. Hattori, "Antireflection Surface with Particle Coating Deposited by Electrostatic Attraction," *Adv. Mater*., **13**: 51 (2001).

[70] T. R. Farhat and J. B. Schlenoff, "Corrosion Control Using Polyelectrolyte Multilayers", *Electrochemical and Solid-State Letters*, **5**(4): B13-B15, (2002).

[71] V. S. Trubetskoy, A. Loomis, J. E. Hagstrom, V. G. Budker and J. A. Wolff, "Layer-by-layer deposition of oppositely charged polyelectrolytes on the surface of condensed DNA particles", *Nucleic Acids Research*, **27(**15): 3090–3095, (1999).

[72] J.R. Heflin, C. Figura, D. Marciu, Y. Liu, and R.O. Claus, "Thickness Dependence of Second Harmonic Generation in Thin Films Fabricated from Ionically Self-Assembled Monolayers," Appl. Phys. Lett., 74:495 (1999).

Thin film fabrication with ISAM offers wide choices of chemical functional groups and combines high flexibility with simplified deposition process. ISAM coated LPGs are the primary focus of this dissertation as the intermedium film for the biosensor design.

2.2.2 Structure and Deposition of ISAM

Each pair of layers of the ISAM film is primarily bound with neighbor layers through electrostatic attraction. The most common materials used in ISAM are polyelectrolytes, which are long polymer chain with charged groups at each unit. When dissolved in water, the counter-ion (*e.g.* H^+, Na^+, Cl^-) dissociates from the charged group. Therefore, ionized polymer chain deposited to the ISAM surface will express net charges in solvent environment. As a result, the oppositely charged polymer chains brought to the ISAM film will be adsorbed via ionic bonds, forming a new layer on top of the film, and flipping the sign of net charges expressed by the ISAM film.

The ISAM deposition technique takes advantages of such features of the polyelectrolyte, and allows an orderly assembly of layer-by-layer thin films on the solid substrate, by sequentially dipping the charged substrate into polyanion solution and polycation solution at room temperature. For instance, assuming a negatively charged substrate is immersed in the polycation solutions first, where dissociated polycation chains are adsorbed to the substrate through electrostatic attractions. The adsorption of the polycation polymers proceeds at an exceptional rapid pace. However, the adsorption process slows down with the accumulation of polycation polymers, where the development of the reversed electric field compensates the attraction forces originated from the layer or substrate beneath, and eventually repulses the deposition of further polycation chains. This means that the ISAM film cannot grow indefinitely if sufficient amount of polyelectrolyte materials are supplied. Instead, the film deposition will automatically cease at

certain stage, which can be predetermined through theoretical estimation and experiment screenings.

The thickness limit for each layer is controlled by several solution parameters, such as pH value, type and salt concentration of the solvent, type of the polyelectrolyte used in the film fabrication ("weak" or "strong"), and its concentration in solution, and the immersion time.

More specifically, a strong polyelectrolyte will dissociate completely under most reasonable pH values, though by contrast, the weak polyelectrolyte will partially dissociate at moderate pH values. Therefore, by adjusting the pH value of a weak polyelectrolyte solution, the ratio of the ionized polyelectrolyte in the solution can be tuned, and ultimately controlling the thickness of the layer. The high salt concentration will screen the repulsive interaction between polyelectrolyte chains, which force the chains to dwell in a tightly compacted conformation, rather than in a stretched conformation under low salt concentration. Such solution-controlled characteristics of the polyelectrolytes offer flexible and easy-to-deploy methods for film thickness adjustment and film configuration control. This is one of the many reasons ISAM are used as the bridging thin film for biosensor applications.

The sign reversal of the surface charges after each deposited layer of the ISAM film has an extraordinary importance in fabrication of more sophisticated thin film structures. The simplest case of assembling a polyelectrolyte multilayer thin film only consists of one polycation (namely, *A*) and one polyanion (namely, *B*). The film deposition procedure can be summarized as alternately dipping the substrate in oppositely charged polyelectrolyte solutions. The dipping sequence with polycation solution and polyanion solution will generate a repeating $(AB)_n$ film structure, and each (*AB*) film layer combine to form one ISAM bilayer, and the thin film is constructed with multiple numbers of such bilayers. More intricate cases generally involve more

polycation or polyanion solution in the repeating structure. For instance, if another polycation solution (namely, *C*) is added into the film constructing process, the layer-structure which repeats itself in the multilayers film could have the expression as $-(ABCB)-_n$. Therefore the structure of the multilayer film can be completely controlled with the dipping sequence and the solution parameters.

Figure 2-16 illustrates deposition process takes place and produces the thin film with repeating bilayer or multilayer structures.

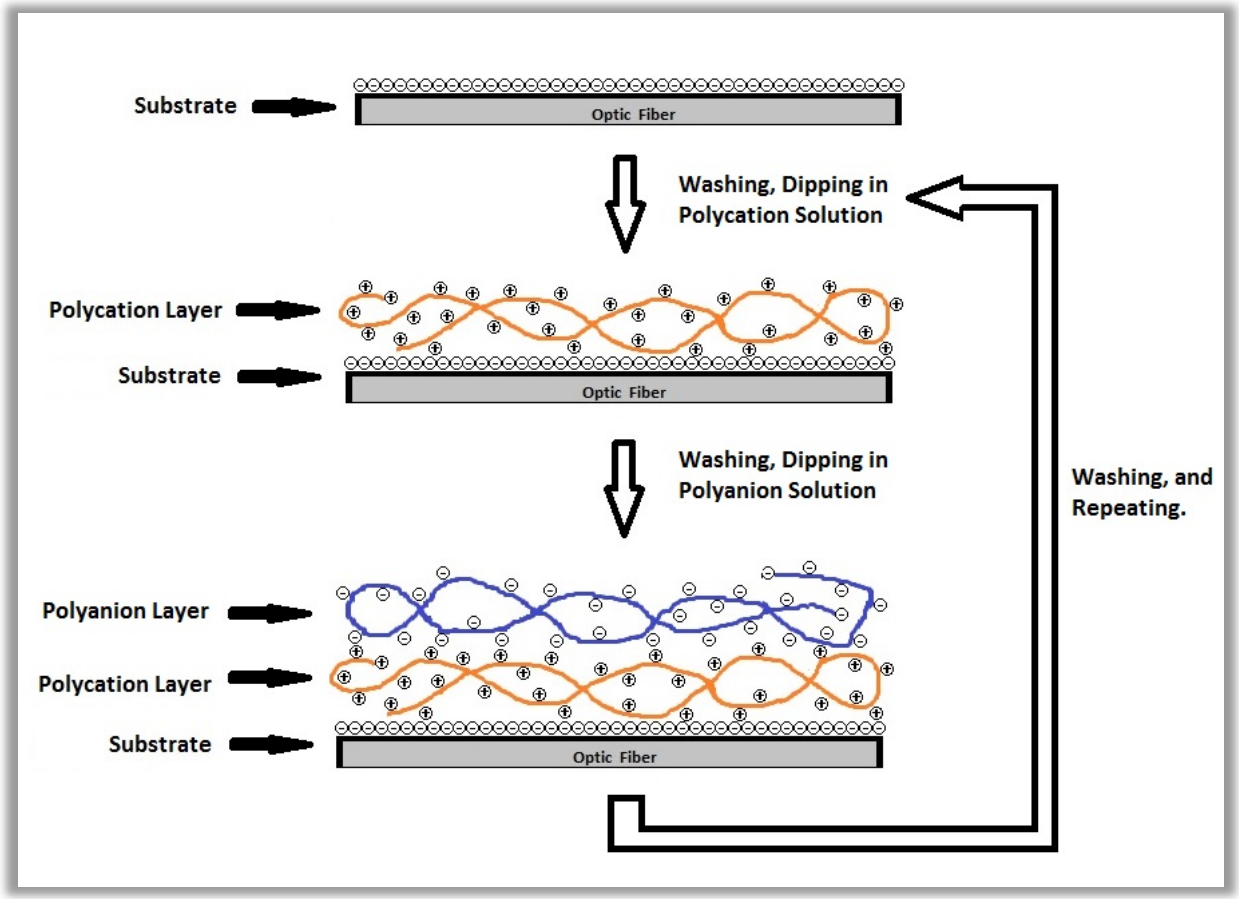

Figure 2-16: The self-assembly process of the ISAM thin film. The negatively charged silica fiber will be dipped in polycation solution first, forming the first nanoscale layer. Then dipping in the polyanion solution will produce the polyanion layer. Together, the polycation-polyanion bilayers generate the basis for constructing the whole ISAM film, with repeated dipping the fiber in the polycation solutions and polyanion solutions sequentially.

Since the ISAM multilayers are conjoined together with the electrostatic interaction between neighboring oppositely charged polyelectrolyte layers, the assembled film construction does not involve any chemical reactions. The surface adsorption of polyelectrolytes is driven by ionic attractions, which takes place spontaneously in the presence of oppositely charged polyelectrolyte chains. Therefore with predetermined polyelectrolyte solution conditions, the polyelectrolytes will perform self-assembling automatically over the substrate until reaching the desired thickness at the nanometer level, without any external intervention or operation.

The fast deposition process of a polyelectrolyte layer and its thickness controllability can be illustrated through the experiments displayed in Figure 2-17. This experiment is carried out with a TAP LPG fiber whose jacket has been stripped off and bears net negative charges on the fiber surface. It was first of all immersed into the polycation solution, where the transmitted optical power at the resonant wavelength was recorded sequentially through a period of 1155 seconds. The fiber was then removed from the polycation solution, rinsed by deionized water 3 times for 15 seconds during each rinsing. After a thorough rinsing, the fiber was dipped into the polyanion solution for the same period of time, and the evolution of the film deposition process is recorded in real time.

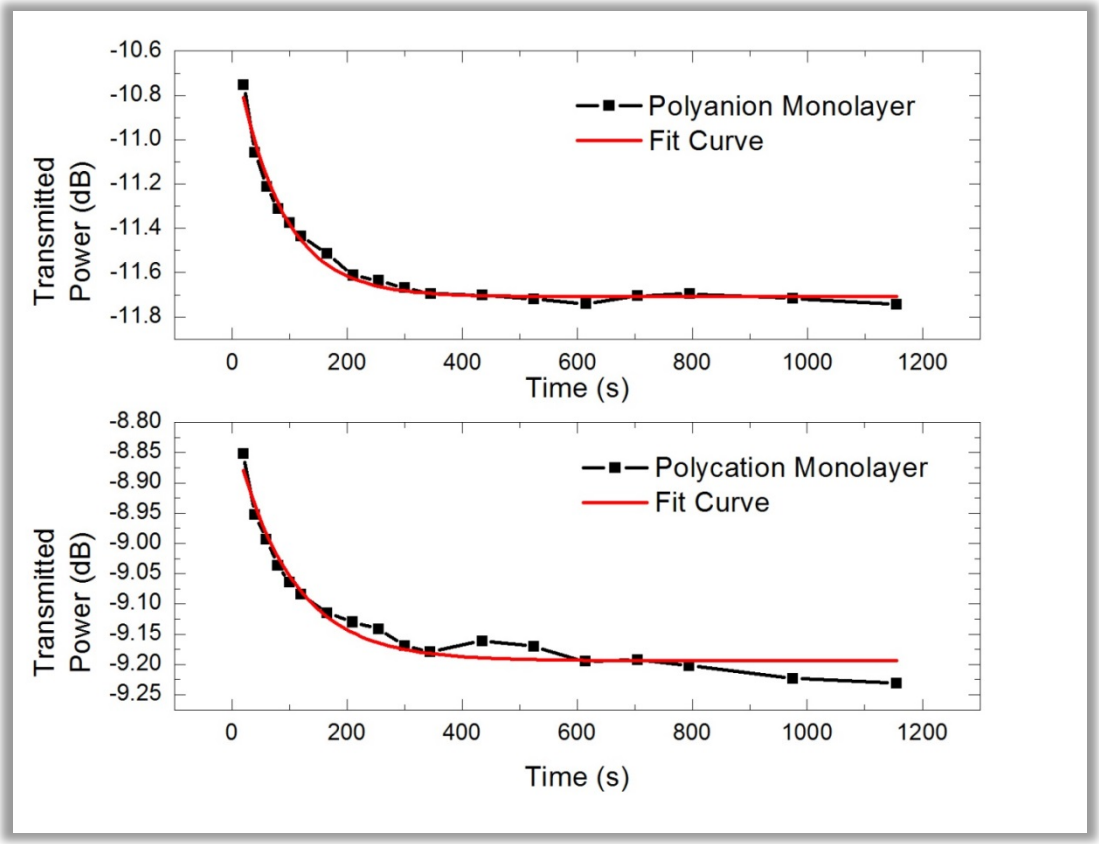

Figure 2-17: Evolution of the ISAM deposition process. The bare TAP-LPG fiber is dipped in both polycation solution and polyanion solution sequentially for 1155 seconds. The transmitted power has a loss of 0.8 dB or 16.8% in the polyanion case, and 0.275 dB or 6.54% in the polycation case. Both power loss curve from polycation layer and polyanion layer saturate after a dipping period of around 400 seconds.

In the first 200 seconds, the transmitted optical power is attenuated in the exponential order, which suggests that the thickness of polycation or polyanion layer increases continuously during this period. The data curve then saturate after about 400 seconds of dipping period, and afterwards the film thickness shows no substantial changes, suggesting the limit of the film thickness has been reached. Numerical analysis of the results is also shown in Figure 2-17. The best fit function we have found for this pair of experiments is $A_0 + A_1 10^{-w \cdot t}$, where w is the rate of the deposition process.

The ISAM film-making technique reaches any solvent accessible surface, regardless of the shape and size of the substrate. This is especially convenient for constructing thin films on optical fibers, as fibers naturally bear negative charges, and its cylindrical symmetry allows the thin film to wrap the entire fiber. Studies have also suggested that the influence from the substrate will be removed after a few bilayers of ISAM,[73] which is especially important for the biosensor design since the receptor film of the sensor can therefore be free from interference from the silica fiber.

2.2.3 PAH and PCBS Polyelectrolytes

The purpose of utilizing ISAM thin film in the architecture of the TAP LPG based biosensor has two major reasons. First, the ambient film layer is needed to expand the transverse ray profile of the cladding and the surrounding film, which requires a subtle and tunable materials combination for precise film thickness control. Second, as the bridging structure between the silica fiber and biological macromolecule probes, the ISAM film can offer diverse biochemistry functional groups available to the cross-linking reactions with antibodies and other probe types.

In this dissertation, based on studies performed by my predecessors, Dr. Erika Gifford[74] and Dr. Zhiyong Wang,[75] PAH(Poly(allylamine hydrochlorine)) and PCBS(Poly[1-[4-(3-carboxy-4-hydroxyphenylazo)benzenesulfonamido]-1,2-ethanediyl,sodium salt) are chosen as the polycation and polyanion specifically for constructing the ISAM film in the biosensor assays.

---

[73] Charles Brands, "*Interface Effects and Deposition Process of Ionically Self-Assembled Monolayer Films: In Situ and Ex Situ Second Hamonic Generation Measurements*", Ph.D Dissertation, ETD-09112003-071527, (Virginia Tech, 2003).

[74] Erika Gifford, "*Sensitivity control of optical fiber biosensors utilizing turnaround point long period gratings with self-assembled polymer coatings*", Ph.D Dissertation, ETD-12082005-094018, (Virginia Tech, 2008).

[75] Zhiyong Wang, "Ionic Self-Assembled Multilayers Adsorbed on Long Period Fiber Gratings for Use as Biosensors", Ph.D Dissertation, ETD-12082005-094018, (Virginia Tech, 2005)

PAH and PCBS are purchased from Aldrich® Chemistry, and diluted in deionized water at pH 7.0 and at 10 mM concentration. The molecular structures of PAH and PCBS are shown in Figure 2-18. PAH will release the chlorine ion at each repeating unit of the polymer chain when dissolved in the solvent, which leave the polymer chain positively charged. In contrast, PCBS will release the sodium ion when dissolved, and express the negative charges along the polymer chain. Correspondingly, PAH serves as polycation in the ISAM thin film, while PCBS serves as polyanion.

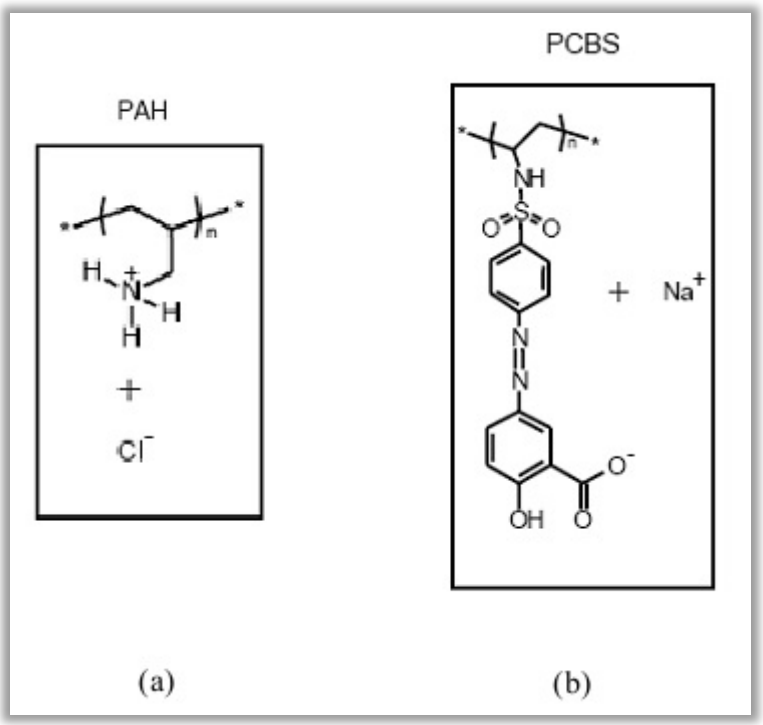

Figure 2-18: The molecular structures of (a) Poly(allylamine hydrochlorine) or PAH, and (b) Poly[1-[4-(3-carboxy-4-hydroxyphenylazo)benzenesulfonamido]-1,2-ethanediyl, sodium salt , or PCBS. PAH is positively charged when dissolved, and serves as polycation in the ISAM thin film, while PCBS is negatively charged, and serves as polyanion.

More importantly, PAH possesses an amine group in each repeat unit when dissociated in solution, while PCBS possesses carboxyl group when the sodium ion is dissociated. Amine and

carboxyl groups are very common functional groups in a wide range of biological compounds. Amine and carboxyl groups are the backbones components of the amino acids, which is the basic element of living tissues and cells. An amine group can crosslink to carboxyl group of another molecule through a peptide bond or an amide bond. Such bonds are a type of covalent bond, therefore it is stable under extreme environment conditions.

The reaction formula can be written as:

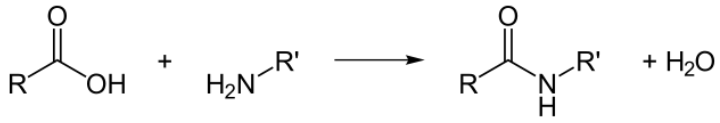

Formation of the amide bond will release free energy, and for each bond a molecule of H_2O is released, thus categorizing the reaction as a dehydration synthesis, or a condensation reaction.[76] The newly formed bond -C(=O)NH- is called peptide link, which bridges amino acids to form the backbone of long polypeptide or protein chains. And with diversified combinations of various amino acids, polypeptides and proteins can exhibit abundant expressions and structures.

Therefore, ISAM films with PAH and PCBS as alternating components have bioconjugation affinity to various biological macromolecules which are protein based. Depending on the deposition sequence, this combination of ISAM can offer either amine or carboxyl groups on the film surface, and engage in crosslinking reactions to incorporate biological probes or receptors to the fiber sensor.

Like many typical polyelectrolytes used for ISAM technique, the thickness of PAH or PCBS layer can be effectively controlled via adjusting the pH values and salt concentration of

[76] R. B. Martin, "Free energies and equilibria of peptide bond hydrolysis and formation", *Biopolymers*, **45**, 351–353, (1998).

corresponding solutions since both chemicals are weak polyelectrolyte,[77,78] which only partially dissociates in the solvent and can be affected by the ionic density of the solvent salt. Dr. Zhiyong Wang has conducted experiments[29] on examining the pH dependence of the thickness of constant amount of PAH/PCBS bilayers. Figure 2-19 below shows the testing results based on 20 bilayers of PAH/PCBS assembled on the RCA cleaned glass slides, with both polyelectrolyte solution concentrated at 10 mM.

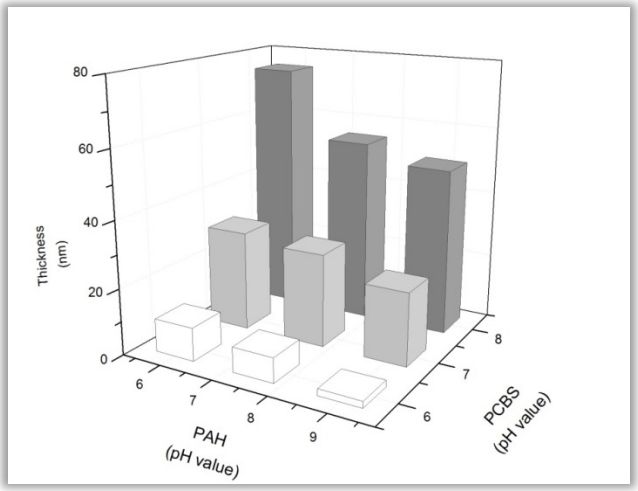

(a)

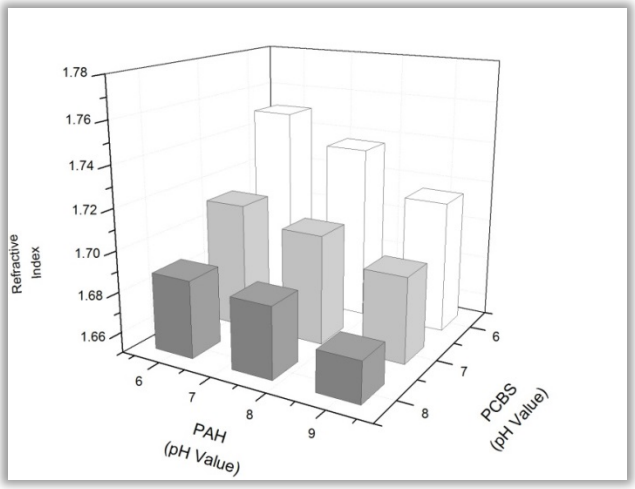

(b)

[77] S. Shiratori, M. Rubner, *Macromol.* **33**, 4213 (2000).
[78] C. Figura, P.J. Neyman , D. Marciu , C. Brands, M.A. Murray, R.M. Davis, M.B. Miller, J.R. Heflin , *Proc. of SPIE,* **3939**, 214 (2000).

Figure 2-19: The pH dependence of (a) thickness and (b) refractive index of the PAH/PCBS bilayers of ISAM film. The ISAM films contain 20 bilayers of PAH/PCBS, therefore each bilayer of the ISAM is at the nm-scale in film thickness. Source:[75].

The results indicates a few intriguing aspects of the ISAM technique that be understood intrinsically. First of all, the thickness of the PAH/PCBS bilayers are dependent on the pH value of the adsorption solution. Higher pH of the PCBS solution and lower pH of the PAH solution generate a thicker film. Similarly, when comparing the refractive index bar chart with the thickness bar chart, it is apparent that thicker PCBS layer will render a smaller refractive index of the final ISAM film, however, thicker PAH layer will produce a larger refractive index film. This is because the conjugated side chain on PCBS has a greater contribution to the refractive index.

Secondly, although both PAH and PCBS solutions are made at same concentration, the pH variation of the PCBS solution has a larger impact on the film's thickness. In comparison, the pH variation of the PAH solution does not change the thickness of the film as much. The pH variation impact on the refractive index is less significant for PCBS, though.

Decher has noticed[20] that for each layers of the ISAM film, the number of anionic and cationic groups has to match. Since the adhesion of each PAH and PCBS layer is accomplished through electrostatic interaction, hence adjusting the solution's pH value will also alter the amount of ionized anionic or cationic groups available for the incoming layer as well as the thickness of the incoming polyelectrolyte layer, and that the top layer charge density has to be identical to the base layer of the thin film. Also, a post-preparation treatment suggestion has been made in the same article by Decher, that consecutively immersing the film-coated substrate in salts and water could help develop a less roughness polyelectrolyte top film, as the desalted

water can dissolve and remove the unattached polymer molecules or other impurities from the film surface, which are the main source of the roughness of the ISAM film.

2.2.4 AFM Studies of the ISAM Thin Film

The film smoothness and controllable thickness of the ISAM film deposition technique can be intuitionally examined utilizing atomic force microscopy (AFM).

The study is performed over RCA cleaned glass slides, which is a comparable substrate to the silica fiber despite the difference in topology. The glass slide was dipped into 10 mM PAH and PCBS solutions at pH=7.0 sequentially for 3 minutes, respectively, which precisely reproduced the same films deposition procedure on the optical fiber. Fig 2-20 displays ISAM thin film AFM height measurement.

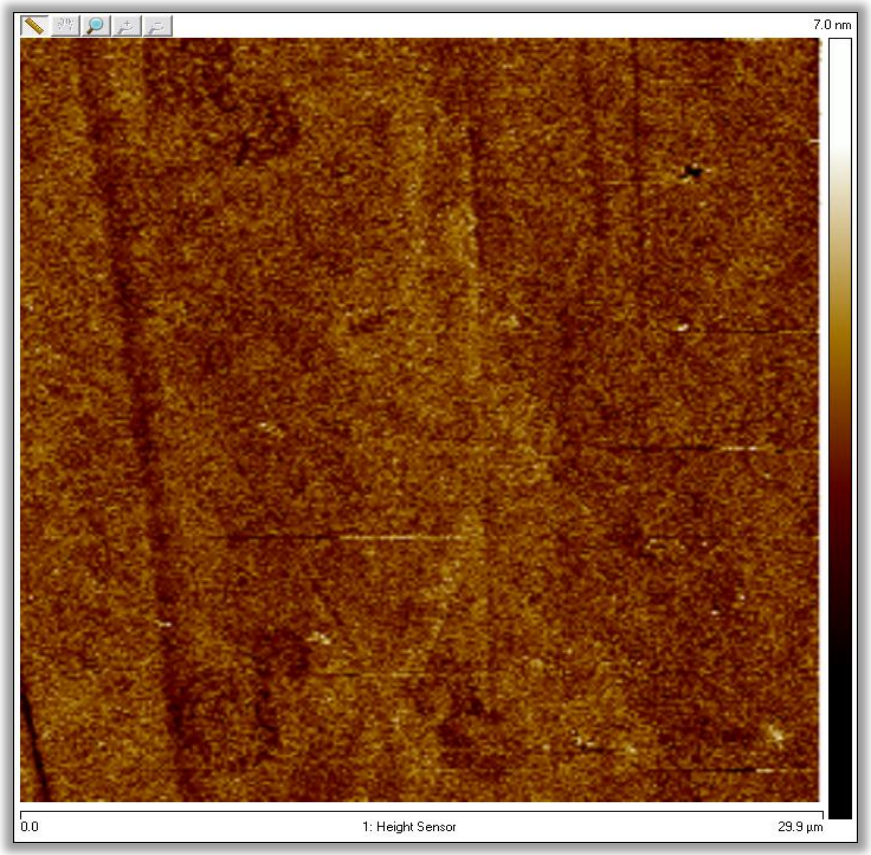

Figure 2-20: AFM image of 3 bilayers of ISAM film adsorbed onto a glass slide. The scale of this image is 30 µm by 30 µm. The surface is smooth and identical in most regions. The scratches may be results of the nitrogen stream which was used to dry the slides after rinsing and cleaning.

A more detailed analysis has been performed on the same region of the thin film coated slides. A random location has been chosen and the surface height along the x-axis and the surface height distribution of a 10 µm by 10 µm region has been scanned. The scanning result is shown in Fig 2-21. The surface height variation of the ISAM thin film is between -0.2 nm and 0.2 nm, and the majority surface height lies between 0.4 nm over the lowest point to 0.8 nm over the lowest point, which agrees with the 0.4 nm variation from the 1D scanning results.

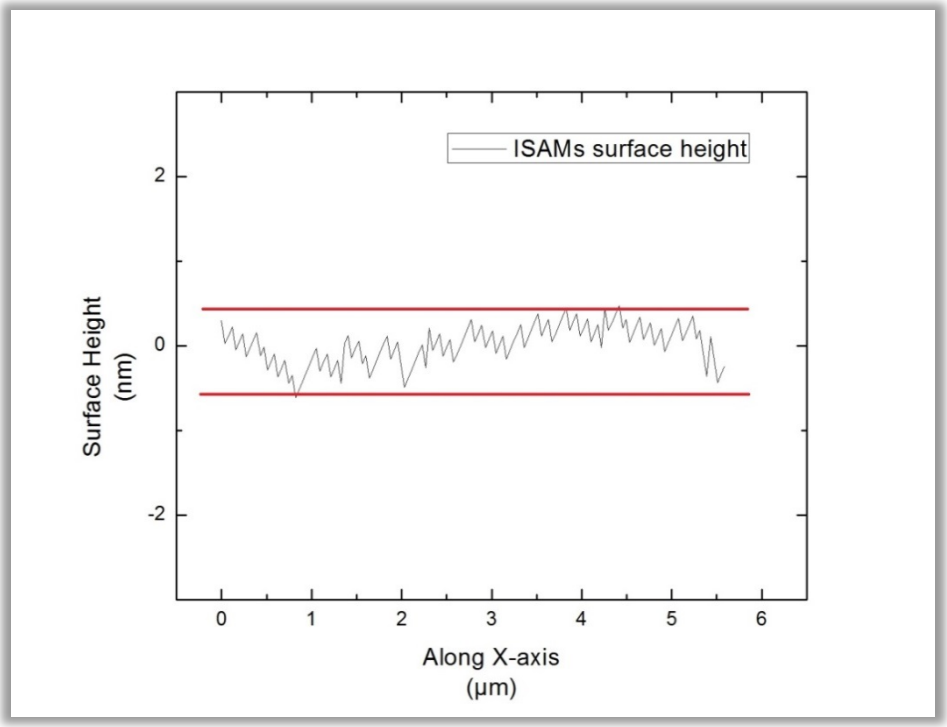

(a)

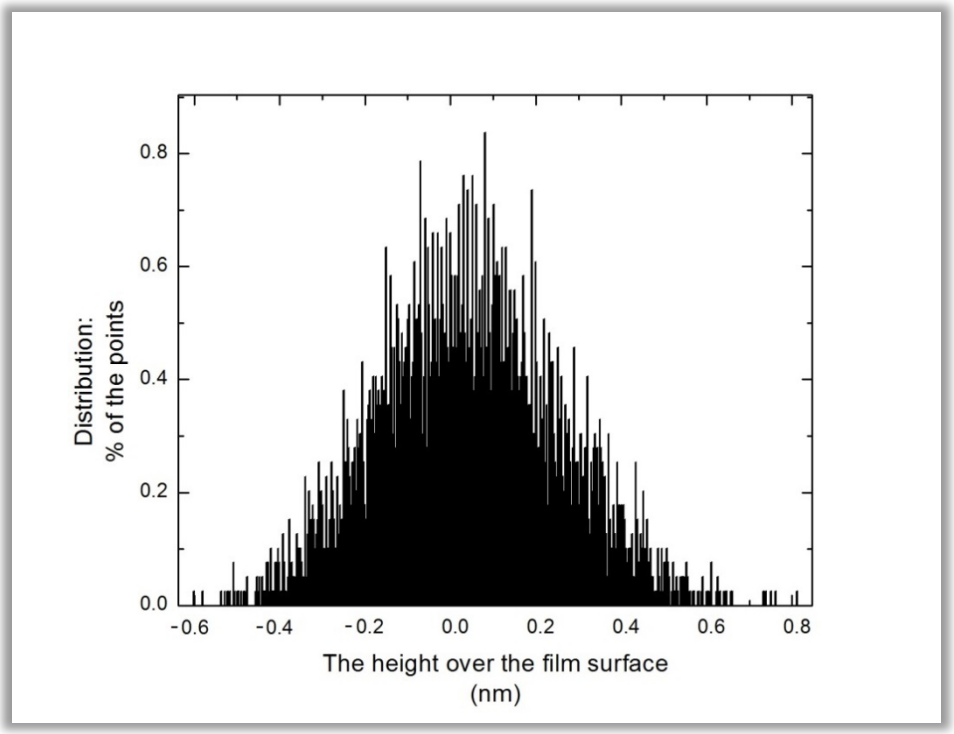

(b)

Figure 2-21: (a) The 1D surface height scanning graph of the ISAM coated glass slides, at a random location. The height variation of the ISAM thin film surface is between plus and minus 0.2 nm. (b) The surface height distribution graph of the ISAM film over a 10 μm by 10 μm area. The majority surface height is between 0.4 nm over the lowest point in this area to 0.8 nm over the lowest point, the variation of the majority surface height agrees with the 1D scanning results.

2.2.5 Discussion of the ISAM Thin Film Coating Technique

The ISAM technique has shown importance in designing the optical fiber biosensor and serves as the substrate on which to immobilize biological molecule onto the fiber surface.

First, the adsorption from polymer solution takes place spontaneously, and the process will halt when the film reaches the designated thickness. The film deposition process occurs swiftly and requires no further intervention or extra mechanism, which limits the cost for producing the biosensor. This is an advantage when the considering commercialization of the sensor system, where the simplicity and accountability of the product system are crucial.

Secondly, the ISAM thin films provide diversified functional groups ready for crosslinking reactions, such as amine group, carboxyl group, sulfhydryl group and so on. With the help of proper crosslinker, these functional groups can react with proteins and other biological macromolecules to produce strong and persistent covalent bonds. In other words, the wide crosslinking options offer multiple immobilization strategies for attaching target biomolecules onto the film surface, and positing such molecules properly so that their paratopes can be facing the outside, rather than buried or blocked by neighbor molecule compound.

2.3 Cross-linking Chemistry

2.3.1 Immobilization of the Biological Molecules on the ISAM Thin Film

In the field of biochemistry, the immobilization of biomolecules and polymers onto certain substrates or materials through cross-linking reactions have been demonstrated to be reliable and is employed in many applications in immunology tests and assays, such as enzyme-linked immunosorbent assays (or ELISA), Western Blotting, Chromatography and so on. In the specific recognition binding between complementary biomolecules (*e.g.* antibody-antigen), such affinity is usually expressed as complex combination of functional groups and the folding architecture of such groups. Such interactions reveal the essence of the precise and selective life process.

With the developments in biochemistry and organic chemistry, it is getting clearer that despite the complexity of the molecular structures and conformations, all the known biological molecules are assembled with only a finite amount of chemical groups. For instance, as the most fundamental and basic element of all life forms, protein is built up with versatile combination of polymer chains, known as amino acids.[79] Each of these amino acids carries a side chain groups

[79] Nelson DL, Cox MM. ***Lehninger's Principles of Biochemistry***(4th ed.). New York: W. H. Freeman and Company. (2005).

which identify and distinguish the residue, and the amino acids are linked together through peptide bonds in orders and fold into primary protein structures that have exhibited various functions in living tissues.[80,81] Another example is the DNA sequence. Despite divergent expressions of a DNA encoding which carries biology information of the host, all the DNA helixes of earthly creatures are architecture upon four basic elements: guanine, adenine, thymine, and cytosine,[82] and the backbone of the sequence itself always ends with a free phosphate group at the 5' end and a free hydroxyl group at the 3' end. Fig 2-22 depicts the generic structures of the amino acid and a simple DNA sequence.

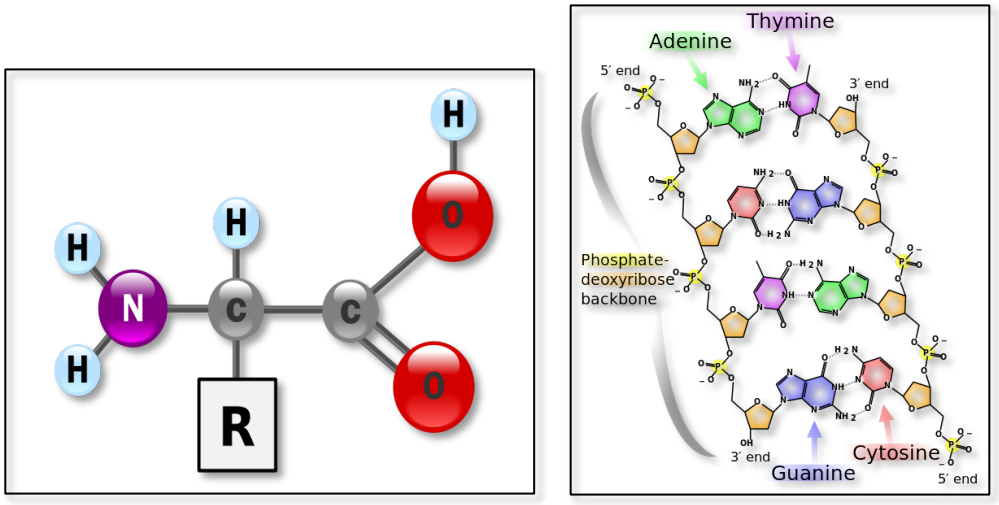

(a) (b)

Figure 2-22: (a) Generic structure of a typical alpha amino acid in its un-ionized form. The amino acid contains an amine group and a carboxyl group, and the reaction between thus groups can form a stable peptide bond. It also carries a *R*-group, which can be certain functional groups, which identifies the amino acid. (b) A simple illustration of a DNA sequence. The backbone is formed with phosphate-deoxyribose, with a phosphate group at the 5' end, and a hydroxyl group at the 3' end.

[80] Murray RF, Harper HW, Granner DK, Mayes PA, Rodwell VW. ***Harper's Illustrated Biochemistry.*** New York: Lange Medical Books/McGraw-Hill. (2006). ISBN 0-07-146197-3.
[81] Branden C, Tooze J. ***Introduction to Protein Structure.*** New York: Garland Pub.(1999). ISBN 0-8153-2305-0.
[82] Wolfram Saenger. ***Principles of Nucleic Acid Structure***. New York: Springer-Verlag.(1984). ISBN 0-387-90762-9.

These functional groups can be further modified and establishing covalent bonds with other molecules through cross-linking reactions. The immobilization of the biomolecules is defined as cross-linking biomolecule onto a much larger subject or macromolecules, plate or film surface. The advantages of the cross-linking reactions can be summarized as follows:[83,84]

- **The specificity and flexibility of the cross-linking target**: As mentioned, the targets of the cross-linking reactions are the limited amount of functional groups that exists universally among biological molecules, such as amines(-NH_2), sulfhydryl(-SH), carboxyl(-COOH), carbonyl(-CHO) or hydroxyl(-OH) groups. The reactions will only modify or cleave the specified primary functional groups or bonds, while leaving the remaining molecules structure intact and active in their supposed function. Moreover, the mentioned functional groups can react with multiple biochemical reagent and establishing unique covalent bonds, therefore opening possibilities for many alternative crosslinking methods and modification reagent options. These give researchers flexibility for choosing the most effective cross-linking reactions for reaching experiment goals.
- **Homobifunctional or heterobifunctional**: To fit different experimental purposes, crosslinkers which have identical reactive groups on both ends can be used for targeting unique functional group and crosslinking same residues (the upper A/A linked molecular structure below). Such linkers are known as homobifunctional crosslinker. On the contrary, the heterobifunctional crosslinkers, are adopted more commonly in a biochemistry experiment, where the linkers will target different reactive groups on separate proteins or molecules and generate conjugations

[83] http://www.piercenet.com/browse.cfm?fldID=63E6BCDB-F15A-49FB-A717-64D46BD93CC8
[84] E. Golemis, **Protein-protein interactions: A molecular cloning manual**. NY: Cold Spring Harbor Laboratory Press. ix, 682, (2002).

between one another to promote variability and specificity of the reaction system (the lower A/B linked molecular structure below).

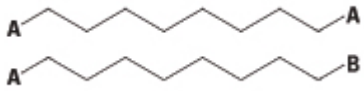

- **Choices on spacer arm length**: The cross-linking chemistry allows diverse choices of crosslinkers for forming conjugation between biological molecules. In principal, the crosslinker can be viewed as a catalyst in the cross-linking reactions. Generally, both reactive moieties of the crosslinker molecules can be consumed or replaced by the functional groups of the biological molecules of interest, and the reaction counterparts are directly linked to each other without owning any external components from the crosslinker. Such crosslinker is categorized as "zero-length" crosslinker reagent. Yet, it is possible to modify the length of the crosslinker molecule by synthesis of crosslinker with stable chemical groups between the reactive groups, such that the bridging region of the crosslinker will be inserted into the bond complex after the reaction. The bridging component is called "spacer arm". Crosslinkers with spacer arm can spatially separate the molecules of interest, which keeps the conjugated biomolecules relatively independent of each other. In the applications of immobilizing biological molecules, it can be useful to increase the spacer arm of the conjugated biomolecule compound in order to float the immobilized molecules above the base or substance, and increase the chance of their involvement in the ensuing biochemistry interactions. The length of spacer arm can be chosen suiting the purpose of the experiment. The cross-linking conjugation with spacer arm (the

upper molecular structure) and zero-length conjugation (the lower molecular structure) can be seen in the figure below:

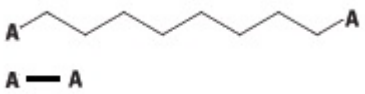

- **Reversibility of the conjugation:** The crosslinkers can also be modified to include chemical bonds or elements in the spacer arm which can be later broken or cleaved, such as esters or disulfide bonds (as shown below). The addition of hydroxylamine will cleave the ester bonds, while the addition of a reducing reagent is able to break the disulfide bonds. Since the spacer arm is cleavable for such crosslinkers, the binding between cross-linked molecules can be set free from one another, or from the substrate on which they are immobilized, if the cleaving reagent is in presence. Such characteristics can be utilized to transfer molecules from one reaction environment to another, or to release the label molecules from the target of interests.

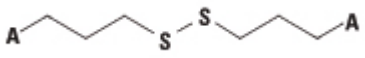

- **Water-soluble or water-insoluble:** The crosslinker molecule can be hydrophobic to acquire access to hydrophobic protein domains or penetrate the cell membrane. However, the hydrophilic crosslinkers are also useful in the situations where the cross-linking reactions occur in the aqueous compartment.

Cross-linking reactions have been tested to attach custom biomolecules onto solid bases or insoluble supports, such as magnetic particles, latex beads, nanoparticles, macro-beads, membranes, microplates, array surfaces, dipsticks and a list of other devices which have an

activated functional group available for cross-linking reactions. Researchers have found applications of immobilization of biomolecules through cross-linking reactions in the area of purification, scavenging or removal of contaminations, catalysis or modification of certain biomolecules of interest.

Though the crosslinkers target specific functional groups of proteins and biological molecules, the reaction usually takes place in a broader view where many conjugations can be formed beyond the designated area of the targeted molecules of interest. For instance, a common protein contains thousands of amino acids units, whose molecular structure will in some cases includes additional amine groups and carboxyl groups within the side *R*-group. Then, with the presence of large excess of cross-linkers that are supposed to target the primary amine groups only, the side-chain amine groups will compete with the primary amine groups for the cross-linking reactions, and yield unintended protein-protein conjugation and sometimes an aggregation of the protein targets. Such nonspecific conjugations threaten the accessibility of the functional groups of the individual proteins within the composite, and will reduce the total reactivity of the final protein compound in the ensuing assays.

In order to address such issue, more sophisticated crosslinker structures have been studied and created, which incorporated photoreactive groups which only respond to the irradiated UV light. If using such crosslinking technique, the specific cross-linking only occurs when the reaction chamber is UV-irradiated at indicated experiment stages. Such approach[85] has been proven to be effective in preventing nonspecific linkages under the assumption that the primary reactive groups of a protein have a better chance to interact with the photoreactive crosslinkers under UV-irradiation.

[85] L. Yang, *et al*. "A photocleavable and mass spectrometry identifiable cross-linker for protein interaction studies". *Anal. Chem*. **82**, 3556-3566, (2010).

2.3.2 Cross-linking Conditions and Efficiency

Cross-linking reactions take place transiently and spontaneously in the presence of the targeted functional group. However, a few factors will affect the efficiency of the cross-linking reactions, such as the temperature, UV-irradiation, concentration of the crosslinker reagents, the length of the reaction period, the pH value of the buffer solution, the ingredient and salt concentration of the buffer solution, *etc.*. Some of the cross-linking reaction parameters may directly determine the strength of the linkage formed, others may have a role in adjusting the cross-linking efficiency.

As is common observed in many organic and biochemistry studies, cross-linking reactions are most active for a certain range of the buffer solution's pH values. For instance, 1-Ethyl-3-[3-dimethylaminopropyl] carbodiimide hydrochloride (EDC or EDAC) and other carbodiimides reagents directly conjugate carboxyl groups to the primary amino groups of the target molecule. Such crosslinking reaction will obtain best performance under acidic conditions[86] (pH=4.5) and with the buffer solution devoid of chemicals containing extraneous carboxyl and amine groups. On the contrary, N-hydroxysuccinimide esters (NHS) and imidoesters are crosslinkers[87] that react with the primary amine groups of the biomolecule and are often used in the recipe of different carboxyl-amine cross-linking methods. The most efficient cross-linking reactions of the NHS-activated compound readily occur at the physiological to slightly alkaline conditions (pH 7.2 to 9) which will yield stable amide bond. Hence, for a carboxyl-amine cross-linking reaction that uses EDC and NHS to active and cross link molecules of interests, there is no overlap of the buffer's pH values under respective efficient reaction conditions. If such situation is inevitable when developing a crosslinking strategy, it is suggested to separate reactions for activating

[86] http://www.piercenet.com/browse.cfm?fldID=F3305493-0FBC-93DA-2720-4412D198A9C9#carbodiimide
[87] http://www.piercenet.com/browse.cfm?fldID=F330F14F-EBCC-97DB-7F6E-9664D3ACE886

corresponding functional groups under the optimal buffer conditions, and then mix the activated molecules reagents at an intermedium pH value for cross-linking reactions. A series of experiments within the range of the intermedium pH values and other reaction parameters need to be executed and examined to determine the best cross-linking conditions.

In the case of certain crosslinkers, the linkage built between targets of interest is feeble and reversible. This means that the reverse reaction is expected to take place at the same time of the according crosslinking reaction. Therefore, with enough reaction time, the cross-linking and counter-reaction rates are approaching equilibrium, where no more conjugation can be produced in the reaction environment. In general cases, if the requirement for the cross-linking reaction does not harm or adversely affect the structure and/or activity of the biomolecules, the experiment designs will allow a relatively long reaction period to link as many molecules of interest as possible. However, if the counter-reaction starts to dominate after certain reaction period, the length of reaction time must be carefully examined to avoid a long reaction period. Another reason for avoiding a long reaction period is the concern about yielding unintended aggregation of the biomolecules complex which may reduce the stability of the linkage due to the increment of the weight of the molecule aggregation. Biomolecules are usually expressed in complicated molecular structures and possess multiple amounts of the functional groups targeted by the crosslinker reagents, which may lead to unbiased conjugations between biomolecules and pile up into a molecule aggregation, instead of forming individual biomolecule compound or film evenly across the substrate.

A reaction length of 30 minutes[88] is generally suggested to begin with for most cross-linking reactions. It is also recommended to add fresh cross-linking reagents into the reaction

[88] G.T. Hermanson***, Bioconjugate Techniques***, 2nd Edition. Academic Press, Inc. 1323,(2008).

environment to maintain proper molar ratio of the crosslinker reagents and suppress the counter-reaction rate at the late stage of the cross-linking reaction procedure.

The concentration of the crosslinker should be prepared accordingly at the vendor's recommendation. Depending on the nature of the cross-linking reactions, the appropriate concentration is usually recommended to be at 20 to 500-fold molar excess. Abundant presence of the cross-linking reagents will increase the reaction rate and form as many linkages as allowed. However, it is not always deemed to be beneficial for a cross-linking reaction with an extremely excess of crosslinkers for the experiment design. The excessive reagents can raise the salt concentration of the solution, which may adversely damage the activity of the biomolecules, alter folding structure of the protein, or lyse whole cells.

For applications of immobilizing biomolecules or purifying proteins, excessive presence of crosslinkers will activate more areas of the solid base than intended, and as long as those activated sites stay open to the proceeding reaction mediums, they would introduce non-specific bindings or pollute the purified protein suspension. Also, when considering conjugating or immobilizing antibodies or enzymes to solid bases, an optimal crosslinker concentration for retaining biological activity of the biomolecules requires a moderate or even low crosslinker-to-protein molar ratio. While on the other hand, a high concentration of cross-linking reaction catalysts will be welcome for preparing immunogen conjugations, where a high degree of conjugation is helpful to saturate the presence of immunogenic probes in the buffer or on the surface of the solid base, and enables more binding sites for antigen detection and capture.

Though there exists a number of alternative crosslinker candidates and cross-linking strategies to immobilize biomolecules of interest onto the support surface, the choice of the most effective cross-linking reactions should consider the following criteria as well: if the final

linkage blocks or adversely affect the structure of the target, such as if the final complex would block or limit the accessibility of the paratope of the monoclonal antibodies; if the crosslinker will affect additional functional groups of the attached molecules such that it could bind with other molecules or reagents in the reaction environment, and introduce pollution or shorten the life time of the immobilized biomolecules; if the linkage compound incorporates easily-disassociated functional groups, which can later become the source of non-specific binding through electrostatic attractions; if the chosen crosslinker alters the surface characteristic of the support and results in a distorted structure of the binding biomolecules, which could devoid the function or activity of such molecules. To obtain the best performance conditions of the cross-linking reactions in an experiment design, it is necessary to examine vast options of the crosslinker reagents and the reaction path-ways empirically.

2.3.3 Common Cross-linking Reactions

Typical crosslinking reagents are synthesized with two general components. The most important component is the reactive groups located at either end of the crosslinker. As shown in its name, the task of such group is to react with the targeting functional groups of the biomolecules and form covalent bonds through the bioconjugation reactions. The other component is the polymer connecting reactive groups, known as the 'backbone' of the crosslinker. Since the backbone will be incorporated into the final bond of the compound, the length of the backbone directly determines the separations between cross-linked molecules.

The structure and composition of proteins are perplex and diverse, and many of them are still waiting for identification and characterization. However, the number of functional groups broadly found in protein structures is under a few dozens. Their roles in organic chemical

reactions have been studied for several decades, and various applications have been found in the field of molecular biology to polymerize or immobilize biomolecules.

The table below shows the most popular chemical groups that have been targeted in the field of biological cross-linking reactions:[89]

Reactive Groups	***Catalyst Chemical Groups***
• Carboxyl Groups (-COOH)	*Carbodiimide (e.g., EDC)*
• Amine Groups ($-NH_2$)	*NHS ester* *Imidoester* *Pentafluorophenyl ester* *Hydroxymethyl phosphine*
• Sulfhydryl Groups (-SH)	*Maleimide* *Haloacetyl (Bromo- or Iodo-)* *Pyridyldisulfide* *Thiosulfonate* *Vinylsulfone*
• Carbonyl Groups (-COH)	*Hydrazide* *Alkoxyamine*
• Phosphate Groups ($-PO_3$)	*Diazirine* *Aryl Azide*
• Hydroxyl Groups (-OH)	*Isocyanate*

The optic fiber biosensor of this dissertation takes advantages of the cross-linking reactions between carboxyl groups and amine groups with the catalyst reagents EDC and sulfo-NHS, which consists of effective chemical groups of Carbodiimide and NHS-ester respectively.

[89] Hemaprabha E., "Chemical Crosslinking of Proteins: A Review", *JESI* **1(1),** 22-26, (2012).

2.3.3.1 The Carboxyl-Reactive Crosslinkers and Reactions

In the application of bioconjugation, the carboxyl-reactive crosslinkers that contain carbodiimide compounds activate the carboxyl groups on the surface of the biomolecule of interest, and link the modified carboxylic acid to the primary amines via an amide bond for molecule labeling or cross-linking purposes.

The most popular and versatile method for activating and cross-linking carboxyl groups makes use of the carbodiimide compounds, and the most common reagent for aqueous reactions is the water-soluble EDC, and the reagent for non-aqueous organic synthesis is the water-insoluble DCC.[90]

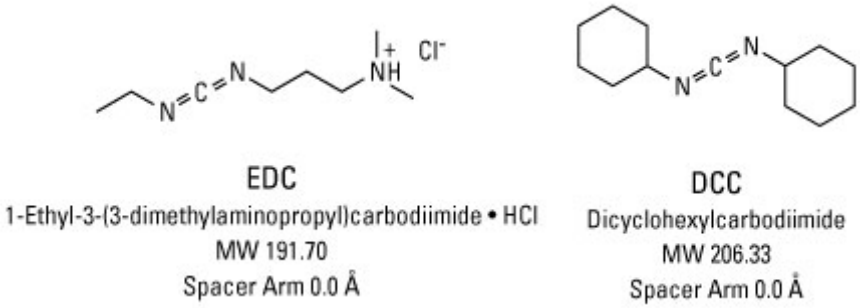

(a) (b)

Figure 2-23: (a) Water-soluble EDC (also called EDAC) is 1-ethyl-3-(-3-dimethylaminopropyl) carbodiimide hydrochloride. EDC is capable of modifying the carboxyl group and enabling reactions with amine groups to form stable amide bonds (b) Water-insoluble DCC, serve as a crosslinker to conjugate carboxyl groups to amine groups very similar to EDC, applied more often in organic synthesis.

The role of the carbodiimide compound in the cross-linking reactions is to intermediate individual biomolecules, one with carboxyl group and the other with an amine group, respectively, and after the amide bond is formed between molecules, the carbodiimide compound will be released from the linkage complex. Therefore, the carbodiimides are referred to as a zero-length crosslinker.

[90] http://www.piercenet.com/browse.cfm?fldID=F3305493-0FBC-93DA-2720-4412D198A9C9#carbodiimide

As applied in our biosensor experiments, the EDC crosslinker reacts with the carboxyl group of PCBS layer of the ISAM thin film. The crosslinker modifies the carboxyl group to form an active O-acylisourea intermediate. This intermediate complex is unstable in aqueous solution and is reversible through the hydrolysis process, which regenerates the carboxyl group and releases the N-unsubstituted urea into the reaction mix. But with the presence of the targeting biomolecules that possess an accessible primary amine group,[91,92] the intermediate complex will be easily replaced from the amino group via nucleophilic attack. The cross-linking strategy can be summarized in Fig 2-24:

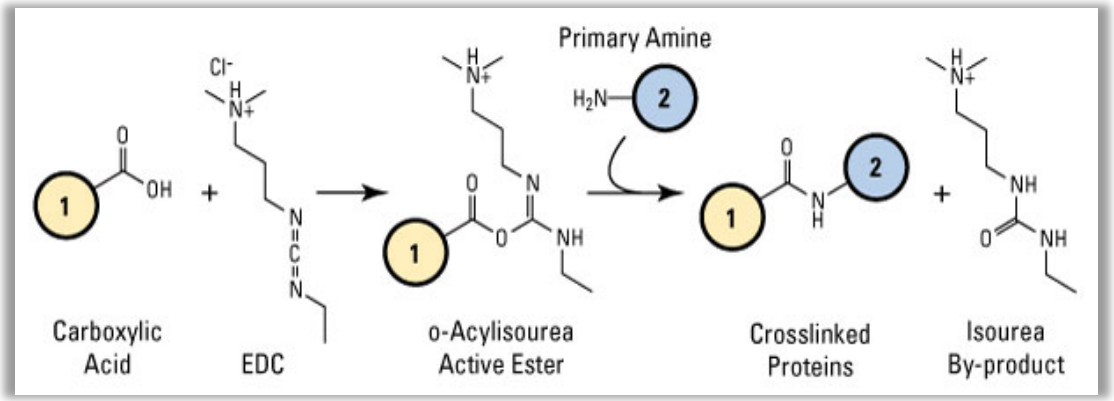

Figure 2-24: EDC activates the carboxyl group on the surface of molecule 1, which form an O-Acylisourea active ester intermediate. The intermediate is unstable, and can be easily replaced by the primary amino group on the surface of molecule 2, and release the Isourea byproduct. If the amine group is not present in the reaction mix, the hydrolysis process will reverse the intermediate complex in an aqueous environment and regenerate the carboxyl group on molecule 1.

The carboxyl cross-linking reaction through a carbodiimide compound is most efficient in acidic buffer conditions with the pH range between 4.5 and 5.5. Such reaction also requires a buffer environment devoid of extraneous reagent with carboxyl and amine groups, otherwise the

[91] A.Panchaud, *et al.,* "Anibal, stable isotope-based quantitative proteomics by aniline and benzoic acid labeling of amino and carboxylic groups". *Mol. Cell. Proteomics*. **7**, 800-12, (2008).
[92] S.Yamashiro, *et al.* "Mammalian tropomodulins nucleate actin polymerization via their actin monomer binding and filament pointed end-capping activities". *J. Biol. Chem*. **285**, 33265-80,(2010).

carbodiimide will also react with buffer reagents and yield non-specific bindings. A very common buffer candidate for carrying out the carboxyl-reaction cross-linking reactions is MES (4-morpholinoethanesulfonic acid). However, in most biochemistry applications, PBS buffer has been extensively used to preserve proteins, peptides, whole cells and so on, since it is capable of maintaining a stable salt concentration and pH value of the suspension. Bioconjugation experiments that must be performed in PBS buffer is compatible with the cross-linking chemistry at a pH value lower than 7.2, though with a reduced reaction efficiency. Elevating the concentration of EDC may help compensate the loss of the reaction efficiency.

In order to achieve better carboxyl-amine cross-linking productivity, NHS (*N*-hydroxysuccinimide) or its water-soluble analog sulfo-NHS can be included in the bioconjugation recipe with EDC. As has been discussed previously, the *O*-acylisourea intermediate is unstable and the compound can be easily reversed if the reaction environment of the mix varies. Addition of sulfo-NHS will replace the *O*-acylisourea intermediate with the amine-reactive sulfo-NHS ester, which is considerably more stable and can sustain transportation or storage of the carboxyl-activated materials in dry form without losing reactivity. The Fig 2-25 shows three reactions occurring simultaneously in the reaction environment, where carboxyl groups of molecule 1 are modified to couple with primary amines of molecule 2 through crosslinkers EDC and sulfo-NHS:

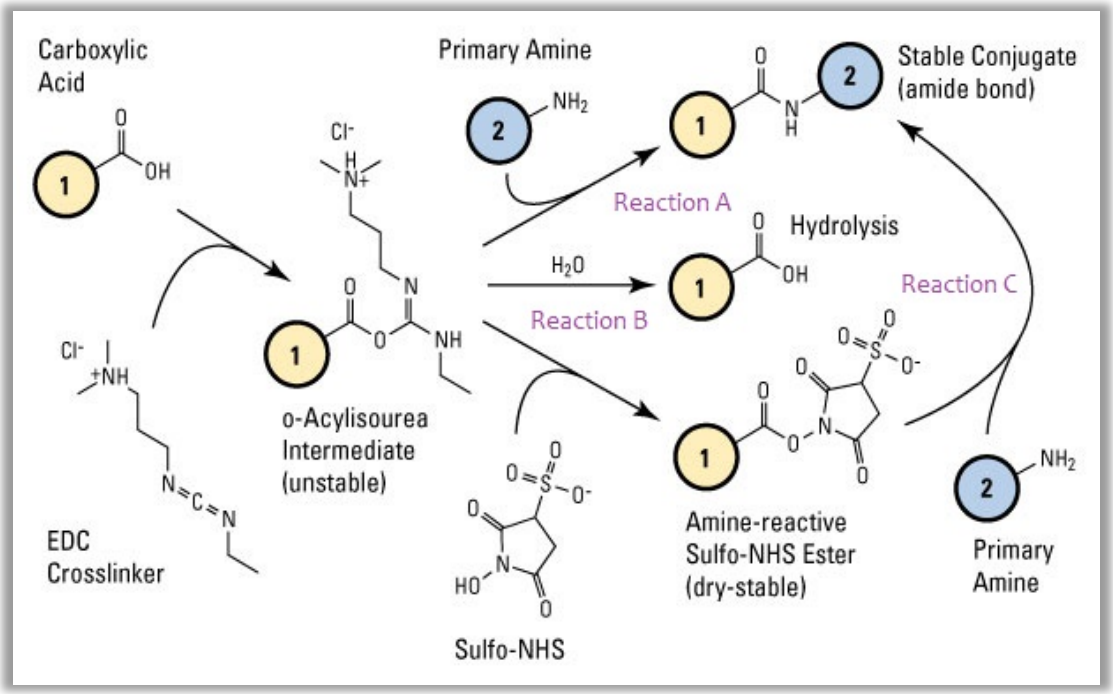

Figure 2-25: A very common cross-linking reaction to link molecule 1 which has a carboxyl group on the surface, to molecule 2 which has a primary amine group. EDC and sulfo-NHS serve as the crosslinkers. Three reactions occur simultaneously: Reaction A links the intermediate from EDC modified molecule 1 directly to the primary amine of molecule 2; Reaction B is the counter-reaction of the EDC modification reaction and regenerates molecule 1 in its original form; Reaction C further modifies the intermediate complex of molecule 1 and generates a stable sulfo-ester compound, which is more stable and reactive with amine groups more efficiently.

The carbodiimide crosslinker EDC is also capable of modifying the phosphate group with the presence of imidazole, and linking it to the amine group.[93] The 5' phosphate group can be located at the 5' end of DNA strands, it also exists at the termini among a large range of RNA strands and can be activated for cross-linking reactions. Therefore, EDC and analog carbodiimide crosslinkers can be useful in DNA or RNA coupling experiments for immobilizing or labeling the targeting strand to the amine groups of biomolecules or solid bases.

[93] http://www.piercenet.com/files/TR0030-Modify-oligos.pdf

An example of chain reactions to cross-link a biomolecule with a 5' phosphate group at its surface to the primary amine group of molecule *R* is illustrated in Fig 2-26:

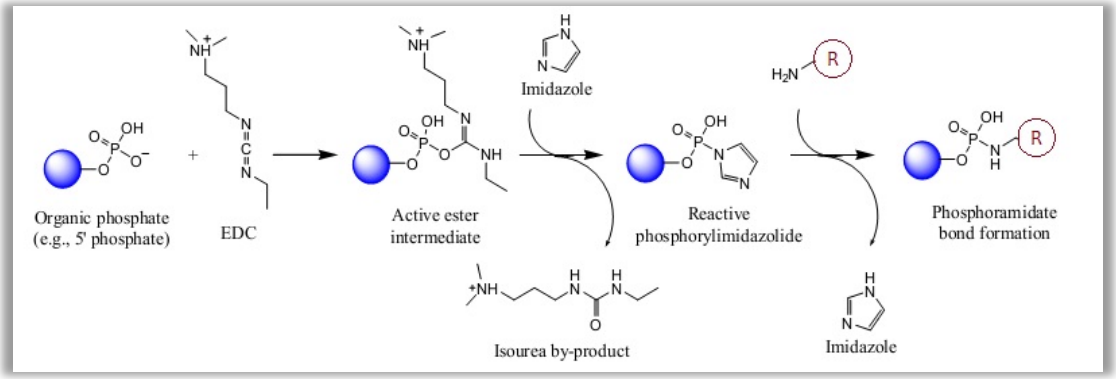

Figure 2-26: An example of chain reactions to couple two molecules with a phosphate group and an amine group, respectively, with crosslinker reagent of EDC and imidazole.

Depending on the goal of the cross-linking reaction and the characteristic of the molecules involved, there are a few alternative cross-linking strategies to fully explore the capacity of the EDC/Imidazole crosslinkers, such as labeling the oligonucleotide with biotin, creation of a sulfhydryl-reactive oligonucleotide or sulfhydryl group on the oligonucleotide, immobilization of oligonucleotide to a beaded support and so on.

Carboxyol-to-Amine crosslinkers and reactions have special advantages in bioconjugation experiments involving proteins and peptides, since they both contain primary amine groups and carboxyl groups at the C-termini and N-termini of the primary molecular structure respectively, which can be useful to posit the molecule correctly to the solid support. Therefore carbodiimide crosslinkers have been popular candidates in many bioconjugation studies and applications.

Crosslinkers such as EDC and DCC have been proven to be versatile and useful in various experimental applications for immobilization onto solid surfaces, affinity binding with carrier beads, labeling or purifying the proteins or peptides, covalently conjugating biomolecules with

other polymer materials which possess carboxyl or amine groups on the molecule surface, protein analysis, cell detections and so on.

2.3.3.2 Amine-Reactive Crosslinkers and Reactions

Amine-reactive cross-linking reactions have been predominantly used in the area of proteins and peptides labeling and coupling, especially when antibodies[94] are involved. Primary amine groups can be universally located at the N-termini of polypeptide chains and C-termini of proteins as well as the side chain amino acid residue of lysine (Lys, K). The primary amine groups possess positive charges at the physiological pH in buffer solution, which allows the amine group to be exposed to the aqueous medium and hence can be easily accessed by the addition of cross-linking reagent targeting amine groups. Furthermore, among other common functional groups targeted in typical bioconjugation experiments, the primary amine group has been found to be particularly nucleophilic, which makes it easier to locate and react with at the presence of certain amine-reactive chemical groups.

Another reason that amine-reactive crosslinking chemistry is popular and simple to apply is due to the fact that numerous chemical groups have been found capable of covalently binding with the primary amine group and forming stable conjugation, such as isothiocyanates, isocyanates, acyl azides, NHS esters, sulfonyl chlorides, carbonates, aryl halides, imidoesters, carbodiimides, anhydrides, and fluorophenyl esters.[95] Most of these chemical groups react with amine groups through either acylation or alkylation.

A primary amine group can react directly with a carbodiimide-activated carboxyl groups to form a stable amide bond, as has been shown in the previous section. However, most

[94] Greg T. Hermanson, ***Bioconjugate Techniques, 2nd Edition***, Academic Press, Inc., (2008).
[95] http://www.piercenet.com/browse.cfm?fldID=F330F14F-EBCC-97DB-7F6E-9664D3ACE886#imidoester

bioconjugation applications which specifically target amine functional groups prefer the cross-linking strategy which uses NHS-ester incorporated synthesis as catalyst.

The NHS-ester activated primary amine group most efficiently at the physiological pH to slightly alkaline conditions (between 7 and 9), where an amide bond is produced with the release of a NHS molecule or its analog, sulfo-NHS, depending on which has been applied to prepare and activate the molecule. The reaction can be triggered at either 4 ℃ or at room temperature, however a reduced temperature of the reaction environment is preferred for enhancing the cross-linking reaction efficiency. The reaction can be described in the Fig 2-27:

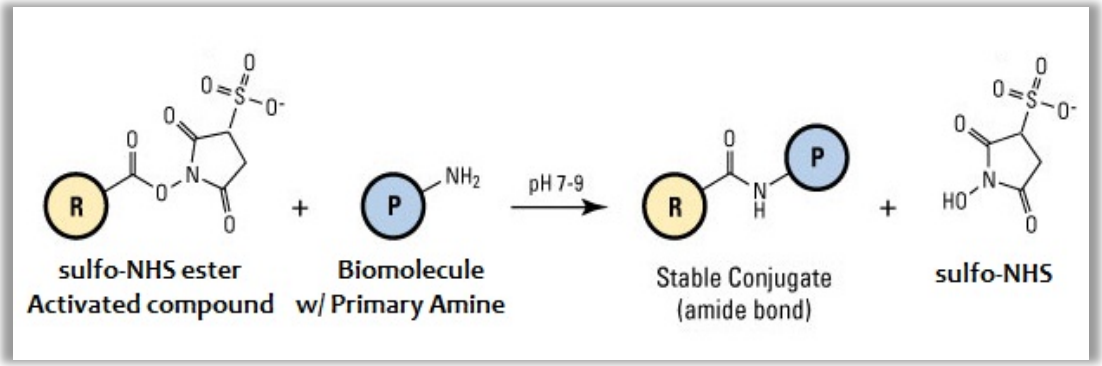

Figure 2-27: Molecule *R* with a sulfo-NHS ester on its surface reacts with the primary amine group on the surface of biomolecule *P*, which yields a stable amide bond and release a sulfo-NHS per generated bond.

Though cross-linking reactions targeting primary amine groups via NHS ester are simple and rapid, the instability of the NHS ester compound within the aqueous medium still brings concerns. The hydrolysis of the ester compound occurs simultaneously with the cross-linking reaction and competes with the primary amine during the process. The hydrolysis rate depends on the temperature and pH of the reaction mix. Higher reaction environment temperature and pH value of the buffer will reduce the reaction efficiency. The reaction efficiency deteriorates quicker at low protein concentration. The half-life of the hydrolysis process of the NHS-ester

compound is 4 to 5 hours at pH 7.0 and 0 ℃, and speeds up to 10 minutes at pH 8.6 and 4 ℃.[47] The buffer solution must not have any reagents containing primary amine group. Therefore, primary amine buffers such as Tris(TBS) and glycine should not be used in the amine-reactive cross-linking reactions. Nevertheless, in some experimental cases, when the cross-linking reaction need to be quenched or the leftover of the NHS-ester compound must be removed from the reaction mix, it can be beneficial to add the buffer solution mentioned above into the reaction environment to halt the bioconjugation reactions.

Another disadvantage of adopting NHS as the crosslinker is its poor water solubility. Since most bioconjugation experiments are performed in aqueous conditions, the low water solubility of the NHS or the molecules with a NHS-ester compound will significantly suppress the cross-linking reaction because of the short supply of dissolved NHS molecules in the reaction medium. A solution is to use the analog synthesis sulfo-NHS instead. Sulfo-NHS is essentially identical to NHS regarding its functionality as an amine-reactive crosslinker. The difference is sulfo-NHS owns an additional sulfonate ($–SO_3$) group on the *N*-hydroxysuccinimide ring. This extra sulfonate group does not affect the chemical function of the *N*-hydroxysuccinimide ring, yet greatly improve the water solubility of the sulfo-NHS or the molecule that owns the ester compound. Moreover, the sulfonate group expresses a negative charge in the aqueous medium, which will prevent the sulfo-NHS molecule or the molecule with the sulfo-NHS ester compound from penetrating the cell membranes. Therefore sulfo-NHS or molecules with its ester compound can be safely used for crosslinking protein or genetic targets that locate at the cell surface and performing cross-linking with whole cells. By contrast, when an inside-cell cross-linking reaction is desired and the corresponding amine-group is targeted, sulfo-NHS ester reagent has to be replaced by NHS ester reagent, even though it has a low water-solubility.

For crosslinking strategies that would not find favorable of a sulfonate group, or if using sulfo-NHS ester reagents may be too expensive, using the water-insoluble NHS-ester reagents can still work, though they need to be dissolved into water-miscible organic buffer first, such as DMSO or DMF, before mixing with the reaction buffer in aqueous form. The typical organic solvent-carryover takes about 0.5 to 10% volume portion of the final reaction buffer.

Some amine-reactive crosslinkers have two identical NHS ester or sulfo-NHS ester groups at both ends of the molecular structure, which is compatible for homobifunctional cross-linking reaction and conjugating proteins of the same sort or couple proteins with other biomolecules which also carry a primary amine group. The typical reagents for carrying out such task are DSS and BS3. Their molecular structure is shown in the Fig 2-28.

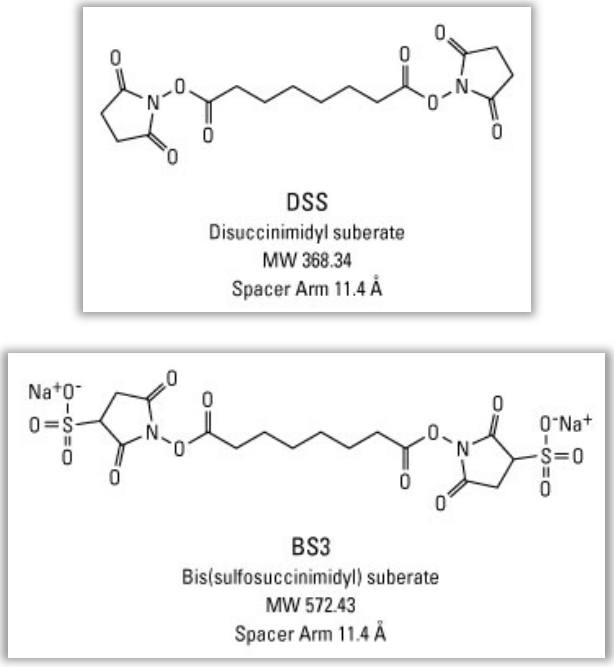

Figure 2-28: Molecular structure of DSS and BS3 (sulfo-DSS), which are both good for carrying out amine-to-amine cross-linking tasks. DSS has NHS-ester compound and has a low water-solubility, though it is capable of penetrating the cell membrane and perform cross-linking reaction inside the cell; by contrast, BS3 owns sulfo-NHS ester compound, and is good for catalyzing amine-reactive bioconjugation experiments in aqueous environment.

Another widely used amine-reactive crosslinker reagent is imidoester. Imidoester requires a higher pH value of reaction buffer for bioconjugation. The reaction develops rather rapidly, however with a shorter half-life. Cross-linking reactions via imidoester at pH 10 have been proven to be most efficient, though amidine favors a reaction environment between pH 8 and 10. When the reaction buffer is set below pH 10, side products or intermediates will be formed, which may react with the remaining amine group and result in the N,N'-amidine derivatives. While at a higher pH value, the amidine bond formed in the cross-linking reaction can be unstable and reversible, and thus compromises the purpose of the bioconjugation. The narrow range of the reaction conditions and strict requirement for a stable pH value of the reaction environment limit the broad application of imidoester as amine-reactive crosslinker, especially when considering cross-linking amine groups to carboxyl groups, where a modified carbodiimide compound intermediate survives at a physiological to acidic environment and whose half-life can be significantly reduced at the compatible pH value for imidoester cross-linking reactions.

Imidoester is mostly used in homofunctional cross-linking reactions. Furthermore, the amidine bond formed between an imidoester compound and protein will possesses a positive charge when dissolved in buffer solutions at physiological pH, meaning the bond replacing the amine group will express the identical charge-property of the original protein, and such characteristic can be useful in certain applications.

The imidoester-to-amine cross-linking reaction chemistry can be described as:

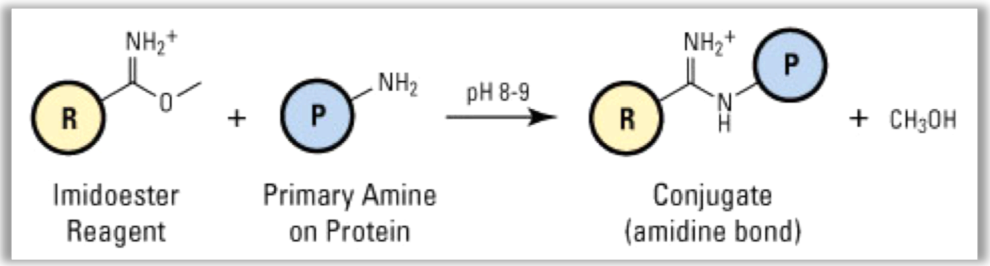

Based on the reaction nature of the imidoester and the amidine bond it forms, most amine-reactive bioconjugation protocols still use NHS-ester as the reaction activator and catalyst.

2.3.4 Application of Carboxyl-to-amine Cross-linking Reaction in Building the TAP-LPG Fiber Biosensor

With understandings of the roles of sulfo-NHS and EDC in the carboxyl-amine crosslinking chemistry, we will follow the protocol where they are used side by side in the affinity binding reactions and immobilizing biology receptors onto the ISAM thin film of the LPG fiber.

The receptors in our biosensor application include monoclonal antibodies, which are proteins and have a primary amine group at the biopolymer end of FC region. With the addition of EDC and sulfo-NHS crosslinkers, the amine groups of the antibodies and carboxyl groups of the ISAM surface will be activated, and react to form amides bonds, which then bind the antibody molecules onto the fiber surface.

Figure 2-29 below illustrates the general structure of the LPG-biosensor:

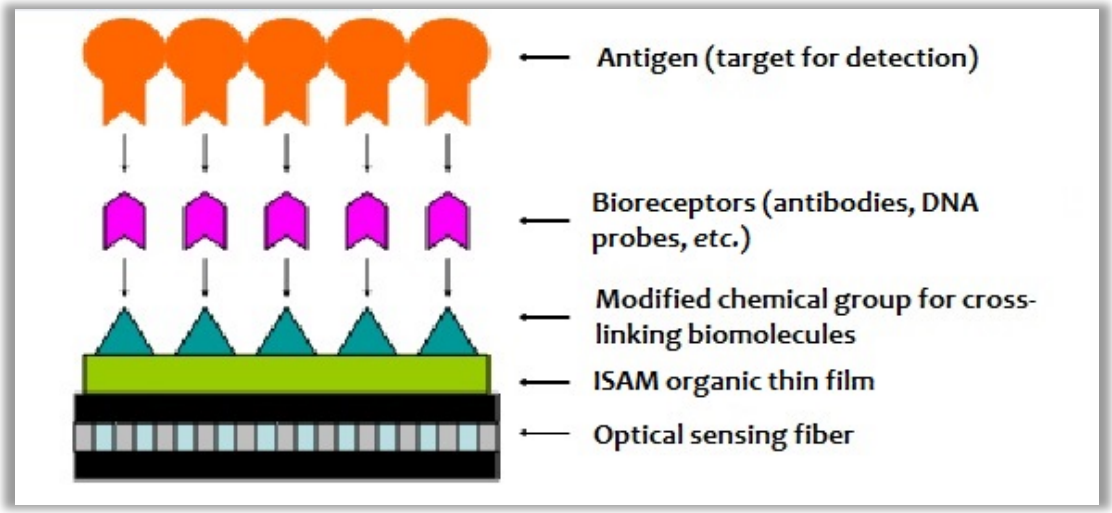

Figure 2-29: General structure of the biosensor. The cross-linking reactions occur with chemical groups on the surface of the bio-affinity ISAM thin film, and attach the detection bioreceptors onto the fiber.

Based on the characteristic of the target bacteria, various bioreceptors can be selected and incorporated into the biosensor system to perform detection and differentiation tasks, such as monoclonal antibodies, polyclonal antibodies, DNA/RNA probe, enzymes, whole cells *etc.*. The bioreceptor compound can be properly posited and firmly linked to the film surface through carefully constructed cross-linking reaction chains. For instance, in order to immobilize biotinylated DNA probe, one possible arrangement of the receptor structure begins with building a sulfo-NHS-biotin layer as the basis, which reacts with carboxyl-group of the PCBS top layer of the ISAM thin film. On top of that, a streptavidin protein layer will be deposited, which possess four biotin-binding sites per molecule to capture lock in the biotinylated DNA probes.

The dynamic and versatile nature of the cross-linking chemistry has provided flexible and abundant options of cross-linking strategies, which can be adopted to attach and immobilize various biology receptors onto the organic polymer films of the fiber sensor. Therefore, the biosensor prototype we proposed has enormous potential in applications of detecting a broad range of bacteria, viruses and other biomolecules which would threaten public health, pollute environment, or contaminate food. Simply by changing the bioreceptor type, this biosensor prototype has already achieved successful demonstration in sensing and differentiating bacteria, including MRSA, *Francisella*, *Brucella*, *H. Somni* and so on. These studies will be presented in the remainder of this dissertation.

2.4 Implemention of immunology Techniques for Biosensing

2.4.1 Overview of Immunology

The Immune system is the primary defense of the human body and other vertebrates[96,97] against foreign pathogens or abnormal changes occurring to the organs such that the proper functions of living tissues, organs and the inner circulation system may be potentially or essentially compromised or damaged. The working status of one's immune system is a reflection of a person's health. It is designed to provide valuable protection against the health risks lurking around human bodies, and point out which organ system is having trouble and what the possible cause might be. The immune system will also respond to any disorders or malfunctions of the organism's health and try to restore it back to the regular state, such as creating antibodies that recognize specific problematic targets, tracing the locations of the antigens presented, removing threats from the human body with the help of white blood cells and lymph fluids, or aggressively removing massive impaired tissues to protect healthy portions from being affected. Through judging the body's responses triggered by the immune system, medical professionals are able to discover the source of the symptoms and ailment, which can lead to a sound diagnosis. The immune system plays a significant role in our daily lives to maintain our bodies functioning properly and keep them free of impending attacks by microorganisms from inside or outside.

Immunology is the study of identifying the relationships between the immune system, pathogen and other disease processes[98]. The development of immunology is aimed at understanding the interactions between antibodies and antigens, and the cellular response of such interaction. In the central scope of this subject is the role of antibody.

[96] Litman G., Cannon J., Dishaw L., "Reconstructing immune phylogeny: new perspectives." *Nat Rev Immunol*. , **5 (11)**: 866–79, (2005).
[97] Gregory B., Habicht G.S., "Immunity and the Invertebrates", *Scientific American*. **November 1996**: 60–66, (1996).
[98] http://en.wikipedia.org/wiki/Immunology

An antibody (Ab) is a special type of glycoprotein, which belongs to the immunoglobulin superfamily. An antibody can also be interchangeably called an immunoglobulin (Ig). The primary structure of antibodies is Y-shaped, as shown in Fig 2-30. There are two identical antigen binding sites, called paratopes, at both tips of the outstretched arms (known as light chain) of the antibody structure. Each of the binding sites is identical as the other, and is capable of recognizing and capturing a specific antigen (Ag). The antibody binding sites and antigen pairing interaction can be analogous to the relation between a key and a lock, where the paratope on the antibody only locks in with one particular epitope of an antigen and distinguishes such antigen from others.

The region that an antibody detects as unique on the antigen is called the epitope, also known as *antigenic determinant*, which is a class of protein and always located at the membrane of the antigen cells. Epitopes accessible to antibodies are expressed on the surface of the organism.

The epitopes are composed of a sequence of amino acids, and by themselves, these epitopes do not necessarily have a particular function to the host cell. Based on the structure and interaction between epitope and paratope, the epitopes can be categorized into two groups: conformational epitopes and linear epitopes. The former epitopes come in direct contact with the paratopes of the immune system, and are detected through their 3D shape in the protein structure; while the latter epitopes are less common in the antibody-antigen interaction, and they are recognized through their primary protein structures.

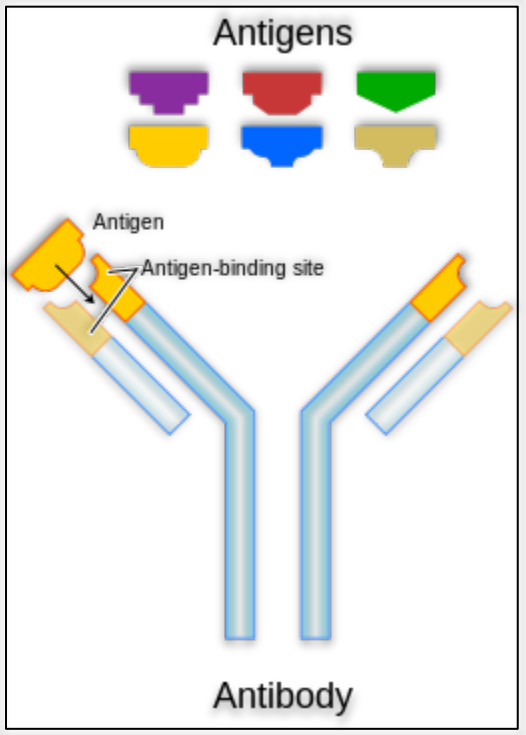

Figure 2-30: The general structure of a monoclonal antibody molecule. The primary structure of an antibody is Y-shaped, with two antigen-identification sites at both ends of the outstretched arm section of the molecule. Each identification and binding sites is capable of locking with one antigen target, and both sites are identical in characteristics and functionality. Monoclonal antibodies are specific to a single type of antigen, therefore they won't bind with antigens from contrasting species.

The antibody-antigen interaction is so exclusive that in most cases, an antibody will even ignore the presence of pathogens from related genera. Therefore, there is a huge family of antibody types, where each one is designed and produced against only one specific type of antigen. However, some antigen species with similar epitopes may bind loosely with other antibodies, such binding is one form of nonspecific binding and is not uncommon when compared with specific antibody-antigen binding.

In the immune system of humans, antibodies originate from B-cells as part of the adaptive immune response. The membrane of B-cells is filled with proteins known as "B-cell receptors",

which are composed of a membrane-bound antibody and a signal transduction protein complex. The membrane-bound antibody is a typical antibody that has two unique and randomly determined binding-site, to ensure the attachment to the antigen. The signal transduction moiety is bound together with the membrane-bound antibody by disulfide bridges, which are responsible for propagating the antibody-antigen binding information in the B-cell and activating it. Each B cell carries one specific type of receptor, which recognizes and binds with one particular antigen. Every day the human immune system generates millions of unique B cells, which will later enter and circulate in the blood and lymphatic system of human bodies to monitor any pathogenic intrusions. The large amount of different types of B cells ensure a high probability of recognizing foreign antigens that may not have been identified before and alerting the immune system of danger at early stage of infection.

Upon contact of the cognate antigen, the B cells will be activated and differentiated into one of two cells – plasma B cell or memory B cell. The plasma B cells duplicate the antibodies that are unique to the one embedded into the cell's receptor complex, and releasing those antibodies into the blood system. These antibodies will bind any remaining antigens matching its type, and help phagocytic cells, the liver and spleen to sweep away the antibody-antigen complex, resulting in the elimination of the intruding antigen threat. The plasma B cells are short-lived cells that die after the antigen threat has been thoroughly dealt with. By contrast, the memory B cells have a long cell life and will remain within the blood and lymphatic systems for decades. These cells are able to response quickly to any ensuing exposures to the same antigens after the first response. Simply speaking, the memory B cells carry the signature information of the cognate antigens from its first appearance in the blood and lymphatic systems, and can react more efficiently to later encounters by the same type of antigens.

Such function of memory B cells have been studied by biomedical researchers and used to produce vaccines, often based on weakened or killed forms of the microbes. The vaccine will trigger the active response of the immune system to the microorganisms and stimulate B cells for antibody production, without causing real damage to the organs or body systems they are designed to protect. The weakened or killed vaccine microorganisms can be easily terminated by the receptor's immune system, while during the process some of the B cells will be transformed into memory B cells, which will record the key epitope configuration of the vaccine microbes. The epitope configuration of an antigen distinguishes its species from others, therefore when the memory B cell meets a familiar epitope configuration while circulating around the immune system, they can secrete the corresponding antibodies immediately without trying to match the antigens with large numbers of randomly generated original B cells. In principle, the vaccine microbes activate B cells ahead of any actual infections, and prepare the receptor's immune system for a possible attack by antigen-induced diseases in the future.

2.4.2 Biological Receptor

The immune system's response to an intruding pathogen relies on the recognition of its types and specie through biological receptors. The biological receptors can vary in composition, yet each of them is exclusive to one specific species of pathogen or antigen. Most of the immune receptors are proteins located on the cell's membrane and wander with the carrier cells along the circulation and/or immune system, and bind with the cognate antigens upon contact. However, there are other types of immune receptors that are specifically designed in the laboratory, whose binding ability and specificity have been enhanced.

Common biological receptors[99] include Fc receptors, B cell receptors, T cell receptors and so on. This dissertation will focus on the characteristics and applications of antibody-antigen interactions, as well as the DNA probes for detecting microorganisms.

The Fc receptor can be found on the membrane of immunological detection and conjugation with pathogens. The binding between the Fc receptor and antibody-antigen complex will activate the immune cell that carries the receptor, and stimulate antibody-mediated phagocytosis or antibody-dependent cell-mediated cytotoxicity[100] to destroy the invading pathogen or infected cells. Figure 2-31[101] illustrates a typical reaction between an immune cell with an Fc-receptor and the antibodies bounded microbe.

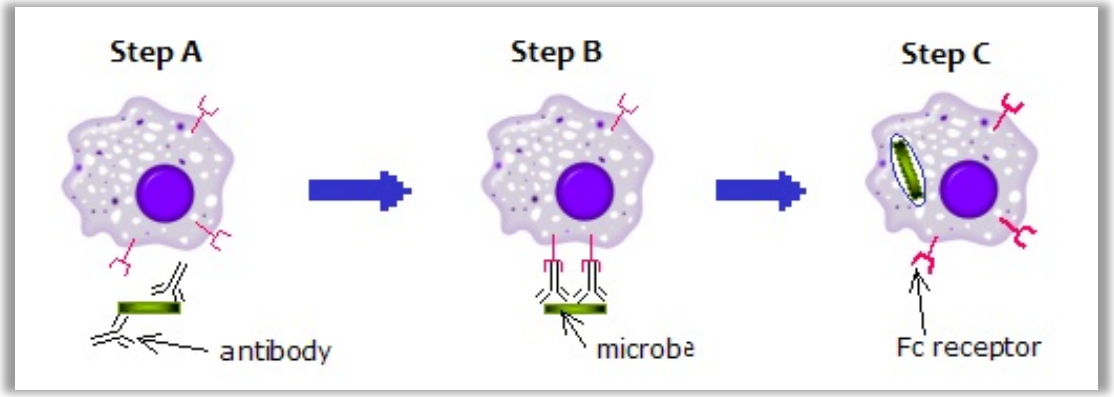

Figure 2-31: The figure shows a typical phagocytosis of a microbe. Step A, the antibodies recognize the invading pathogen and attach to it with their Fab detection region. Step B, the immune cell with the Fc receptor combines with the antibodies that are bounded to the microbe. Step C, the Fc receptor stimulates the immune cell to phagocytize and terminate the microbe.

[99] Lippincott Williams *etc.*, ***Lippincott's Illustrated Reviews: Immunology*** (ISBN 0-7817-9543-5), Page 20, (July 1, 2007)
[100] Peter Parham, ***The Immune System***, Garland Science, 2nd edition.
[101] http://en.wikipedia.org/wiki/Fc_receptors

There exist a few classes of Fc receptors,[102,103] where each of them differs in binding affinity to the antibody. For example, the Fc-receptor that binds to the mostly common class of antibodies—IgG, is named as *Fc-gamma receptors* (FcγR). Similarly, those that bind with IgA and IgE are called *Fc-alpha receptors* (FcαR) and *Fc-epsilon receptors* (FcεR), respectively.

2.4.3 Immunoassays and Immunological Tests

The versatile immunological interactions have inspired and motivated researchers to take advantage of the affinity binding reactions and develop analytic biochemistry assays for creating diagnostic tools, pathology studies, quality control in industry, detection of analyte in the homogenate or extract tissue samples, *etc.*. Among all biochemistry techniques developed through affinity binding interactions, the most widely and commonly used tests are ELISA and Western Blotting tests.

The ELISA test, or enzyme-linked immunosorbent assay, is a test that exploits the specific binding between antibodies and their cognate antigens, and uses enzyme-linked molecules to color (or not, if no binding occurs) the sample suspension as the testing result indicator.

In a sandwich ELISA procedure, illustrated in Figure 2-32, the assay starts with immobilizing the capture antibodies onto a solid substrate (usually in multiple-well polystyrene plates). Then, the coated substrate is exposed to antigen, followed by primary antibodies that are specific to the antigen and then enzyme-linked secondary antibodies. Primary antibodies and secondary antibodies need to be harvested from distinct animals species to minimize the chance of non-specific bindings. Additionally, the wells need to be thoroughly washed between each step to remove unbound antigens and antibodies. If the specific antigen is in presence of the

[102] Janeway, Charles A.; Travers, Paul; Walport, Mark; Shlomchik, Mark. ***Immunobiology.*** 5th ed.. New York and London: Garland Publishing; c2001.
[103] Abul K. Abbas, Andrew H. Lichtman ; illustrations by David L. Baker, Alexandra Baker. ***Cellular and molecular immunology.*** Philadelphia, PA : Elsevier Saunders, c2005

sample tested and captured, the enzyme or tagging molecules of the complex[104] will generate color or other type of detectable signal.

In order to quantitatively analyze the concentration of the sample antigen, a serial dilution of known-concentration of antigens needed to be made and tested with ELISA. The optical density (OD) of antigen at each concentration can be determined separately in the inhibition array, and summarized into a standard OD-concentration curve. For ELISA test of an unknown concentration antigen sample, researchers can simply compare the OD value from the preceding built standard curve, and find the corresponding concentration value of the sample suspension. Figure 2-33 illustrates the plate matrix for quantitative comparison and determination of antigen concentration in a double antibody sandwich ELISA assay.

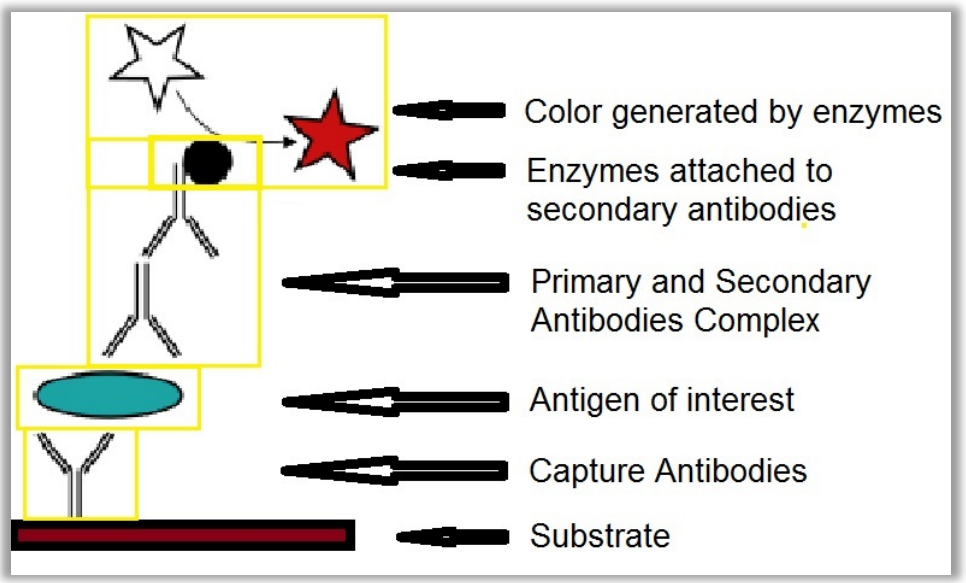

Figure 2-32: A complex in an ELISA test. Capture antibodies are immobilized onto substrate well first, then antigen will be captured, if in presence. Primary and secondary antibodies complex will be formed on top of the bound antigen, which will color the solution to indicate the existence of the antigen-antibody complex. Source: [105, 106]

[104] http://www.piercenet.com/browse.cfm?fldID=F88ADEC9-1B43-4585-922E-836FE09D8403
[105] http://en.wikipedia.org/wiki/Immunoassay

Figure 2-33: A 96-well microtiter plate used for performing a human anti-IgG, double antibody sandwich ELISA.[106] The deeper the color of the well is, the higher the antigen concentrations are.

The basis of a successful ELISA assay depends mostly on quality of immobilizing antigens (in direct and indirect assays) or capture antibodies (in sandwich assays) on the solid surface. Therefore, when developing a specific ELISA assay, it is natural and essential to optimize the plate-coating conditions for the antigens or capture antibodies of interest. Unlike some biochemistry experiments that require a low protein binding container or substrate, the plate well for ELISA assays usually favor microplates with a minimum protein-binding capacity of 400 ng/cm^2, and a low binding variation. The low binding variation guarantees that the amount of the antigen adsorbed by the solid substrate would only depend on its original concentration in the serum or sample suspension, so that the quantitative analysis can be trustworthy and reliable as the antigen binding condition remains the same when comparing an unknown-concentration ELISA assay result with the points on an OD-curve from known-concentration ELISA assays.

[106] http://en.wikipedia.org/wiki/ELISA

The coating of antigen or capture antibodies occurs passively and spontaneously via hydrophobic interactions between the substrate and non-polar protein residues, though in some cases the plates need to be prepared to meet the optimal binding conditions. The process is usually performed in an alkaline buffer such as phosphate-buffered saline (pH 7.4) or carbonate-bicarbonate buffer (pH 9.4) with the molecule of interest concentration within the range of 2-10 μg/ml. Low protein concentration will help the process of substrate adsorption. Nevertheless it will reduce the assay sensitivity and prolong the experiment length to obtain detectable signals. A typical ELISA assay can be conducted at 4 – 37 °C, and initial incubation of antigens or capture antibodies can take several hours to overnight, depending on the optimal conditions for coating each individual type of protein. The concentration of capture antibodies is usually high to ensure its coverage of the plate surface to be as large as possible. Though for subsequent steps when primary and/or secondary antibodies are applied, the concentrations are usually set lower than the maximum binding capacities. This is because the primary structure of antibodies has two outstretched arms, which can trap or hook nonspecific binding or unbound proteins from being washed off by washing buffers.

Except for rare cases, the ELISA assays require a blocking step before applying the primary antibodies to ensure that all the empty binding sites on the substrate are well covered by the blocking reagent and unavailable for antibodies or other protein bindings in the subsequent steps. The blocking reagent can be a solution of irrelevant proteins, mixture of proteins (such as milk solutions) and so on. An ideal blocking reagent should be able to cover every nonspecific binding site, without diminishing the amount of available specific binding sites. There is no ideal blocking reagent for each antigen of the ELISA assay, the best blocking reagent formula needs to be determined through empirical tests. An inadequate amount of blocking reagent will raise the

non-specific binding rates and create higher background noise, while excessive blocking reagent can bind with specific binding sites and consequently reduce the sensor's sensitivity to the antigen detection. General purpose blocking and washing buffers for ELISA assays are available commercially (Thermo Fisher Scientific Inc.: N502). Most blocking reagents are prepared in the laboratory before usage. Depending on the characteristic of the substrate surface to be blocked and the purpose of the experiment, a few common blocking options can be considered, including detergent blockers (such as Tween 20 and Triton X-100, which are non-ionic detergents), protein blockers (such as bovine serum albumin (BSA), non-fat dry milk or casein, whole normal serum, and fish gelatin), and miscellaneous blockers (such as polyethylene glycol (PEG), polyvinyl alcohol (PVA), and polyvinylpyrrolidone (PVP), usually for hydrophobic surface blockings). Ten percent whole sera are recommended when facing extremely difficult non-specific binding situations.[107] Blocking agents containing 10% serum from the host to which the enzyme conjugated secondary antibodies was made of can reduces nonspecific binding of secondary antibodies.

Washing the plate thoroughly between each step is also critical for improving the assay's sensitivity and obtaining the best signal-noise rate. Insufficient washing may result in residual unbound proteins or molecules, which will increase the chance of creating false positive signals as well as background noise; while excessive washing may damage the antigen-antibody complex, or even remove the entire complex from the substrate surface. Therefore, a gentle yet firm rinsing step needs to be evaluated to ensure the best outcomes of the assay. Tris-buffered saline (TBS) and phosphate-buffered saline (PBS) at physiologic pH and without additional agents are common washing buffers used in ELISA assays. Detergents such as 0.05% Tween-20 are usually included in the formula of the washing buffer to remove nonspecific bound molecules.

[107] http://catalog2.corning.com/Lifesciences/media/pdf/elisa3.pdf

However, a high-purity for the detergent is essential for preventing the introduction of the impurity pollution.

For sandwich ELISA assays, the spontaneous adsorption process does not guarantee a proper orientation of the capture antibodies. If the capture antibodies are attached to the substrate through residues on the Fab branches, or on the side chain residues in the Fc branch, one or both of the antigen binding sites will be facing towards the plate. This cause inaccessibility to the antigens they are supposed to bind with, which results in a lower antigen binding capacity. The deposition process may also cause the denaturation of antibodies, or introduce contaminants. Therefore, direct deposition of antibodies onto the solid substrate in a sandwich ELISA assay is usually avoided. Instead, a base layer of affinity-purified antibodies is usually coated onto the plate first. These proteins can be Protein A, G or A/G recombinant protein. Such proteins express specific and high binding affinities to IgA, IgE, IgG, IgM and so on only through the Fc heavy chain regions. Depending on the types of the capture antibodies used in the assay, proper protein candidates can be selected to coat the plate ahead of applying the antibodies to preserve their binding capacities. Commercial products that have a coated wall layer of glutathione, metal-chelate, streptavidin or NeutrAvidin Protein are available and ready for applying capture antibodies or other proteins directly in a sandwich ELISA assay.

In a sandwich ELISA assay, monoclonal and polyclonal antibodies can both be used as capture and detection antibodies. However, polyclonal antibodies are more common as the capture antibodies, since they have multiple antigen-binding sites on each molecule and are suitable for adsorbing as many antigens as possible from the serum or sample suspensions. In contrast, monoclonal antibodies are considered a better candidate as detection antibodies, since they provide an improved specificity compared to polyclonal antibodies and are able to

differentiate antigen epitopes with slight differences. Nevertheless, when designing a Sandwich ELISA assay, the capture antibodies and primary/secondary antibodies have to be of different animal species so that the secondary antibody does not bind to the capture antibody. The capture and detection antibodies that satisfy all the mentioned criteria are called "matched pairs".

The most popular tag molecules for an ELISA assay are enzymes, which will convert a substrate into a detectable product. The production rate depends on the amount of enzyme present and the allowed length of the reaction period. Therefore for a given length of the reaction period, the amount of detectable products reflects the proportional amount of antigen immobilized and conjugated with the detection reagents. The variety and flexibility of detectable products generated by enzyme-linked antibodies gives the ELISA assay vast applications. Other signal conversion options in ELISAs include using radioactive or fluorescent tags.

The ELISA has received a widespread popularity among university biochemistry laboratories, biopharmacy corporations' R&D centers, medical laboratories in hospitals and other versatile applications in microbiology and drug screening. The quantitative ELISA has become a standard test to evaluate the concentration of an antigen present in serum or sample suspensions, before proceeding with ensuing analysis. Many commercial products for diagnosis of diseases such as HIV or West Nile virus have been developed and are available based on the ELISA. Dr. Dennis Bidwell and Alister Voller initially developed the ELISA technique and created standard diagnostic tests for malaria, Chagas disease, and Johne's disease[108] utilizing the ELISA. Their work has inspired extension of the use of ELISA for diagnosis of many other microorganisms. However, the ELISA is almost impossible to perform rapidly and is not easy to use for non-medical professional personnel.

[108] J. Frank Griffin, *etc.,* "Immunoglobulin G1 Enzyme-Linked Immunosorbent Assay for Diagnosis of Johne's Disease in Red Deer (Cervus elaphus)". ***Clin. Diagn. Lab. Immunol***. 12 12 (12): 1401–1409, (**Dec. 2005**).

The first technical barrier a typical ELISA assay would encounter is limited detection. An optimized ELISA assay for absolute diagnosis of a specific antigen can reach the detection limit of 10^6 cfu/ml. This is due to factors that are difficulty to control: limited amount of antigen-antibody binding sites, low color producing efficiency by enzymes, complexity from multilayer structure and so on. Such concentration level is in general higher than the damage-controllable threshold for many microorganisms. Thus, the unmodified ELISA tests are not suitable for early stage diagnostic purposes.

By these means, a standard ELISA cannot meet the needs for a commercially cost-efficient, portable and easy-to-deploy diagnostic kit for personnel without technical expertise.

Chapter 3 Experimental Detail of Optical Fiber Sensor for Detecting and Differentiating various Bacteria

3.1 Immunoassay Based Fiber Biosensor

Though an ELISA assay can be difficult to design and deploy for rapid diagnosis, the principle of ELISA can be inspiring in developing biosensors based on the multilayer designs of the assay. The core of the ELISA test is the antigen-antibody combination. All the technical details lie in immobilizing and supporting the conjugation of the complex onto a solid surfaces, and expressing the specific existence of such a complex with detectable signals. Thus, if a sensor is able to transform the physical variation of the biofilm (such as thickness of the film, the change of conductivity, the variation of the refractive indices and so on) into measureable signals, it is feasible to transform the ELISA techniques and build a smaller, rapid response biosensor system.

As has been discussed in Chapter 2, the ionic-self-assembled-multilayer based LPG fiber sensor system can meet the requirements mentioned above and is a promising candidate as a rapid diagnostic test. A well-tuned, ISAM LPG sensor can be very sensitive to small variations on the cladding of the fiber. Or optically speaking, the LPG fiber can translate the nanometer-scale increment of the biofilm into a significant attenuation of the transmitted light, especially at and around the resonant wavelength.

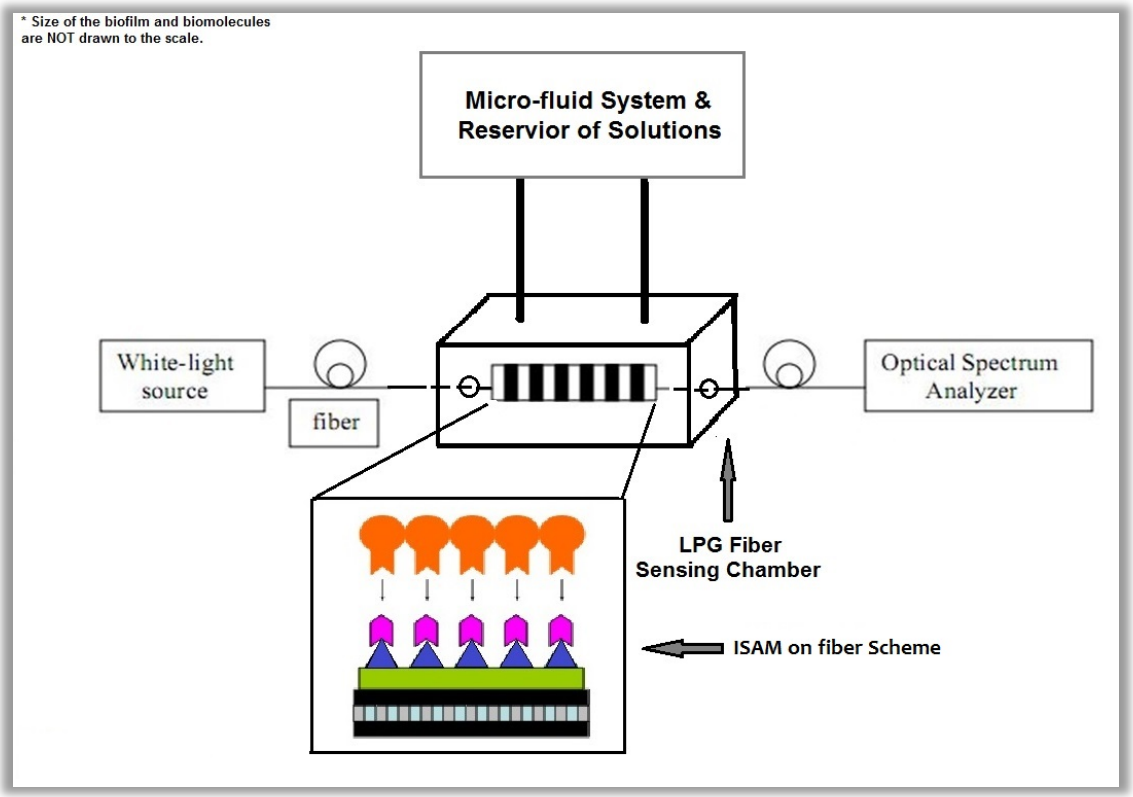

Figure 3-1: General scheme of a complete biosensor system developed on the basis of the ISAM integrated LPG fiber.

The LPG-fiber sensor integrates the standard biological receptor-target scheme with the latest fiber grating technique to make a potentially highly automated and easy-to-operate diagnostic system possible. Figure 3-1 shows the backbone components that comprise the sensing system: (a) light source, which injects a continuous beam of consistent optical power into the inscribed fiber; (b) single-mode fiber which is written with a customized and optimized periodic grating to carry out the biosensing tasks, and transform the physical signal of the attached biomolecule to the analyzable optical power signal; (c) nanoscale organic film and target-specific receptor film that has been pretreated and deposited onto the LPG fiber to detect, differentiate and determine whether the tested sample suspensions contain the biomolecule of interest; (d) fiber and reaction chamber, where the sample suspensions contact the sensing fiber,

and allow the reactions to occur between antigen receptors, which occupy the fiber surface and the analyte flowing through with the sample suspension fluid; (e) micro-fluidic system, which consists of control and fluid injection systems, is programmed to supply and circulate solutions from various reservoirs into the reaction chamber at each stage of the test, and provide necessary fluid media for optical power measurement; (f) optical spectrum analyzer (or photodetector), which measures the remaining power of the transmitted light after passing the LPG sensing portion, and displays the optical power at or around the predetermined resonant wavelength to reflect the shifting of the transmitted spectrum, if any.

Since the LPG fiber sensor is fabricated from silica fibers, the existence of the sensor itself does not interfere with the immunoassay process, or alter the nature of the interactions between biomolecule components.

In the ensuing sections, the dissertation will discuss the components of the system, how the sensor system works, and display the testing results with various immunoassay applications with pure culture samples and or clinic swab samples.

3.2 The Components of the Fiber Biosensor System

3.2.1 Biosensor System Setup

The envisioned commercialized biosensor system design will be able to be packed into a briefcase size, which can be easily carried around or placed on a medical clinic table, and the testing can be conducted with minimum manual operations.

The current size of the prototype system developed here is limited by the white light source and optical spectrum analyzer, which provide the capacity for optical power for a range of wavelengths. Such feature is not required under the future commercialized version of the design, where the expensive white light source can be replaced by a compact laser diode that generates

monochromatic, and a small photodiode that can be used to measure the transmitted optical power instead of the more powerful and programmable optical spectrum analyzer.

The system shown in Fig 3-2 gives the currently deployed instrumental setup that generates all the data displayed and discussed in the later sections. It should be noted that when comparing this setup with the general sketch proposed in Fig 3-1, the current sensor system doesn't combine the microfluidics system yet, which is still under development by another team of the project (the company: Virginia nanoTech), and will be briefly shown and discussed at the end of the chapter.

Hereby, the current system operates manually (as can be seen in Fig 3-2(b)) with a plastic block, which has a shallow grove to fit the LPG fiber as well as holding the liquid to allow interaction between the fiber sensor and the respective solution. All the solutions are added into the grove using a pipette with adjustable volume. The total volume of the solution-holding grove is 0.5 ml, however in a typical experiment, a total volume of 0.6 ml of solution is added into the volume to ensure the fiber sensor is completely covered and soaked in the solution liquid, the additional 0.1 ml liquid volume is able to be held over the groove.

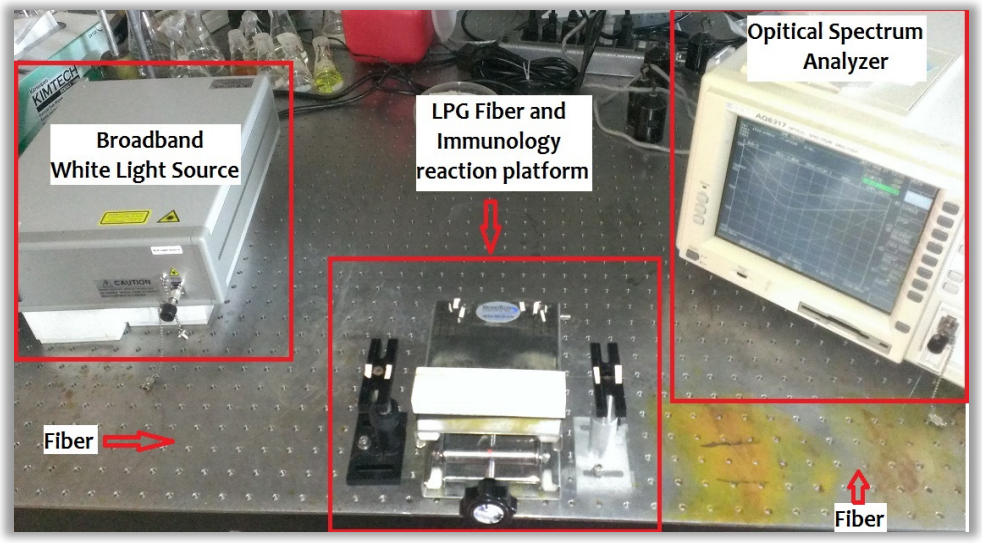

(A)

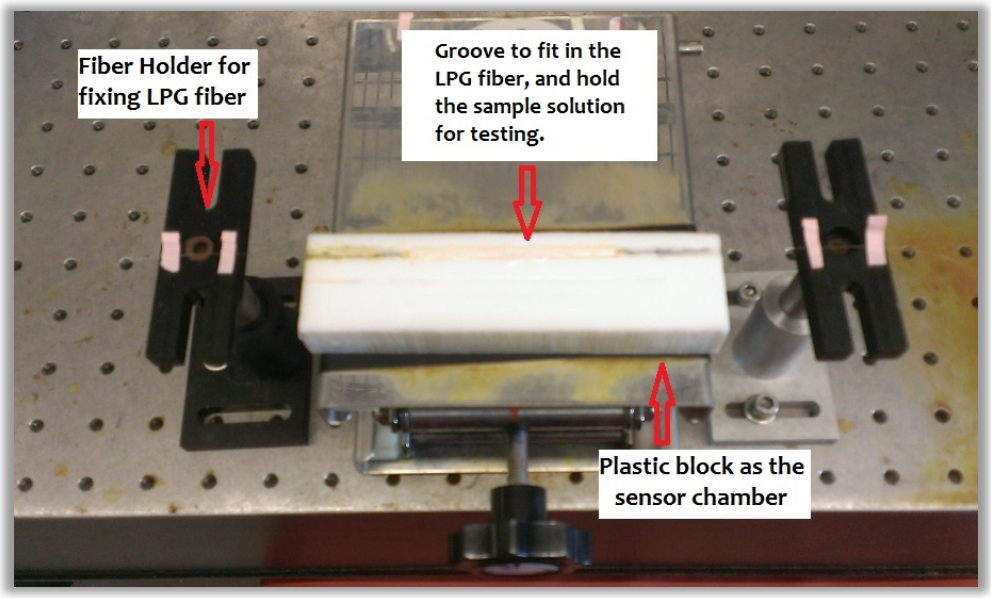

(B)

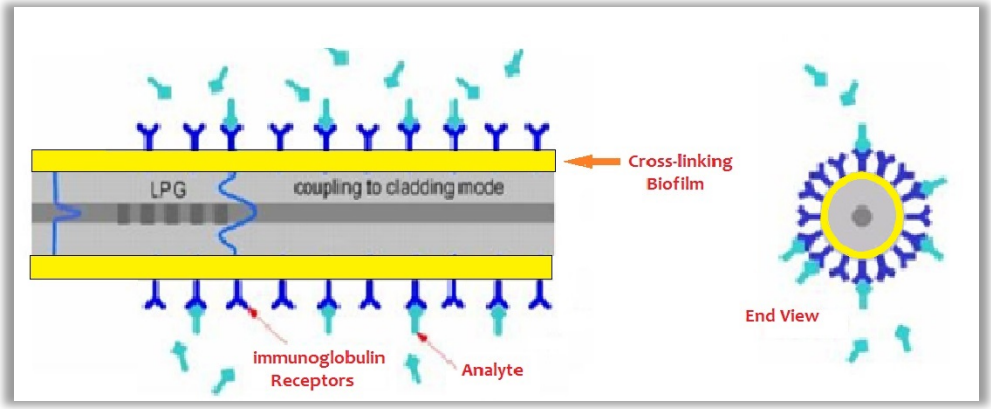

(C)

Figure 3-2: Experimental setups of the fiber sensor system. (A) the overview including white light source, which emits broadband white light; LPG fiber in the immunology reaction platform, where the sensing tasks are performed; and the optical spectrum analyzer, which will read the optical power of the transmitted light, display the scanning spectrum of the transmitted light and record the results. (B) a closer look of the reaction platform, where the fiber holder suspends the fiber and fixes the fiber over the platform, the plastic block with a groove to fit the pretreated LPG sensing fiber in and hold the sample suspension for immunology interactions. (C) illustration of the sensor built on the LPG fiber.

The LPG sensing portion of the fiber is pretreated with nanoscale ISAM films and specific immunoglobulin receptors prior to the test of the sample suspensions. In the commercial application, the fiber sensor can be sealed into a cartridge, and be removed or replaced with a

fresh sensor once a diagnosis has been done. Since the cartridge that will be supplied in the future commercialized version of the sensor system with the assay already embedded onto the LPG sensing fiber, the entire time for handling and processing a diagnosis can be significantly reduced and the procedures be greatly simplified that personnel with minimal training can be qualified for operating the diagnosis system and interpreting the results.

3.2.2 White Light Source

The white light source used in this setup is provided by FiberLabs Inc., whose model number is SLD-11OESL003. The total output power of the light source is +12.2 dBm, with power stability variation at +/- 0.0004 dB. Figure 3-3 shows the power of the whole spectrum provided by the light source from 1200 nm to 1700 nm. The major spectrum range used in the experiments is 1500 nm to 1580 nm, with 1540 nm as the center, since the LPG fibers used in the experiments are fabricated with the resonant wavelength between 1530 nm to 1560 nm. Some experiments are done under a wider range of the spectrum, with the scanning wavelength range from 1450 to 1650 nm, however the most useful data are obtained around 1540 nm during those tests. Therefore, the data analysis in the later chapters focuses on the operating wavelength, that ranges from 1500 nm to 1580 nm.

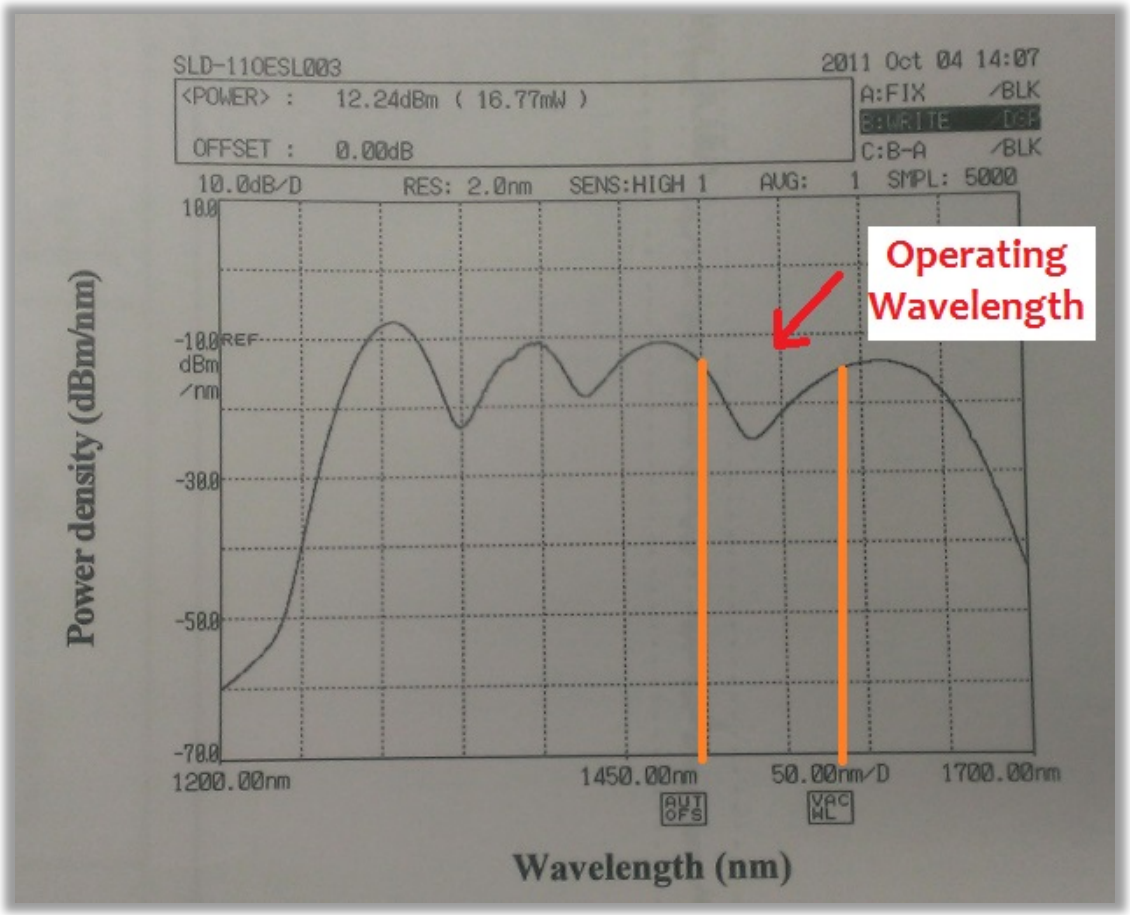

Figure 3-3: Whole spectrum offered by the SLD-110ESL003 light source, which is scanned and printed by the optical spectrum analyzer. The operating wavelength represents the wavelength that are recorded and adopted in the data analysis of the experimental results.

Figure 3-4 shows a stability study of the light source. The stability issue is important, because if the total output power of the light source varies on a large scale, than it is implausible to compare the attenuation of the spectrum between soaking the sensor in different solutions or samples, as any variation of the signal may be due to the shifting of the output power as a result of the instability of the light source. For instance, a constant decline of the optical power over time will generate a false reduced transmitted optical power, and create false positive results.

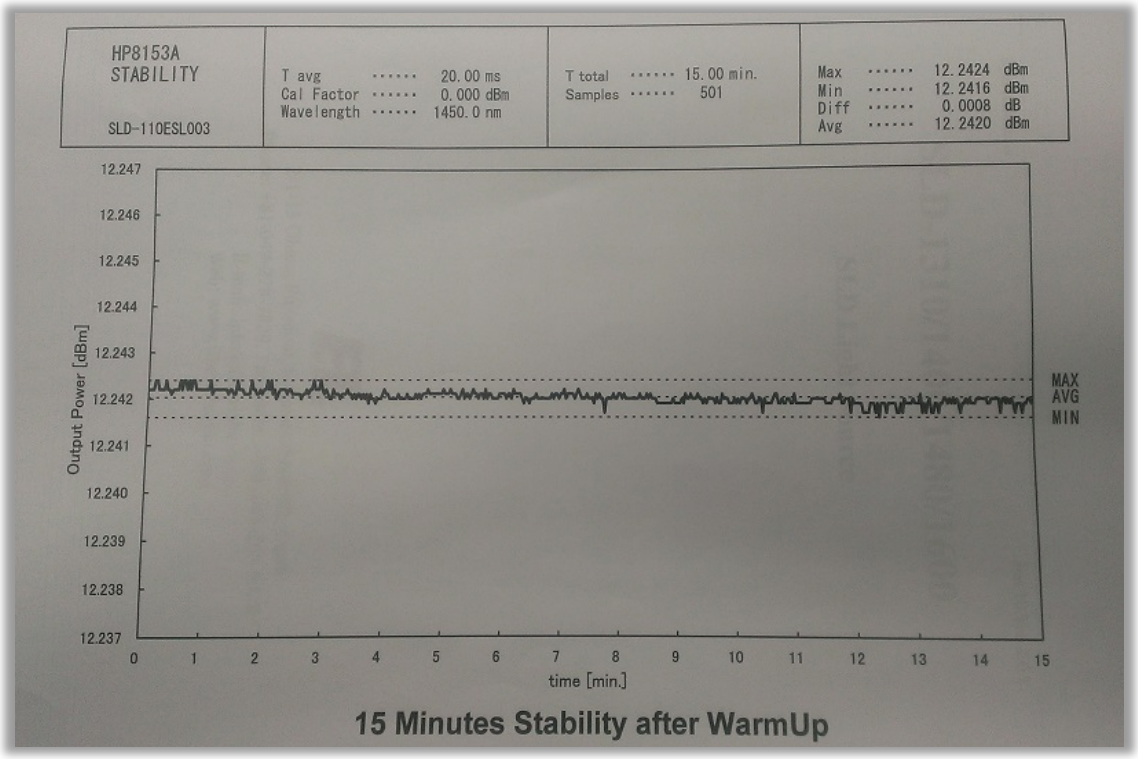

Figure 3-4: Whole spectrum offered by the SLD-110ESL003 light source, which is scanned and printed by the optical analyzer. The operating wavelength represents the wavelengths that are recorded and adopted in the data analysis of experiment results.

Based on the data sheet bundled with the white light source when purchased, it showed that after the light source warms up, a 15 minutes stability study has been conducted by measuring the output optical power. The average output optical power is at 12.240 dBm, with a variation of 0.0008 dB at the wavelength of 1450 nm. This means that for a typical diagnostic test that takes about 60 minutes, the variation of optical power can be well maintained within a 0.01 dB range, which is about 0.2% change of the transmitted optical power. Therefore, a system error of about 0.2% should be considered when analyzing all the experiment results.

3.2.3 Optical Spectrum Analyzer

The optical spectrum analyzer is manufactured by ANDO with the model No. ANDO AQ6317. The data sheet shows that this model is capable of providing +/- 0.05 nm wavelength accuracy in the 1550 nm band (the same band the data were taken at), and +/- 0.01 nm wavelength linearity, with the achievable wavelength resolution at 0.015 nm. The analyzer can cover and display the spectrum of light from 600 nm to 1750 nm, with the minimum measurement down to -90 dBm and the resolution at +/- 0.05 dB. Adding up with the output optical power variation from the white light source, it can be concluded that the system error can be set at +/-0.06 dB, which equals around 1.2%. Therefore statistically speaking, for experiments conducted on this system, a positive signal should be showing optical power attenuation about 3 times higher than the system error, which is 3.6% in percentage change.

3.2.4 Stability and Repeatability Study of the Biosensor System

In order to examine the total stability and repeatability of the biosensor system introduced above, a 5 hours stability study has been performed, and the results are shown in Fig 3-5. The system was assembled as shown in Fig 3-2 (A), which is also the setup for daily experiment and data collection. The data was taken at the wavelength 1525 nm after 30 minutes of warm-up period for the white light source, which is the location of the resonant wavelength for the LPG fiber tested, and the data was taken every 10 minutes. The average transmitted optical power recorded in this 5 hours period located at -26.05 dB, and the statistic study showed the standard deviation equals 0.24 dB. Therefore the data variation is less than 1% due to system instability, and this result agrees with the theoretical estimation calculated above.

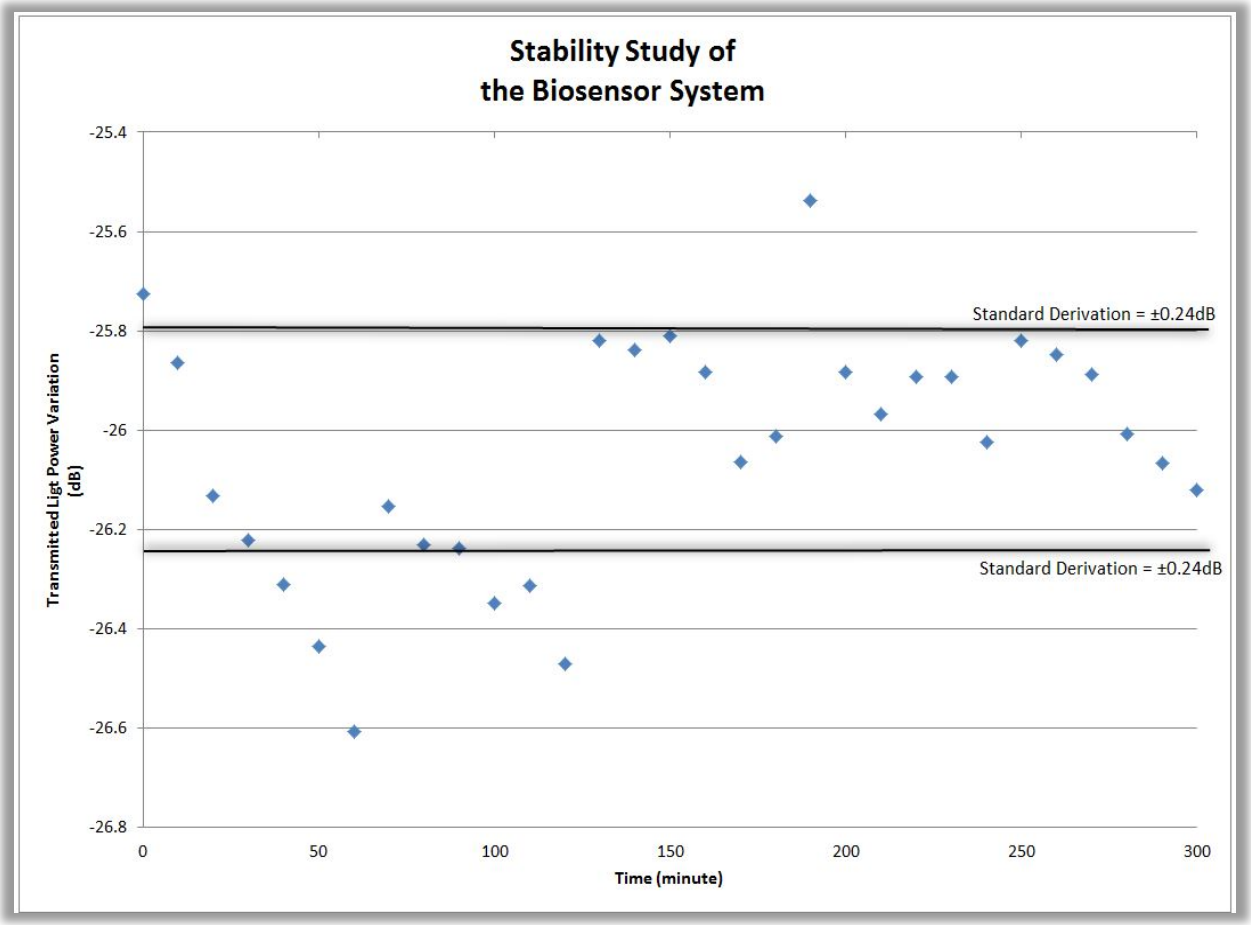

Figure 3-5: Stability study of the biosensor system. The average transmitted optical power is -26.05 dB, with standard deviation equals 0.24 dB. The two parallel dark lines mark the upper and lower boundaries for the data region within standard deviation.

It is also seen that after 120 minutes of the measurement, most of the data points fall within the standard deviation boundaries and are more close to one another. This characteristic suggests that a 2.5 hours warm-up period (which includes the initial 30 minutes warm-up) is highly recommended for yielding trustworthy readings from this equipment, as the influence from the system error after this warm-up period can be reduced.

3.2.5 Optical Fiber Preparation

The Long-Period-Gratings are fabricated over a stripped region over the single mode fiber (SMF-28, Corning), and both ends of the fiber are also carefully stripped, cut with a high precision fiber cleaver (High Precision Fiber Cleaver, Fujikura) to yield a neat and clean fiber end. The fiber ends are gently wiped with paper which has dipped in 70% ethanol. Then both bare fiber ends are inserted into FC fiber jackets (F18294 FIS FC Buffered Fiber Adapter, Fiber Instrument Sales, Inc.), with the fiber end sticking out of the jacket tip for about 0.5 mm.

It needs to be pointed out that preparing the fiber ends is a critical step for yielding a high level of transmitted optical power. Insertion loss due to unclean or uneven fiber ends can greatly sabotage the accuracy of the measurement of transmitted power. Based on experience, an ideal and successful experiment would require the transmitted optical power at 1400 nm to stay above -45 dB to ensure that the optical power at the greatest attenuation is able to float over -80 dB, where the optical power becomes too weak for a precise evaluation and analysis by the spectrum analyzer. Figure 3-6 shows a typical spectrum measurement (1400 nm to 1700 nm) of the LPG fiber. The total optical power evaluated in this case is relatively low, with high of -39 dB and low of -51 dB. The principle for determining whether the insertion loss is acceptable, is by checking whether the spectrum shifting figure is clear and sharp, since the difference between the shifted spectrum and the reference spectrum is what this research hinges on. In Fig 3-6, the spectrum is measured when the LPG fiber is exposed to air and PBS solution separately, which have different refractive indices. It is manifest that the shifting of the spectrum between the two media is largest at the resonant wavelength, which is located at 1540 nm. While further away from this resonant wavelength, the spectrum hardly varies. This observation agrees with theoretical estimations made in previous sections *2.1.3* and *2.1.4*.

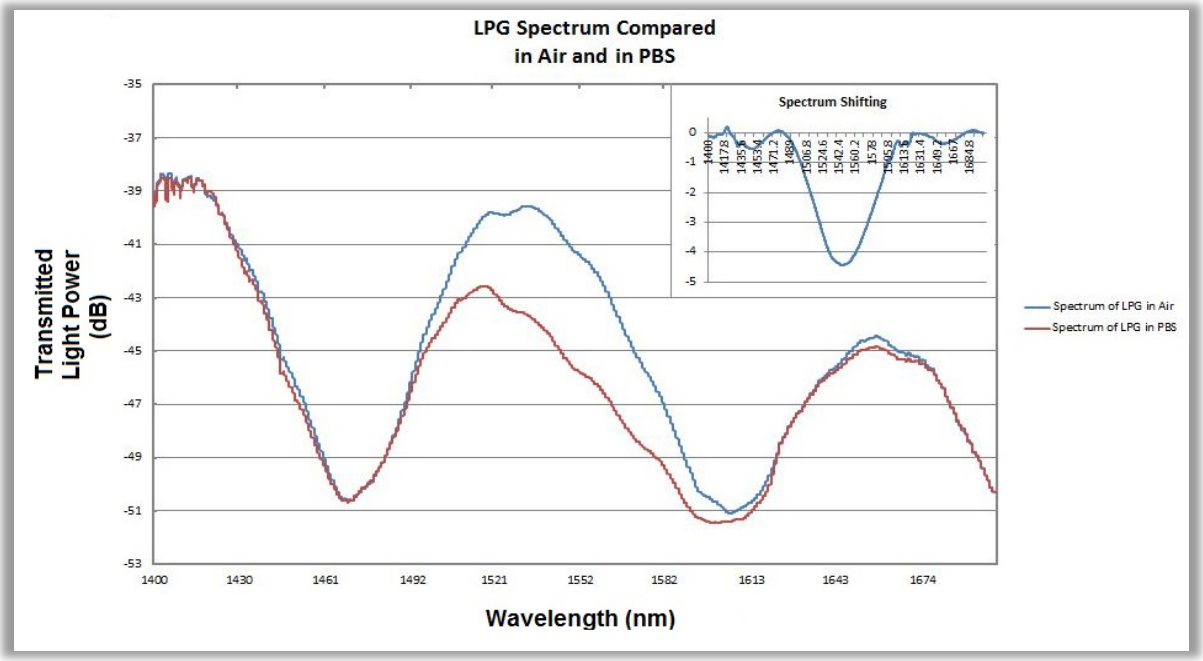

Figure 3-6: Spectra of LPG fiber exposed to air and PBS solution are measured and compared in this figure. It is manifest that at the resonant wavelength (1540 nm), the shifting is the largest; while further away from this wavelength, the attenuation of the spectrum is difficult to notice.

The fiber sensor system is built up around the TAP LPG fiber. In most cases the TAP LPG fiber is fabricated[109] with double-peaks straddling the working resonant wavelength. Then soaking the LPG fiber in 10% HF solution so that part of the cladding thickness will be removed from the fiber surface, causes double-peaks to merge into a TAP style single peak, as has been described in section *2.1.5*. The LPG in our work were provided by Prof. S. Ramachandran of Boston University.

The length of the HF etching period needs to be determined case by case, which is largely due to the cladding thickness of the LPG fiber to be etched, the distance between the double-peaks, the sensitivity and depth of the merged single peak, *etc.*. The etching has to be conducted with the light source and spectrum analyzer connected to monitor the spectrum shifting. The

[109] X. Lan, Q. Han, T. Wei, J. Huang, H. Xiao, "Turn-Around-Point Long-Period Fiber Gratings Fabricated by CO Laser Point-by-Point Irradiations," *IEEE PHOTONICS TECHNOLOGY LETTERS* , **vol. 23, no. 22**, pp. 1664–1666, (2011).

etching process can be viewed as the reverse approach of the manufacture of the biosensor, as etching removes materials from the fiber versus the biosensor deposits materials onto the fiber. Therefore the TAP LPG's sensitivity to the small variation of the cladding thickness also applies to the etching process. In a typical etching, it may take a dozen minutes to bring the double-peak together and merge into one; however after etching before the TAP region, the sole peak becomes shallower much more rapidly. It can take less than a few seconds to see the mode-coupling vanish and the single peak disappear entirely. Under the assumption that the material removal rate remains the same for the same acid solution regardless of the cladding thickness, the etching process serves as an additional demonstration that the LPG fiber is much more sensitive in the vicinity of the TAP.

LPGs can be written by exposure to UV or CO_2 lasers. Wang's[110] review article produce a broad view of the LPG fiber fabrication technique using CO_2 laser, and such technique utilizes laser pulses focusing on the single mode fiber surface to inscribe a small asymmetric groove to the cladding, and generating a refractive index disturbance at those grooves of the cladding and resulting in a periodic RI difference required by the long-period-gratings theory. The CO_2 laser inscribed fiber as can be viewed closely in Fig 3-7.[111]

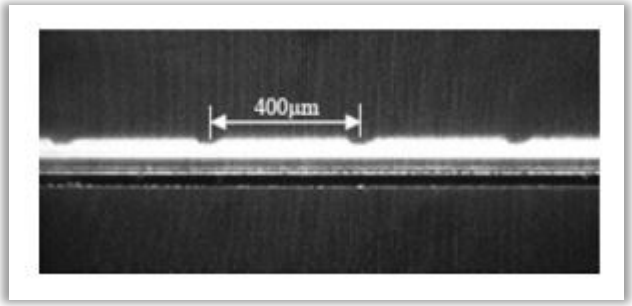

[110] Y. Wang, "Review of long period fiber gratings written by CO[sub 2] laser," *Journal of Applied Physics*, **vol. 108, no. 8, p. 081101**, 2010.
[111] Y.-P. Wang, D. N. Wang, W. Jin, Y.-J. Rao, and G.-D. Peng, "Asymmetric long period fiber gratings fabricated by use of CO2 laser to carve periodic grooves on the optical fiber", *Appl. Phys. Lett*. **89**, 151105 (2006).

Figure 3-7: Photograph[102] of an asymmetric LPFG with periodic grooves, taken from Reference 61. The grooves can be seen 400 μm away from each other, indicating the grating period for this fiber is 400 μm.

3.2.6 Test of LPG Sensor

The central component of the whole diagnostic system is the LPG fiber. It contacts the testing sample suspensions and translates the physical change due to the immunoassay reactions into the optical signals for quantitative analysis.

Fiber mode theory predicts that the LPG fiber responds swiftly and sensitively to the variation of the cladding thickness and the additional material's refractive index. And for the LPG fiber with Turn-Around-Point (TAP) characteristics, the resonant wavelength of the transmitted light does not shift due to physical variations taking place on the cladding, but instead the optical power of the spectrum peak changes at the fixed resonant wavelength.

To demonstrate this further, a simple experiment can be crafted: set up the whole system according to the design introduced above, then deposit 1 bilayer of ISAM thin film at a time, and take measurements, and compare the results. Since the thickness of 1 bilayer of ISAM film is solely determined by the concentration and pH values of the materials solution after a sufficiently long deposition period, this parameter should remain constant as long as the same solutions are used in the experiment.

Figure 3-8 reflects the spectrum shifting due to adding each extra bilayer to the LPG sensor:

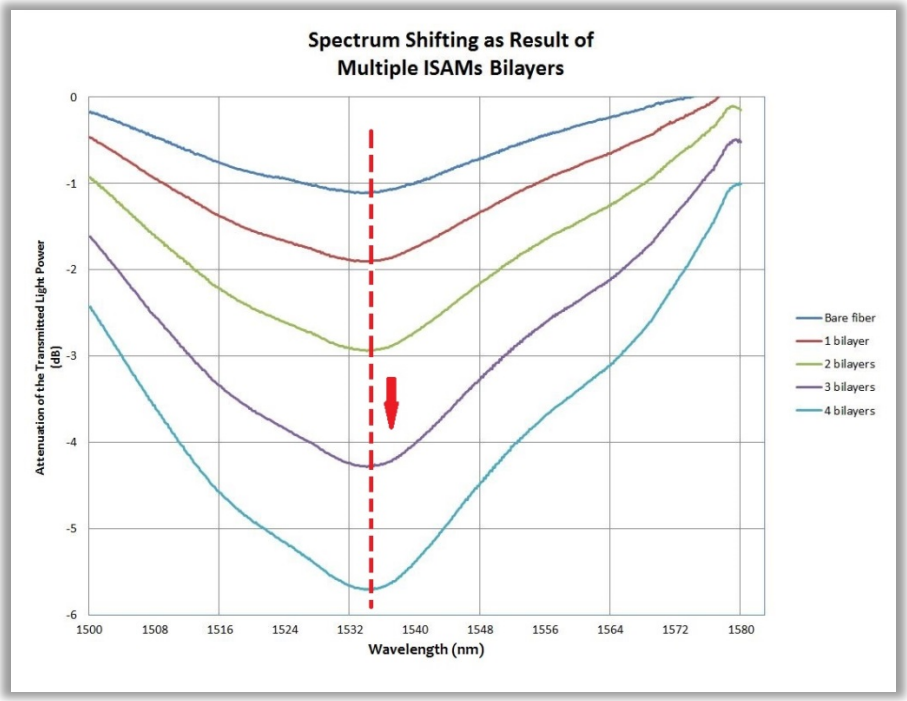
Spectrum Shifting as Result of Multiple ISAMs Bilayers
Attenuation of the Transmitted Light Power (dB)
0
-1
-2
-3
-4
-5
-6
1500
1508
1516
1524
1532
1540
1548
1556
1564
1572
1580
Wavelength (nm)
Bare fiber
1 bilayer
2 bilayers
3 bilayers
4 bilayers

(A)

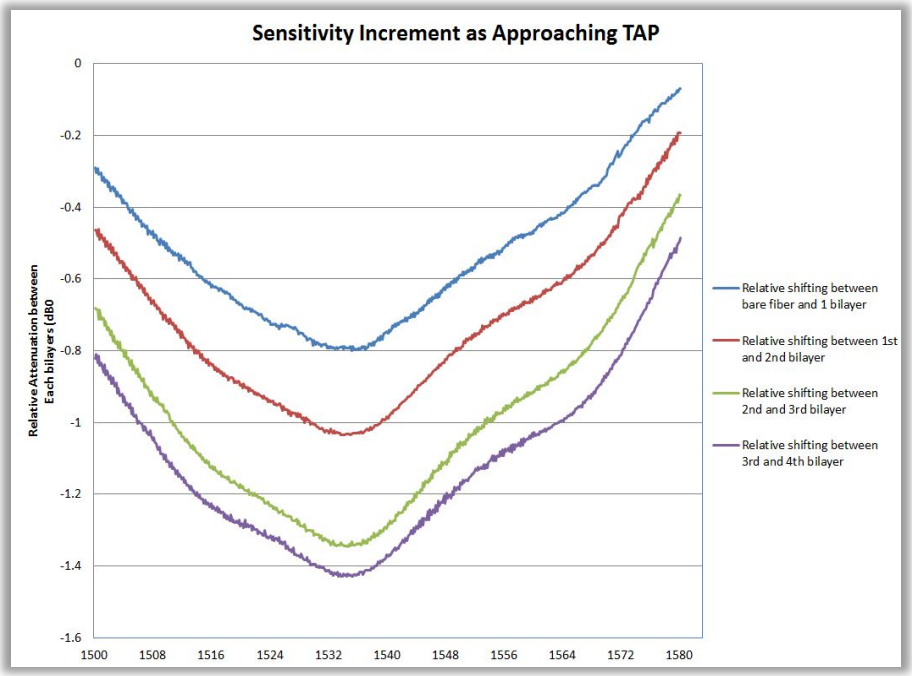
Sensitivity Increment as Approaching TAP
Relative Attenuation between Each bilayers (dB0
0
-0.2
-0.4
-0.6
-0.8
-1
-1.2
-1.4
-1.6
1500
1508
1516
1524
1532
1540
1548
1556
1564
1572
1580
Relative shifting between bare fiber and 1 bilayer
Relative shifting between 1st and 2nd bilayer
Relative shifting between 2nd and 3rd bilayer
Relative shifting between 3rd and 4th bilayer

(B)

Figure 3-8: (A) With addition of a constant thickness to the cladding, the spectrum peak shifts lower without drifting to other wavelengths. (B) The shifting of the peak at the resonant wavelength accelerates while approaching the TAP. The relative shifting of the spectrum between each additional bilayers increases.

Fig 3-8 (B) is the difference between consecutive spectra with each additional bilayer deposited onto the LPG fiber. This figure reflects the fact that while approaching the TAP, the sensitivity of the fiber accelerates, with more attenuation added to the spectrum, and especially at the spectrum peak with a constant thickness increment to the cladding.

This is crucial for tuning the sensor to reach its maximum sensitivity. As has been mentioned above, the received fiber is pretreated with 10% HF acid to etch back the attenuation peak, so that there is room for building up ISAM films and immunoassay receptors for further antigen detection. Thereby, the ISAM thin films whose thickness can be controlled at the nanometer level is capable of tuning the LPG sensor to its most sensitive region by carefully building up the thickness of the cladding. The most sensitive region of the LPG fiber varies from case to case, as the initial bare fiber spectrum may not be the same due to etching conditions and length. Yet it is possible to initially build up multiple layers of ISAM thin films and overshoot the TAP, determine the number of the bilayers for best sensitivity, then remove the ISAM easily by treating the fiber with heated weak acid.

However, Fig 3-8 (B) also implies that while moving very close to the TAP, the sensitivity increment may stall, since the attenuation reaches its maximum and then decreases again after the TAP as the result of the spectrum splitting (refer to Fig 2-9). It would be unwise to push the spectrum peak too close to the TAP with the ISAM film and/or immunoassay receptors, as the additional attachment of the target material has the possibility of overshooting the TAP and causing the spectrum to split. In such cases, especially for commercial applications where monitoring the whole spectrum would be too expensive, it will create an increased optical power

and perplex the automated quantitative analysis system. In this sense, it is recommended to leave at least 1 bilayer's room for additional molecule binding to avoid overshooting the TAP.

As has been discussed, the best working condition for the LPG fiber sensor is close to but before reaching the TAP. Therefore, the quality of the LPG fiber can directly determine the sensitivity potential to the biosensor system. Peng *et al.*[61] has shown experimentally that adding grating periods can create a deeper TAP. Their result is shown below in Fig 3-9:

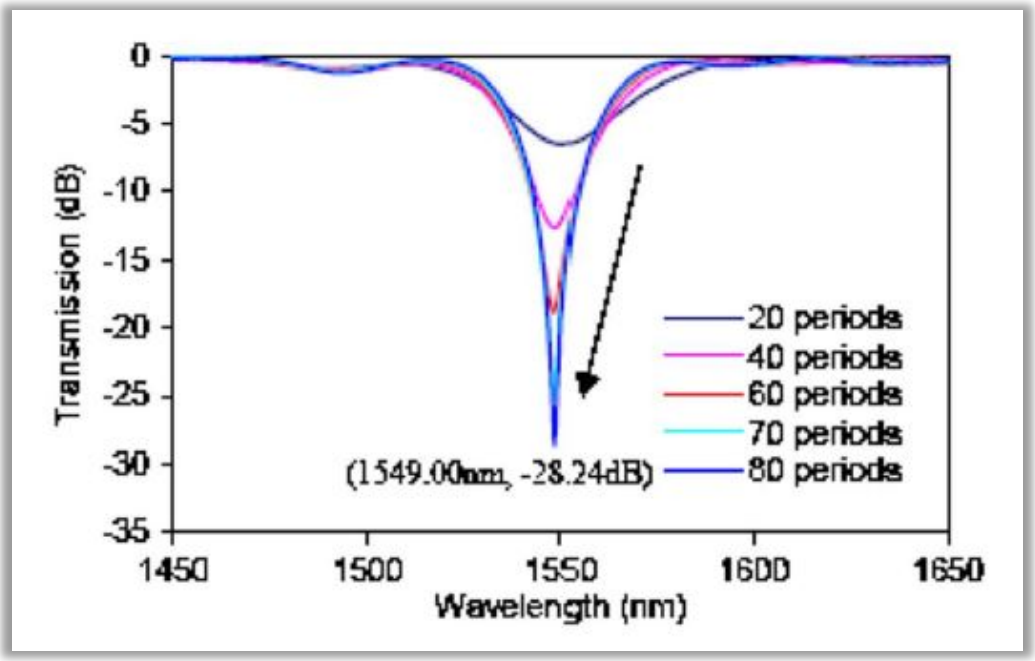

Figure 3-9: Spectrum of LPG fibers which have various numbers of grating periods. The peak of the transmitted optical power is attenuated from -5 dB for 20 periods to -28 dB for 80 periods.

In this dissertation, two series of LPG fibers have been integrated into the system and utilized for experiments. One is with less grating periods, whose TAP capacity is at the -10 dB ~ -12 dB level, and for convenience such fibers will be called "less sensitive fibers"; the other series of LPG fibers have many more periods inscribed, whose peak could reach TAP at the power level of -30 dB ~ -35 dB, and those fibers will be referred as "sensitive fibers".

Chapter 4 Application of the LPG Biosensor for MRSA Detection

4.1 Introduction to Methicillin-resistant *Staphylococcus aureus* (MRSA)

Our primary motivation for developing the LPG based fiber biosensor is to provide a novel, fast and accurate diagnostic device for detecting and differentiating microorganisms that are substantial threat to the health and public safety. The key for disease control and suppressing a potential epidemic lays on early identification and diagnosis of the microorganisms. However, the current diagnostic technologies and equipment for accurate identification of the infection source are limited to large regional hospitals, due to their high investment and operation costs. The time to diagnosis also needs to be shortened to adopt the necessary medical actions. Doctors have to depend on their own medial experience and intuition to make treatment decisions without having solid laboratory evidence of some of the most contagious antigen.

Staphylococcus aureus (*SA*), which obtain antibiotic resistance in a swift and efficient manner, is responsible for various soft-tissue and skin infections. *SA* strains that develop resistance to methicillin are referred to as methicillin-resistant *Staphylococcus aureus* (MRSA).[112,113,114] Those strains that do respond to oxacillin on methicillin are referred to as methicillin-sensitive *Staphylococcus aureus* (MSSA). Early diagnosis and treatment is crucial for controlling MRSA infection and restoring the patient's health. As emphasized in its name, such bacteria are resistant to most beta-lactam antibiotics, and are therefore difficult to treat. MRSA

[112] H.F.Chambers, "The changing epidemiology of Staphylococcus aureus?" *Emerg Infect Dis*, **7**(2):178-182, (2001).
[113] GT Stewart, RJ Holt, "Evolutio of natural resistance to the newer penicillins." *Br Med J*, **1**(5326):308-311, (1963).
[114] EJ Benner, FH Kayser, "Growing clinical significance of methcillin-resistant Staphylococcus aureus." *Lancet*, **2**(7571):741-744, (1968).

infections can rapidly progress if no properly diagnosed in a short time. Fortunately, there still remain a few antibiotics, such as vancomycin, to which MRSA is susceptible. However, physicians would like to be certain that such antibiotics are required before using them in order to reduce the probability that bacteria will develop resistance to them as well.

Figure 4-1: MSSA cells (on the left) compared to MRSA cells (on the right) under scanning-electron-microscopic. Both strains are close to spherical in shape and are similar in diameter (0.5 µm ~ 0.8 µm). Differentiating MRSA from MSSA based on their physical profiles is impossible. (Pictures taken from Wikipedia: *http://en.wikipedia.org/wiki/Methicillin-resistant_Staphylococcus_aureus* and *http://en.wikipedia.org/wiki/Staphylococcus_aureus*)

Patients suffering from MRSA infection have a higher morbidity and mortality.[115] Reports[116] have indicated a substantial increase in *S. aureus* isolates that are resistant to methicillin found from clinical samples. Studies conducted in an urban hospital has concluded that patients whose skin and soft tissue infections are the result of MRSA strains tend to stay on average 7 days longer in the hospital compared with those suffering solely from MSSA infections (20.1 days

[115] SE Cosgrove, *etc.*, "Comparison of mortality associated with methicillin-resistant and methicillin-susceptible Staphylococcus aureus bacteremia: a meta-analysis." *Clin Infect Dis*, **36(1):**53-59, (2003).
[116] EW Tiemersma, *etc.,* "Methicillin-resistant Staphylococcus aureus in Europe, 1999-2002." *Emerg Infect Dis,* **10(9):**1627-1634, (2004,).

versus 13.7 days).[117] The same study also pointed out that overall cost for treating a MRSA-infected patient is almost doubled ($22,735 versus $11,205).

Early identification of MRSA is accepted as the most efficient means to diminish the threat of MRSA strains to patients or public health. A MRSA infection can progress rapidly over several days. If the infection reaches the heart or lungs, death can come rapidly. The standard method for identification of MRSA is culture growth, requiring 2-3 days at a specialized facility. In this dissertation, we demonstrate that our LPG-fiber based biosensor can provide a low cost, rapid diagnostic device that could provide early identification of MRSA. We have shown that our device can detect MRSA strains at the concentration as low as 100 cfu/ml, and yields diagnostic results within 1 hour.

4.2 MRSA biosensor using monoclonal antibodies as receptor

4.2.1 Monoclonal Antibodies to MRSA

The cause of broad-spectrum β-lactam resistance by MRSA strains is due to penicillin-binding protein 2a (PBP2a) that is encoded by the *mecA* gene.[118,119] MRSA strains are the most common carriers of the PBP2a protein, and is not found on MSSA strains. Consequently, in this dissertation's design for a MRSA biosensor, the PBP2a protein is selected as antigen target, and mouse monoclonal antibodies (Mab) to PBP2a are used in the biosensor assay as the receptor.

[117] TP Lodise, PS McKinnon, "Clinical and economic impact of methicillin resistance in patients with Staphylococcus aureus bacteremia." *Diagn Microbiol Infect Dis*, **52(2):**113-122, (2005).
[118] K Murakami, etc., "Identification of methicillin-resistant strains of staphylococci by polymerase chain reaction." *J Clin Microbiol*, **29(10):**2240-2244, (1991).
[119] C Ryffel, etc., "Sequence comparison of mecA genes isolated from methicillin-resistant Staphylococcus aureus and Staphylococcus epidermidis." *Gene*, **94(1):**137-138, (1990).

In this section of the dissertation, if not explicitly stated, all the MRSA antibodies (PBP2a antibodies) were acquired from CalBioreagents (San Mateo, CA) with catalog #6G10.

Before testing with the biosensor system, the monoclonal antibodies were tested by immunoblot procedures for specificity and sensitivity. Our collaborator, Dr. Aloka Bandara of Dr. Thomas Inzana's research group has used Mab purchased from CalBioreagents as primary antibodies and confirmed their appropriateness through immune-blotting tests with MSSA and MRSA whole cells. Figure 4-2 shows that such antibodies are capable of differentiating MRSA strains from MSSA strains with the cell concentrations of 10^8cfu/ml (the colored spot indicates a positive response). However, the immune-blotting tests also have a low sensitivity for MRSA detection, as further tests showed that neither MSSA nor MRSA cell samples at or below concentration of 10^7cfu/ml yielded any visible signals.

Figure 4-2: Immunoblotting test conducted by Dr. Bandara to determine the specificity and sensitivity of the monoclonal antibodies to PBP2a shows a dark spot on the right, which means a clear positive response from MRSA strains, versus a blank spot on the left which is a negative response from MSSA strains.

Therefore, the PBP2a antibodies tested above are qualified as the antigen receptor in the biosensor system, and in the ensuing sections the dissertation will utilize this Mab in the TAP LPG biosensor.

4.2.2 Experimental Methods and Procedure

A standard experimental procedure for assembling and testing the biosensor is composed of three major stages: depositing ISAM organic nanofilms on the cladding surface; depositing the receptor layer of the sensor; and sensor testing with sample suspensions. All experiments are conducted under standard biological safety conditions, and the experimental environment is considered to be aseptic as sterilize precautions are performed before and after each experiment. 'Sensitive' LPG fibers are used in all the experiments mentioned in this section, and all the data were acquired on the biosensor system built around these LPG fibers whose TAP depth was around 30 dB to 35 dB. The detailed step of each experimental stage is described as below:

Depositing ISAM organic nanofilms:

1. Turn on white light source and optical spectrum analyzer. Allow 30 minutes to warm up.
2. If preparing new LPG fiber, strip the buffer coatings off both fiber ends first. Clean the fiber ends with Kimwipes which has been dipped in 70% ethanol. Put on fiber adapters with a 0.5 mm tip sticking out of the adapter. Then connect one of the adapters to the light source and the other to the optical analyzer.
3. Suspend the LPG-inscribed segment of the fiber between fiber holders. Make sure the LPG fiber (if not specified otherwise, simply referred to as "fiber" below) is slightly tightened between the fiber holders, but avoid asserting too much stress to the fiber.
4. Rinse the fiber with DI water for 3 minutes. Take a broad spectrum measurement as Reference spectrum.

5. Raise the sample holder block (if not specified otherwise, referred to as "block" below) to the fiber, make sure the fiber is located within the solution-holding-grove, and yet avoid having the fiber in physical contact with any part of the sample holder block*.
6. Add 0.5 ml of deionized (DI) water to the groove of the block** and make sure the fiber is entirely covered by the liquid. Take measurement and record the spectrum after 3 minutes.
7. Remove the DI water, rinse the fiber again, thoroughly wash the sample holder with detergent and sterilize the block with 70% ethanol. Air dry the block with strong air flow, and make sure no liquid droplet is visible on the block surface.
8. Raise the block to the fiber, add 0.5 ml of 10 mM PAH at pH 7.0 to the groove.
9. Wait for 1 minute, then remove the PAH solution. Rinse the fiber and clean the block as described in **Step 7**.
10. Raise the block to the fiber, add 0.5 ml of 10 mM PCBS at pH 7.0 to the groove.
11. Wait for 1 minute, then remove the PCBS solution. Rinse the fiber and clean the block as described in **Step 7**. Steps 8 to 11 deposit 1 ISAM bilayer.
12. Repeat steps 8 to 11 until the desired number of ISAM bilayers is built. If the top ISAM film is desired to have amine groups, then the final layer deposition shall be stopped at step 9 and skip step 10 and 11***.

Depositing the receptor layer of the biosensor:

(Wearing sterilized gloves and face mask are required for the following steps)

13. Leave PCBS as top layer of the ISAM film, and make sure the spectrum is close to but not reaching the TAP (the value in dBs varies from fiber to fiber, usually 15 dB for sensitive fiber, and 5 dB for less-sensitive fiber).

14. Take the EDC out of freezer and sulfo-NHS out of refrigerator respectively, wait 15 to 30 minutes to allow the chemical containers to rise to room temperature[†].

15. Measure 20 mg of EDC and 12 mg of sulfo-NHS and seal the chemicals in a 1.5 ml vial. Add 0.5 ml of autoclaved PBS solution at pH 6.0 to the vial to dissolve the chemicals. Vortex the vial at medium level until all the powder is dissolved into the solution.

16. Tap the Mab container gently and flip over a few times. Measure 90 μg of PBP2a Mab[††] immediately after step 15, and add the Mab to the crosslinker solution, gently tap the mixture for better crosslinking reaction. The final Mab concentration should be 180 μg/ml (Mab are usually supplied in liquid form, therefore the amount of liquid added depends on the original concentration of the antibody product, *ie.,* 36 μl of Mab whose original concentration is 2.5 mg/ml).

17. Rinse the fiber, clean and sterilize the block, then raise the block to the fiber without direct contact. Tap the crosslinker vial, and then add the crosslinker solution to the fiber.

18. Allow the crosslinker plus Mab mixture to react with the fiber overnight (or at least 6 hours). Stir the mixture with pipette every 5 minutes for the first 15 minutes, then every 15 minutes for the first hour. It is recommended to keep the solution stirred every 30 minutes after the first hour until the reaction period is over.

19. Remove the solution. Rinse the fiber for 3 minutes. Wash the block and soak fiber in autoclaved DI water for 10 minutes. Stir 30 seconds for every 3 minutes.

20. Remove the water, Rinse the fiber again and wash the block. Soak the fiber in autoclaved DI water for 3 minutes, then take a measurement. If the spectrum shifts

higher instead of lower, repeat step 19[†††] until the peak of the spectrum reaches the level of ISAM measurement or lower.

21. Rinse the fiber and wash the block. Measure 10 mg of dry milk powder and dissolve it with 1 ml of DI water, which makes a 1% dry milk as blocking reagent[††††] (in early studies of the *MRSA* Mab biosensors, 50 mg/ml of Ethanolamine solution has also been used as an alternative blocking reagent, though with less blocking efficiency. Using 10% whole serum is recommended if effective blocking is difficult to achieve). Add the blocking reagent to fiber for 3 minutes. Stir over the period.

22. Remove the dry milk solution. Rinse the fiber thoroughly for 3 minutes. Wash the block and soak the fiber in DI water for 10 minutes.

23. After 10 minutes water soaking, rinse the fiber again and take a measurement after putting on new DI water and soaking the fiber in it for 3 minutes. If the spectrum shifts up for more than 1 dB, repeat the soaking and rinse steps. This measurement will give the reference reading for the ensuing sample tests.

Testing samples with the biosensor:

(Wearing sterilized gloves and face mask are required for the following steps)

24. Take the sample suspension out of storage and allow it to reach room temperature.

25. Remove any buffer solution that is soaking the fiber. Rinse the fiber gently and thoroughly. Wash the block with detergent and spray with 70% ethanol.

26. Add the sample suspension to the fiber for 50 minutes. Stir the solution for 30 seconds every 10 minutes.

27. Remove the sample suspension. Rinse the fiber gently yet thoroughly. Soak the fiber in DI water for 10 minutes, and stir 30 seconds every 3 minutes.

28. Rinse the fiber again, and take a measurement of the spectrum after soaking the fiber in DI water for 3 minutes. Upon this step, the test with one sample suspension is accomplished.

29. For sequential tests with further sample suspensions, repeat steps 24 to 28.

Notes and Tips:

**** Maintaining constant stress on the suspended LPG fiber between fiber holders:***

As discussed in section 2.2, the LPG fiber can be used as a stress sensor as well. Therefore, maintaining a constant pressure on fiber between fiber holders has a substantial analytical importance to avoid introducing significant systematic errors to the results and ensuring that any spectrum shifting is due to the cladding variation on the LPG fiber, rather than environmental or systematic fluctuations.

***** Using DI water as measurement and rinsing buffer:***

In ELISA tests, 1x PBS solutions at pH 7.0 has been used as regular buffer for making solutions or for dilution purpose, and 1x PBS at pH 7.0 with 0.5% v/v Tween-20 as detergent has also been used as standard washing buffer in biochemistry laboratories. Nevertheless, PBS solution or its detergent-containing washing buffer version has been constantly creating problems for our LPG biosensor measurement. It has been found and will be further discussed in the AFM imaging section that, after applying solutions made by PBS or after rinsing fiber with PBS washing buffer, it is difficult to remove all the salt left over from the fiber surface. And these salt crystals attached to the fiber cladding will interact with the coupled-mode transmitting along the sensor as well as the background medium (usually solutions), adding

uncontrollable fluctuations to the experimental measurement. PBS has a human-body-like osmotic and ion concentration, and it can also help maintain a constant pH to the solution, therefore it is very helpful for preserving culture samples that favors human-body-like biochemistry conditions. However, in our biosensor design, biomolecules do not have to maintain a long period activity or remain intact throughout the assay as long as the protein structure of the receptors and epitope of the antigen remain functional. Therefore, DI water can be used to replace the role of PBS as the buffer solution and background medium when running measurements. Using ***DI water*** *has been proven to be generating* ***more consistent*** *results compared to using PBS, and the experimental results seldom deviate from expectations. But DI water has a smaller refractive index than PBS solution due to lack of solvent, therefore using* ***DI water*** *as the measurement background medium will reduce the signal reduction ratio under the same cladding thickness increment, and consequently* ***reduce the sensitivity*** *of the fiber. The pros and cons of using DI water and PBS as measurement background can be summarized in the table below:*

	Advantages	*Disadvantages*
DI water	• Consistent readings • Less fluctuations	• Reduced sensitivity • Reduce biomolecule activity in the long term
1x PBS	• Higher sensitivity • Good for preserving biomolecules and retaining their activities	• Leaves salt residue on to the fiber surface • Creating inconsistent readings and fluctuations

****** ISAM shall always be prepared fresh:***

Though ISAM films are considered robust and able to sustain high film quality for a long period of time, it is not recommended to assemble the ISAM films hours before depositing the biofilms. Exposure of the ISAM deposited LPG fiber to air should also be avoided, since dusts and fine particles suspended in the air would be attracted to and attached on the film surface due to static electric attraction, resulting in uneven film surface. Uneven film will compromise the biofilm quality lying on top of it, and increase nonspecific bindings.

† ***Storage requirement of EDC and sulfo-NHS to keep them from humidity:***

EDC and sulfo-NHS/NHS are moisture sensitive chemicals. EDC is especially easy to adsorb water from the air. Allowing the chemical containers to thermally equilibrate with the environment can help keep the humidity in the air from entering the container, and damaging the chemical quality. A degraded EDC powder is usually the essential cause for a failed experiment. It is therefore helpful to split the original EDC into a series of smaller sealed containers, and discard the smaller containers after 2 weeks of use. Using a desiccant can or box for EDC and sulfo-NHS storage can help prevent the chemicals absorbing moisture as well.

†† ***Monoclonal antibodies storage:***

Monoclonal antibodies are proteins and usually recommended by the vendor to be stored at $4^{o}C$. They have a natural affinity to the walls of many common containers used in a biochemical laboratory at concentration lower than 1 mg/ml. It is highly recommended to split the original antibody purchase into a series of smaller, low-protein-binding vials and remain at the original concentration for better antibody preservation, as exposure to air would increase the degradation rate of the antibodies.

Therefore, each split vial should not contain an antibodies quantity for more than two uses. The ratio of active antibodies decays over time, thereby even the split antibodies vials that have never been opened shall not be considered in working order after 2 months in storage.

††† ***Rinsing fiber to remove left-over salt:***

If the left-over PBS salt crystals are not entirely removed from the biosensor fiber surface, they tend to deliver a disastrous phenomenon: the spectrum of the transmitted optical power will shift upwards instead of downwards with a thicker cladding layer. The reason for this phenomenon has yet to be answered, but experimentally such phenomenon can be reversed by soaking the fiber in DI water and stirring the water vigorously, and by doing this the remaining PBS salt crystals will be dissolved and removed from the fiber surface.

†††† ***Using 1% dry milk suspension as blocking reagent:***

Typical ELISA tests generally use 3% to 5% dry milk as blocking reagent. However, a high dry milk concentration or a longer blocking period will reduce the available antibody binding sites by blocking the antigen's accessibility to such sites. Consequently, a dry milk concentration higher than 1% or soaking period longer than 5 minutes has been found to diminish the total antibody sites available for antibody-antigen binding, leading to the attenuation of the sensitivity of the sensor. Yet, swab samples from a human subject may require a higher blocking concentration, as such solutions may contain biomolecules more likely to exhibit nonspecific binding.

4.2.3 Preparation of the Sample Suspensions

We refer to sample solutions as pure when they contain only pure culture bacterium in a PBS solution. The sample suspensions used in our tests are diluted in series from original solutions at high concentration ranging between 10^7cfu/ml to 10^8cfu/ml, provided by collaborator Dr. Bandara.

All the vials and tubes used in dilution and final sample suspension storage are autoclaved. The original pure culture samples are suspended in 1x PBS at pH 7.4, and the same PBS solution is used for serial dilution from higher concentrations.

The pure culture dilutions should not exceed 10 ml per tube, and shall be discarded after 2 months in storage whether opened for tests or not.

For mouse tissue samples, the sample suspensions provided for the biosensor assays are made of organs of mice inoculated with *MRSA* strain 1961B or MSSA strain ATCC 29213. The tissues were confirmed to contain the respective bacterial strains the mice were inoculated with by viable plate count on Brain Heart Infusion broth (BHIB) agar (Becton-Dickinson).

The original mouse tissue samples also contained some organ fragments of the mice, which create nonspecific binding problems for the biosensor. However, when diluting the original mice tissue solutions at a ratio of 1:5, the nonspecific binding can be efficiently suppressed with the help of blocking the sensor with dry milk. Therefore, for any later experiments regarding mouse tissue samples, a 1:5 dilution from the original solutions were performed to obtain best results.

Each of eight volunteers from Virginia Tech has provided three human swabs that have touched their ears, noses and skin, respectively. Suspensions were made from those swabs to acquire Staphylococcal cultures for biosensor assays. Studies for whether the suspensions

contain MRSA strains or not were conducted through plate counts on BHI agar or BBL™ CHROMagar™.

Patient swabs were provided by Dr. Clements of Carilion Roanoke Memorial Hospital. The swabs were taken from patients' open wounds of a suspected MRSA. The swab samples are marked only with numbers, and the medical condition or the identity of the patient are never disclosed, except whether or not the swabs were identified as positive with MRSA strains from the laboratory of the hospital. All the work done with human subject samples and clinical swab samples met the criteria for exemption 4, based on the Exemption 4 statement: "Research involving the collection or study of existing data, documents, records, pathological specimens, or diagnostic specimens, if these sources are publicly available or if the information is recorded by the investigator in such a manner that subjects cannot be identified, directly or through identifiers linked to the subjects".

The swab samples are received in sealed biosafety swab-containers and stored in the freezer at -20 ^{o}C. The swabs are taken out of the freezer 1 hour prior to the experiments to allow time for containers and swabs to reach room temperature. Each sample includes two swabs taken from the same patient. After reaching room temperature, the swab is carefully taken out of the container and dipped into 5 ml of sterilized PBS solution at pH 7.0. The swab is stirred in the solution to ensure the majority of the microorganisms and biomolecules carried by the swab will be transferred into the sample suspension, while keeping the cotton head immersed within the buffer liquid all the time during the stirring. The suspension is vortexed for better mixing and then split into 10 vials, each containing 0.5 ml of sample suspension. One vial of the suspension is put on a fiber immediately after the suspension is made, the rest are stored in the freezer for later repeating the tests or for confirmation tests via ELISA.

4.2.4 Biosensor Assay Results with Pure Culture Samples

As the initial and most fundamental studies, assays with pure cultures can provide answers to two major questions: 1) if the biosensor system is **sensitive** enough for actual use in hospitals, and 2) how specific is the system when facing a large range of the bacteria strains and only responding to the existence of antigen of interest?

In order to address these two questions, two series of experiments were designed. The first experiment explores the biosensor's sensitivity and contrast ratio of the signals, Strains tested in such experiments are serially diluted from stock solutions at a concentration of 10^{8}cfu/ml. In a typical experiment, MSSA 29213 and MRSA 1556 at the same concentration were tested sequentially over the same biosensor fiber to compare the signal response between the two. This is called "one pair" of tests, referring to the intention that any positive signal response is not generated by nonspecific binding as the negative controls at the same concentration tested prior to MRSA strain samples.

In most experiments within this experimental design, multiple culture sample pairs at escalating concentration are tested sequentially. The results for subsequent tests after the first pair are still valid and meaningful as immobilized MRSA Mab sites are not saturated after the first experiment pair, and are sufficient for sequential test with sample pairs at higher concentration. Under this experimental design, the first pair of samples is at the lowest concentration – 100 cfu/ml, the next pair is at 10^{4}cfu/ml, and the third pair is at the concentration of 10^{6}cfu/ml, which means we are expecting increased transmitted power attenuation from each exposure to MRSA solution. A positive reading is presented as the percentage of power loss, and it is referred as a signal reduction higher than threshold at the resonant wavelength, which is set at 7.5% of power attenuation based on the statistic analysis. A negative reading is also presented

as the percentage of power loss, and it is referred as a signal reduction below the set threshold. A well blocked biosensor shall return negative readings at or around 0% of signal reduction to non-MRSA strains.

The experimental results discussed below have confirmed the expectations, and showed the Mab-based biosensor fiber is not saturated even after 2 pairs of tests, and capable of continuous sensing tasks. Figure 4-3 shows the result of a sequential MRSA vs. MSSA pairing tests, where the samples are serially diluted from 10^8cfu/ml source solution.

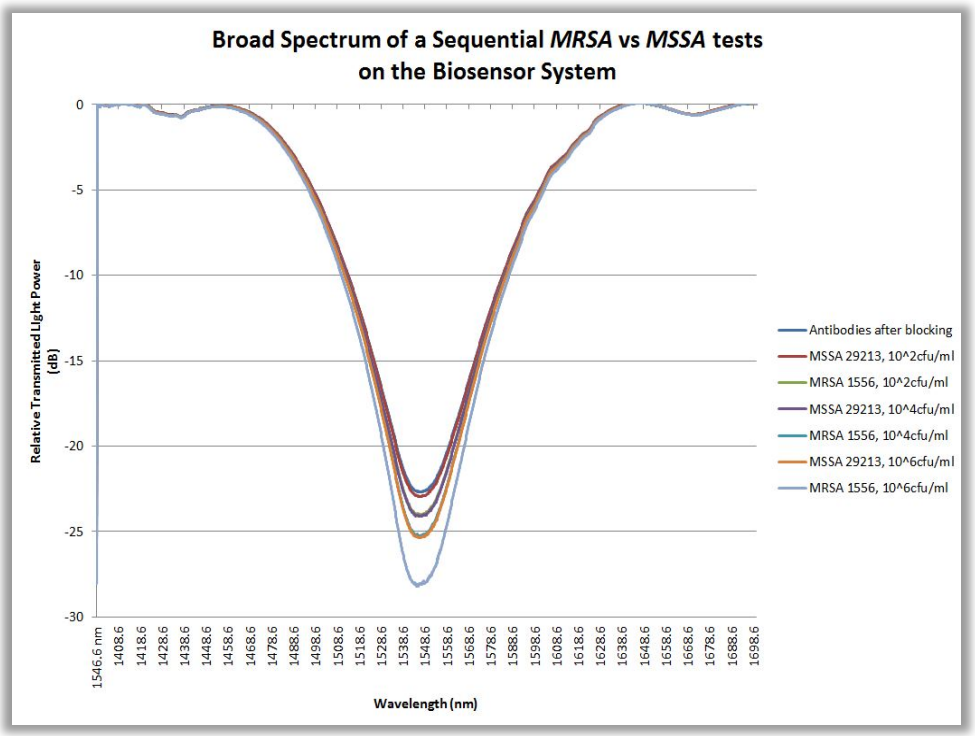

(A)

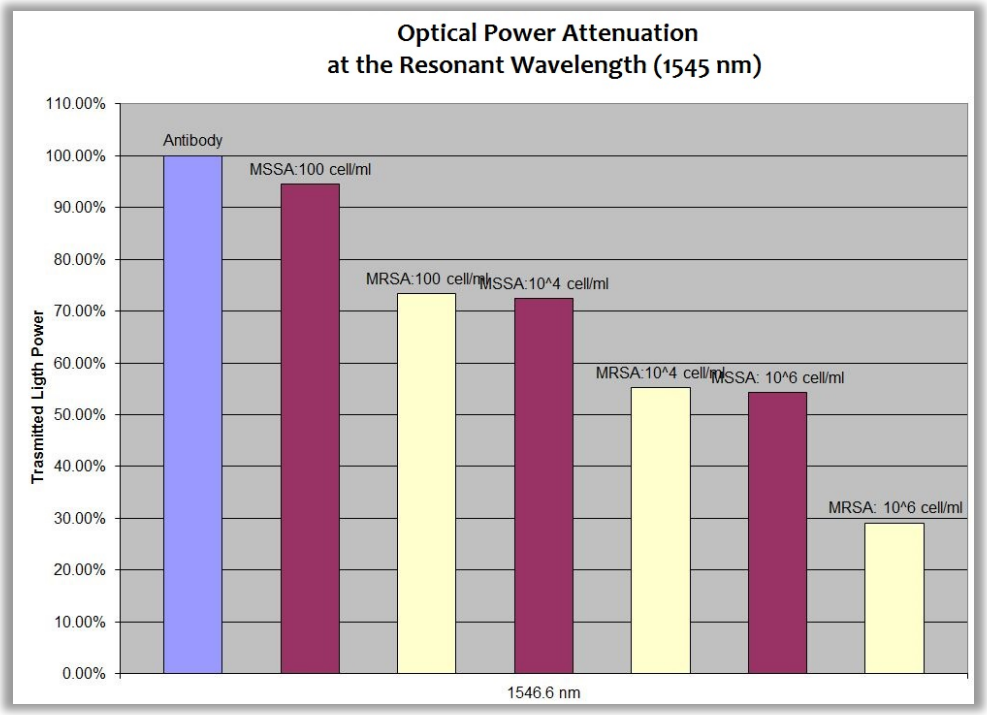
Optical Power Attenuation
at the Resonant Wavelength (1545 nm)
Trasmitted Ligth Power
110.00%
100.00%
90.00%
80.00%
70.00%
60.00%
50.00%
40.00%
30.00%
20.00%
10.00%
0.00%
Antibody
MSSA:100 cell/ml
MRSA:100 cell/ml
MSSA:10^4 cell/ml
MRSA:10^4 cell/ml
MSSA: 10^6 cell/ml
MRSA: 10^6 cell/ml
1546.6 nm

(B)

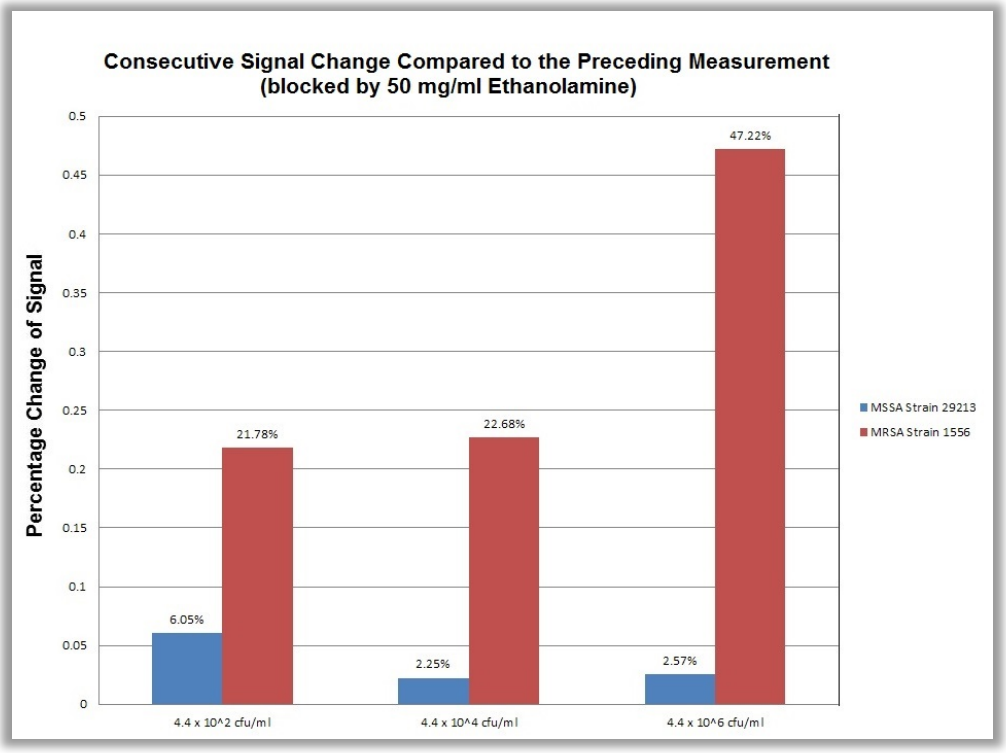
Consecutive Signal Change Compared to the Preceding Measurement
(blocked by 50 mg/ml Ethanolamine)
Percentage Change of Signal
0.5
0.45
0.4
0.35
0.3
0.25
0.2
0.15
0.1
0.05
0
6.05%
21.78%
2.25%
22.68%
2.57%
47.22%
4.4 x 10^2 cfu/ml
4.4 x 10^4 cfu/ml
4.4 x 10^6 cfu/ml
MSSA Strain 29213
MRSA Strain 1556

(C)

Figure 4-3: (A) Broad spectrum measurement of the transmitted optical power after each pure culture test. (B) The percentage of the transmitted optical power at the resonant wavelength after each pure culture test. (C) The sequential comparison of the signal reduction generated by each pure culture sample.

Fig 4-3 (A) displays the full picture of the broad spectrum scanned after each pure culture sample tested. It explicitly reflects the most valuable trait of the TAP LPG fiber – that the attenuation of the spectrum is along a fixed wavelength, the resonant wavelength to the coupled-mode the LPG fiber works on. At this resonant wavelength, the transmitted optical power is attenuated much more than nearby wavelengths.

Fig 4-3 (B) shows the transmitted optical power at the resonant wavelength after each sample test, presented in percentage form compared to the reading after the biosensor is fully assembled and properly blocked by ethanolamine (50 mg/ml). It is clear that the major signal reduction is by the MRSA strain cultures, and the amount of the signal reduction agrees with the broad spectrum measurement, meaning that by simply monitoring the power variation at the single resonant wavelength, the biosensor is able to tell if any material is attached to the fiber after each test.

Fig 4-3 (C) displays the sequential signal reduction added by each sequential pure culture test. This figure provides a more detailed look at the biosensor behavior and its response to the applied culture samples, and it will be the major chart type for analysis and data reporting in this dissertation. In this graph, each bar represents the relative transmitted optical power attenuation compared with the previous measurement, where each measurement after the test becomes the new reference level for the next test measurement. Two major conclusions can be extracted from this figure:

1) The change in transmission for MRSA strain samples is much greater than the background signals generated from MSSA samples and nonspecific binding. This means it is

possible to set up a critical level for this sensor design, where any signal below this critical level could be generated by nonspecific binding or by a sample that contains a methicillin-sensitive bacterium, yet any signal above this level is considered to be generated by antigen-antibody binding and the sample is considered to contain MRSA. Also, it can be concluded that nonspecific binding sites are fairly limited in this study, as the largest nonspecific binding response is produced by MSSA 29213 strains at 100 cfu/ml, however, the negative responses remain below 3% for higher MSSA concentration and further negative control tests. Selecting a more efficient blocking reagent, such as 1% dry milk or bovine serum albumin (BSA) or increasing the length of the blocking step can help reduce the nonspecific binding, though it will also reduce the possible signal level of the MRSA samples. An experiment using 3% dry milk as blocking agent has been shown to be a better choice than ethanolamine, and it will be examined closely later.

2) The biosensor system is able to detect MRSA pure cultures at a concentration as low as 100 cfu/ml. Also, the signal reduction is larger at higher MRSA concentrations. The signal attenuation from 10^4cfu/ml MRSA sample is 22.68%, and the signal attenuation from 10^6cfu/ml MRSA sample doubled to 47.22%. For a sequential test where multiple culture samples are tested, this result indicates that the available Mab binding sites are more than 10 million, the binding sites are evenly spread over the sensor surface so that over a small amount of antigen binding does not significantly affect the neighboring binding sites, and they do not substantially diminish the MRSA detecting capacities for further tests. Furthermore, the signal attenuations from 100 cfu/ml MRSA sample and 10^4cfu/ml sample are almost identical. Though not fully understood, this may be partially due to some of the antibody binding sites being blocked by exposure to the 100 cfu/ml solution. In this experimental design, the negative threshold, or the

"grey zone", is 7.5% of signal reduction. Any samples generating a signal response equal or smaller than 7.5% shall be considered to not contain a significant amount of methicillin-resistant bacteria.

A supplemental experiment for comparing how change of the blocking reagent will affect the sensitivity and specificity of the biosensor system has also been performed. In such experiments, all the procedures, the constitution of biofilm, the sample concentration and strain type remain the same, the only difference is from the choice of blocking reagent: 3% dry milk replaced 50 mg/ml Ethanolamine as the blocking reagent. The results are shown in Fig 4-4.

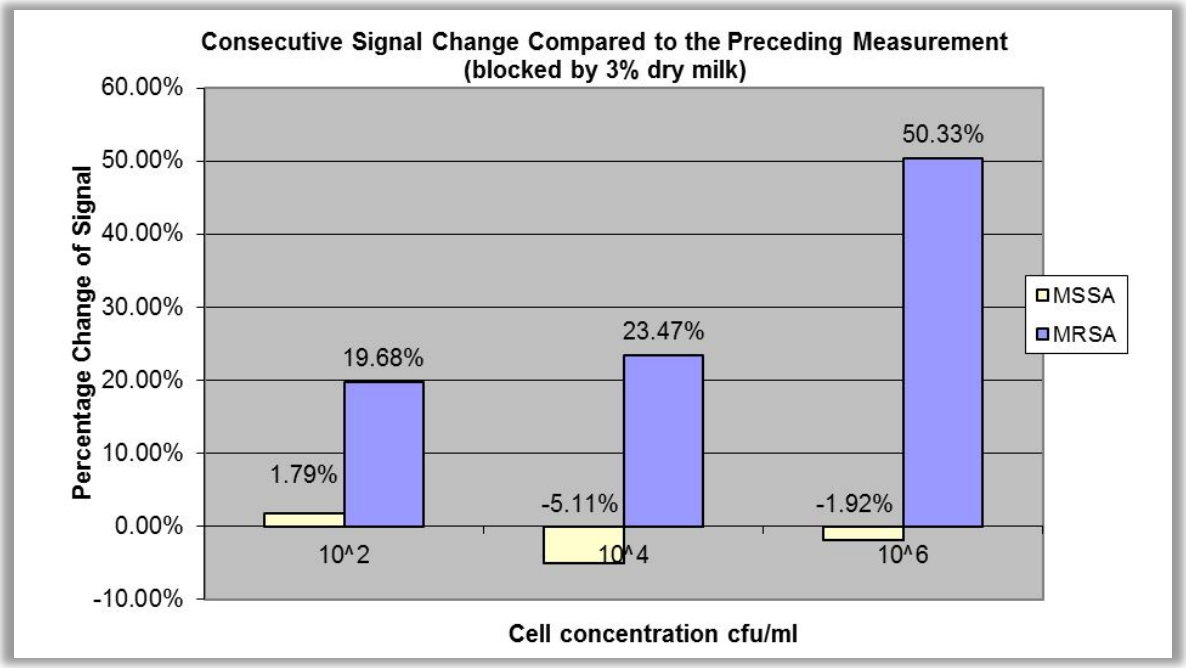

Figure 4-4: The sequential test with the same procedure, biofilm composition, sample concentration and strain type as the one conducted in Figure 3-17. The only difference is 3% dry milk was applied as a blocking reagent instead of 50 mg/ml ethanolamine.

This experiment indicates that 3% dry milk is a much better choice for blocking reagent than 50 mg/ml ethanolamine in sensitivity and specificity. First, all of the MSSA 29213 pure culture samples returned a 2% or lower response, which significantly lowered the threshold level for a positive diagnosis by 2/3. Second, compared to the preceding experiments using ethanolamine as

blocking reagent, switching to dry milk only reduced the positive reading for the first MRSA sample by about 2%, and readings for the next two MRSA samples at higher concentration returned a close or even higher response. This means that the sensitivity of the biosensor is only slightly affected by using the more 'aggressive' blocking reagent. Therefore, all the following experiments to be presented here were conducted with dry milk as blocking reagent, if not stated otherwise.

The next issue to address is to verify if this biosensor design is capable of responding to a broader range of MRSA strains. Researchers have discovered over a hundred distinct types of MRSA strains that differ at the genetic level and have various degree of immunity to various antibiotics. A community-acquired MRSA strain (CA-MRSA) known as USA300 had been rarely reported in communities across the country by 2000.[120] However, today over 70% of patients who suffer from MRSA infections are identified to be carrying MRSA strain USA300. The dynamic and quick evolution of MRSA strains in communities requires the biosensor to be effective and adaptive to identify with every possible strain that is methicillin-resistant.

The broad screening of a vast collection of all known MRSA strains by the biosensor is important for validating the credibility of diagnostic reports generated by the system. In the longer term this is possible as the sensor system can return diagnostic results within an hour's period. However, acquiring the full collection of strains is difficult, as the transportation of these strains from distant storage locations are subject to strict biological safety requirements, and require cooperation between various parties, which makes such a complete screening process cost-ineffective at the current stage of the biosensor development.

[120] http://www.bcm.edu/molvir/index.cfm?pmid=16508

Despite the difficulties of acquiring a large number of distinct MRSA strains, our collaborators Dr. Inzana and Dr. Bandara have been able to supply dozens of different MRSA strains for biosensor testing, which they have amassed in the course of other research projects.

The screening of a wide range of various MRSA strains is done by testing only one pair of samples, which is a sequential test of a *non*-MRSA strain culture solution at 10^4cfu/ml as the control group, and a MRSA strain culture solution at the same concentration. If the biosensor operates as desired, it should return below-threshold optical power attenuation after exposure to the *non*-MRSA culture sample, and return large optical power attenuation after the various MRSA culture samples. The paired strain samples put into the tests were selected randomly.

As the negative controls tested in this series of experiments includes a vast category of bacteria families, the biosensor needed to be upgraded to suppress the nonspecific bindings which was a serious problem in the first experimental series. Ethanolamine at concentration 50 mg/ml is not powerful enough to block out all the nonspecific binding sites exposed to the testing sample suspension. Therefore, 3% dry milk are used as the blocking reagent in this strain screening series.

The results are shown below in two separate tables -- the treatment group, and negative control group, which should have little to no signal reductions.

Table 4-1 **Summary of pure culture tests:**

Treatment Group

MRSA Strains	***Light Attenuation Percentage Change***	***Data Range***	***BBL CHROMagar Result***
MRSI,09-2908	**23.94%**	**±1.09%**	+
MRSS,10-2737	**18.73%**	**±0.43%**	+
MRSI,11-2934	**33.82%**	**±2.85%**	+
MRSA,1961-B	**18.68%**	**±0.14%**	+

MRSI,11-3332	**20.98%**	**±0.59%**	+
MRSA,2754	**26.97%**	**±0.13%**	+
MRSA,12-0057/58	**9.12%**	**±1.28%**	+
MRSA,1171	**34.55%**	**±0.31%**	+
MRSA,3376.3	**19.30%**	**±0.15%**	+
MRSI-gr,3-24-10	**32.49%**	**±1.10%**	+
MRSS,12-0504	**10.55%**	**±0.63%**	+
MRSI-gr, 4-6-10	**9.55%**	**±0.12%**	+
MRSA,94045	**10.02%**	**±0.07%**	+
MRSA,1565	**18.92%**	**±0.06%**	+
MRSI,11-2716	**25.09%**	**±0.02%**	+
MRSA,12-1746	**30.47%**	**±0.10%**	+
MRSI,12-0220	**13.48%**	**±2.50%**	+
MRSS,12-1309	**23.09%**	**±0.40%**	+
MRSI,12-1316	**27.87%**	**±0.76%**	+
MRSA,1573	**16.78%**	**±0.13%**	+
MDR-MRSI 11-0803	**17.75%**	**±1.50%**	+
MRSA,9122	**31.85%**	**±1.45%**	+
MRSE	**31.36%**	**±1.34%**	+
MRSH	**20.67%**	**±0.45%**	+
S.aureus T.R	**27.78%**	**±0.44%**	+
MRSI,2-16-09	**15.45%**	**±0.31%**	+

** The BBL CHROMagar results are provided by collaborator Dr. Bandara, and performed with strains at culture concentration of 10^8cfu/ml.*

*** All pure culture samples were tested at the concentration of 10^4cfu/ml*

Table 4-2 **Summary of pure culture tests:**

Negative Control Group

Non-MRSA Strains	***Light Attenuation Percentage Change***	***Data Range***	***BBL CHROMagar Result***
MSSI, 12-1789	**1.95%**	**±0.17%**	**-**
E.coli,S17-1	**-0.44%**	**±0.32%**	**-**

E.coli,Top-10	**-0.07%**	**±0.61%**	**-**
E.coli, XL Blue	**1.85%**	**±1.20%**	**-**
GPG, 12-1308	**-4.13%**	**±1.99%**	**-**
GPG,12-1736	**-1.85%**	**±0.02%**	**-**
Entero. faeliaes., 12-1864	**-2.99%**	**±0.69%**	**-**
MSSI,12-1290	**1.80%**	**±2.23%**	**-**
MSSI,12-1853	**1.99%**	**±0.07%**	**-**
MSSH,12-1286	**-2.00%**	**±0.16%**	**-**
Strep,12-1825	**-0.62%**	**±0.80%**	**-**
P.M.,12-1923	**1.78%**	**±1.56%**	**-**
Entero. faeliaes., 12-1857	**-2.22%**	**±0.27%**	**-**
MSSI,12-1290	**2.67%**	**±0.08%**	**-**
MSSA,29213	**0.80%**	**±0.99%**	**-**
Pseudomonas aeruginosa	**-0.69%**	**0.30%**	**-**

* *The BBL CHROMagar results are provided by collaborator Dr. Bandara, and performed with strains at culture concentration of 10^8cfu/ml.*

** *All pure culture samples were tested at the concentration of 10^4cfu/ml*

Choosing 10^4cfu/ml as the standard concentration for all the culture samples – methicillin-sensitive or methicillin-resistant – is based on the sensitivity limit consideration of the biosensor. Testing 100 cfu/ml MRSA samples with biosensor could explore the low sensitivity limit. However, for some strains such a concentration would yield a signal reading below the set threshold, which contradicts the purpose of these experiments of answering whether the biosensor could return affirmative results to MRSA strains in general.

For the control group (non-MRSA strains), there are negative readings associated with some strains in Table 4-2. There are two possible reasons for this. First, as has been examined in section 3.2.4, the system itself tends to inevitably vary at a range of ±1.5% as the system error

due to instability of the light source and optical spectrum analyzer. Therefore, for a control sample that has added nothing to the fiber, there is still the chance of getting a negative reading due to the instability of the sensor system. Second, in principle, after the biosensor is assembled, the surface film composition should remain the same, if not considering further antigen-antibody or nonspecific bindings with the tested sample suspensions. However, in reality the binding between receptors and the base ISAM film tends to deteriorate over time and exposure to salts. In addition, every time the fiber surface is flushed by deionized (DI) water for rinsing, the strong liquid flow may remove some of the receptors and blocking reagent. With all these effects added together, and if they all coincide in one negative control sample test, it is not surprising to see an occasionally negative reading from the biosensor.

Most importantly, one can see that the largest reading for the negative control group is 2.7%, while the smallest signal for the positive group is 9.1%. Thus, the LPG biosensor does work to the expectation of distinguishing methicillin-resistant and methicillin-sensitive bacteria, and the 7.5% cutoff setting is a proper choice for threshold.

4.2.5 Biosensor Assay Results with Human Subject Samples

Another important test series was designed to test the sensor capacity for samples collected from human subjects, which is the ultimate goal for this biosensor system. Swab samples taken from athlete volunteers at Virignia Tech have been collected by Dr. Inzana's research group. Blood agar cultures were used to make sample solutions. Therefore, these human subject samples are less complex than sample suspensions made directly from swab samples of infected tissues. Nevertheless, testing human subject samples extracted from common community carriers has significance, as these samples represent randomly selected CA-MRSA strains the biosensor

system may encounter in future community screening tests, and the successful differentiation of such CA-MRSA from other bacteria found commonly in humans.

The chart below summarizes the testing results of the human subject samples. These samples were also tested by BBL CHROMagar. A positive agar response is referred to as growth on the agar, while for negative responses, the agar did not show any trace of growth that are suppose to indicate the existence of antigen-antibody binding in any of the repeating tests

Table 4-3 **Summary of human subject sample tests:**

Culture Sample	*Light Attenuation Percentage Change*	*Data Range*	*BBL CHROMagar Result*
CG-N	**20.11%**	**±2.80%**	+
YP-N	**9.53%**	**±0.21%**	+
AC-H	**18.19%**	**±0.55%**	+
CG-E	**10.22%**	**±0.89%**	+
CG-H	**20.56%**	**±0.13%**	+
AB-E	**20.70%**	**±0.65%**	+
YP-E	**17.14%**	**±3.79%**	+
AC-E	**21.39%**	**±0.10%**	+
AC-H	**11.09%**	**±0.93%**	+
KF-H	**-0.44%**	**±0.58%**	-
KF-E	**-1.68%**	**±0.41%**	-
AB-N	**-1.38%**	**±0.92%**	-
HAK-H	**-0.30%**	**±0.05%**	-
HAK-E	**-2.18%**	**±0.26%**	-
BF-N	**-3.25%**	**±1.25%**	-
AH-H	**-0.72%**	**±0.32%**	-
AH-E	**-4.12%**	**±0.17%**	-
YP-H	**1.06%**	**±0.15%**	-
AB-H	**0.03%**	**±0.26%**	-

** The BBL CHROMagar results are provided by collaborator Dr. Bandara and performed with strains at culture concentration of 10^8cfu/ml.*

*** The capital letter after the dash symbol in each culture sample's name indicates the body parts where the volunteers got the swab touch. E – ear, H— hand, N – nose.*

*** *The agar tests for human subject culture samples are harder to evaluate, since the MRSA strain concentration is unknown and the swabs may carry various bacteria to the sample suspension from the human subject as well. Therefore, the human subject swab samples that were tested positive are marked with the degree of the results as well. Some – a visible yet not strong color changing, indicating some MRSA bindings, concentration may be low; High – a strong and clear color changing, indicating lots of MRSA binding, concentration may be high.*

The results from the biosensor system and the agar culture tests agree with each other. Though all of the agar-positive samples also displayed above-threshold readings from the biosensor system, the detectable degree of these samples varies from case to case.

4.2.6 Biosensor Assay Results with Mice Tissue Samples

The human subject tests showed that the biosensor system is capable of detecting random CA-MRSA strains. Another key question is whether the biosensor can bind only with any MRSA strain from a more complex sample. Therefore, experiments for testing biosensor system with mouse tissue samples were designed. Organ tissues harvested for making sample suspensions contain a wide array of biomaterials, such as blood cells, proteins, and enzymes, which might potentially interfere with reactions occurring on the fiber sensor surface. Therefore, such tissue samples are a close simulation of clinical swab samples taken directly from a patient's suspected infection. The method and procedures for preparing mice tissue samples are described in section 4.2.3 and provided by Dr. Bandara.

Though the mice were inoculated with about 10^7cfu of either MRSA 1956 or MSSA ATCC 29213 strains, no information about the respective strain concentration was available prior to the test. Only what strain the mice were infected with was given during the execution of experiments.

Based on such information, tissue samples prepared from the same organ of the mice inoculated by either MSSA strains (referred as "MSSA tissue samples" below) or MRSA strains (referred as "MRSA tissue samples" below) were paired for a sequential test, and each fresh

biosensor was used for each pair of tissue samples. The first few trials were failed due to difficulties in differentiating MRSA tissue samples and MSSA tissue samples. Therefore, the dry milk concentration was increased to 5%, and the tissue sample suspensions were diluted with autoclaved 1x PBS at pH 7.0 at 1:6 ratio. The results are encouraging, and shown in Figure 4-5:

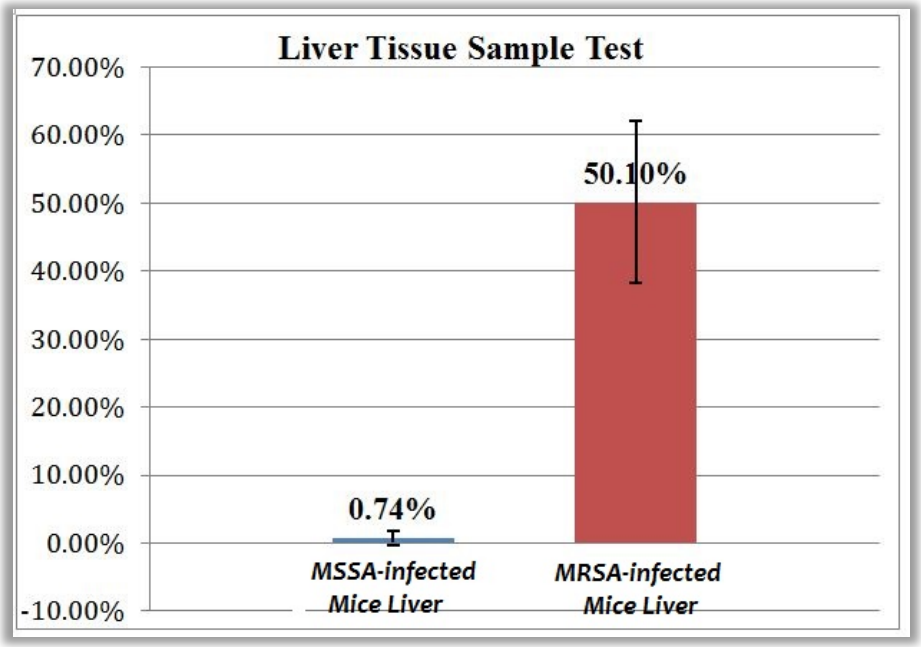

(A)

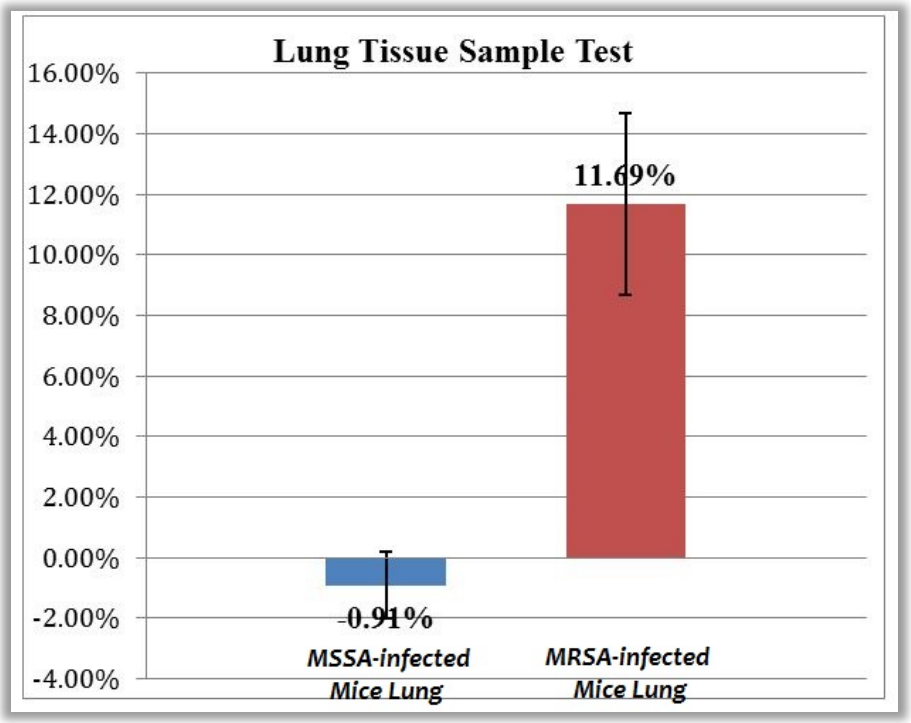
Lung Tissue Sample Test
16.00%
14.00%
12.00%
10.00%
8.00%
6.00%
4.00%
2.00%
0.00%
-2.00%
-4.00%
11.69%
-0.91%
MSSA-infected Mice Lung
MRSA-infected Mice Lung

(B)

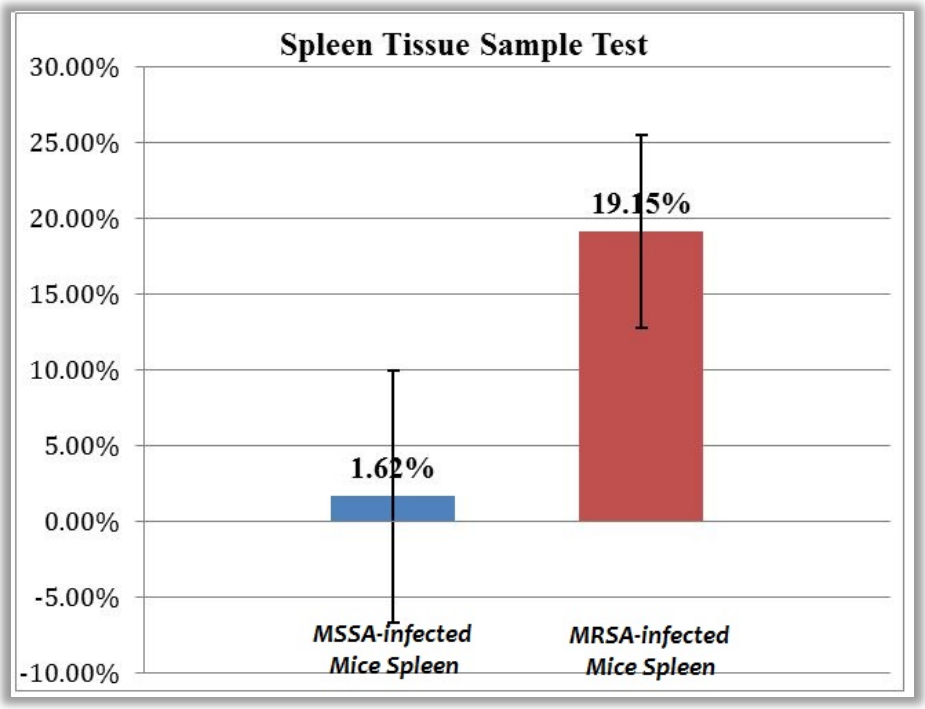
Spleen Tissue Sample Test
30.00%
25.00%
20.00%
15.00%
10.00%
5.00%
0.00%
-5.00%
-10.00%
19.15%
1.62%
MSSA-infected Mice Spleen
MRSA-infected Mice Spleen

(C)

Figure 4-5: Mouse tissue sample pairing tests: (A) Liver tissue samples; (B) Lung tissue samples; (C) Spleen tissue samples.

Three repeated experiments were conducted for each tissue sample pair to evaluate the statistical significance of the results, and standard deviation bars are indicated on the data charts above.

The pairing comparison tests showed large signal differences, with liver tissue samples collected from MRSA infected mice returning an average power attenuation of 50.11%, and samples from MSSA infected mice only yielding 0.74% optical power attenuation with a small standard deviation bar as well. The contrast between positive readings and negative readings are clear and without doubt.

The lung tissue sample pairing tests also gave a relatively clear result, as signals from lungs of MRSA infected mice is averaged power attenuation of 11.69% and its standard deviation bar sets the lowest positive reading level well above 8%, compared with the negative readings ranging between -2% to 0%. This lower positive measurement compared to data of liver and spleen tissue testes implies that the lung might be the least affected organ became the mice were infected with MRSA by Intraperitoneal injection.

The spleen tissue samples returned a fairly high positive reading for MRSA infected mouse samples, which averaged 19.15%. However, the variation of the readings cannot be ignored in these tests. The standard deviation for both MRSA tissue samples and MSSA tissue samples were above 7%, with the upper negative control result at 10% and lower positive test result at 12%. Therefore, the signal distinction between positive and negative readings is too small to set a clear cut-off for diagnostic. The large variation may be due to the complexity of the

composition of the spleen tissue sample suspensions, which may reflect the role of spleen as blood filter, adding complexity to the composition of the spleen tissue samples.

The data obtained from mouse tissue sample tests are summarized in the Table 4-4:

Table 4-4 **Summary of the mouse tissue sample tests on the antibodies based MRSA biosensor**

Mouse Number	***Spleen Tissue Suspension***	***Liver Tissue Suspension***	***Lung Tissue Suspension***	***Mice infected by MRSA***
Mouse #4	19.2% ± 6.4%	50.1% ± 11.9%	11.7% ± 3.0%	Yes
Mouse #2	1.6% ± 8.3%	0.7% ± 1.0%	-0.9% ± 1.1%	No

** The data is presented as "average ± standard deviation".*

Based on the data obtained from mouse tissue samples, one can draw two conclusions: first, the biosensor is able to detect MRSA in a sample suspension that contains a complex mixture of biomolecule components. However, in order to avoid a large amount of nonspecific bindings, the sample suspensions may require serial dilution and the fiber sensor may need a more aggressive blocking approach. Both measures may also potentially reduce the sensitivity of the fiber sensor to recognize and bind MRSA strains, especially when the strains are at very low concentrations. Second, though necessary precautions must be taken to reduce the interference of nonspecific bindings and background noise, the fiber sensor is still capable of detecting MRSA from a complex sample suspension such as mouse tissue samples. More importantly, the biosensor did not react with MSSA or similar strains from tissue specimen, which could induce similar symptoms as MRSA, necessitating sound treatment decisions.

4.2.7 Biosensor Assay Results with Clinical Swab Samples

The biosensor setup based on monoclonal antibodies to MRSA has been proven in the preceding experiments to be effective and capable of detecting a wide range of strains, even from

complex solutions. The platform should thus be ready for testing clinical swab samples collected from patients suspected of MRSA infections.

Since whether a swab suspension containing a MRSA strain is unknown, it makes such an experiment a blind test. A typical swab sample test is designed to consist of 4 sequential tests to confirm any signal change is valid:

1) In the first test, the sensor is treated with a clean MSSA strain culture at 10^6 cfu/ml, to confirm the sensor is insensitive to nonspecific binding. Therefore, all subsequent signal reduction shall come from MRSA-antibody binding.

2) After the test 1, one swab suspension solution is applied to the fiber, and a measurement is taken.

3) After the test 2, a clean MRSA strain culture at 10^6 cfu/ml is tested, to confirm that the sensor is reactive to MRSA. If no positive reading obtained from test 2, it should be sufficient to prove the swab suspension tested did not contain a MRSA strain.

4) Another swab suspension coming from the same patient is tested last. This is a double checking measure and could help reduce uncertainty of the test.

Despite incorporating confirmation experiments to reduce random variation and uncertainties among the blind tests, the swab suspension tests failed to deliver trustworthy results. The most common cases would show contradictory results generated from tests 2 and 4. Though there is possibility that the original swab suspension was not well mixed, or the MRSA concentration is so low that the biosensor may not always be able to detect a MRSA strains' existence from a complicated suspension, the unmatched results have to be discarded to support a solid diagnostic decision. For about half of the remaining positive results, the hospital laboratory culture results have negative.

Therefore, for the first 16 swabs received and tested, only 6 samples matched results to the clinical culture test. It will be shown in section 3.3.3 that using MRSA DNA probe on the biosensor is able to improve the stability and sensitivity of the diagnostic results with clinical swabs.

4.2.8 Statistical Importance of the Biosensor Assays

This section focuses on the analysis of the statistical significance of the data presented in the discussions above. It is evident from the data shown in preceding sections that for individual tests that compare MRSA containing samples with non-MRSA containing samples, the distinction between positive responses and null/negative responses is reliable. However, it is important to quantify how well the Mab based biosensor could differentiate methicillin-resistant and methicillin-sensitive bacteria.

All the statistical analyses presented below is based on the raw data from pure cultures, which are the data sets used for calculating mean and standard deviation for Table 3-1 through Table 3-3. These data were obtained from the same experimental settings, following identical procedures and sample suspension preparation protocols, and have large enough data numbers for valid statistical analyses.

Figure 4-6 shows a scattered point chart of the percentage power attenuation distribution in MRSA strain samples and non-MRSA strain samples, respectively:

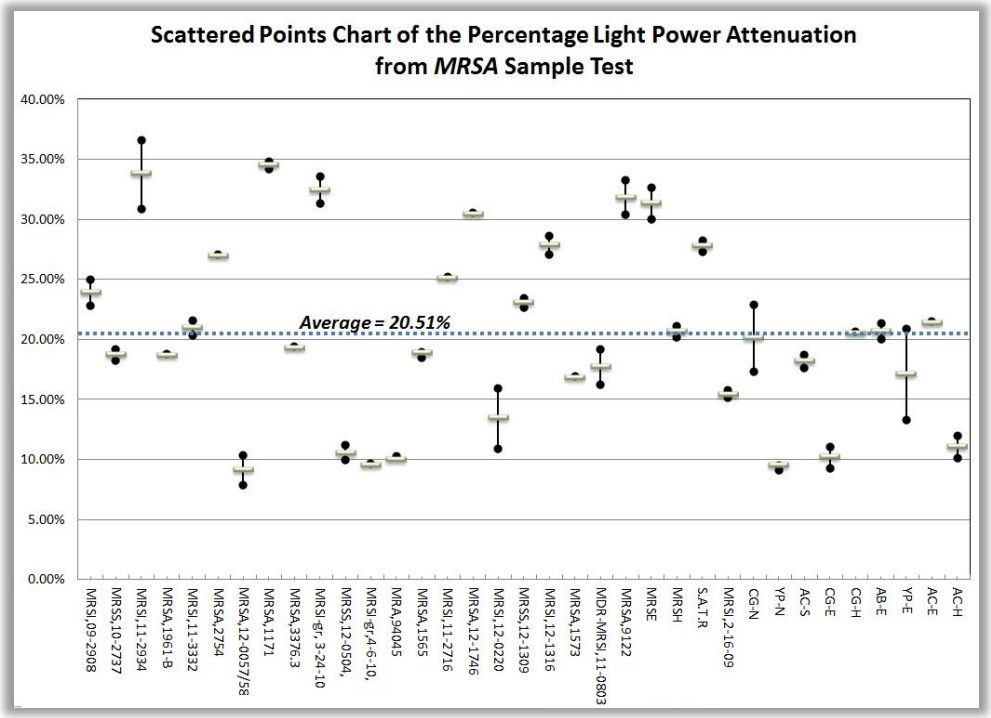
Scattered Points Chart of the Percentage Light Power Attenuation from MRSA Sample Test
40.00%
35.00%
30.00%
25.00%
20.00%
15.00%
10.00%
5.00%
0.00%
Average = 20.51%
MRSI,09-2908
MRSS,10-2737
MRSI,11-2934
MRSA,1961-B
MRSI,11-3332
MRSA,2754
MRSA,12-0057/58
MRSA,1171
MRSA,3376.3
MRSI-gr,3-24-10
MRSS,12-0504,
MRSI-gr,4-6-10,
MRA,94045
MRSA,1565
MRSI,11-2716
MRSA,12-1746
MRSI,12-0220
MRSS,12-1309
MRSI,12-1316
MRSA,1573
MDR-MRSI,11-0803
MRSA,9122
MRSE
MRSH
S.A.T.R
MRSI,2-16-09
CG-N
YP-N
AC-S
CG-E
CG-H
AB-E
YP-E
AC-E
AC-H

(A)

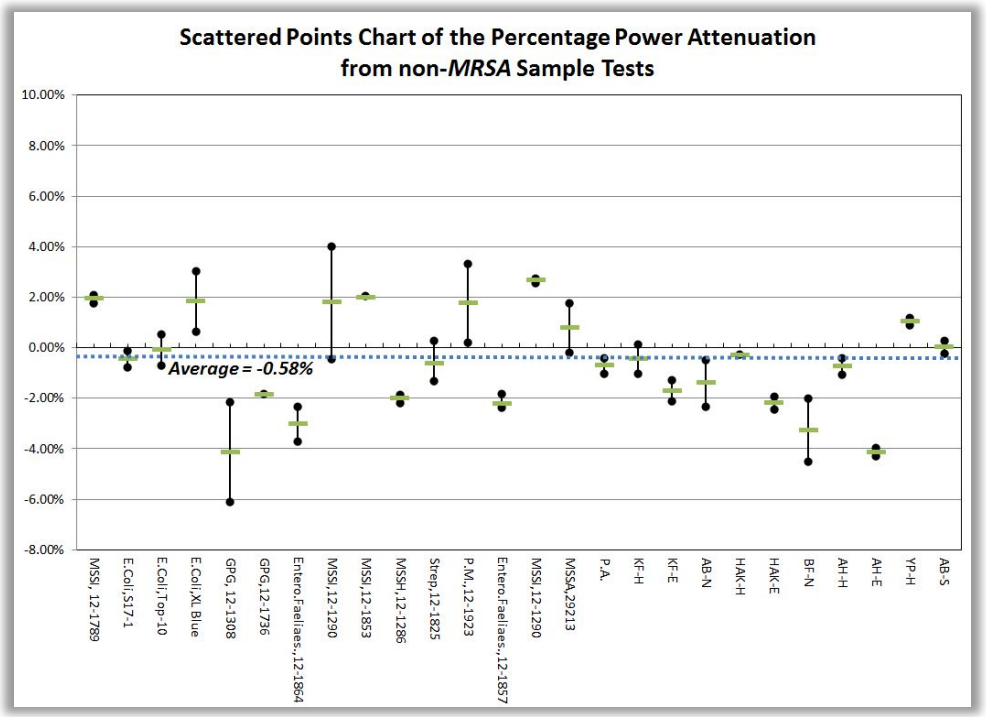
Scattered Points Chart of the Percentage Power Attenuation from non-MRSA Sample Tests
10.00%
8.00%
6.00%
4.00%
2.00%
0.00%
-2.00%
-4.00%
-6.00%
-8.00%
Average = -0.58%
MSSI, 12-1789
E.Coli,S17-1
E.Coli,Top-10
E.Coli,XL Blue
GPG, 12-1308
GPG,12-1736
Entero.Faeliaes.,12-1864
MSSI,12-1290
MSSI,12-1853
MSSH,12-1286
Strep,12-1825
P.M.,12-1923
Entero.Faeliaes.,12-1857
MSSI,12-1290
MSSA,29213
P.A.
KF-H
KF-E
AB-N
HAK-H
HAK-E
BF-N
AH-H
AH-E
YP-H
AB-S

(B)

Figure 4-6: Scattered point chart of the average percentage power attenuation from (A) MRSA strain sample tests, and (B) non-MRSA strain sample tests. The circles indicate the upper and lower reading boundaries of the multiple tests to the corresponding strain sample.

The differences between these two charts are clear, indicating all the positive readings from MRSA_sample tests were at or above 10% signal reduction, with an average of 20.51% and a standard deviation of 7.62%. In comparison, the negative readings from non-MRSA sample tests were settled closely in a range of ±4%. The table below gives more detailed statistical information of the two data groups:

Table 4-5 **Statistical factors of each data group (*MRSA* samples vs. non-MRSA samples)**

	MRSA Samples Data Group	**Non-MRSA Samples Data Group**
Data Group Size	70	52
Mean	20.5%	-0.57%
Standard Deviation	7.62%	2.11%
95% confidence interval for Mean	19.1% ~ 21.9%	-2.2% ~ 1.06%
Median	20.1%	-0.44%
Average Absolute Deviation from Median	6.09%	1.63%
p-value	*p-value* << 0.0001	

The p-value shown in the above table is calculated based on the Student's T-Test, which measures if the two compared data groups are significantly different. The well accepted significant difference requires a p-value less than 0.05. The calculation for the MRSA and non-MRSA sample data groups shows a p-value much smaller than 0.0001. Therefore, it is

reasonable to conclude that the biosensor has successfully differentiated MRSA strain samples from other negative control group samples in the pure culture tests.

The table also shows the 95% confidence interval for the mean, which represents the interval where that the mean of all the possible pure culture tests (including those of strains not tested or to be tested) would possibly fall in such interval with a 95% chance. This indicates that the biosensor is very likely to produce a mean transmitted power attenuation of 19.1% ~ 21.9% when testing a large set of unidentified pure MRSA culture samples whose concentration is 10^4cfu/ml (at which concentration all the data were collected).

Since the mean of the negative control (non-MRSA) group had a mean of -0.57% and standard deviation of 2.11%, the upper boundary for a clear negative response is at 1.5%. In the context of molecular immunoassays, a prudent protocol usually is 3 times of the standard deviation added to the mean to identify a so-called grey area. To be consistent with the experimental results, in this dissertation, the grey area is set to 5% ~ 7% for the Mab based 'sensitive fiber' sensor (since the 'less sensitive fibers' have very different fiber parameters and returns smaller responses for both MRSA and non-MRSA samples, their grey area shall be determined separately).

The histogram for MRSA and non-MRSA sample readings, shown in Fig 4-7, also supports this definition of grey area for the Mab based biosensor,

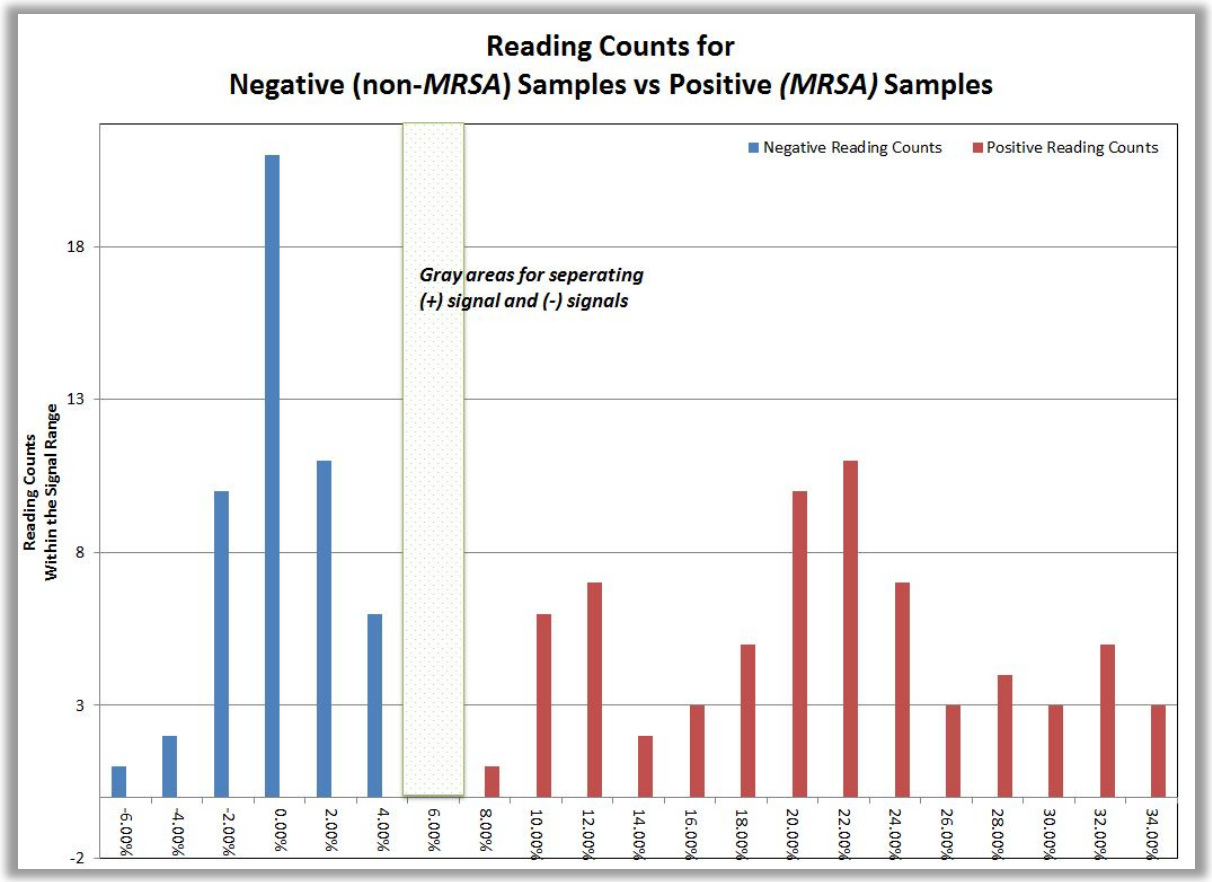

Figure 4-7: Histogram of the number results in each 2% interval from all the data of the MRSA and non-MRSA tests.

The two data group readings obtained from MRSA samples and readings from non-MRSA samples, have no overlapping results and are separated by a gray area spanning between 5% and 7%. On the left side of the grey area, the majority of the readings fall in the ±1% range, and the number of results exponentially decays beyond such range. The right side, where the positive responses are located, has a greater distribution of the transmission changes. The data ranges near the mean (20.5%) have the most reading counts. However, the other data points are less concentrated around such range, and two other sub-peaks can be observed in the 12% and 32% range. Such spread data distribution could be a reflection of the nature of the antibody-affinity variation among MRSA strains. The primary antibodies used in the sensor system may be

extremely responsive to some strain types, while for other strains it would only be a moderate response, and there are some strain types that have a very low affinity to the antibodies used to build the biosensor. There would render a small, but clearly distinguishable signal reduction under the same strain concentration in the tests.

4.3 The MRSA Biosensor Using DNA Probe as Receptor

4.3.1 Replacing Mab with DNA-probes for MRSA Biosensor

We have shown that although the monoclonal antibody based MRSA biosensor was shown successful with pure cultures, and it is specific for MRSA strains, it lacks consistency for returning reliable results for clinic swab, and would require substantial modification to develop the assay into a commercial version. Thereby, there is a need for a more sensitive and specific receptor to replace Mab on the biosensor.

As described for the *Brucella* studies in section 5.3, DNA probes as the receptor on the biosensor have exceptional consistency in attaining results as expected across all tests and various solution formulations. The hope is that a MRSA DNA probe would be more effective as a MRSA diagnostic tool for clinical swab samples.

In molecular biology, a DNA or gene probe is relatively short (usually a few hundreds bases long) and is a single-strand (*ss*-) segment of DNA (ss-DNA) that is complementary to the target DNA's unique sequence. Thus, the probe sequence and target sequence will hybridize due to complementarity between the two sequences. Since the hybridization between DNA sequence and probe demands base-pairing at every nucleobase along the sequence, the probe is extremely exclusive to the targeting DNA sequence.

The unique base sequence of the probe may be only in the range of tens of base pairs. Therefore, when comparing to epitope proteins or even whole cells that are targeted for affinity

binding in the Mab biosensor design, the ss-DNA probe is smaller in size and its linear primary structure facilitates more accessibility to its nucleobases on the backbone chain, such that the corresponding gene probe has a better chance of contact and hybridizing with the targeting gene segment, by combine the ss-DNA sequence to the probe.

It is possible to select and design a gene probe that is of high affinity and specificity to the target DNA sequence by carefully examining the DNA sequence of the targeting biomolecule and determining a unique identifying gene fragment.

The *mecA* gene that controls the production of the PBP2a responsible for the methicillin resistance has been long studied and deemed as "gold standard" for identifying methicillin resistant *S. aureus* strains.[121,122,123,124,125,126] The promoter of the *mecA* gene is composed of 300 nucleotides.[127]

Since the DNA probe targets the DNA sequence and only binds the complementary sequence on the chromosome. Nonspecific bindings with whole cells, proteins or other biomolecule that can be found in a clinical swab sample suspension should not occur. Therefore, DNA probes have been widely considered and also proven to be a more specific probe for

---

[121] P Francois, J Schrenzel, *etc., "*Rapid detection of methicillin-resistant Staphylococcus aureus directly from sterile or nonsterile clinical samples by a new molecular assay.", *J Clin Microbiol,* **41(1):**254-60, (2003).

[122] A Huletsky, M. G. Bergeron, *etc.,* "New real-time PCR assay for rapid detection of methicillin-resistant Staphylococcus aureus directly from specimens containing a mixture of staphylococci." *J. Clin. Microbiol*. **42:**1875-1884, (2004).

[123] A. J. Grisold, E. Leitner, G. Mühlbauer, E. Marth, and H. H. Kessler. "Detection of methicillin-resistant Staphylococcus aureus and simultaneous confirmation by auTomated nucleic acid extraction and real-time PCR." **J. Clin. Microbiol**. **40**:2392-2397, (2002).

[124] D. Jonas, M. Speck, F. D. Daschner, and H. Grundmann. " Rapid PCR-based identification of methicillin-resistant Staphylococcus aureus from screening swabs." *J. Clin. Microbiol*. **40**:1821-1823, (2002).

[125] B. Strommenger, C. Kettlitz, G. Werner, and W. Witte. " Multiplex PCR assay for simultaneous detection of nine clinically relevant antibiotic resistance genes in Staphylococcus aureus." *J. Clin. Microbiol*. **41**:4089-4094,(2003).

[126] K. Murakami, and W. Minamide. "PCR identification of methicillin-resistant Staphylococcus aureus," p. 539-542. In D. Pershing, T. Smith, F. Tenover, and T. White (ed.), *Diagnostic molecular microbiology: principles and application.* ASM Press, Washington, D.C., (1993).

[127] HENRY CHAMBERS, "Methicillin Resistance in Staphylococci: Molecular and Biochemical Basis and Clinical Implications", *CLINICALMICROBIOLOGY REVIEWS,* **10 (4):** p. 781–791, (1997).

specimen detection. Replacing the Mab with a *mecA* specific DNA probe is a reasonable plan to prepare the LPG-based biosensor for tackling clinical swab samples.

4.3.2 DNA Probe Biosensor Assembly and Testing Methods

The assembly of the biosensor using a DNA probe closely follows the same procedure for building Mab based biosensors. It begins with the same method for preparing the bare LPG fiber, depositing ISAM films and leaving PCBS as the topmost layer.

The DNA probe is obtained commercially based on a sequence identified by our collaborator Dr. Bandara. The probe is designed to be a nucleic acid sequence specifically complementary to a segment of the *mecA* gene at a few dozen nucleobases length, with a biotin molecule attached. Biotin has an extremely high affinity, large binding rate, and high specificity for streptavidin and avidin. In addition, the bond formed between biotin and streptavidin/avdin is stable under extremes of heat, pH and proteolysis conditions, making the biotinylated DNA probe easy to be captured and immobilized onto a substrate that is pretreated or covered by streptavidin/avidin molecules.

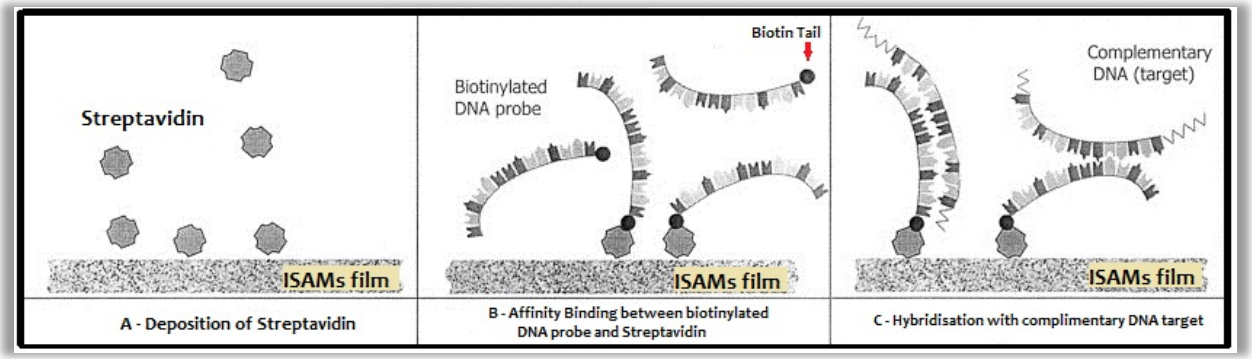

Figure 4-8: DNA probe for the biosensor: (A) Deposition of streptavidin onto the ISAM film with PCBS as top layer, and using EDC/Sulfo-NHS as crosslinker; (B) Attach biotinylated DNA probe to the streptavidin to immobilize to the fiber surface; (C) If complementary DNA target sequences meet with the probe, the two chains hybridize and coil, therefore adding the thickness of fiber cladding and reducing the transmitted optical power[128]. The figure is modified from Fig.2 of literature [126].

The cross-linking chemistry used to attach the DNA probe to the ISAM film is similar to the immobilization of monoclonal antibodies. Streptavidin is a type of protein, which is enriched with primary amine and carboxyl groups on its protein structure. These groups can easily conjugate with carboxyl groups or amine groups of the substrate organic polymer film, making the bioconjugation and immobilization of the streptavidin an identical process to attaching antibodies to the same organic polymer film via EDC plus sulfo-NHS crosslinkers. In the application of the biosensor, we have found that ISAM films with terminal carboxyl groups have displayed higher affinity to the streptavidin. Therefore, this dissertation will describe in detail the cross-linking method for immobilizing the streptavidin onto the PCBS layer of the ISAM. However, it is still possible to link streptavidin to the PAH layer of the ISAM, only with a lower binding rate. Then the biotinylated DNA probe can be directly applied to the fiber surface that is now covered with streptavidin and be captured.

The following paragraphs describe the step-by-step experimental procedure for assembly of the biosensor using biotinylated DNA probes as sensing receptors:

Deploying the DNA probe to the fiber surface:

1. Prepare the LPG bare fiber as described in section 4.2.2, and build ISAM organic nanofilm with PCBS as the top layer. Rinse the fiber and clean the sample holder.

[128] M.I Pividori, A Merkoçi, S Alegret, "Electrochemical genosensor design: immobilisation of oligonucleotides onto transducer surfaces and detection methods", *Biosensors and Bioelectronics,* **15(5-6):** 291-303, (2000).

2. Make 0.42 ml of EDC/sulfo-NHS crosslinker solution, with EDC concentration at 40 mg/ml and sulfo-NHS concentration at 20 mg/ml. Solvent is autoclaved 1x PBS at pH 7.4.
3. Prepare the streptavidin solution. The streptavidin is purchased commercially (Life Tech, #43-4301) in the lyophilized form and reconstituted with 2 ml of DI water, making a final concentration of 0.5 mg/ml. Using syringes to extract 0.08 ml of the streptavidin, mix with the crosslinker solution made from step 2. The final streptavidin concentration is 80 μg/ml.
4. Tap and rotate the streptavidin-crosslinker mixture for 1 minute. DO NOT VORTEX. Apply the mixture to the fiber, allowing deposition period for 6 hours to overnight.
5. Remove the mixture. Rinse the fiber and clean the sample holder. Immerse the fiber in fresh DI water for 10 minutes. Stir the soaking liquid every 30 seconds during the process to thoroughly remove the unbound salt and streptavidin molecules.
6. If necessary, take one measurement of the fiber in PBS, make sure to repeat step 5 if this measurement step is taken.
7. Take the DNA probe out of the freezer, and allow 30 minutes to let the probe solution thaw and reach room temperature. Apply 0.5 ml of the 60 pmol/ml biotinylated DNA probe to the fiber and allow 4 hours reaction time for biotin-streptavidin affinity binding.
8. Remove the DNA probe solution. Rinse the fiber thoroughly, clean the sample holder, and soak the fiber in fresh DI water for 10 minutes, stirring every 3 minutes.
9. Remove the soaking water. Make 1% dry milk solution in DI water, and add it to fiber for 1 minute. Stir during the process.

10. Remove the dry milk blocker, rinse the fiber thoroughly and clean the sample holder. Then soak the fiber in fresh DI water for 10 minutes, stir every 3 minutes.

11. Remove the soaking water, and apply PBS at pH 7 to the fiber. Wait 3 minutes for the fiber to be stable, take one measurement of the spectrum and record the result.

12. If the transmittance is found to shift upwards instead of down in step 6 or 10, repeat the rinsing and soaking procedures in step 8 and run the measurement again.

Testing specimen samples with the DNA probe:

13. Take lysostaphin stock[†] and the sample suspension to be tested out of the refrigerator, and allow 15 minutes to let the liquid reach room temperature. Extract 20 µl of the 1 mg/ml lysostaphin and add it to the sample suspension.

14. Put the sample suspension in the oven set at 37^{o}C, and allow 2 to 4 hours incubation for thorough lysing of any existing MRSA whole cells.

15. Remove the MRSA-lysed sample suspension and water-bathe the sample suspension in boiling water for 10 minutes[††]. Wrap the cap of the sample vial to prevent the cap popping open during the heating and reduce the chance of introducing contaminations to the sample suspension or releasing biohazard materials to the laboratory environment.

16. Immediately soak the boiled sample suspension in ice water, wait 1 minute to allow the sample suspension to cool down[†††].

17. Apply the ice-cold solution to the DNA probe based biosensor, and wait 1 hour for the reaction. Stir every 5 minutes during the period, and it is recommended to stir more often in the first 5 minutes of the reaction period[††††].

18. Remove the sample suspension. Rinse the fiber thoroughly and clean the sample holder. Soak the fiber in DI water for 10 minutes and stir every 3 minutes. Then remove the soaking solution and add PBS buffer, wait 3 minutes for the fiber to get stabilized and make a measurement afterwards.

19. If more samples need to be tested, repeat steps 11-16.

† ***Using Lysostaphin to lyse MRSA cells in the sample suspension:***

Lysostaphin from Staphylococcus staphylolyticus is commercially obtained from Sigma-Aldrich, catalog #L7386-1MG. The sample suspension usually contains whole MRSA cells which confine the DNA polymer within the cell wall and thus inaccessible to the DNA probe deployed on the sensor surface. Therefore it is important to break the cell and release the DNA polymer into the solution liquid.

†† ***Water-bathing the sample suspension to dehybridize DNA helices:***

The DNA sequences of microorganisms are rarely in the single stranded form. Therefore it is necessary to melt the double helices of the DNA sequences by disrupting the hydrogen bonds between the complementary bases, and release the single strand DNA(ss-DNA) target, which can then be recognized by the DNA probe and be immobilized onto the fiber surface. The most common method for denaturing DNA helices is by heating the solution to the denaturation temperature of 94-98 ^{o}C, and the majority of the helices shall be dehybridized after 10 minutes of boiling. Extreme heat can also help lyse some of the bacteria, as will be seen in the Brucella and H. Somni DNA sensing cases.

††† ***Rapid cooling of the boiled sample suspension:***

The separated ss-DNA is still active and can hybridize with its complementary sequence at the moderate temperature range, generally around 30 to 80 ^{o}C. The hybridization rate increases quickly after the solution temperature drops from the denaturation temperature, and such hybridization must be prevented to the ss-DNA to hybridize with the DNA probe on the fiber. The best way for keeping the ss-DNA apart from its complementary chain is to cool the solution temperature from the denaturation temperature to 10 ^{o}C or lower as swiftly as possible.

†††† ***Slow down the temperature rising of the sample suspension:***

As mentioned above, when the temperature of the sample suspension raises to a moderate temperature range, say room temperature, the rate for rehybridization increases. However, the hybridization rate for sensor-DNA interactions is also temperature related, therefore it's not necessary to keep the sample suspension ice-cold for the whole reaction period. Allowing the temperature inside the reaction chamber (mainly the sample suspension and sample holder) to slowly rise back to room temperature before the end of each sample testing period is highly recommended. Applying this technique has seen extensive and effective improvement to the sensitivity of the biosensor in experiments.

Due to eventual breakage of the sensitive LPG fibers, all the experiments conducted and displayed for the MRSA DNA probe sensor were done using the 'less sensitive' fiber, whose TAP capacity is usually in the -9 dB ~ -11 dB range. Therefore, though not fully comparable, the results for all testing results would be considered to be two times larger or more if performed with the 'sensitive' fiber for the same test.

4.3.3 DNA Biosensor Assay Results with Pure Culture Samples

Following the procedures described above, the pure culture samples at concentrations 10^4cfu/ml to 10^7cfu/ml were paired up as "negative control group vs. treatment group", and tested in 3 separate runs, with each runs only testing one pair of samples and using a fresh fiber sensor. The pure culture samples are the same as used in Mab sensor tests. All the MRSA and MSSA samples were serially diluted to the working concentration from the original 10^8cfu/ml solution, respectively. The summary of the results is shown in Fig 4-9:

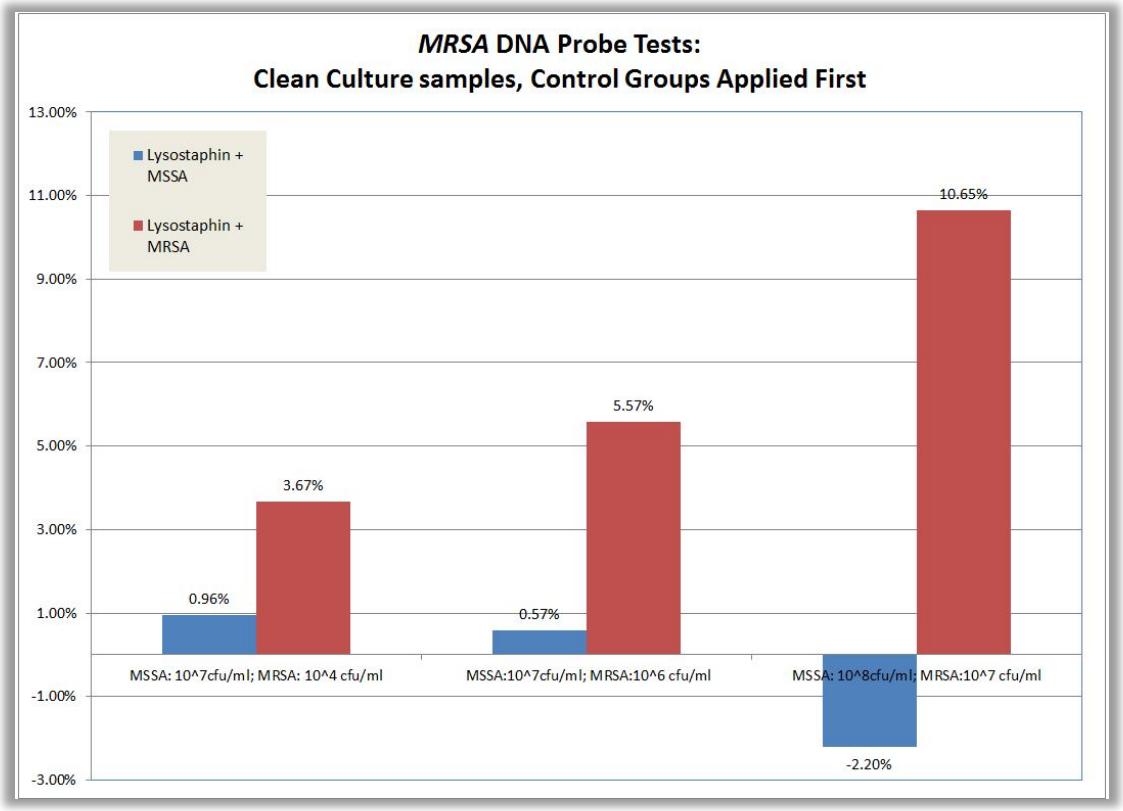

Figure 4-9: 3 individual pure culture runs were performed to examine the sensing capacity of the DNA sensor. In each run, MSSA samples at high concentration were applied, and then MRSA samples each at 10^4 cfu/ml, 10^6 cfu/ml and 10^7 cfu/ml were tested next.

In a complementary experiment, the treatment group samples were applied before the negative control group samples. The same 3 individual sample pairs were tested and each using fresh fiber sensor. The results are shown in Fig 4-10:

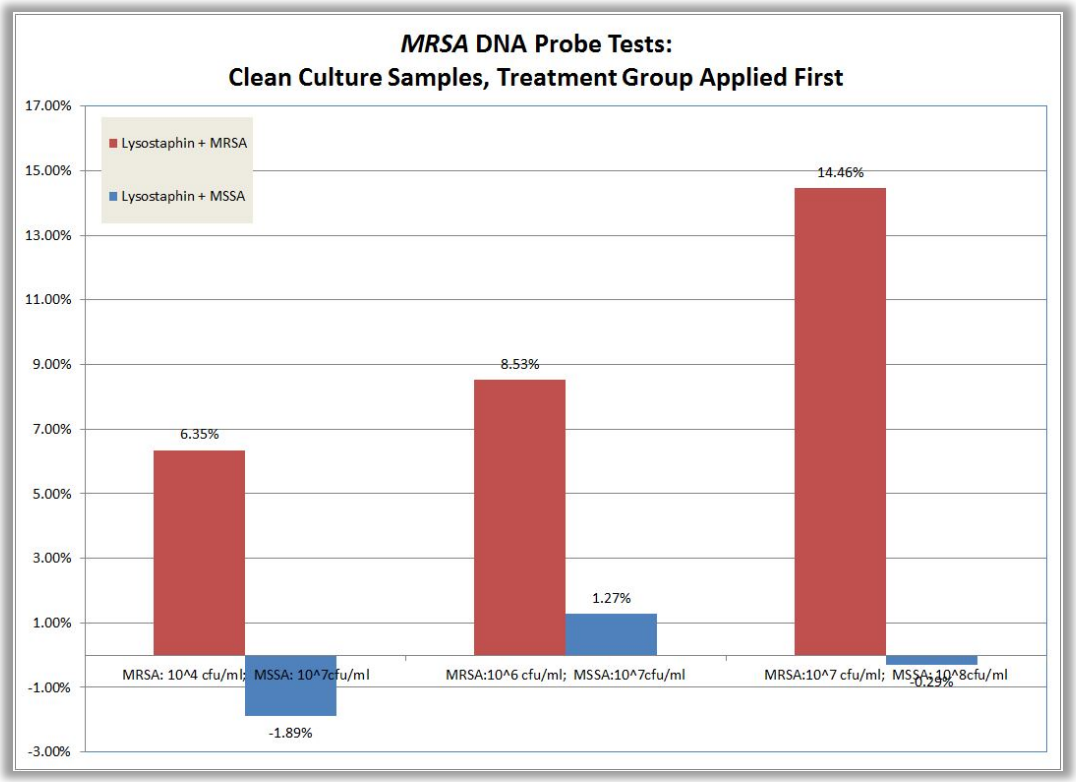

Figure 4-10: Three individual pure culture runs. The only difference from the experiment series in Figure 4-9 is that during this experiment series, the *MRSA* samples were applied first, then the MSSA samples were applied.

The first experimental series focused on testing the specificity of the DNA sensor. Therefore, the negative control groups were always tested first, then the treatment group samples were applied and showed a positive response. This shows that the null response from the negative control group was not the result of the biosensor malfunctioning, and that the biosensor is specific to MRSA strains only.

The second experimental series focuses on testing the sensitivity of the DNA probe. Therefore, the treatment group samples were always applied first, then the negative control group samples were applied to prove that all the positive responses reported by the biosensor

were coming from the specific probe-DNA hybridizations, rather than random nonspecific bindings.

Notice that at each strain concentration, the MRSA response is always higher if it is first applied to the fiber sensor, implying some responses might be due to nonspecific binding. However, it is the contrast between treatment group and control group that we need to be concerned with. Fig 4-11 compares the results of the first test in each separate run, which reflects how the biosensor would most likely respond when faced with an unknown culture sample and how the positive signals and negative/null signals would look:

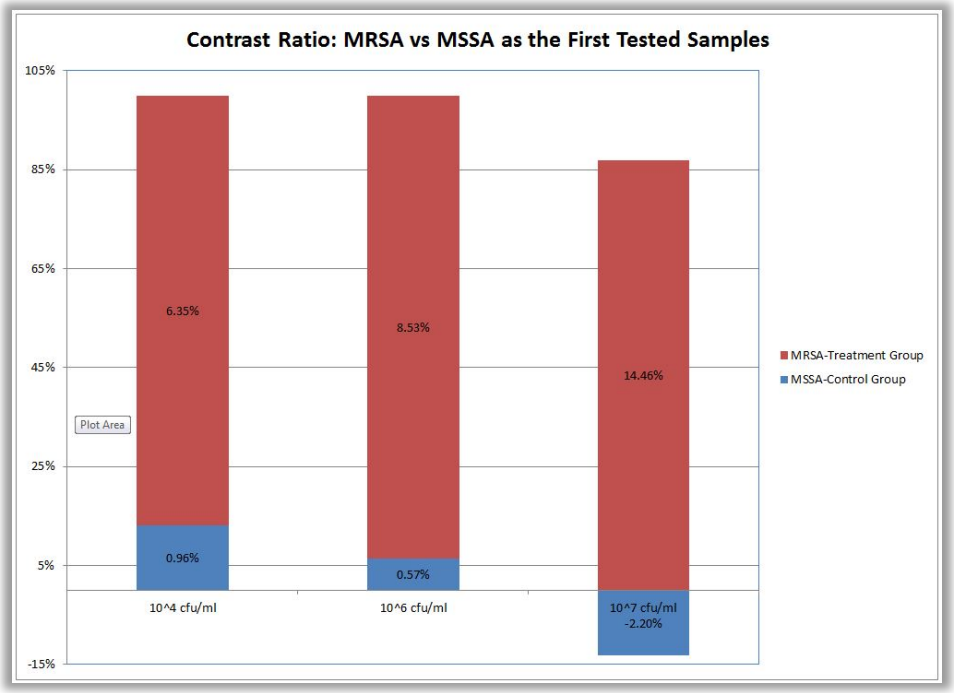

Figure 4-11: Difference in signal for the first tested samples: MRSA vs. MSSA.

In the Fig 4-11, the total bar lengths have been all adjusted to 100%. The red weight of each bar indicates the weight coming from MRSA samples, and the blue weight indicates the weight coming from MSSA samples. As discussed in section 4.2.8, it is reasonable to set the decision threshold at 4.5%, as the standard deviation of the control group is 1.41%.

Both of the two experimental series also show an increase of the response to the MRSA strain samples as the concentration rises. This means the sensor is responding quantitatively to the concentration of MRSA in the sample.

4.3.4 DNA Probe Biosensor Assay Results with Clinical Swab Samples

In the pure culture samples, both MSSA and MRSA culture samples have mixed with lysostaphin to ensure the release of DNA by the cells to the sample suspension. Therefore, the choice of blocking agent has been optimized for the existence of the working concentration of lysostaphin in the probe-DNA reaction environment. This means that as the composition of a clinical-obtained swab sample is unknown, it should still be pretreated with the lysostaphin whose final concentration stays above the optimized working level of 20 μg/ml.

The experiment procedures of testing swab samples with the DNA probe based biosensor followed the same 4-run protocol described in Mab based sensor in section 4.2.7. Pure MSSA culture is tested with biosensor as the first step to evaluate the specificity. Then, the first swab sample will be tested and results recorded. After the first swab sample, pure MRSA culture will be examined with biosensor to confirm its ability to reactive with MRSA strain. Next, if a duplicate swab sample is available, it shall also be tested with biosensor. The last step is especially valuable when the swab sample test yields a null/negative signal outcome and suspicions over a false negative need to be dealt with.

The swab samples tested with the DNA probe fiber sensor have displayed some overall improvement of the result's consistency. However, based on the results returned from the clinical laboratory that also performed culture tests on over the swab samples collected from the same source, only 3 out of the total 6 swab samples tested (swab 18 to 23) generated agreement with

diagnostic results. The other three swab tests are either too ambiguous to make a clear call, or suggest an opposite diagnostic results from the clinical culture test results.

The three swab tests that agree with culture growth are: swab 18, MRSA positive; swab 19, MRSA positive; swab 22, MRSA negative. Both swab 18 samples tested in this sequential test suggest MRSA positive responses. The test for swab 19 returned a much clearer picture, where the 1st run with the MSSA pure culture generated a negative response, and both swab samples and the MRSA pure culture sample generated a positive response. Therefore, swab 19 is clearly MRSA positive. The test for swab 22 started with directly testing the swab sample in the 1st run. However, neither of the swab tests before or after the first MRSA culture yielded a positive peak shift, while the MRSA culture generated a clear positive signal, suggesting the DNA fiber sensor is working. Therefore swab 22 would be MRSA negative.

The remaining swabs all showed positive results with the LPG biosensor, but were culture negative. This suggests the largest problem at the moment is nonspecific binding yielding false-positive results, where the blocking inefficiency may be the main cause. Some sources argue[129] that dry milk, which is currently used for blocking Mab or DNA probe biosensor for swab tests, is a poor choice for hybridization. Hence, searching for a capable blocking agent for swab sample tests shall become the main focus of the next sensor development stage.

4.4 AFM Imaging Studies

The design of an efficient and effective immunoassay can be strikingly complicated, as there are numerous aspects that need to be taken into consideration for experimental design, and there are hidden factors that may cause fluctuations or false signals. A close investigation of the fiber surface with the help of atomic force microscopy (AFM) after each procedure could be highly

[129] http://catalog2.corning.com/Lifesciences/media/pdf/elisa3.pdf

valuable in providing direct observation of how the surface is altered after each step, how the film coverage and quality might affect the sensor, where the abnormal readings might come from, and how to improve the biosensor design to solve the deficiencies. However, a direct look at the LPG fiber sensor can be risky and impractical for two reasons. First, the LPG fibers are valuable experimental assets, checking its surface configuration using a sharp tip scanning technique can expose the fiber to the hazard of being damaged or broken. Second, AFM is optimized towards scanning level surfaces. Therefore a scanning image will not easily visualize the surface of the curved fiber. Figure 4-13 shows an example of directly looking at a Mab based biosensor fiber surface after blocking by dry milk and later exposed to boiled MRSA cultures.

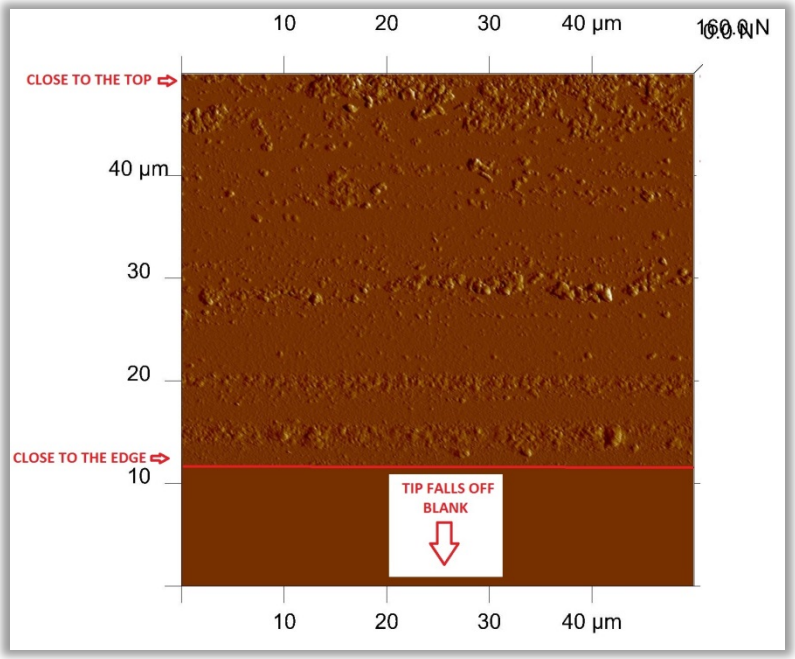

Figure 4-12: AFM image of the biosensor fiber surface. The biosensor has been blocked by dry milk, and used for testing boiled MRSA pure culture samples. Towards the top of the fiber, the image is clear, however when the scanning tip moves towards the fiber edge, the surface profile becomes blurred, and the tip falls off the fiber before reaching the scanning limit.

Though it is difficult to examine the sensor surface directly under AFM, it is possible to replicate the biochemistry treatment steps on the fiber, and reassemble the entire experiment on a silica glass slide. Silica is the material from which the fiber is fabricated, and silica glass slides

are often used to study and characterize ISAM films. Therefore, silica glass slides can simulate the LPG fiber as the substrate to the organic films that comprise the biosensor.

All the AFM imaging and processing work reported here were done with the help of Mr. Moataz Khalifa.

Prior to the deposition of any organic or biochemistry materials, the glass slide is RCA cleaned and dried with high nitrogen flows. This step is taken to remove any impurities from the slide surface to ensure the best film quality of the ISAM. Then the slide is immersed in PAH and PCBS 10 mM solution for 3 minutes each sequentially to form 1 ISAM bilayer. Between each dipping step, the slide is washed with DI water and dried by nitrogen. After this step, an image of the ISAM film on the silica slide is taken by AFM.

Then, the same crosslinker-Mab mixture as described in section 4.2.2 is made and exposed to the ISAM coated region of the slide for 6 hours to overnight. The volume of the mixture is as low as 0.5 ml, therefore the solution is only be put on one side of the slide which is lying flat. Using slow rotate motor to keep the mixture solution stirred can help the antibodies bioconjugate to the ISAM. Then the slide will be rinsed by DI water, and instead of drying by strong nitrogen flow, an oven that's set to 37 ^{o}C is used to dry the slide. The dried slide is then scanned by AFM again to generate the image of the antibodies on top of the ISAM film.

The slide is then blocked with 1% dry milk for 1 minute, and after this, the MRSA pure culture samples at the highest possible concentration 10^{8}cfu/ml are added to the biofilm-deposited side of the slide, and the slide is placed on the rotate motor for 1 hour. Then the slide is rinsed by DI water and also dried in oven, and then can be put under AFM for imaging. The purpose for only applying the highest MRSA concentration is to maximize the cell deposition

and reduce the work needed for searching the whole slide for the most congregated binding region, as each scan only checks at most a 90 μm by 90 μm square.

Fig 4-14 displays the topography of the slide surface after each major stage of the experiment.

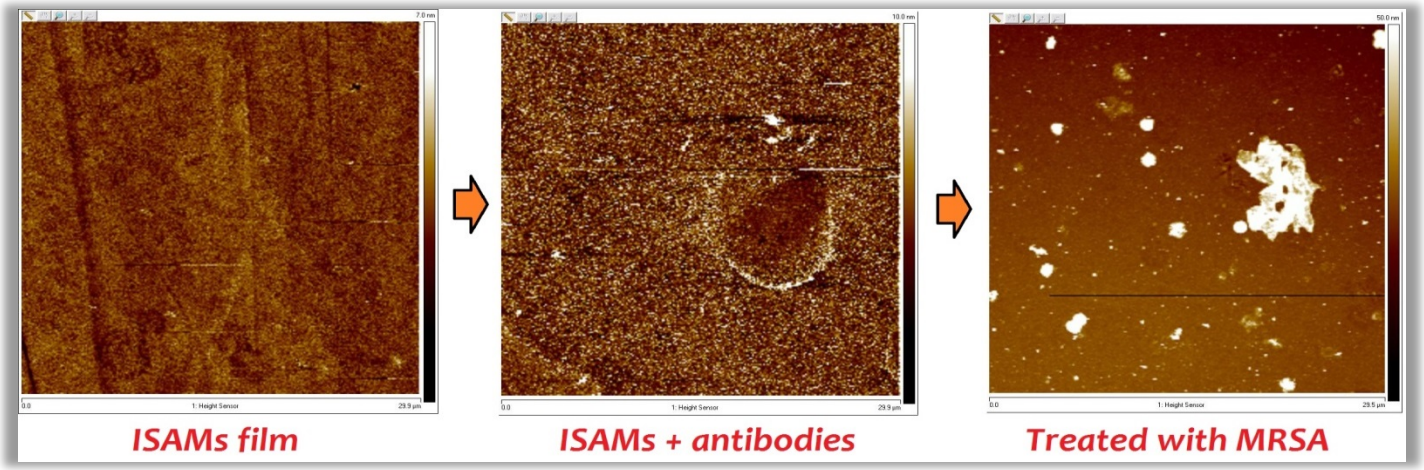

(A) (B) (C)

Figure 4-13: AFM image of the slide after been treated with: (A) ISAM film; (B) antibodies + crosslinkers; (C) MRSA pure culture samples.

The first graph displays a very smooth and even ISAM film surface. The legend indicates the height ranges from 0 nm to 7 nm in the graph, however the majority of the film height stays within 2~5 nm range.

The second graph displays the antibody surface after the protein molecule is immobilized onto the ISAM. The bright spots refer to the 10 nm height and are believed to represent antibody molecules. Such size also agrees with the estimated size for a single monoclonal antibody molecule. Though not every bright spot necessarily corresponds to a well-positioned antibody site (meaning one or two of its paratope is facing off the film), the antibody coverage is still considered decent in this figure.

The third graph displays the slide surface image after being treated with MRSA pure culture samples. The height legend has dramatically increased to 50 nm, indicating the brightest circles which are 1μm in diameter, are about 50 nm above the film surface. These large, bright spots are believed to be antibody-conjugated MRSA whole cells.

The heights of the conjugated cells are much smaller than their diameter. This could have two causes: first, the slide-drying process may remove part of the liquid stored inside the cells, and the cell lies flat on the film surface on top of the binding antibody site. Secondly, the AFM scanning tip exerts strong force on the cell for the imaging process, and such forces can easily squash the cell and flatten the cell structure.

A more close examination in Fig 4-15 at a smaller imaging scale over such bright and rounded spots has revealed more details, and it's easier to identify these spots as the relics of MRSA whole cells.

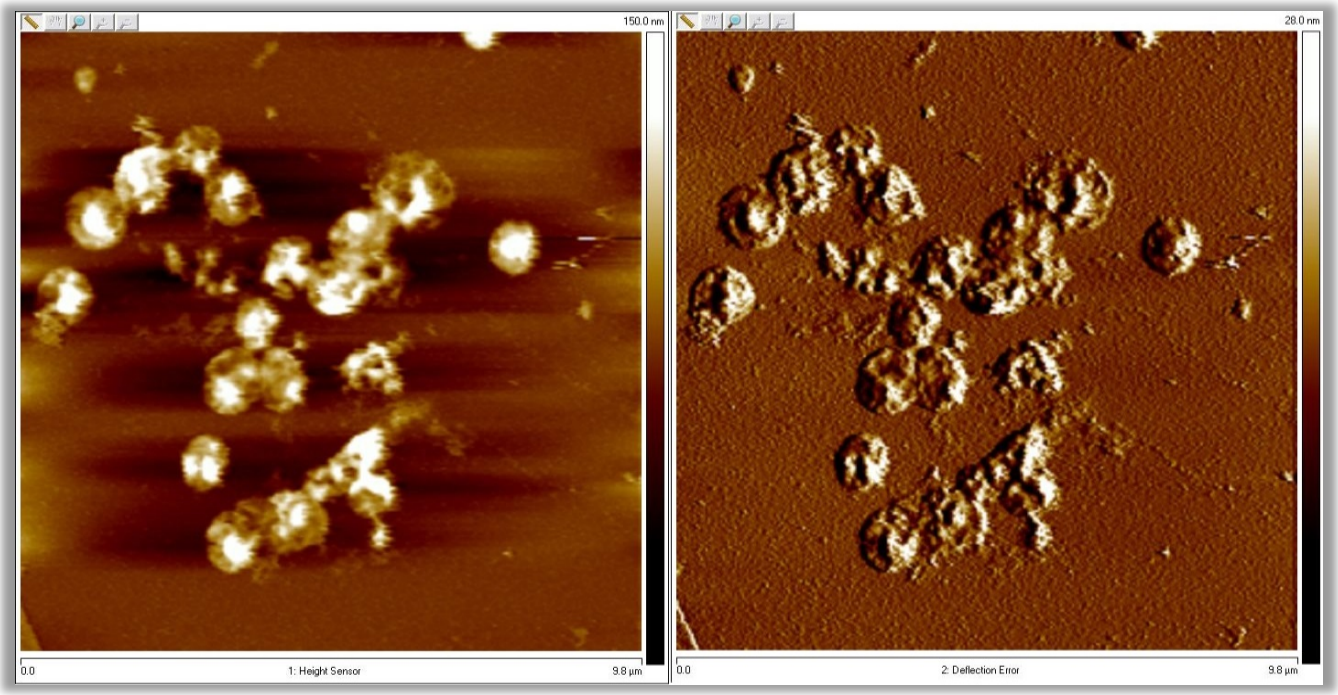

Figure 4-14: 10 μm by 10 μm AFM images of the bright spots that are believed to be MRSA bindings. Left: height sensor image; Right: deflection Error image.

And at a larger scale, Fig 4-16 shows that the 10^8 cfu/ml MRSA pure culture sample has provided a relatively dense binding coverage on the biofilm surface:

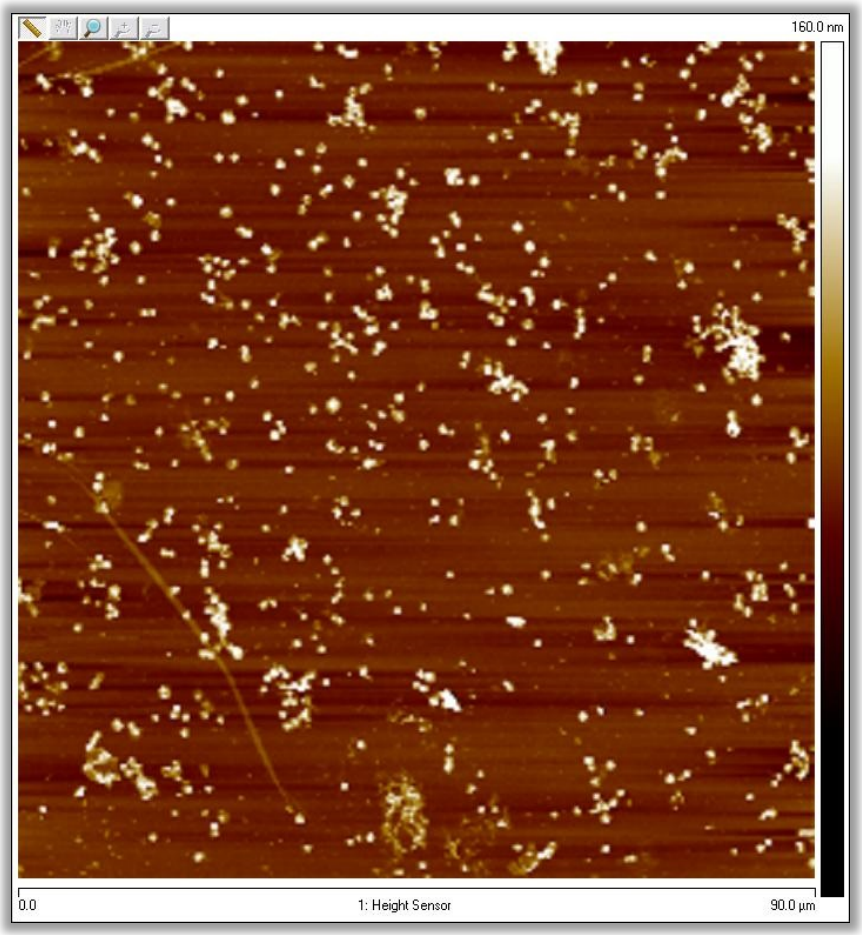

Figure 4-15: 90 µm by 90 µm AFM images of the slide covered by MRSA Mab and then treated by 10^8 cfu/ml MRSA pure culture sample

From the Fig 4-16, it is plausible to conclude that on the fiber sensor surface, even when exposed to a high concentration of MRSA samples, the film still has open regions that theoretically should be available for further MRSA binding. However, such phenomena are not quite evident from experimental observations. One possible explanation is that those antibody left-over binding sites may belong to ill positioned antibodies, whose paratopes may be facing towards the substrate and therefore blocked for any MRSA binding. If this is true, then it implies

the crosslinking biochemistry is not very efficient, and an improved method needs to be found to replace the current EDC/sulfo-NHS method.

A built-in analysis tool also enables the AFM instrument to render information on the height distribution of a selected image area. This tool could help us get a more comprehensive idea of the antibody deposition on the fiber surface. Fig 4-17 shows the film height distribution of the slide that has ISAM and antibodies deposited and the analysis is performed in the 1µm by 1µm marked block, where the film is smoother in the height sensor view and away from bright spots, which could be dust or pollution pulled to the surface due to static electric attraction.

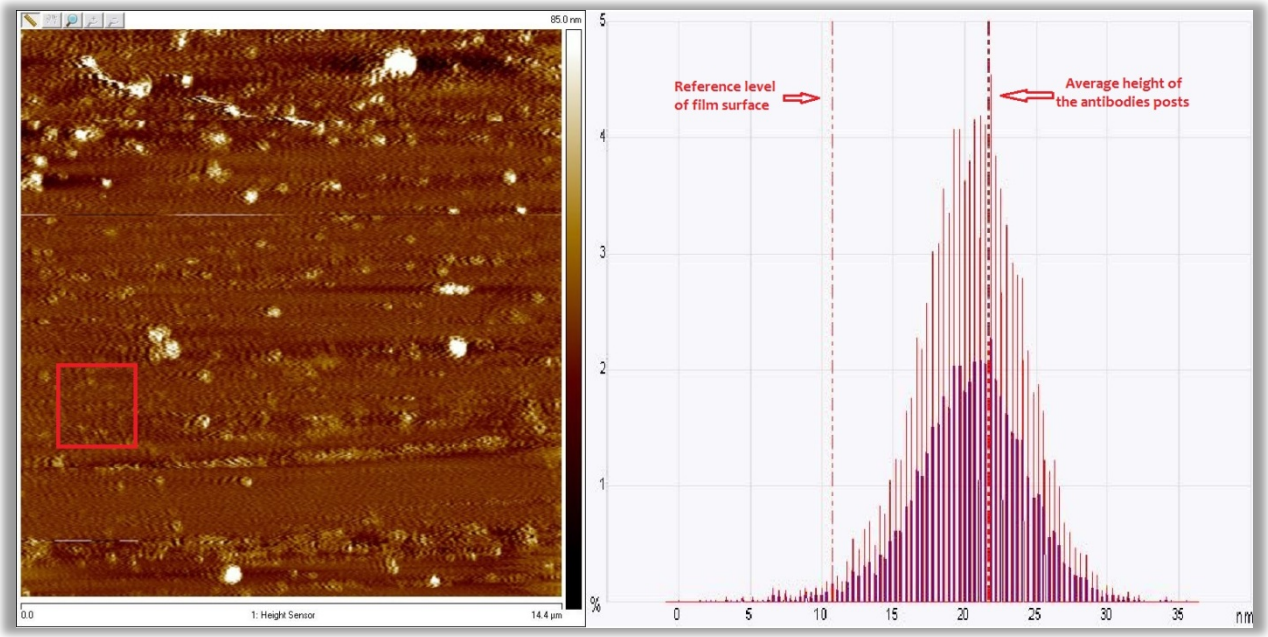

Figure 4-16: Film height distribution on a slide deposited with ISAM and antibodies. The left figure shows the location of the 1µm by 1µm block on the slide, and the right figure shows the height distribution.

The height distribution has confirmed that the majority of the materials above the ISAM film level are of 10 nm in average height, which agrees with the estimation from the height sensor image above and indicates such film materials likely belong to antibodies. Moreover, the height distribution consists of discrete bars, which reflects that antibody sites are located rather

remotely from neighboring sites and well scattered over the fiber surface, meaning the antibodies layer of the fiber sensor does not cover the whole ISAM film underneath, and those exposed ISAM film regions can be the source for nonspecific bindings.

Another finding from the AFM imaging is the discovery of the unintended precipitation from PBS. Figure 4-18 displays the image of the slide after depositing antibodies and then vigorous rinsing by PBS solution, instead of DI water.

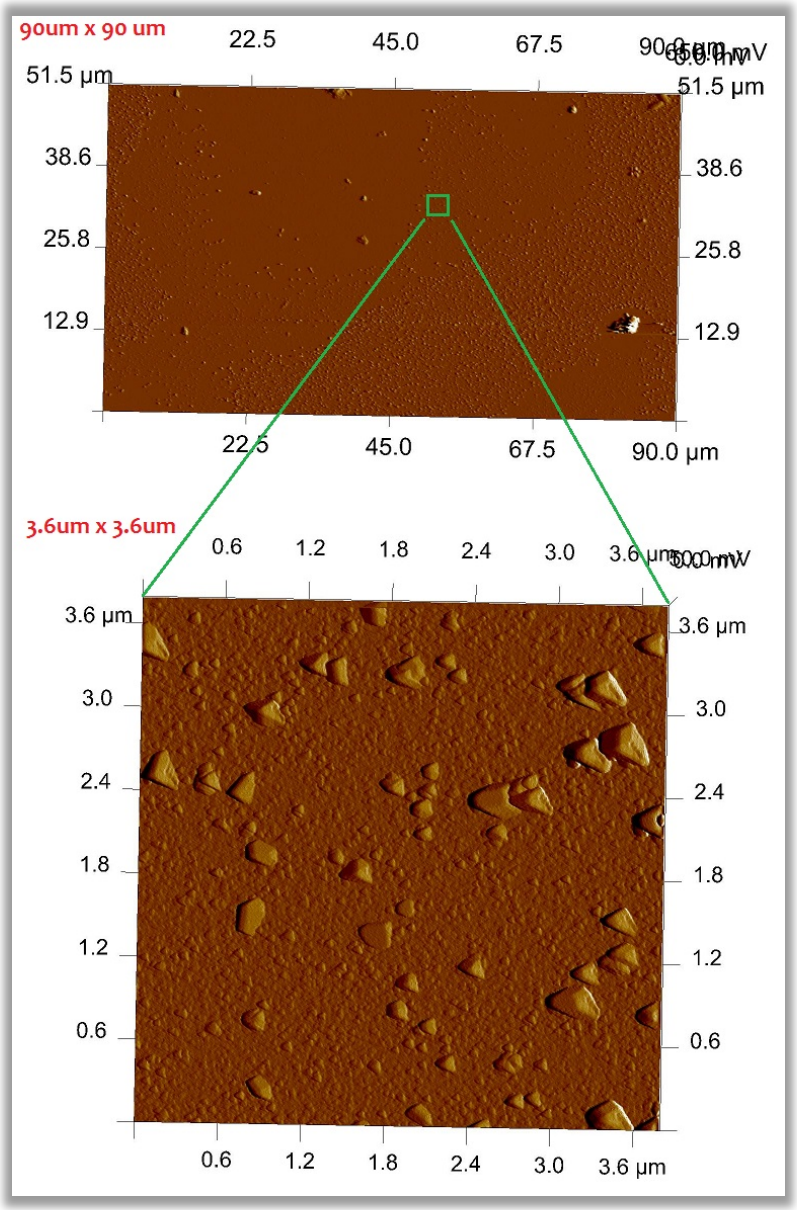

Figure 4-17: Unintended salt precipitation from PBS solution. The trace of the salt crystal is very clear from the 90 µm by 90 µm and 3.6 µm by 3.6 µm view.

Similar traces of left-over salt have also been discovered from a slide that has been further treated with MRSA pure culture samples. However, after rinsing the same slide again with DI water, all the salt structures were gone. And with repeated rinsing or rinsing by strong water flow to remove all of the salt precipitation, most of the bound MRSA cell structures were damaged or destroyed at the same time, though their trace can still be found:

PBS Salts Observed: Before DI Water Rinsing

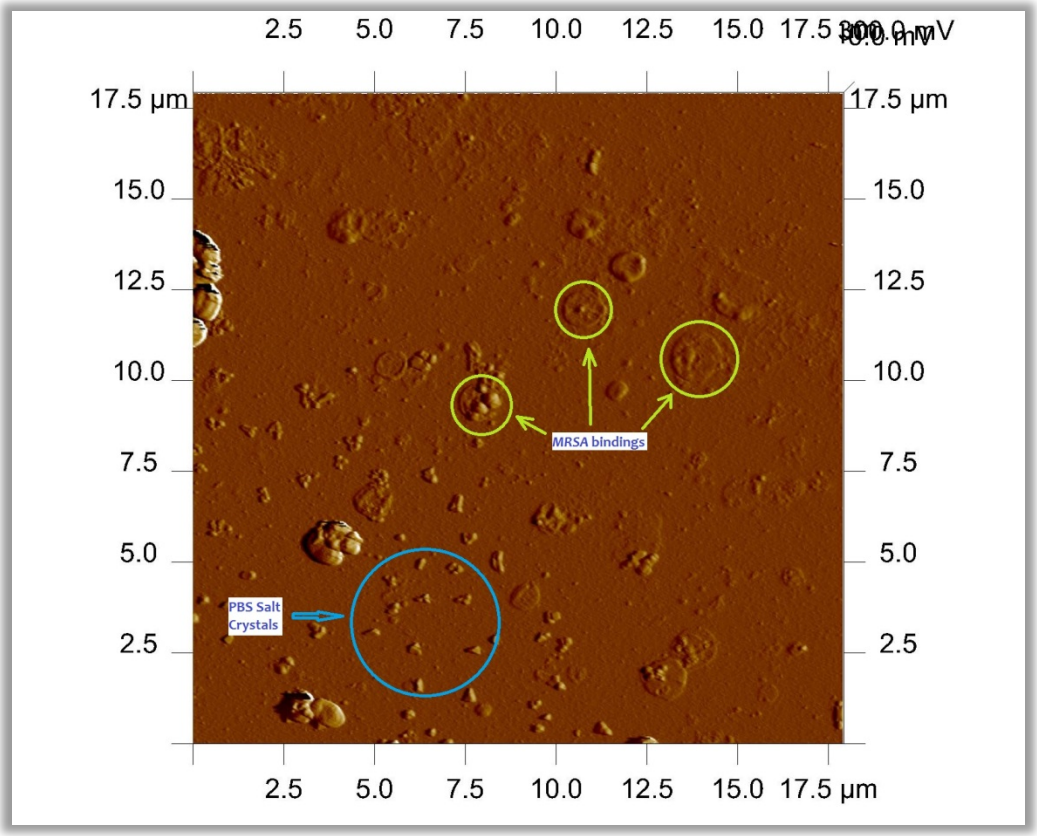

(A)

PBS Salt All Gone: After DI Water Rinsing

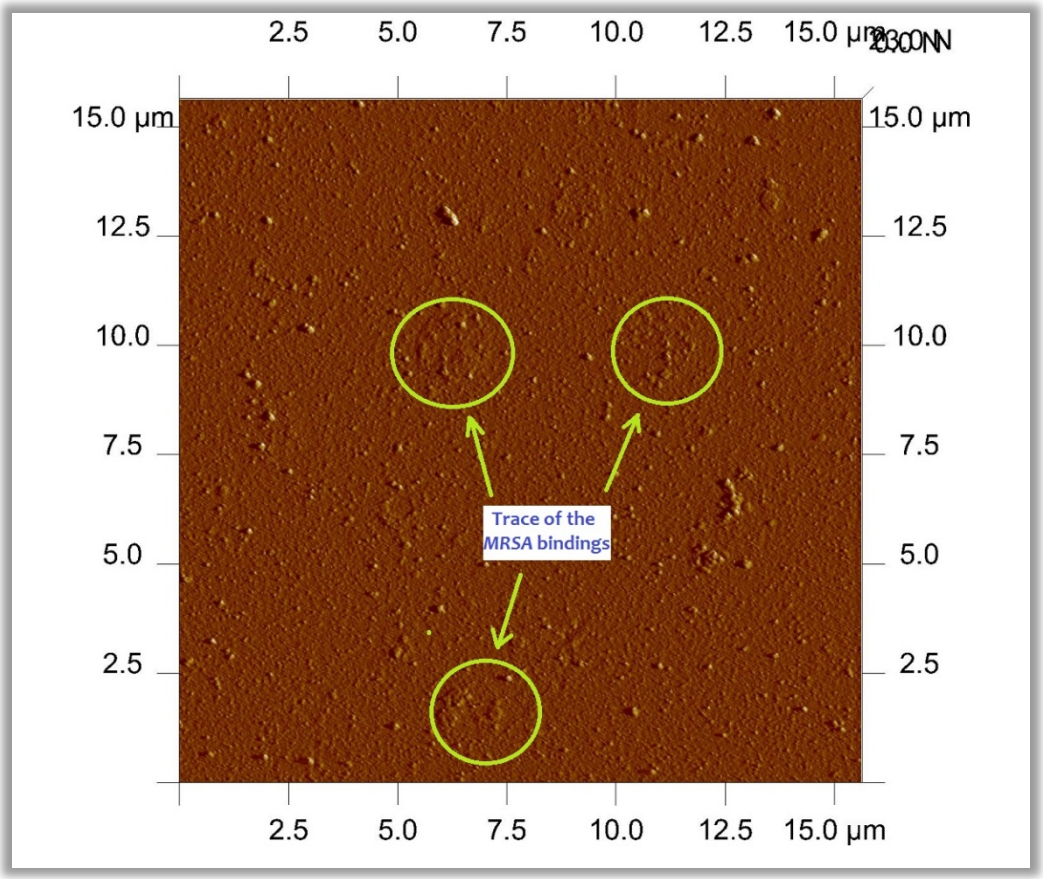

(B)

Figure 4-18: The salt precipitation is entirely removed from the fiber surface after rinsing by DI water. (A) before rinsing, the salt crystals are observed; (B) after rinsing, all salt crystals are removed from the slide.

This finding has answered some puzzling and contradictory observations from prior trials that used PBS as the rinsing buffer and measurement background, as the precipitation of salt on the fiber surface is not controllable and can vary from run to run. Such unintended and unaccounted for salt precipitations increase the cladding thickness and create false positive signals; similarly on the counter process, when the surface fluid is altered which leads to the dissolution of the precipitation layer, the average cladding thickness will be reduced and mask any MRSA cell binding to the fiber which should increase the average cladding thickness, with an ultimate result of false negative readings.

Therefore, the precipitation of PBS salt or any other impurities must be thoroughly removed from the fiber before making a measurement, meaning that PBS is not appropriate for fiber rinsing or to serve as measurement background. Thus unlike other common immunoassay designs, PBS or its detergent addition version is removed from the experiment procedure as the rinsing buffer, and serves no other roles than the solvent for the biochemical components in the biosensor experiments.

Chapter 5 Identification of Other Bacteria with the LPG Biosensor

5.1 Adaptive Biosensor Platform

The MRSA biosensor system is a valuable platform that can be modified easily for detection of pathogenic bacteria and viruses that are contagious in the community or hospital, and can be better controlled or healed at early stage of the infection.

Based on the antigen type, an immune receptor specifically targeting the species can be found. Since the ISAM film is able to provide the two most commonly used functional groups in bioconjugation assays (amine and carboxyl groups), it is possible to find a cross-linking chemistry to immobilize the corresponding receptor to the fiber surface. The immune receptor binds to molecules on the fiber surface, causing the power attenuation to the transmitted light with a magnitude that is proportional to the amount of analyte attached.

The current MRSA biosensor platform has been adapted to perform diagnostic trials on three other intriguing pathogenic species: *Francisella tularensis, Brucella,* and *Histophilus somni. The F. tularensis* study used a monoclonal antibody as in Mab-based MRSA sensor; while the *Brucella* and *H. somni* studies used DNA probe as detection receptors. The ensuing sections will present each of these biosensors in detail.

5.2 The *F. tularensis* Biosensor

Francisella tularensis (F. tularensis) is a Gram-negative bacterium that is the causative agent of tularemia,[130] which without proper treatment can be fatal to the host. As a Gram-negative organism, the *F. tularensis* membrane structure distinct from the Gram-positive bacteria.

[130] http://en.wikipedia.org/wiki/Francisella_tularensis

The outer membrane structure can protect the cell from being attacked by a range of antibiotics, dyes, and detergents that have been demonstrated to be effective in disassembling the membrane or cell wall of Gram-positive species. Due to its low infectious dose (down to a few bacteria), *F. tularensis* has been used to develop biological weapons and is classified as a Class A select agent by the federal government. Therefore, identification of *F. tularensis* infection in a patient at an early stage and initiating antibiotics to contain the infection could help the patient's immune system from being overrun by the infection, and increase the chance of full recovery and reduce the mortality rate. Also, detection of *F. tularensis* can alert the authorities of a potential biohazard threat, which could help minimize the damage by a potential bioterrorist act. For all these reasons, the need for a rapid *F. tularensis* diagnostic device is urgent, and our LPG-fiber based Mab biosensor system could be modified only by changing the receptor layer in order to potentially meet such a need.

The assembly of the *F. tularensis* biosensor largely follows the procedures of building the MRSA Mab based biosensor. The only difference is using the antibody to *F. tularensis* (Meridian Life Science Inc.) rather than the antibody to PBP2a as biological receptor, which is a monoclonal antibody to the lipopolysaccharide (LPS). The final working concentration of the *F. tularensis* antibody in the mixture is 200 μg/ml.

The *F. tularensis* experiments were conducted using the 'sensitive' LPG-fiber, and blocked with 50 mg/ml ethanolamine. The *Francisella* experiments were designed at the early stage of the Mab biosensor platform development, therefore the experiments for comparing various blocking reagent efficiency was not been accomplished at that time, and the *F. tularensis* sensor's assembly protocol used ethanolamine rather than dry milk as the blocking reagent. The samples were tested on the same sensor in sequential order from low concentration to high

concentration, and negative control group samples (namely, WBTI strain) are tested prior to the treatment group samples (namely, LVS, or Live vaccine strain of *Francisella tularensis*) under the same concentration. WBTI is a mutant of LVS that lacks O-antigen of the LPS, to which the Mab is directed. Therefore, WBTI is selected as the negative control strain for the biosensor assays.

The consistently encountered issues during testing of the *F. tularensis* sensor system were nonspecific binding and false positive readings from pure WBTI culture samples, which are utilized as the underlying control group strains. Another commonly seen issue was the sensor's positive saturation level. A typical MRSA antibody based sensor could quantitatively reflect the concentration of the tested positive sample up to 10^6cfu/ml in a sequential test. However, for the *F. tularensis* sensor, the fiber sensor is saturated at 10^6cfu/ml of tested LVS sample suspension, and in subsequent tests with higher concentrations, the sensor is unable to exhibit a larger optical power attenuation. However, the sensor still managed to collect a number of promising data, and Fig 5-1 displays an example of a *F. tularensis* sensor test:

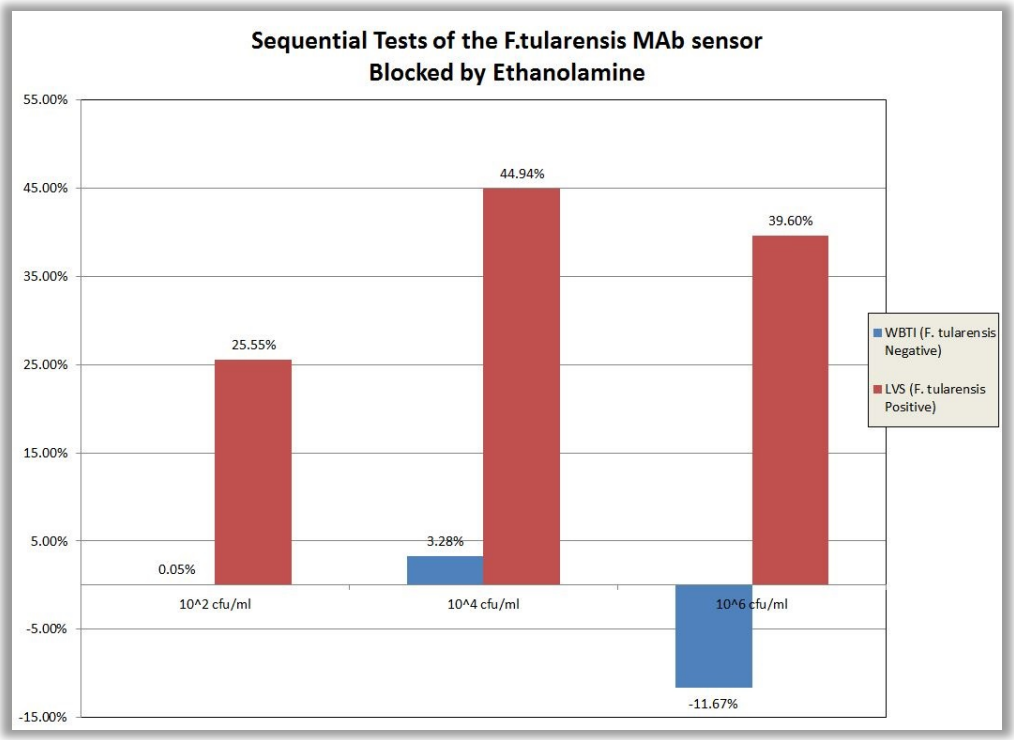

Figure 5-1: Sequential sample tests with *F. tularensis* biosensor. The sample pairs at cell concentrations of 10^2 cfu/ml and 10^4 cfu/ml were according to the expectation. However, the last sample pair at 10^6 cfu/ml was unexpected.

The experimental data above displayed consistent readings at cell concentration of 10^2 cfu/ml and 10^4 cfu/ml for both WBTI and LVS pure culture samples. However, the higher concentration sample pair, which is tested on the same sensor fiber after the preceding 4 individual runs, did not meet the expectation. The WBTI sample at a concentration of 10^6 cfu/ml returned a -11.67%, which is beyond the normal range of a random upward shift of the spectrum, and the shift for 10^6 cfu/ml is somewhat smaller than for 10^4 cfu/ml.

5.3 The *Brucella* Biosensor

Brucella is a Gram-negative bacterium that is small in size (0.5~1.5 μm), rod shaped (coccobacilli), non-motile and non-spore-forming.[131] Human beings obtain *Brucella* infections through ingestion of contaminated meat, direct contact with infected animals, or inhaling

[131] http://en.wikipedia.org/wiki/Brucellosis

aerosols of *Brucella.* Infection by *Brucella* will cause a highly contagious zoonosis called Brucellosis, whose symptoms resemble influence, though with emphasis on muscle and joint pains. The human infectious dose of *Brucella* is very low, between 10-100 organisms.[132,133] The duration of the disease varies from a few weeks to years. As a member of Gram-negative families, complete eradication of *Brucella* infection can be difficult, as the bacteria function as facultative intracellular parasites inside cells. The recommended treatment includes the use of multiple antibiotics (such as a combination of rifampicin and doxycycline) for several weeks.

Diagnostic confirmation of *Brucella* infection is commonly accomplished through serology because isolation would require BSL-3 containment facilities. In additional, diagnosis of *Brucella* through blood culture requires a prolonged incubation period (up to 6 weeks) as they are slow-growing, even with the help of modern automated machines the cultures would still need up to seven days to show a positive result. A better diagnostic technique is real-time PCR. However, such diagnostic systems are expensive and require advanced training for laboratory staff, and therefore are not practical to deploy the system for community clinics. However, fast and reliable diagnosis of *Brucella* can be crucial, as it is one of the earliest species to be weaponized due to its high survival in aerosol form and resist to some drying, only a few dozen organisms can infect human hosts. Therefore, finding an alternative diagnostic tool that is cost-efficient for massive *Brucella* specimen screening and has easy to operate interface is an important goal.

[132] KJ Ryan, CG Ray (editors) (2004). *Sherris Medical Microbiology (4th ed.*). McGraw Hill. ISBN 0-8385-8529-9.
[133] V. L. Atluri, M. N. Xavier, M. F. De Jong, A. B. Den Hartigh, R. E. M. Tsolis, "Interactions of the Human PathogenicBrucellaSpecies with Their Hosts". *Annual Review of Microbiology,* **65**: 523–541, (2011).

The *Brucella* optical biosensor is inspired from studies for the development of *Brucella* genus-specific PCR assays.[134] Recent research[135,136,137] has found that the DNA sequence of *Brucella* spp. such as *B. abortus, B. melitensis* and *B. suis* contains at least one complete copy of IS711 element at a unique chromosomal location of the species-specific DNA clone. Therefore, a DNA probe designed using IS711 as a template and target region of the corresponding sequence can be efficient and specific for *Brucella* spp. detection. In the scope of this dissertation, the *Brucella* biosensor will adopt the DNA probe platform and use a IS711 DNA probe as the receptor.

The biosensor assembly and diagnostic assay is based on the procedure described in section 4.3.2, replacing the MRSA DNA probe with *Brucella* probe IS711, which has commercially obtained in biotinylated form. The *Brucella* probe concentration is 60 pmol/ml, which is similar to that of the MRSA DNA probe. The sample solution for the test is made of pure culture isolates that are suspended in PBS pH 7.4. The negative control group for the assays includes *E. coli, Salmonella,* and *Pseudomonas aeruginosa.* Since the *Brucella* spp. probe IS711 has been demonstrated to be specific and efficient, no blocking reagent has been applied to the fiber sensor after the deposition of the biotinylated probe, and the lysing step only involves a boiling water bath without addition of further lysing enzymes.

[134] BJ Bricker, SM Halling, "Differentiation of Brucella abortus(biovars 1, 2 and 4), Brucella melitensis, Brucella ovis, and Brucella suis(biovar 1) by the polymerase chain reaction." *J. Clin. Microbial.* **32:** 2660-2666, (1994).
[135] R. Redkar, S. Rose, B. Bricker, and V. DelVecchio, "Real-time detection of Brucella abortus, Brucella melitensis, and Brucella suis." *Mol. Cell. Probes* **15:**43-52, (2001).
[136] BJ Bricker, "PCR as a diagnostic tool for brucellosis." *Vet.Microbiol.* **90(1):** 435-446, (2002).
[137] William S. Probert, Kimmi N. Schrader, Nhi Y. Khuong, Susan L. Bystrom and Margot H. Graves, "Real-Time Multiplex PCR Assay for Detection of Brucella spp., B. abortus, and B. melitensis", *J. Clin. Microbial.* **42(3):** 1290-1293,(2004).

The summary of three separate tests is shown in the Fig 5-2. Each experiment tested one *Brucella* strain (*B.abortus, B.melitensis* or *B.suis*) in sequential order and of different concentrations.

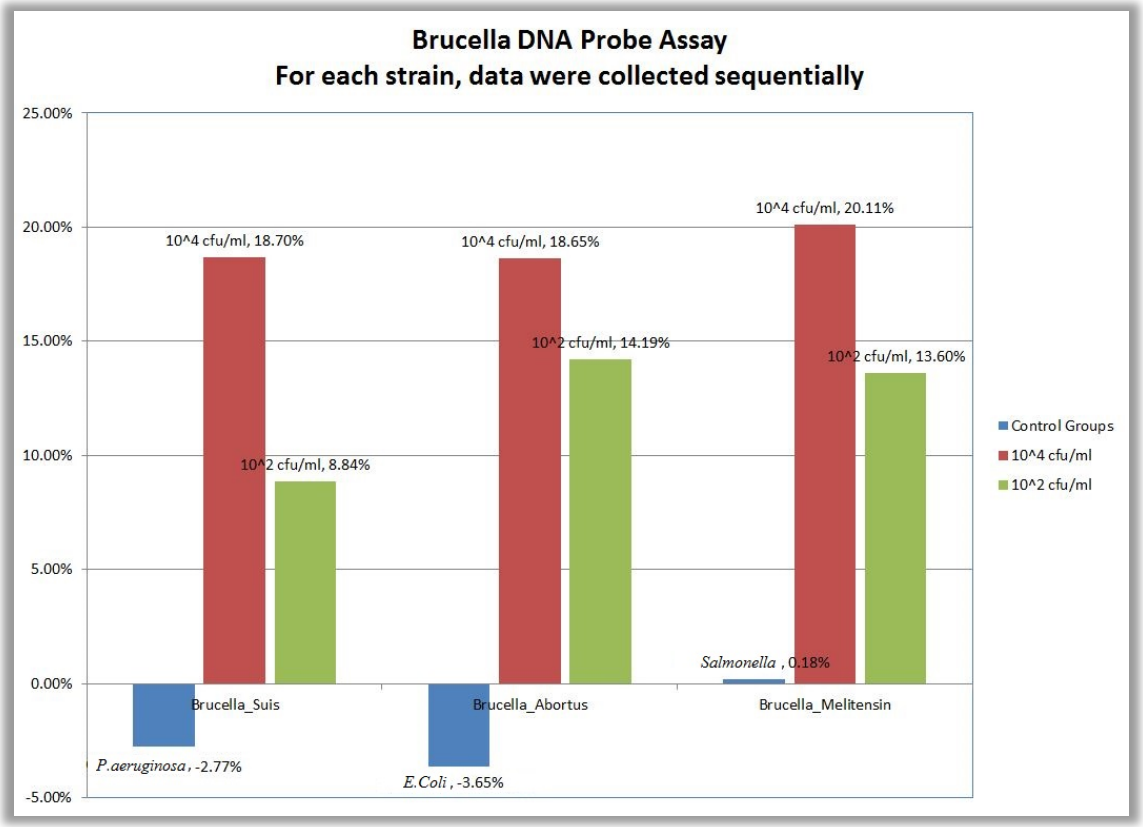

Figure 5-2: Comparison of the *Brucella* DNA biosensor with three *Brucella* spp.: *B. abortus, B. melitensis, and B. suis*. Each experiment comprises of 3 sequential tests. First, test biosensor with a randomly chosen negative control sample (*E. coli, Salmonella or P. aeruginosa*). Then a *Brucella* culture suspension at 10^4cfu/ml was tested, followed by a test with culture suspension at 10^2cfu/ml.

Each experiment tested three sample suspensions sequentially. The first sample tested was a negative control group sample whose cell concentration was 10^5cfu/ml, then a *Brucella* species suspension at a concentration of 10^4cfu/ml, followed by the same strain suspension at 10^2cfu/ml. The difference between the signal responses of the negative control group samples and *Brucella* culture samples is evident. All control samples returned a negative to null reading, and all three

Brucella species tested at a concentration of 10^4cfu/ml rendered a 18%-20% signal attenuation, while at a one-hundredth lower concentration. The signal response ranges from 8.84% to 14.19%, depending on the type of the strain tested. The attenuation of the optical power also correlated to the concentration of the *Brucella* pure culture suspension tested. Therefore, a quantitative analysis could be performed to a concentration-unknown *Brucella* culture suspension. Since the sample holder can only accommodate 0.5 ml of the sample solution, the fiber sensor actually reacts with as little as 50 organisms in the assay for a concentration of 10^2cfu/ml and is still able to return a positive reading. Therefore, it is a plausible conclusion that the *Brucella* DNA fiber sensor is very sensitive, and is capable of detecting *Brucella* strains at or below 100 cfu/ml within 1 hour.

5.4 The *H. somni* Biosensor

Histophilus somni (H. somni) is a Gram-negative, nonmotile, pleomorphic coccobacillus[138]. *H. somni* is the main cause for histophilosis diseases, which have been widely reported in North American cattle. The disease primarily affects the respiratory system of cattle, causing bovine respiratory disease. Prevention of an epidemic of *H. somni* within livestock relies on early detection and separation of infected animals. In order to obtain maximum cost efficiency, diagnostic tools need to be inexpensive to deploy and simple to operate.

The *H. somni* biosensor uses the DNA probe based fiber sensor platform, and follows the same sensor assembly protocols as described in section 4.3.2 for creating the receptor layer on the cladding of the LPG-fiber. The *H. somni* DNA probe is prepared by Dr. Inzana's group, and supplied as a biotinylated probe suspension at 60 pmol/ml. The probe is cross-linked to the

[138] http://www.merckmanuals.com/vet/generalized_conditions/histophilosis/overview_of_histophilosis.html

PCBS layer of the ISAM film via EDC/sulfo-NHS, culture samples are lysed, and the DNA denatured by boiling for 10 minutes; then cooled to 10^{o}C before being applied to the fiber sensor.

Fig 5-3 summarizes the sensitivity study of the *H. somni* DNA bionsensor:

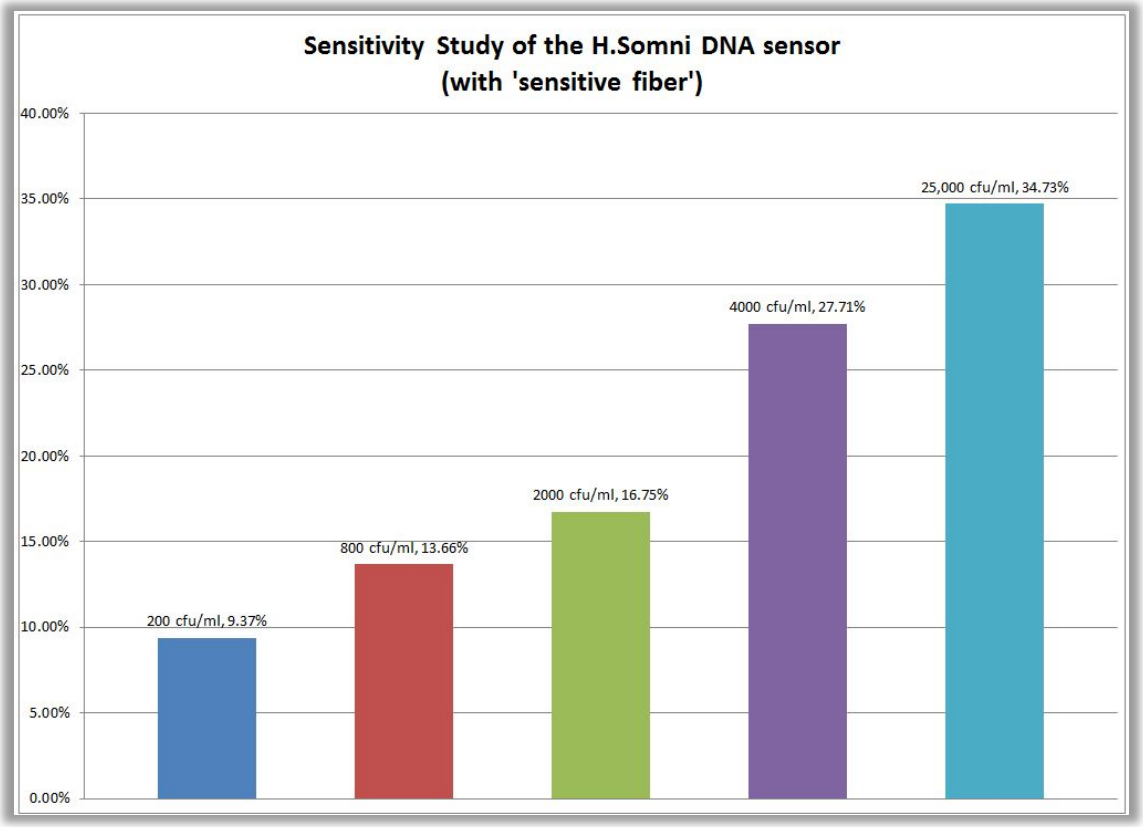

Figure 5-3: Sensitivity of the *H. somni* DNA sensor. Pure *H. somni* culture suspensions from 200 cfu/ml to 25,000 cfu/ml were tested in separate tests. The DNA sensor is built on the 'sensitive fiber'. Therefore, it is capable of detecting presence of 100 cfu/ml of *H. somni*.

In this study, *H. somni* culture suspensions from 200 cfu/ml to 25,000 cfu/ml were tested in 5 separate tests. Each test was performed on the freshly prepared fiber sensor, which is built on the 'sensitive fiber'. Therefore, this series of experiments shows high sensitivity in detecting *H. somni* strains. With increment of the suspension's concentration, the percentage signal also increased. Therefore, the biosensor is quantitative and results reflect the concentration of the *H. somni* suspension tested.

Another interesting study designed and conducted based on the *H. somni* biosensor is to see if streptavidin layer enhances the sensitivity of the biosensor. Studies[139,140] have reported of using EDC/sulfo-NHS cross-linking chemistry to conjugate oligonucleotides, which refers to the sequence end of the biotinylated DNA probe, directly to the primary amine groups of a protein. Therefore if such cross-linking chemistry could also be applied to the assembly process for building DNA probe based biosensor, it could help reduce the complexity of adding streptavidin, limit the source of nonspecific binding and control the material cost to manufacture the biosensor.

Fig 5-4 shows the comparison experiments for the *H. somni* biosensor assembled with or without streptavidin layer.

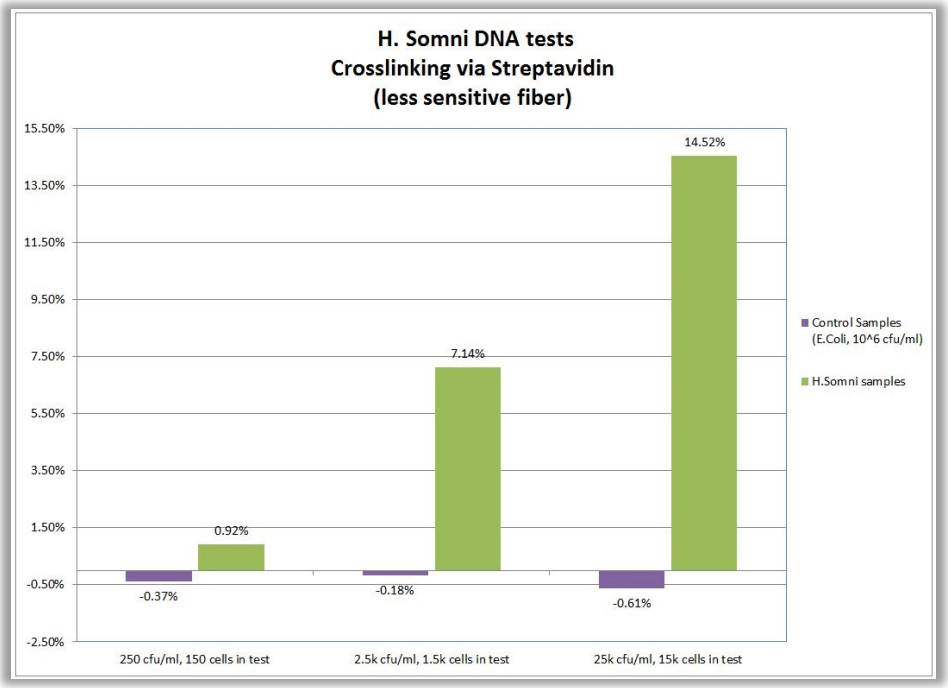

(A)

[139] http://www.piercenet.com/files/TR0030-Modify-oligos.pdf

[140] Gurman Singh Pall, Carles Codony-Servat, Jane Byrne, Leigh Ritchie, and Andrew Hamilton, "Carbodiimide-mediated cross-linking of RNA to nylon membranes improves the detection of siRNA, miRNA and piRNA by northern blot", *Nucleic Acids Res.,* **35(8):** e60, (2007).

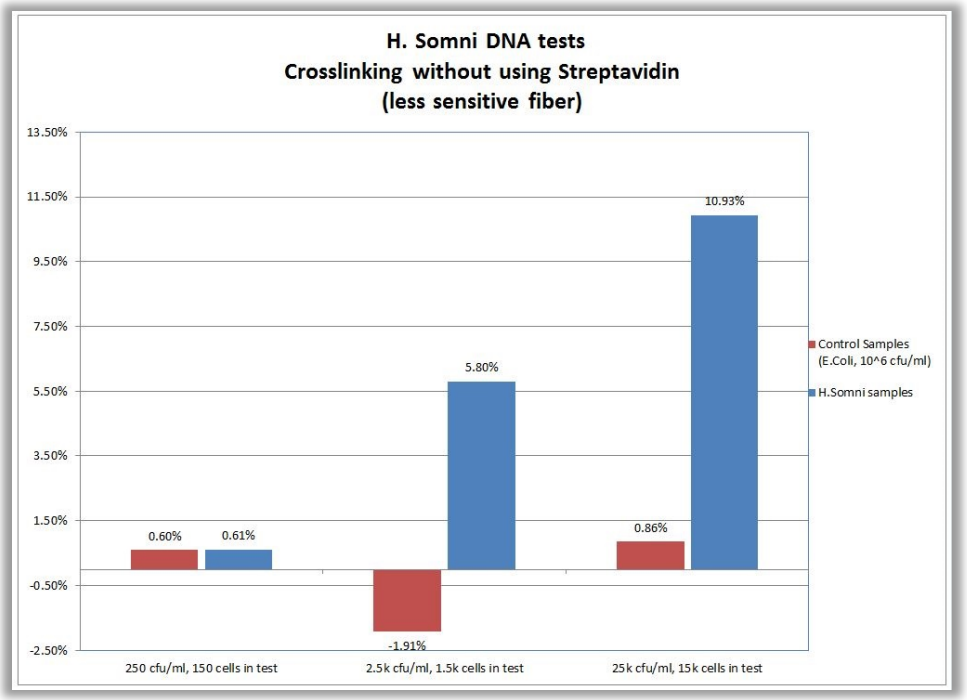

(B)

Figure 5-4: Comparison experiments to check the specificity and sensitivity of the *H. somni* biosensor which is assembled with or without streptavidin.

The experiments tested three sample pairs in separate runs on each biosensor design: the one using streptavidin to immobilize the DNA probe, and the one that directly links the DNA probe to the PAH of the ISAM film. Each sample pair contains one control sample (*E. coli* at 10^6 cfu/ml) and one *H. somni* sample at escalating concentrations (200 cfu/ml, 2.5k cfu/ml and 25k cfu/ml). Each sample pair was tested on a freshly prepared biosensor.

The *H. somni* suspension samples at 2.5k cfu/ml and 25k cfu/ml showed strong positive readings in both sensor designs. Under the same sample pair, the biosensor with streptavidin layer has displayed a larger positive reading compared to the biosensor without streptavidin (7.14% vs 5.8% at 2.5k cfu/ml *H. somni* suspension, and 14.52% vs 10.93% at 25k cfu/ml *H. somni* suspension). All of the negative control samples universally returned negative to null readings, which means both designs passed the specificity test, though the biosensor with the

streptavidin layer is slightly more sensitive than the one without the streptavidin layer. It also confirmed that the step for deposition of a streptavidin layer between ISAM and DNA probes is valuable for retaining high sensitivity.

It should also be noted that since all the experiments were performed on the 'less sensitive fiber', that all the positive signals under respective sample concentration are relatively smaller than what are generated from the biosensor built on the sensitive fiber, and that the same biosensor built on the basis of 'less sensitive fiber' could not effectively distinguish signals between 200 cfu/ml *H. somni* culture sample and *E. coli* control sample at 10^6cfu/ml.

Chapter 6 Conclusion and Future Work

6.1 Conclusion

This dissertation has presented the combination of turnaround point long period gratings and ionic self-assembled multilayer films as an optical fiber based biosensor. With interdisciplinary integration of knowledge from biochemistry, molecular biology, immunology and immunoassays, this dissertation has demonstrated a novel biosensor for MRSA detection that is able to perform fast and accurate identification, is compact in the size of the system's core components, and is much cheaper and easier to operate than its competitors.

A series of experiments have been conceived and performed to explore the specificity and sensitivity of the biosensor system. It has been found that the Mab based MRSA biosensor is capable of sensing MRSA strains1556 at concentrations as small as 100 cfu/ml (signal reduction of 21.78%) or less in pure culture samples and properly yielding negative results to control samples containing MSSA strains. Table 6-1 summarizes the results of testing different strain suspension samples:

Table 6-1 **Summary of various strain suspension sample tests on the antibodies based MRSA biosensor**

Strains	***Number of Tested Samples***	***Number of Positive/Negative***	***Light Attenuation*** *(Percentage Change)*	***Standard Deviation***	***BBL CHROMagar Result***
MRSA pure culture suspensions[*]	26	26/0	21.89%	±7.82%	+
Control pure culture suspensions[*]	14	0/14	-0.12%	±0.12%	-
Human subject sample suspensions	20	9/11	16.52% (+) -1.45% (-)	±4.94% (+) ±1.59% (-)	9 (+) 11 (-)

** The pure culture suspensions were tested at concentration of 10^4cfu/ml.*

From the table, it is evident that the antibody-based MRSA biosensor achieved similar results as the BBL CHROMagar culture tests performed on the same batch of pure cultures. Since each individual sample suspension represents a distinct strain type (either a methicillin-resistant strain or methicillin-sensitive strain), the agreement between the expectation of the outcomes and the testing results in the total 71 samples indicate the biosensor is capable of detecting a wide range of MRSA strains with good sensitivity.

Statistical analysis has also been conducted on the data of the pure culture sample tests on the antibodies based MRSA biosensor. The *p-value* between the data obtained from the methicillin-resistant strain suspensions and that from the methicillin-sensitive strain suspensions are smaller than 0.0001, proving the biosensor is extremely effective in distinguishing the MRSA strain group from the control strain group.

Additional studies of the antibody-based MRSA biosensor has also demonstrated the sensor system is able to properly identify tissue samples from the mice infected with MRSA strains. Each tissue suspension was tested in a pair (tissue sample from mouse #2 and the same organ tissue samples from mouse #4 become one pair) on a freshly prepared biosensor. The summary of the results is shown in Table 6-2

Table 6-2 **Summary of mouse tissue sample tests on the antibodies based MRSA biosensor**

Mouse Number	***Spleen Tissue Suspension***	***Liver Tissue Suspension***	***Lung Tissue Suspension***	***Mice infected by MRSA***
Mouse #4	19.2% ± 6.4%	50.1% ± 11.9%	11.7% ± 3.0%	Yes
Mouse #2	1.6% ± 8.3%	0.74% ± 1.02%	-0.91% ± 1.11%	No

***** *The data is presented in the form of "average ± standard deviation".*

Based on the success of the antibody based MRSA fiber sensor platform, four other types of biosensor (MRSA DNA probe biosensor*, F. tularensis* Mab biosensor, *Brucella* DNA biosensor

and *H. Somni* DNA biosensor) have been designed and tested with preliminary success in differentiating corresponding pure culture samples from control strain suspensions.

The DNA probe MRSA biosensor was developed in response to the inability to obtain good correlation of the Mab MRSA biosensor with clinical culture tests with human patient swabs. More specifically, the experiments for testing the DNA probe based MRSA biosensor were performed in sequential order with the 'less sensitive' fiber sensor. In such cases, MSSA (as control strain) at low concentration is applied to the fiber sensor first for 1 hour, and the spectrum shift is measured after the sample soaking period. Then, without cleaning the fiber sensor, MRSA (as MRSA treatment strain) at the same concentration to the MSSA suspension tested previously is applied for 1 hour and shift of the spectrum is measured. These two measurements represent one strain concentration run, and two more runs at higher concentration are also performed on the same fiber sensor sequentially afterwards. One set of experiments was run with the MSSA control strain first and another series with the MRSA strain applied first. The data of a representative experiment can be viewed in Table 6-3. Unfortunately, the DNA probe MRSA biosensor was still found to suffer from significant false positives on clinical human patient swabs.

Table 6-3 **Summary of pure culture sample tests on DNA probe based MRSA biosensor**

Strain Suspension	***Control Strain Suspensions Applied First***	***MRSA Strain Suspensions Applied First***
MRSA, 10^4cfu/ml	3.67%	6.35%
MRSA, 10^6cfu/ml	5.57%	8.53%
MRSA, 10^7cfu/ml	10.65%	14.46%
MSSA, 10^7cfu/ml†	-0.22%	-0.3%

† *The data of "MSSA, 10^7cfu/ml" is obtained via averaging data points of 3 individual tests performed between the MRSA strain suspensions.*

The experiments for testing the antibody based *F. tularensis* biosensor were also performed in sequential order. In such cases, WBTI (as negative control strain) at low concentration is applied to the fiber sensor first for one hour, and the spectrum shift is measured. Then without stripping the fiber sensor clean, LVS (as *F. tularensis* treatment strain) at the same concentration as the WBTI suspension tested previously is applied for one hour and shifting of the spectrum is measured afterwards. These two measurements represents one strain concentration run, and two more runs at 100 times higher concentration are also performed on the same fiber sensor sequentially afterwards. The data of a representative experiment can be viewed in Table 6-4:

Table 6-4 **Summary of pure culture sample tests on antibody based *F. tularensis* biosensor**†

Strain Suspension Concentration	***WBTI*** *(Control Strain)*	***LVS*** *(Treatment strain)*
10^2*cfu/ml*	0.05%	25.55%
10^4*cfu/ml*	3.28%	44.94%
10^6*cfu/ml*	-11.67%	39.60%

† Data is obtained via a sequential tests, where the Control strain suspensions (WBTI) is applied before the treatment strain suspensions (LVS) at the same cell concentration.

The experiments for examining the DNA probe based *Brucella* biosensor were conducted separately for three *Brucella* strain types. In each strain type run, the biosensor is prepared freshly, then a negative control strain (one of *P. aeruginosa, E. coli,* or *Salmonella*, initially chosen randomly and remaining the same in the ensuing sequential runs) at 10^6 cfu/ml is applied first to the fiber sensor for one hour, and the spectrum afterwards is measured and compared to the spectrum level before soaking in the suspension. A *Brucella* strain suspension (one of *B. suis, B. abortus or B. melitensis*, initially chosen randomly and remaining the same in the ensuing sequential runs) at concentration 10^4 cfu/ml, is added to the fiber sensor for one hour, and the spectrum shifting is recorded. An additional experiment run with the same *Brucella* strain type

but at 10^2 cfu/ml is conducted afterwards, and the spectrum is also recorded. Thus three runs represent a full test series for one *Brucella* strain type test, and the three tests with different *Brucella* strain types were performed on the biosensor system. The data for testing the DNA probe based *Brucella* biosensor with three individual strain types can be viewed in Table 6-5:

Table 6-5 **Summary of pure culture sample tests on the DNA probe based *Brucella* biosensor**

Strain Concentration	***B. suis***	***B. abortus***	***B. melitensis***	***Average with S.D.***
Negative Control Strains† *(Strain name listed below)*	-2.77% (*P. aeruginosa*)	-3.65% (*E. coli*)	0.18% (*Salmonella*)	-2.08% ± 1.64%
10^4cfu/ml	18.70%	18.65%	20.11%	19.15% ± 0.68%
10^2cfu/ml	8.84%	14.19%	13.60%	12.21% ± 2.40%

† Control strains are at concentration of 10^6cfu/ml, and arealways applied first in the sequential tests, each Brucella strain type is tested in an individual sequential test series, where control strains, Brucella pure culture suspensions at 10^4cfu/ml, and then Brucella suspension at 10^2cfu/ml were tested in order.

The experiments for testing the DNA probe based *H. Somni* biosensor are similar to the experimental designs of testing the Mab based MRSA biosensor. The experiments were conducted in pairs and sequentially. This means that each concentration pair consists of a sequential run with a negative control strain suspension (*E. Coli* at 10^6 cfu/ml) and then a *H. Somni* suspension at various strain concentrations. Each freshly prepared biosensor is tested with three strain concentration pairs in order, starting from *H. Somni* suspension concentration of 10^2 cfu/ml till 10^6 cfu/ml. Also, the comparison experiments for crosslinking the DNA probe to the fiber sensor with, or without Streptavidin, were performed, and the data for the two crosslinking methods are summarized and compared in Table 6-6:

Table 6-6 **Summary of pure culture sample tests on the DNA probe based *H. Somni* biosensor**

(*Crosslinking Methods Comparison*)

Strain Concentration	***Crosslinking with Streptavidin*** *(vs. control strain suspensions†)*	***Crosslinking without Strepavidin*** *(vs. control strain suspensions†)*
10^2cfu/ml	0.92% (*vs*. -0.37%)	0.61% (*vs*. 0.6%)
10^4cfu/ml	7.14% (*vs*. -0.18%)	5.80% (*vs*. -1.91%)
10^6cfu/ml	14.52% (*vs*. -0.61%)	10.93% (*vs*. -0.86%)

† All control strain suspensions were E. Coli at concentration of 10^6 cfu/ml.

All of the biosensors studied above have displayed adequate sensitivity and specificity to the analyte suspensions tested, and each of them is able to respond only to the target strains or DNA strands. Although the design of each biosensor system is slightly different from one another in terms of the receptor layer, the assembly of the biosensor platform of the TAP LPG optical fiber and ISAM film are the same in all cases. Therefore, the biosensor platform is proven to be versatile and can be easily modified for or detection of a variety of specific analytes. The rapid response and label-free feature make this biosensor approach a very competitive candidate for rapid, low-cost sensing devices in the application of medical diagnostic, forensics, environmental protection, counter-biowarfare or bioterrorism, protection of public health, and monitoring food safety. The future for commercialization of the biosensor system is optimistic if the issues related to finding an appropriate blocking agent for complex human swab samples can be resolved.

6.2 Future Work

Despite success thus far in various applications of pathogen detection and differentiation, the development of the optical fiber based biosensor is still at a primitive stage, and many questions need to be answered. The following sections will list a few topics that could be very interesting to study and could substantially improve the performance of the biosensor platform.

6.2.1 Introducing Protein-G to Improve Bioconjugation of Antibodies

Monoclonal antibodies contain a large number of amine groups on the Fab and Fc regions of their primary protein structures. These groups can be targeted by crosslinkers and conjugate with the carboxyl groups expressed on the surface of the substrate ISAM film. Therefore, the orientation of the immobilized antibodies on the fiber surface can be widely varied. Some of the orientation directions may be inefficient, because one or both of the antibodies' paratopes can be facing the film and inaccessible to the sample.

Protein-G is an immunoglobulin-binding protein that has a high protein-antibody affinity and primarily binds with the Fc region of the antibodies.[141] Therefore, at least one paratope of the antibody can be guaranteed to be available for each immobilized antibody molecule. Furthermore, bioconjugation between protein-G and antibodies can take place at a higher rate than solely mixing antibodies with crosslinkers and attaching them to the ISAM film. Using protein-G can be cost-saving and sensing-efficient.

As a protein, protein-G can be conjugated to the carboxyl groups of the ISAM film via EDC/sulfo-NHS catalyst in the same way as for antibodies. The procedure for biosensor assembly only differs in replacing antibodies with protein-G (final working concentration at 50 μg/ml) in the crosslinker mixture. After that, antibodies are added at the working concentration for 4 more hours to attach antibodies to the protein-G. A few tests have been conducted with the extra protein-G layer deposited between the ISAM film and antibodies on the fiber. However, no significant improvement has yet been observed, which contradicts the expectation. A possible explanation may be that each protein-G only possesses two antibody binding sites, and if protein-G deposition has a low density, it would subsequently reduce the amount of antibody binding as

[141] http://www.piercenet.com/browse.cfm?fldID=978FBB48-DCD3-F4E4-66E7-069349D16FEE

well. Optimizing the protein-G deposition process and exploring the alternative cross-linking chemistry might solve the issue and increase the sensitivity of the Mab-based fiber sensor.

6.2.2 Improvement of the DNA Biosensor with Swab Tests

As has been discussed in the DNA probe section, there are a few aspects of the biosensor that require improvement for commercialization. The first possible measure is to improve streptavidin conjugation to the fiber surface. As each streptavidin can at most host four biotin molecules, the coverage of the streptavidin on the ISAM film directly determines the maximum amount of biotinylated DNA probe that can be attached to the biosensor. The more DNA probe sites the sensor has on the cladding, the larger the chances a target sequence would hybridize with the probe, and the more sensitive the sensor would be. A current bottleneck has been set by the EDC/sulfo-NHS cross-linking chemistry. It has been found in experiments that well-preserved EDC and sulfo-NHS chemicals are vital to the bioconjugation quality and efficiency. However, the storage requirement for maintaining high quality is so strict that the chemical powder captures enough moisture after first exposure to air within a two-week period. Degradation of the quality of cross-linker may be accountable for many issues encountered in the sample tests, such as sudden drop of cladding thickness, poorly deposited streptavidin, which may barely bind with any DNA probe so that the biosensor would show little to no response to the presence of treatment group samples, and so on. Finding alternative cross-linking chemistry may help resolve the problem, or finding a better way of storing and maintaining EDC and sulfo-NHS.

A second critical measure is to screen a wide range of blocking reagents that can help reduce the nonspecific binding from swab sample tests while not disrupting the antigen-receptor (ie, antibody-antigen binding, or DNA sequence hybridization) binding mechanism. The blocking

efficiency study for blood or swab suspension solutions has been a major topic of immunoassays. There are many commercially available products such as recombinant proteins, detergents, buffers and so on. Each blocker behaves differently in how it would neutralize nonspecific binding sites. Applying some of the blockers may be efficient for reducing nonspecific binding, yet they might react with chemical groups on the receptor and hence modify the functionality of the receptor. Also, the blocking efficiency of the blocker varies largely on the condition of the solvent, the reagent concentration and the composition of the film they are supposed to treat. Therefore, a series of experiments needs to be designed to test the quality and efficiency of a blocker.

6.2.3 Statistical Significance and Stability Studies

One weakness of the current biosensor prototype is the result-reproducibility. The quality of the crosslinker and the activity of the receptor (monoclonal antibodies, or DNA probe) could significantly affect the quality of the data collected from the respective experiment. Therefore, the variation in measurement is still large for complex samples, such as tissue sample tests or swab sample tests.

A possible solution is to run multiple repeating experiments on the same biosensor design and sample set, and derive the statistical significance from a large data size that could reduce the influence of the unknown system parameters and random fluctuations.

6.2.4 Regenerating the Biosensor

Currently, after each experiment, the biosensor fiber is treated with heated weak acid to remove the entire set of organic films deposited onto the fiber. This is an inefficient use of time and materials used to assemble the biosensor. However, there are biochemistry treatments that

target the bioconjugation bonds formed between biomolecules and their substrate or the antigen-anbody bonds, which could help regenerate the biosensor. The literature[142] has reported that dipping the target sequence hybridized DNA sensor in 90% formamide TE buffer (10 mM Tris-HCl, pH 8.3, 1 mM EDTA) for 10 seconds at room temperature can remove antibodies from the organic film substrate. And the DNA probe can be naturally dehybridized with the complementary sequence with the help of enzymes or high heat. However, these biosensor regeneration methods may be strong enough to terminate the activity of the respective receptor or damage the ISAM film, resulting in a regenerated yet potentially disabled biosensor.

Therefore, more work should be done to determine whether a regeneration method used in other assays could still be helpful to the fiber sensor case, and if such method is suitable, what the best reaction conditions would be.

6.2.5 Determination of the Necessary Assay Length

Currently a complete assay for one sample test takes one hour. However, it may be possible to shorten this period and still have sufficient sensitivity of the optical biosensor. The literature has reported biosensor platforms based on DNA probes are able to return reliable readings after 1-5 minutes of contact with the sample solution, as the hybridization process occurs spontaneously at room temperature with a high reaction rate. It may be possible to limit our biosensor assay period to a few minutes as well, and if such experiments succeed, it could immensely enhance the speed of diagnosis with this biosensor system. A detailed study of the results, as a function of time of exposure of the sample to the fiber surface should be carried out.

[142] Ferguson JA, Christian Boles T, Adams CP, Walt DR, "A fiber-optic DNA biosensor microarray for the analysis of gene expression", *Nature Biotechnol,* **14**:1681–1684, (1996).

Bibliography

1. A Farmer, A Wade, E Goyder, et al., “Impact of self-monitoring of blood glucose in the management of patients with non-insulin treated diabetes: open parallel group randomized trial". *BMJ,* **335 (7611):** 132, (2007).
2. H. C. Gerstein, M. E. Miller, et al. "Effects of intensive glucose lowering in type 2 diabetes". *The New England Journal of Medicine*, **358(24):** 2545–59, (2008).
3. M. E. Khamseh, M. Ansari, M. Malek, , G. Shafiee, H. Baradaran, "Effects of a structured self-monitoring of blood glucose method on patient self-management behavior and metabolic outcomes in type 2 diabetes mellitus". *Journal of diabetes science and technology*, **5(2):** 388–393, (2011).
4. T. Vo-Dinh, B. Cullum, "Biosensors and biochips: Advances in biological and medical diagnostics". *Fresenius' Journal of Analytical Chemistry*, **366 (6–7):** 540, (2000).

5. E. Marazuela, A. Moreno-Bondi, "Fiber-optic biosensors - an overview". *Analytical and Bioanalytical Chemistry* **372(5-6):** 664–682, (2002).
6. Donzella V, Crea F. "Optical biosensors to analyze novel biomarkers in oncology." *J Biophotonics.* **4(6):**442-52, (2011).
7. R. Rizzuto, P. Pinton, M. Brini, A. Chiesa, L. Filippin, T. Pozzan, "Mitochondria as biosensors of calcium microdomains". *Cell Calcium*, **26(5):** 193–199, (1999).
8. M. Bragadin, S. Manente, R. Piazza, G. Scutari, "The Mitochondria as Biosensors for the Monitoring of Detergent Compounds in Solution". *Analytical Biochemistry,* **292 (2):** 305–307, (2001).
9. C. Védrine, J.-C. Leclerc, C. Durrieu, C. Tran-Minh, "Optical whole-cell biosensor using Chlorella vulgaris designed for monitoring herbicides." *Biosensors & bioelectronics*, **18(4):** 457–63, (2003).
10. R. S. Dubey, S.N. Upadhyay, "Microbial corrosion monitoring by an amperometric microbial biosensor developed using whole cell of Pseudomonas sp." *Biosensors & bioelectronics*, **16(9-12):** 995–1000, (2001).
11. M. Campàs, R. Carpentier, R. Rouillon, "Plant tissue-and photosynthesis-based biosensors". *Biotechnology Advances*, **26(4):** 370–378, (2008).
12. S.Q. Lud, M.G. Nikolaides, I. Haase, M. Fischer and A.R. Bausch, "Field Effect of Screened Charges: Electrical Detection of Peptides and Proteins by a Thin Film Resistor" *ChemPhysChem,* **7(2):** 379-384, (2006).
13. G Liu, Y. Lin, "Nanomaterial labels in electrochemical immunosensors and immunoassays." *Talanta*. **74(3):**308-17, (2007).
14. María Dolores Marazuela, María Cruz Moreno-Bondi, "Fiber-optic biosensors – an overview." *Anal Bioanal Chem* **372**:664–682,(2002).
15. I. Vockenroth, P. Atanasova, W. Knoll, A. Jenkins, I. Köper, "Functional tethered bilayer membranes as a biosensor platform". *IEEE Sensors 2005 the 4-th IEEE Conference on Sensors*: 608–610, (2005).
16. Kyung Wook Weea, *etc.,* "Novel electrical detection of label-free disease marker proteins using piezoresistive self-sensing micro-cantilevers." *Biosensors and Bioelectronics*, **20(10):** pp. 1932–1938, (2005).
17. Bong Seop Kwaka, *etc*.,"Quantitative analysis of sialic acid on erythrocyte membranes using a photothermal biosensor." *Biosensors and Bioelectronics,* **35(1):** pp.484–488, (2012).
18. Guan H, Cai M, Chen L, Wang Y, He Z., "Label-free DNA sensor based on fluorescent cationic polythiophene for the sensitive detection of hepatitis B virus oligonucleotides." *Luminescence*. **25(4):**311-6,(2010).
19. M. Zhang, S. Ge, W. Li, M. Yan, X. Song, J. Yu, W. Xu, J. Huang, "Ultrasensitive electrochemiluminescence immunoassay for tumor marker detection using functionalized Ru-silica@nanoporous gold composite as labels." *Analyst.* **137(3):**680-5,(2012).
20. Li P, Sherry AJ, Cortes JA, Anagnostopoulos C, Faghri M., "A blocking-free microfluidic fluorescence heterogeneous immunoassay for point-of-care diagnostics." *Biomed Microdevices.* **13(3):**475-83,(2011).
21. Anjum Quershia, Yasar Gurbuza, Weng P. Kangb, Jimmy L. Davidson, "Anjum Quershia, Yasar Gurbuza, Corresponding author contact information, E-mail the corresponding author, Weng P. Kangb, Jimmy L. Davidson." *Biosensors and Bioelectronics,* **25(4):** 877-882, (2009).
22. Deblina Sarkar, Kaustav Banerjee, "Proposal for tunnel-field-effect-transistor as ultra-sensitive and label-free biosensors." *Appl. Phys. Lett.,* **100:** 143108 (2012).
23. Ankit Jain, Pradeep R. Nair, Muhammad A. Alam, "Flexure-FET biosensor to break the fundamental sensitivity limits of nanobiosensors using nonlinear electromechanical coupling". *PNAS*, **109(24):** 9304-9308, (2012).

24. E. Anderson, J. Graham Smith, et al., “Investigation and verification of a bioluminescent biosensor for the quantitation of ara-CTP generation: A biomarker for cytosine arabinoside sensitivity in acute myeloid leukaemia”, Biosensors and Bioelectronics, 52: 345-353, (2014).
25. S. Rodriguez-Mozaz, M. de Alda, D. Barceló, “Biosensors as useful tools for environmental analysis and monitoring.” Anal Bioanal Chem, 386: 1025–1041, (2006).
26. CA Rowe-Taitt, JP Golden, MJ Feldstein, JJ Cras, KE Hoffman, FS. Ligler, “Array biosensor for detection of biohazards.” Biosens Bioelectron. 14(10-11):785-94, (2000).
27. Daniel Berdat, Annick Marin, Fernando Herrera, Martin A.M. Gijs, “DNA biosensor using fluorescence microscopy and impedance spectroscopy.” Sensors and Actuators B, 118:53–59, (2006).
28. Andreas P. Abel, Michael G. Weller, Gert L. Duveneck , Markus Ehrat , H. Michael Widmer,“Fiber-Optic Evanescent Wave Biosensor for the Detection of Oligonucleotides.” *Anal. Chem.,* **68 (17):** pp 2905–2912,(1996).
29. Tempelman LA, King KD, Anderson GP, Ligler FS , “Quantitating Staphylococcal Enterotoxin B in Diverse Media Using a Portable Fiber-Optic Biosensor.”*Anal Biochem,* **233**:50–57, (1996).
30. Bartolomeo Della Ventura, Luigi Schiavo, Carlo Altucci, Rosario Esposito, Raffaele Velotta, “Light assisted antibody immobilization for bio-sensing.” *Biomedical Optics Express*, **2(11):** pp.3223-3231,(2011).
31. D. A. Bergstein, E. Ozkumur, A. C. Wu, A. Yalcin, J. Needham, R. Irani, J. Gershoni, B. B. Goldberg, C. DeLisi, M. F. Ruane, M. S. Ünlü, "Resonant Cavity Imaging: A Means Toward High-Throughput Label-Free Protein Detection," *IEEE Journal of Selected Topics in Quantum Electronics***, 14(1)**:131-139, (2008).
32. B.H Schneider, E.L Dickinson, M.D Vach, J.V Hoijer, L.V Howard, “Highly sensitive optical chip immunoassays in human serum.” *Biosens. Bioelectron.* **15(1-2)**:13-22, (2000).
33. M.M. Varma, H.D. Inerowicz, F.E. Regnier, D.D. Nolte, “High-speed label-free detection by spinning-disk micro-interferometry.” *Biosens. Bioelectron*. **19**(11):1371-1376, (2004).
34. M. Zhao, D. Nolte, W. Cho, F. Regnier, M. Varma, G. Lawrence, J. Pasqua, “High-Speed Interferometric Detection of Label-Free Immunoassays on the Biological Compact Disc.” *Clin. Chem.* **52:**2135-2140, (2006).
35. B. Liedberg, C. Nylander, I. Lunstrom, “Surface plasmon resonance for gas detection and biosensing” *Sens. Actuators,* **4:** 299-304, (1983).
36. Xudong Fan, Ian M. White, Siyka I. Shopova, Hongying Zhu, Jonathan D. Suter, Yuze Sun, “Sensitive optical biosensors for unlabeled targets: A review”, *Analytica Chimica Acta,* **620**: 8–26, (2008).
37. Homola J., “Present and future of surface plasmon resonance biosensors.” *Anal Bioanal Chem.,* **377(3):**528-39,(2003).
38. K.H. Smith, B.L. Ipson, T.L. Lowder, A.R. Hawkins, R.H. Selfridge, S.M. Schultz, “Surface-relief fiber Bragg gratings for sensing applications.” *Appl. Opt.,* **45**:1669, (2006).
39. T.L. Lowder, J.D. Gordon, S.M. Schultz, R.H. Selfridge, “Volatile organic compound sensing using a surface-relief D-shaped fiber Bragg grating and a polydimethylsiloxane layer.” *Opt. Lett.,* **32:**2523, (2007).
40. W. Liang, Y. Huang, Y. Xu, R.K. Lee, A. Yariv, “Highly sensitive fiber Bragg grating refractive index sensors.” *Appl. Phys. Lett.* **86**: 151122, (2005).
41. M.P. DeLisa, Z. Zhang, M. Shiloach, S. Pilevar, C.C. Davis, J.S. Sirkis, W.E. Bentley, “Biofunctionalized tilted Fiber Bragg Gratings for label-free immunosensing.” *Anal. Chem.,* **72:**2895, (2000).
42. L. Rindorf, J.B. Jensen, M. Dufva, L.H. Pedersen, P.E. Hoiby, O.Bang, “Photonic crystal fiber long-period gratings for biochemical sensing.” *Opt. Express*, **14:**8224, (2006).
43. ARC Electronics (2007-10-01). "Fiber Optic Cable Tutorial"
44. http://www.arcelect.com/fibercable.htm
45. “Long-period grating theory”, http://gratings.fo.gpi.ru/index.php?page=11#ref
46. T. Tamir, ed., "Integrated Optics", Vol.7 of Topics in Applied Physics, Springer-Verlag, (1975).
47. T. Erdogan, "Fiber grating spectra*", J. Lightwave Technol.,* **15**, pp. 1277-1294, (1997).
48. http://en.wikipedia.org/wiki/Fiber_Bragg_grating
49. Patrick H J, Kersey A D and Bucholtz F, “Analysis of the response of long period fibre gratings to external index of refraction*”, J. Lightwave Technol*. **16:**1606–42, (1998).

50. S. A. Vasiliev, E. M. Dianov, A. S. Kurkov, O. I. Medvedkov, V. N. Protopopov, "Photoinduced in-fibre refractive-index gratings for core-cladding mode coupling", *Quantum Electron*., **27**: pp.146-149, (1997).
51. T. Erdogan, "Cladding-mode resonances in short- and long-period fiber grating filters", *J. Opt. Soc. Am. A*, **14**: pp.1760–1773, (1997).
52. S.W. James, R.P. Tatam, "Optical fibre long-period grating sensors: characteristics and application", *Meas. Sci. Technol.*, **14**: R49–R61 (2003).
53. O.V. Ivanov, S.A. Nikitov, Yu.V. Gulyaev, "Cladding modes of optical fibers: properties and applications", *Physics-Uspekhi*, **49**:175-202 (2006).
54. Turan Erdogan, "Fiber Grating Spectra", *Journal of Lightwave Technology,* **15**:1277-1294, (1997).
55. Vengsarkar A M, Lemaire P J, Judkins J B, Bhatia V,Erdogan T and Sipe J E, "Long-period fibre gratings as band rejection filters", *J. Lightwave Technol.,* **14:** 58–64, (1996)
56. A. Yariv, Optical Electronics, 3rd ed. New York: Holt, Reinhart and Winston, pp. 57–77, (1985).
57. K.S. Kim and M.E. Lines, "Temperature dependence of chromatic dispersion in dispersion-shifted fibers: Experiment and analysis," *J.Appl. Phys*., **73**: pp. 2069–2074, (1993).
58. S.W. James, R.P. Tatam, "Optical fiber long-period grating sensors: characteristics and application," *Meas. Sci. Technol.* **14:** R49–R61, (2003).
59. Zhiyong Wang, "Ionic Self-Assembled Multilayers Adsorbed on Long Period Fiber Gratings for Use as Biosensors", Ph.D Dissertation, ETD-12082005-094018, (Virginia Tech, 2005)
60. Victor Grubsky and Jack Feinberg, "Long-period fiber gratings with variable coupling for real-time sensing applications", *OPTICS LETTERS*, **25:** 203-205, (2000).
61. V. Bhatia "Applications of long-period gratings to single and multi-parameter sensing", *Opt. Express*, **4:** 457–66, (1999).
62. Xuewen Shu, et. al., "Sensitiv ity Characteristics of Long-Period Fib e r Gratings", *J. Lightwave Technol.,* **20**: pp. 255–266, (2002).
63. S. Khaliq, S. W. James and R. P. Tatam, "Enhanced sensitivity fibre optic long period grating temperature sensor," *Meas. Sci. Technol.,* 13792–5, (2002).
64. Khaliq S, James S W and Tatam R P, "Fibre-optic liquid level sensor using a long-period grating," *Opt. Lett.,* **26:** 1224–6, (2001).
65. G. Decher, "Fuzzy Nanoassemblies: Toward Layered Polymeric Multicomposites", *Science*, **277:** pp.1232-1237, (1997).
66. F. Caruso, K. Niikura, D.N. Furlong, Y. Okahata, "Assembly of Alternating Polyelectrolyte and Protein Multilayer Films for Immunosensing," *Langmui*r, **13:** 3427–3433 (1997).
67. G. Mijares, D. Reyes, M. Gaitan, B. Polk, D. DeVoe, "Polyelectrolyte multilayer-treated electrodes for real-time electronic sensing of cell proliferation". *Journal of Research of the NIST*., **115**: 61(13), (2010).
68. Z. Wang, J.R. Heflin, K. Van Cott, R.H. Stolen, S. Ramachandran, S. Ghalmi, "Biosensors Employing Ionic Self-Assembled Multilayers Adsorbed on Long-Period Fiber Gratings," *Sensors and Actuators B*, **139**:618-623, (2009).
69. H. Hattori, "Antireflection Surface with Particle Coating Deposited by Electrostatic Attraction," *Adv. Mater*., **13**: 51 (2001).
70. T. R. Farhat and J. B. Schlenoff, "Corrosion Control Using Polyelectrolyte Multilayers", *Electrochemical and Solid-State Letters*, **5**(4): B13-B15, (2002).
71. V. S. Trubetskoy, A. Loomis, J. E. Hagstrom, V. G. Budker and J. A. Wolff, "Layer-by-layer deposition of oppositely charged polyelectrolytes on the surface of condensed DNA particles", *Nucleic Acids Research*, **27**(15): 3090–3095., (1999).
72. J.R. Heflin, C. Figura, D. Marciu, Y. Liu, and R.O. Claus, "Thickness Dependence of Second Harmonic Generation in Thin Films Fabricated from Ionically Self-Assembled Layers," *Appl. Phys. Lett.,* **74**:495 (1999).

73. Charles Brands, “Interface Effects and Deposition Process of Ionically Self-Assembled Layer Films: In Situ and Ex Situ Second Hamonic Generation Measurements”, Ph.D Dissertation, ETD-09112003-071527, (Virginia Tech, 2003).
74. Erika Gifford, “Sensitivity control of optical fiber biosensors utilizing turnaround point long period gratings with self-assembled polymer coatings”, Ph.D Dissertation, ETD-12082005-094018, (Virginia Tech, 2008)
75. Zhiyong Wang, “Ionic Self-Assembled Multilayers Adsorbed on Long Period Fiber Gratings for Use as Biosensors”, Ph.D Dissertation, ETD-12082005-094018, (Virginia Tech, 2005)
76. R. B. Martin, "Free energies and equilibria of peptide bond hydrolysis and formation", Biopolymers, 45: 351–353, (1998).
77. S. Shiratori, M. Rubner, *Macromol*. **33**, 4213 (2000).
78. C. Figura, P.J. Neyman , D. Marciu , C. Brands, M.A. Murray, R.M. Davis, M.B. Miller, J.R. Heflin, *Proc. of SPIE*, **3939**: 214 (2000).
79. Nelson DL, Cox MM. *Lehninger's Principles of Biochemistry*(4th ed.). New York: W. H. Freeman and Company. (2005).
80. Murray RF, Harper HW, Granner DK, Mayes PA, Rodwell VW. ***Harper's Illustrated Biochemistry.*** New York: Lange Medical Books/McGraw-Hill. (2006). ISBN 0-07-146197-3.
81. Branden C, Tooze J. ***Introduction to Protein Structure.*** New York: Garland Pub.(1999). ISBN 0-8153-2305-0.
82. Wolfram Saenger. ***Principles of Nucleic Acid Structure.*** New York: Springer-Verlag.(1984). ISBN 0-387-90762-9.
83. http://www.piercenet.com/browse.cfm?fldID=63E6BCDB-F15A-49FB-A717-64D46BD93CC8
84. E. Golemis, ***Protein-protein interactions: A molecular cloning manual***. NY: Cold Spring Harbor Laboratory Press. ix, 682, (2002).
85. L. Yang, *et al*. “A photocleavable and mass spectrometry identifiable cross-linker for protein interaction studies”. *Anal. Chem*. **82:** 3556-3566, (2010).
86. http://www.piercenet.com/browse.cfm?fldID=F3305493-0FBC-93DA-2720-4412D198A9C9#carbod
87. http://www.piercenet.com/browse.cfm?fldID=F330F14F-EBCC-97DB-7F6E-9664D3ACE886
88. G.T. Hermanson***, Bioconjugate Techniques***, 2nd Edition. Academic Press, Inc. 1323,(2008).
89. Hemaprabha E., “Chemical Crosslinking of Proteins: A Review”, *JESI* **1(1),** 22-26, (2012).
90. http://www.piercenet.com/browse.cfm?fldID=F3305493-0FBC-93DA-2720-4412D198A9C9#carbodiimide
91. A.Panchaud, *et al.,* “Anibal, stable isotope-based quantitative proteomics by aniline and benzoic acid labeling of amino and carboxylic groups”. *Mol. Cell. Proteomics*. **7:** 800-12, (2008).
92. S.Yamashiro, *et al.* “Mammalian tropomodulins nucleate actin polymerization via their actin monomer binding and filament pointed end-capping activities”. *J. Biol. Chem.* **285**: 33265-80,(2010).
93. http://www.piercenet.com/files/TR0030-Modify-oligos.pdf
94. Greg T. Hermanson, ***Bioconjugate Techniques, 2nd Edition***, Academic Press, Inc., (2008).
95. http://www.piercenet.com/browse.cfm?fldID=F330F14F-EBCC-97DB-7F6E-9664D3ACE886#imidoester
96. Litman G., Cannon J., Dishaw L., “Reconstructing immune phylogeny: new perspectives.” *Nat Rev Immunol*. , **5 (11)**: 866–79, (2005).
97. Gregory B., Habicht G.S., “Immunity and the Invertebrates”, *Scientific American*. **November 1996**: 60–66, (1996).
98. http://en.wikipedia.org/wiki/Immunology
99. Lippincott Williams *etc.*, ***Lippincott's Illustrated Reviews: Immunology*** (ISBN 0-7817-9543-5), Page 20, (July 1, 2007)
100. Peter Parham, ***The Immune System***, Garland Science, 2nd edition.
101. http://en.wikipedia.org/wiki/Fc_receptors

102. Janeway, Charles A.; Travers, Paul; Walport, Mark; Shlomchik, Mark. ***Immunobiology.*** 5th ed.. New York and London: Garland Publishing; c2001.
103. Abul K. Abbas, Andrew H. Lichtman ; illustrations by David L. Baker, Alexandra Baker. ***Cellular and molecular immunology.*** Philadelphia, PA : Elsevier Saunders, c2005
104. http://www.piercenet.com/browse.cfm?fldID=F88ADEC9-1B43-4585-922E-836FE09D8403
105. http://en.wikipedia.org/wiki/Immunoassay
106. http://en.wikipedia.org/wiki/ELISA
107. http://catalog2.corning.com/Lifesciences/media/pdf/elisa3.pdf
108. J. Frank Griffin, *etc.,* "Immunoglobulin G1 Enzyme-Linked Immunosorbent Assay for Diagnosis of Johne's Disease in Red Deer (Cervus elaphus)". *Clin. Diagn. Lab. Immunol*. **12 12 (12):** 1401–1409, (2005).
109. X. Lan, Q. Han, T. Wei, J. Huang, H. Xiao, "Turn-Around-Point Long-Period Fiber Gratings Fabricated by CO Laser Point-by-Point Irradiations," *IEEE PHOTONICS TECHNOLOGY LETTERS* , **23(22):** pp. 1664–1666, (2011).
110. Y. Wang, "Review of long period fiber gratings written by CO[sub 2] laser," *Journal of Applied Physics*, **v 108(8):** p. 081101, (2010).
111. Y.-P. Wang, D. N. Wang, W. Jin, Y.-J. Rao, and G.-D. Peng, "Asymmetric long period fiber gratings fabricated by use of CO2 laser to carve periodic grooves on the optical fiber", *Appl. Phys. Lett*. **89**: 151105 (2006).
112. H.F.Chambers, "The changing epidemiology of Staphylococcus aureus?" *Emerg Infect Dis*, **7(2**):178-182, (2001).
113. GT Stewart, RJ Holt, "Evolutio of natural resistance to the newer penicillins." *Br Med J*, **1(5326)**:308-311, (1963).
114. EJ Benner, FH Kayser, "Growing clinical significance of methcillin-resistant Staphylococcus aureus." *Lancet*, **2(7571):**741-744, (1968).
115. SE Cosgrove, *etc.*, "Comparison of mortality associated with methicillin-resistant and methicillin-susceptible Staphylococcus aureus bacteremia: a meta-analysis." *Clin Infect Dis*, **36(1):**53-59, (2003).
116. EW Tiemersma, *etc.,* "Methicillin-resistant Staphylococcus aureus in Europe, 1999-2002." *Emerg Infect Dis,* **10(9):**1627-1634, (2004,).
117. TP Lodise, PS McKinnon, "Clinical and economic impact of methicillin resistance in patients with Staphylococcus aureus bacteremia." *Diagn Microbiol Infect Dis***, 52(2):**113-122, (2005).
118. K Murakami, etc., "Identification of methicillin-resistant strains of staphylococci by polymerase chain reaction." *J Clin Microbiol*, **29(10):**2240-2244, (1991).
119. C Ryffel, etc., "Sequence comparison of mecA genes isolated from methicillin-resistant Staphylococcus aureus and Staphylococcus epidermidis." *Gene*, **94(1):**137-138, (1990).
120. http://www.bcm.edu/molvir/index.cfm?pmid=16508
121. S Gregory*, etc.,* "The DNA sequence and biological annotation of human chromosome 1". *Nature,* **441 (7091):** 315–21, (2006).
122. P Francois, J Schrenzel, *etc., "*Rapid detection of methicillin-resistant Staphylococcus aureus directly from sterile or nonsterile clinical samples by a new molecular assay.", *J Clin Microbiol,* **41(1):**254-60, (2003).
123. A Huletsky, M. G. Bergeron, *etc.,* "New real-time PCR assay for rapid detection of methicillin-resistant Staphylococcus aureus directly from specimens containing a mixture of staphylococci." *J. Clin. Microbiol*. **42:**1875-1884, (2004).
124. A. J. Grisold, E. Leitner, G. Mühlbauer, E. Marth, and H. H. Kessler. "Detection of methicillin-resistant Staphylococcus aureus and simultaneous confirmation by auTomated nucleic acid extraction and real-time PCR." **J. Clin. Microbiol**. **40**:2392-2397, (2002).

125. D. Jonas, M. Speck, F. D. Daschner, and H. Grundmann. " Rapid PCR-based identification of methicillin-resistant Staphylococcus aureus from screening swabs." *J. Clin. Microbiol*. **40**:1821-1823, (2002).
126. B. Strommenger, C. Kettlitz, G. Werner, and W. Witte. " Multiplex PCR assay for simultaneous detection of nine clinically relevant antibiotic resistance genes in Staphylococcus aureus." *J. Clin. Microbiol*. **41**:4089-4094, (2003).
127. K. Murakami, and W. Minamide. "PCR identification of methicillin-resistant Staphylococcus aureus," p. 539-542. In D. Pershing, T. Smith, F. Tenover, and T. White (ed.), *Diagnostic molecular microbiology: principles and application.* ASM Press, Washington, D.C., (1993).
128. HENRY CHAMBERS, "Methicillin Resistance in Staphylococci: Molecular and Biochemical Basis and Clinical Implications", *CLINICALMICROBIOLOGY REVIEWS,* **10 (4):** p. 781–791, (1997).
129. M.I Pividori, A Merkoçi, S Alegret, "Electrochemical genosensor design: immobilisation of oligonucleotides onto transducer surfaces and detection methods", *Biosensors and Bioelectronics,* **15(5-6):** 291-303, (2000).
130. http://catalog2.corning.com/Lifesciences/media/pdf/elisa3.pdf
131. http://en.wikipedia.org/wiki/Francisella_tularensis
132. MA Apicella, et al., "Identification, Characterization and Immunogenicity of an O-Antigen Capsular olysaccharide of Francisella tularensis", PLoS ONE, 5(7): e11060, (2010).
133. Maier TM, Havig A, Casey M, Nano FE, Frank DW, et al. "Construction and characterization of a highly efficient Francisella shuttle plasmid." Appl Environ Microbiol, 70: 7511–7519, (2004).
134. http://en.wikipedia.org/wiki/Brucellosis
135. KJ Ryan, CG Ray (editors) (2004). ***Sherris Medical Microbiology (4th ed.)*** McGraw Hill. ISBN 0-8385-8529-9.
136. V. L. Atluri, M. N. Xavier, M. F. De Jong, A. B. Den Hartigh, R. E. M. Tsolis, "Interactions of the Human PathogenicBrucellaSpecies with Their Hosts". *Annual Review of Microbiology,* **65**: 523–541, (2011).
137. BJ Bricker, SM Halling, "Differentiation of Brucella abortus(biovars 1, 2 and 4), Brucella melitensis, Brucella ovis, and Brucella suis(biovar 1) by the polymerase chain reaction." *J. Clin. Microbial.* **32:** 2660-2666, (1994).
138. R. Redkar, S. Rose, B. Bricker, and V. DelVecchio, "Real-time detection of Brucella abortus, Brucella melitensis, and Brucella suis." *Mol. Cell. Probes* **15:**43-52, (2001).
139. BJ Bricker, "PCR as a diagnostic tool for brucellosis." *Vet.Microbiol.* **90(1):** 435-446, (2002).
140. William S. Probert, Kimmi N. Schrader, Nhi Y. Khuong, Susan L. Bystrom and Margot H. Graves, "Real-Time Multiplex PCR Assay for Detection of Brucella spp., B. abortus, and B. melitensis", *J. Clin. Microbial.* **42(3):** 1290-1293,(2004).
141. http://www.merckmanuals.com/vet/generalized_conditions/histophilosis/overview_of_histophilosis.html
142. http://www.piercenet.com/files/TR0030-Modify-oligos.pdf
143. Gurman Singh Pall, Carles Codony-Servat, Jane Byrne, Leigh Ritchie, and Andrew Hamilton, "Carbodiimide-mediated cross-linking of RNA to nylon membranes improves the detection of siRNA, miRNA and piRNA by northern blot", *Nucleic Acids Res.,* **35(8):** e60, (2007).
144. http://www.piercenet.com/browse.cfm?fldID=978FBB48-DCD3-F4E4-66E7-069349D16FEE
145. http://www.piercenet.com/browse.cfm?fldID=978FBB48-DCD3-F4E4-66E7-069349D16FEE
146. Ferguson JA, Christian Boles T, Adams CP, Walt DR, "A fiber-optic DNA biosensor microarray for the analysis of gene expression", *Nature Biotechnol,* **14**:1681–1684, (1996).